Universidad de Alcalá

PhD. Program in Electronics: Advanced Electronic Systems. Intelligent Systems

# Predictive Techniques for Scene Understanding by using Deep Learning in Autonomous Driving

PhD. Thesis Presented by

**Carlos Gómez Huélamo**

2023

Universidad de Alcalá

PhD. Program in Electronics: Advanced Electronic Systems. Intelligent Systems

# Predictive Techniques for Scene Understanding by using Deep Learning in Autonomous Driving

PhD. Thesis Presented by

**Carlos Gómez Huélamo**

Advisors

**Dr. Luis Miguel Bergasa Pascual**

**Dr. Rafael Barea Navarro**

Alcalá de Henares, July 24th

**A mi Madre, allá donde esté ..... .**

*"En este vasto mundo*
*navegáis en pos de un sueño,*
*surcando el ancho mar*
*que se extiende frente a vosotros.*
*El puerto de destino es el mañana*
*cada día más incierto.*
*Encontrad el camino,*
*cumplid vuestros sueños,*
*estáis todos en el mismo barco*
*y vuestra bandera es la libertad"*
Opening 3 de One Piece
Autor: The Babystars

# Acknowledgements

Esta Tesis Doctoral supone el culmen a cuatro años (Abril 2019 - Abril 2023) realmente duros, cargado de emociones, triunfos, pandemias, estafas y tropiezos, todo a partes iguales. Este es probablemente (aunque como diría Sean Connery interpretando a James Bond en 1983, *Never Say Never Again*) mi último gran documento individual, académicamente hablando.

Durante mi etapa universitaria (2013 hasta el momento, 2023) he tenido ciertos momentos puntuales en los que he sentido un salto cualitativo como profesional: El primero fue en el segundo cuatrimestre de segundo de carrera, cuando las cosas se pusieron tensas con Control II e Informática Industrial. Vaya sudores. El segundo probablemente fue con el fallecimiento de mi madre durante mi ERASMUS+ en Irlanda. Duros y oscuros momentos, alejado de mis seres queridos. El tercer momento llega en segundo de máster, durante mi querido ERASMUS+ en Finlandia, donde compagino una estancia preciosa en Tampere con el máster y un pre-inicio de doctorado. Me equivoqué al empezar tan pronto con la beca, "queriendo cobrar" cuanto antes, en vez de terminar tranquilamente el TFM y plantear la tesis, pero eso no lo sabría hasta tiempo después. Pero no es hasta la tesis donde empezaron los quebraderos de cabeza reales. Continuamente altibajos, mala planificación por mi parte, momentos puntuales donde me equivoqué rotundamente al empecinarme en soldar una estructura compleja para nuestro vehículo sin ayuda, no estudiar PyTorch tras el congreso WAF 2018 tras la sugerencia de mi tutor, no enfocarme en técnica individual hasta bien entrado el doctorado, no querer hacer nada hasta que no tuviese la teoría perfectamente asimilada, tener demasiado respeto a la Inteligencia Artificial y escurrir el bulto de mi tesis en un compañero mientras yo me dedicaba a integrar y corregir los bugs del grupo que para mí *era lo fácil*. Mal. Todo mal. Pero todo cambió tras mi segunda estancia, en Estados Unidos, cuando tras llorar por no entender el camino a seguir, nadie que me ayudara, decidí crear mi propio camino, con paciencia y fé, práctica y error compaginado con lectura de artículos, para mejorar mi confianza y autoestima, y finalmente logré empezar a entender lo que era el Deep Learning. Gracias a todos mis errores, desventuras y discusiones, a día de hoy, excepto momentos inevitables, me encuentro con muchísima capacidad para atacar y gestionar prácticamente cualquier problema, consultar documentación y organizarme, aunque esta sigue siendo mi tarea pendiente.

Cada año, desde hace ya varios, mi primera publicación en Instagram viene seguida de la frase "Trabaja duro en silencio y deja que tu éxito haga todo el ruido". Filosofía Kaizen, de mejora y aprendizaje continuo, para así cada día entender el mundo un poquito mejor. Si toda la dedicación y estudio que he depositado en este trabajo sirven para algo en mi futuro, sé que todo el esfuerzo habrá merecido la pena.

Después de este particular monólogo, a lo cual soy muy propenso y de lo cual mis amigos y compañeros no cesan en su empeño de recordádmelo, debo, como no puede ser de otra manera, dar paso a los agradecimientos.

En primer lugar, me gustaría agradecer a mis profesores del grupo RobeSafe, especialmente a mis tutores Luis Miguel Bergasa Pascual y Rafael Barea Navarro, por ofrecerme estar en el grupo (así como aguantarme) durante todos estos años e intentar que tuviésemos el mejor *experimental setup* y *roadmap* en el laboratorio, aunque no fuese siempre sencillo. Sin dudas considero realmente interesante la temática propuesta en esta tesis doctoral, predicción de agentes en el contexto de vehículo inteligente, ya que entra en el plano filosófico sobre cómo razonar el futuro de los objetos y cómo podría afectar a la capacidad ejecutiva del agente que deba tomar una decisión. Mi mente hace tiempo que cambió y me fijo siempre que conduzco de todo lo que intento reproducir con mis estudios. Habrá que seguir esta tendencia muy de cerca en los próximos años, porque personalmente considero que sus aplicaciones son fantásticas.

A mis tutores en las estancias de doctorado, Christoph Stiller y Eduardo Molinos en el Karslruhe Institute of Technology (KIT, Alemania) y Wei Zhan y Masayoshi Tomizuka en la University of California, Berkeley (UCB, Estados Unidos). Se suele decir que unas veces se gana y otras se aprende, y yo en estas estancias quizás aprendí demasiado ... No obstante, me guardo grandísimos momentos (admirar las secuoyas gigantes o hacer mi primera escalada en roca entre ellos) y amigos, como Su Shaoshu o Frank Bieder, con los que aún guardo un cierto contacto.

A mis compañeros, mejor dicho, amigos, de laboratorio: Javier Araluce, Rodrigo, Felipe (chavalín), Santiago, Miguel Antunes, Miguel Eduardo, antiguos compañeros como Javier del Egido, Óscar, Alejandro, Eduardo, Roberto y Pablo Alcantarilla, y a nuevos becarios como Fabio, Navil y Pablo. Gracias de corazón por estar ahí, en nuestras charlas sobre tecnología, empleos, el camino correcto a seguir y la vida en general.

Especial mención vuelvo a hacer a Miguel Eduardo y mi compañero Marcos Conde, cuya apoyo intenso ayudó a centrar mi camino en técnica y escritura. Muchísimas gracias por todo lo que aprendí a vuestro lado. Especial mención a mi querido profesor Ángel Álvarez, por sus valiosos consejos para afrontar mi carrera profesional y mi vida en general de la mejor forma posible. Eres muy grande.

A mis amigos de la universidad, especialmente a Rocío, Juan Carlos, Esther, Sergio, Pablo, Rubén y Adrián Rocandio. Aún me acuerdo de cuando empezamos con la carrera

y como el paso inexorable del tiempo nos moldea a conveniencia. Os deseo lo mejor en vuestro futuro.

A mis buenos amigos Samuel y Adrián, con quien gran parte de mi vida he compartido. Con especial cariño guardo las interminables charlas sobre la vida y el futuro después de Karate, de comer, de cenar, en el coche, siempre quejándonos de la hora que marcaba el reloj al final de tan interminables conversaciones.

A mi familia, uno de los pilares de mi vida. A mi padre Juan Antonio y a mi madre Petra, que en paz descanse, les debo todo lo que soy y es por ello por lo que les estaré siempre agradecido. Querido padre, gracias por ser tan Genaro, arisco y pesado. Siempre has sido mi ejemplo a seguir, aunque cuando tenga 42 años me sigas regañando por subir con las zapatillas puestas. Querida madre, no se muere quien se va, sólo se muere el que se olvida, y tú nunca caerás en el olvido. A mi querida hermana-calili-chessmaster Silvia, con quien tantas regañinas he tenido, pero el cariño que nos tenemos las supera a todas. A mi perrita Nuka (a.k.a. Dragón, ChupaChups cuando le cortamos el pelo o Nuki-Nuki), cuyos paseos matutinos son probablemente el ingrediente secreto para la elaboración de esta tesis, dando rienda suelta a mi cabeza para imaginar nuevas propuestas mientras miraba el cielo azul. A mi querido *experimental setup* que me ha acompañado durante toda mi vida académica: silla de madera de la cocina, ratón de Hello Kitty tomado prestado de mi hermana y mi querido portátil táctil. Sois la base de todo mi trabajo.

Al resto de la familia, amigos, compañeros, entrenadores y profesores, gracias por todo.

Y, por último, la persona más importante de mi vida ahora mismo. Mi querida Marta, la persona más maravillosa y buena que conozco. Hemos compartido risas, lloros, besos y abrazos. Nunca me cansaré de repetirte lo suave que tienes la piel tras darte un beso en la mejilla y después hacerte de rabiar. Espero que esta situación esté dentro de un while cuya condición sea *True*.

*"Te quiero más que ayer, pero menos que mañana. Hoy, y siempre"*

Mi querido lector, disculpa mi monólogo de agradecimientos, es mi forma de ser y la cual tengo por bandera, aunque creo que ha quedado bonito. Podría decir mil anécdotas más de mi doctorado, pero como diría Aragorn, legítimo Rey de Gondor, enfrente de la mismísima Puerta Negra: *Hoy no es ese día*.

Vamos a la lectura importante, que empiece el *Rock and Roll* !!

# Resumen

TBD

**Palabras clave:** Autonomous Driving, Deep Learning, Motion Prediction, Scene Understanding.

# Abstract

TBD

**Keywords:** Autonomous Driving, Deep Learning, Motion Prediction, Scene Understanding.

# Contents

# List of Figures

# List of Tables

# List of Source Code

# List of Acronyms

| | |
|---|---|
| AD | Autonomous Driving. |
| ADS | Autonomous Driving Stack. |
| AI | Artificial Intelligence. |
| BEV | Bird's Eye View. |
| CA | Constant Acceleration. |
| CMP | Conditional Motion Prediction. |
| CNN | Convolutional Neural Network. |
| CTRA | Constant Turn Rate and Acceleration. |
| CTRV | Constant Turn Rate and Velocity. |
| DL | Deep Learning. |
| FLOP | FLoating-point Operations per second. |
| GAN | Generative Adversarial Network. |
| GNN | Graph Neural Network. |
| ITS | Intelligent Transportation Systems. |
| LSTM | Long Short-Term Memory. |
| MHSA | Multi-Head Self-Attention. |
| minADE | minimum Average Displacement Error. |
| minFDE | minimum Final Displacement Error. |
| MOT | Multi-Object Tracking. |
| MP | Motion Prediction. |
| PMP | Passive Motion Prediction. |

RNN Recurrent Neural Network.

SOTA State-of-the-Art.

VRU Vulnerable Road User.

# Chapter 1

# Introduction

*Aaay, el oro, la fama, el poder.*
*Todo lo tuvo el hombre que en su día se autoproclamó*
*el rey de los piratas, ¡GOLD ROGER!*
*Mas sus últimas palabras no fueron muy afortunadas:*
*"¿¡MI TESORO!? Lo dejé todo allí, buscadlo si queréis,*
*ojalá se le atragante al rufián que lo encuentre.*

Opening 1 de One Piece: "We are"
Autor original: Hiroshi Kitadani

## 1.1. Motivation

AD have held the attention of technology enthusiasts and futurists for some time as is evidenced by the continuous research and development of this topic in Intelligent Transportation Systems (ITS) over the past decades, being one of the emerging technologies of the *Fourth Industrial Revolution*, and particularly of the Industry 4.0.

The concept *Fourth Industrial Revolution* or Industry 4.0 was first introduced by Klaus Schwab , CEO (Chief Executive Officer) of the World Economic Forum, in a 2015 article in Foreign Affairs (American magazine of international relations and United States foreign policy). A technological revolution can be defined as a period in which one or more technologies are replaced by other kinds of technologies in a short amount of time. Hence, it is an era of accelerated technological progress featured by Researching, Development and Innovation whose rapid application and diffusion cause an abrupt change in society. In particular, the *Fourth Industrial Revolution* conceptualizes rapid change to industries, technology, processes and societal patterns in the 21st century due to increasing interconnectivity and smart automation. This industrial revolution focuses on operational efficiency, being the following four themes which summarize it:

- Decentralized decisions: Ability of cyber physical systems to make decisions on their own and to perform their tasks as autonomously as possible.

- Information transparency: Provide operators with comprehensive information to make decisions. Inter-connectivity allows operators to gather large amounts of information and data from all points in the manufacturing process in order to identify key areas or aspects that can benefit from improvement to enhance functionality.
- Technical assistance: Ability to assist humans with unsafe or difficult tasks and technological facility of systems to help humans in problem-solving and decision-making.
- Interconnection: Ability of machines, sensors, devices and people to communicate and conect with each other via the Internet of Things (IoT) or the Internet of People (IoP).

Based on the aforementioned principles, this revolution is expected to be marked by breakthroughs in emerging technologies in fields such as nanotechnology, quantum computing, 3D printing, Internet of Things (IoT), fifth-generation wireless technologies (5G), Robotics, Computer Vision (CV), Artificial Intelligence (AI) or the scope of this PhD thesis, Autonomous Driving Stacks (ADSs). The sum of all these advances are resulting in machines that can potentially see, hear and what is more important, think, moving more deftly than humans.

An ADS, also referred in the literature as Intelligent Vehicle (IV), driverless car or autonomous car, is a vehicle tan can sense its surrounding and moving safely with little or even no human input. These ADSs must combine a variety of sensors to understand the traffic scenario, like RADAR (RAdio Detection A Ranging), LiDAR (Light Detection and Ranging), cameras, Inertial Measurement Unit (IMU), wheel odometry, GNSS (Global Navigation Satellite System) or ultrasonic sensors, and detect, track and predict (which is the main purpose of this thesis) the most relevant obstacles around the ego-vehicle. Then, advanced control and planning systems process this sensory information in combination with a predefined global route to calculate the corresponding control commands to drive throughout the environment, ensuring a safe driving.

The dream of seeing fleets of ADSs efficiently delivering goods and people to their destination has fueled billions of dollars and captured consumer's imaginations in investment in recent years. Nevertheless, according to the "Autonomous driving's future: Convenient and connected" report, published by the global management consulting firm McKinsey & Company in January 2023, even after some setbacks have pushed out timelines for AD launches and delayed customer adoption, the transportation community still broadly agrees that AD has the potential to transform consumer behaviour, transportation and society at large. AD is considered as one of the solutions to the aforementioned problems and one of the greatest challenges of the automotive industry today.

Statistics show that 69 % of the population in the European Union (EU), including associated states, lives in urban areas. According to the World Health Organization,

nearly one third of the world population will live in cities by 2030, leading to an overpopulation in most of them. Aware of this problem, the Transport White Paper published by the European Commission in 2011 indicated that new forms of mobility ought to be proposed so as to provide sustainable solutions for people and goods safely. For example, regarding safety, it sets the ambitious goal of halving the overall number of road deaths in the EU between 2010 and 2020. Nevertheless, this goal does not seem to be easy since only in 2014 more than 25,700 people died on the roads in the EU, many of them caused by an improper behaviour of the driver on the road. A similar study made by the National Highway Traffic Safety Administration (NHTSA, tranportation organization of the United States) reported in 2015 that around 94 % of traffic accidents happen because of human error. In that sense, the existence of reliable and economically affordable ADSs are expected to create a huge impact on society affecting social, demographic, environmental and economic aspects. It can produce substantial value for the auto industry, drivers and society, making driving safer, more convenient and more enjoyable. While the human driver or not could select whether to drive, in autonomous mode hours on the road previously spent driving could be used to work, watch a funny movie or even to video call a friend. For employees with long commutes, AD might shorten the workday, increasing worker productivity. Since workers, specially those related to digital jobs or related fields, may perform their jobs from an ADS, they could more easily move further away from the office, which, in turn, could attract more people to suburbs and rural areas. Besides this, it is estimated to cause a reduction in road deaths, reduce fuel consumption and harmful emission associated and improve traffic flow, as well as an improvement in the overall driver comfort and mobility in groups with impaired faculties, such as disable or elderly people, providing them with mobility options that go beyond car-sharing services or public transportation. Other industrial applications of autonomous vehicles are agriculture, retail, manufacturing, commercial and freight transport or mining.

## 1.2. Historical Context

ADSs have become a challenge for auto competitions and technology companies, which has derived in an intense competition. Though today companies such as Mercedes, Ford or Tesla are racing to build ADSs for a radically changing consumer world, the research and development of autonomous robots is not new.

In 1500, centuries before the invention of the automobile, Leonardo da Vinci designed a cart that could move without being pulled or pushed. In 1868, Robert Whitehead invented a torpedo that could propel itself underwater in order to be a game-changer for naval fleets all over the world. In terms of robotic solutions for intelligent mobility, the study was started in the 1920s, being the concept of Autonomous Car defined in Futurama, an exhibit at the 1939 New York Wolrd's Fair. General Motors created the exhibit to display its vision of what the world would look like in 20 years, including an

automated highway system that would guide ADS. By 1958, General Motors made this concept a reality (at least as a proof of concept) being the car's front end embedded with sensors to detect the current flowing through a wire embedded in the road. The first semi-automated car was developed in 1977 by Japan's Tsukuba Mechanical Engineering Laboratory. The vehicle reached speeds up to 30 km/h with the support of an elevated rail.


Figure 1.1: Stanley, 2005 DARPA Grand Challenge winner
Source: *Stanford university*

Nevertheless, the first truly autonomous cars appeared in the 1980s with Carnegie Mellon University's Navlab and ALV projects funded by the USA company DARPA (Defense Advanced Research Projects Agency) in 1984 and EUREKA Prometheus project (1987) developed by Mercedes-Benz and Bundeswehr University Munich's. By 1985, the ALV project had shown self-driving speeds on two-lane roads of 31 km/h with obstacle avoidance added in 1986 and off-road driving in day and night conditions by 1987. Furthermore, from the 1960s through the second DARPA Grand Challenge in 2005 (212 km off-road course near the California-Nevada state line, surpassed by all but one of the 23 finalists), automated vehicle research in the United States was primarily funded by DARPA, the US Army and US Navy, yielding rapid advances in terms of speed, car control, sensor systems and driving competence in more complex conditions. This caused a boost in the development of autonomous prototypes by companies and research organizations, most of them from the United States. Figure 1.1 shows Stanley, the 2005 DARPA Gran Challenge winner, from Stanford university.

Even though self-driving cars have not yet displaced conventional cars, there can be found several examples of how it has become a hot topic for powerful companies such as Delphi Automotive Systems, Audi, BMW, Tesla, Mercedes-Benz or Waymo. In 2005 Delphi broke the Navlab's record achievement (driving 4,584 km while remaining 98 % of the time autonomously) by piloting an Audi, improved with Delphi technology, over 5,472

km through 15 states while remaining in self-driving mode 99 % of the time. Moreover, in 2005 the USA states of Michigan, Virginia, California, Florida, Nevada and the capital, Washington D.C., allowed the testing of automated cars on public roads.

In 2017, Audi stated that its A8 car prototype would be automated at speeds up to 60 km/h by using its perception system named "Audi AI". Also, in 2017 Waymo (self-driving technology development company subsidiary of Alphabet Inc) started a limited trial of a self-driving taxi service in Phoenix, Arizona.

Figure 1.2 shows the total number of autonomous test miles and miles per disengagement in California (Dec 2019 - Nov 2020) by some of the most important AD technology development companies around the world. The concept disengagement is quite useful to assess the quality of an ADS, defined as the deactivation of the autonomous mode when a failure of the autonomous technology is detected or when a safe operation requires that the autonomous vehicle test driver disengages the autonomous mode, resulting in control being seized by the human driver.

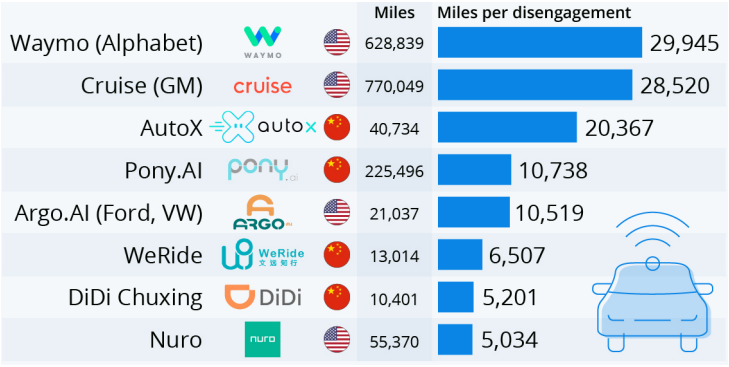


Figure 1.2: Number of autonomous test miles and miles per disengagement (Dec 2019 - Nov 2020)
Source: *DMV California, via The Last Driver License Holder*

At the moment of writing this thesis (2023), many vehicles on the road are considered to be semi-autonomous due to safety features like braking systems, assisted parking, lane boundaries detection or predict the long-term behaviour of the users around the vehicle to execute the most optimal action in a safely way. Regarding this, the Society of Automotive Engineers (SAE) published the concept of autonomy levels in 2014, as part of its "Taxonomy and Definitions for Terms Related to On-Road Motor Vehicle Automated Driving Systems" [1] report. Figure 1.3 illustrates the six levels of autonomy (the higher the level, the more autonomous the car is), where it can be appreciated that Level Zero means "No Automation", being the acceleration, braking and steering controlled by a human driver at all times, and Level Five represents Full Automation, where there is a full-time automation of all driving tasks on any road, under any conditions, whether there is a human on board or not.

In that sense, today most vehicles only included basic Advanced Driver Assistance Systems (ADAS), but major advancements in AD capabilities are on the horizon. According to a 2021 McKinsey consumer survey, growing demand for AD systems could create bil-

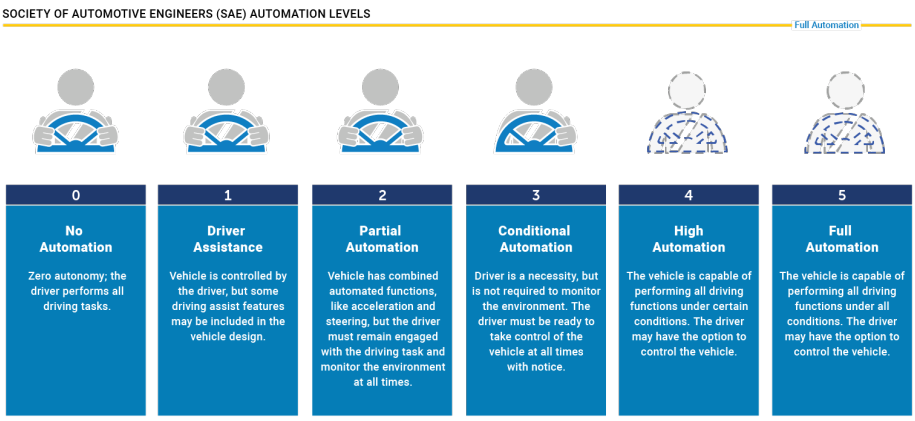


Figure 1.3: Society of Automotive Engineers (SAE) automation levels
Source: *NHTSA (National Highway Traffic Safety Administration)*

lions of dollars in revenue. Based on a consumer interest in AD features and commercial solutions available on the market today, ADAS and AD could generate between $300 and $400 billions in the passenger car market by 2035. Figure **??** illustrates an interesting study reporting the revenues of ADAS and AD from Level 1 (Driver Assistance) to Level 4 (High Automation). As expected, Level 5 is excluded from this study due to the huge difficulties the automotive companies would have to face to adapt their systems under totally different environmental conditions.

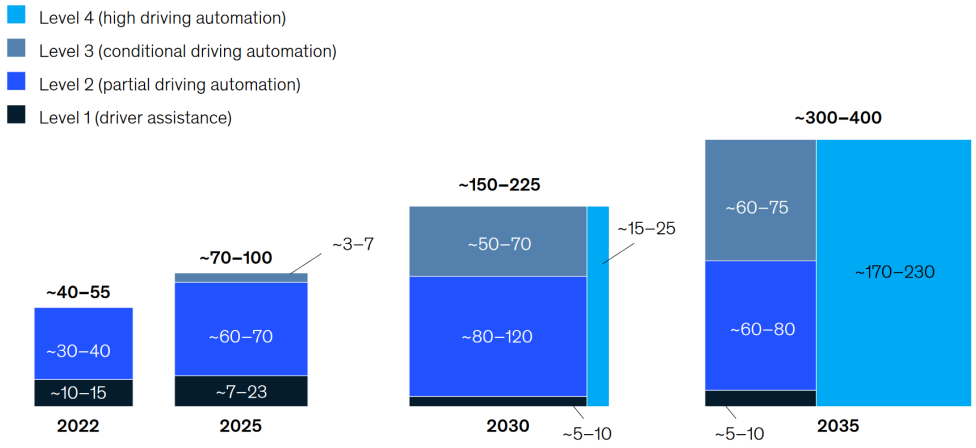


Figure 1.4: Advanced Driver Assistance systems (ADAS) and Autonomous Driving (AD) revenues in $ billion
Source: *McKinsey Center for Future Mobility*

## 1.3. Autonomous Driving architecture

To sum up what commented above, increasing the level of autonomous navigation in mobile robots (from agriculture to public and private transport) are expected to create tangible business benefits to those users and companies employing them. However, designing an autonomous navigation system does not seem to be an easy task. In the SOTA

we can distinguish two main kind of software architectures: End-to-End and modular. Figure 1.5 illustrates the entire AD architecture starting from sensing, all the way to longitudinal (throttle/brake) and lateral (steering angle) control of the vehicle, which are the commanded signals that feed the low-level electronic system that moves the vehicle, like a drive-by-wire system [2]. End-to-End are considered black-box models, where a single neural network performs the driving task (throttle/steering/brake) from raw sensor data, in such a way the error be may vanished since intermediate representations are jointly optimized, but these are not very interpretable. On the other hand, modular architectures (considered as glass models as counterpart to End-to-End approaches) separate the driving task into individually programmed or trained modules. This solution is more interpretable, since the know-how of a research group or company is easily transferred, they allow parallel development, being the standard solution in industrial research, but the error is propagated, where intermediate representations can led to suboptimal performance. For example, incorrect object detection can lead to low-quality tracking and motion prediction.

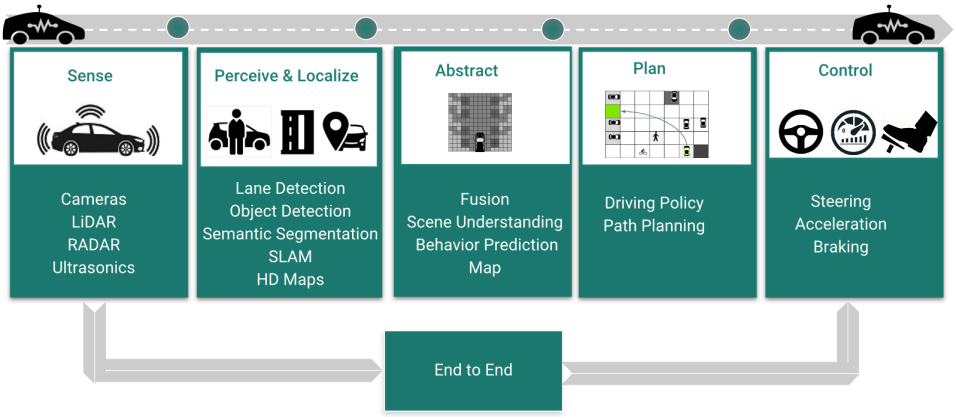


Figure 1.5: Autonomous Driving Stack (ADS) modular vs end-to-end pipeline
Source: *Vrunet: Multi-task learning model for intent prediction of vulnerable road users* [3]

Considering the RobeSafe (Robotics and eSafety) research group and the main projects (Techs4AgeCar, AIVATAR) where this thesis has been developed, we integrate our algorithms in a software modular approach. An example of a software modular approach is shown in Figure 1.6. Despite the fact in literature some authors disagree on the specific software architecture of an ADS, specially the motion prediction module, which is usually classified as a perception algorithm but sometimes is included as part of the planning or decision-making layers, we can hierarchically break down (from raw data to the driving task) a standard AD architecture into the following software layers:

- Localization layer: Positions and locates the vehicle on a map with real-time and centimetric accuracy approach. The main source of information is a robust differential-GNSS, though IMUs, wheel odometry and even cameras are commonly employed.

- Perception layer: Understand the environment around the ego-vehicle thanks to the information collected by the sensors. If defined as multi-stage, the perception layer first detects the most relevant obstacles, then track them over time to finalize long-term predict with plausible predictions. In order to perform object detection, LiDAR, camera and RADAR are the main sensors that provide the corresponding raw data. Additionally, HD map information is frequently used in the motion prediction tasks by most SOTA algorithms.
- Mapping layer: Responsible for creating a topologic, semantic and geographical modeling of the environment through which the vehicle drives, being the HD Map graph the most common source of information.
- Planning layer: This layer is comprised of three components: route, behaviour and trajectory planner. The route planner computes the most optimal (in terms of distance, time and so forth and so on) global route from some predefined start and goal. It uses the localization and mapping output. On the other hand, the behaviour planner, also referred as decision-making layer by some authors, it performs high-level decision-making of driving behaviours such as lane changes or progress through intersections, mostly focused on the previously computed global route and current localization. It can be seen as an atomization of the global route in different behaviors to reach the goal. Finally, the trajectory planner, also known as local planner, generates a time schedule for how to follow a path given constraints such as position, velocity and acceleration in order to meet the previously decided behaviour and taking into account the prediction from the perception layer, avoiding obstacles in optimal direction and speed conditions.
- Control layer: Once the local plan is calculated, the control layer is responsible for generating the commands that are sent to the actuators. It receives as input some waypoints from the calculations made in the trajectory planner. Once these waypoints are received, most authors perform spline interpolations and a velocity profile that ensures a smooth and continous trajectory.

## 1.4. Problem statement

As commented in previous sections, in order to operate efficiently and safely in highly dynamic, complex and interactive driving scenarios, ADS need to smartly reason like human beings via predicting future motions of surrounding traffic participants during navigation. Nevertheless, achieving accurate and robust MP in one of the most difficult and interesting challenges to achieve full-autonomy, since it is equivalent to a bridge between the former stages of the perception layer, where the scene is understood detecting and tracking static and dynamic objects of the environment, and the planning and control

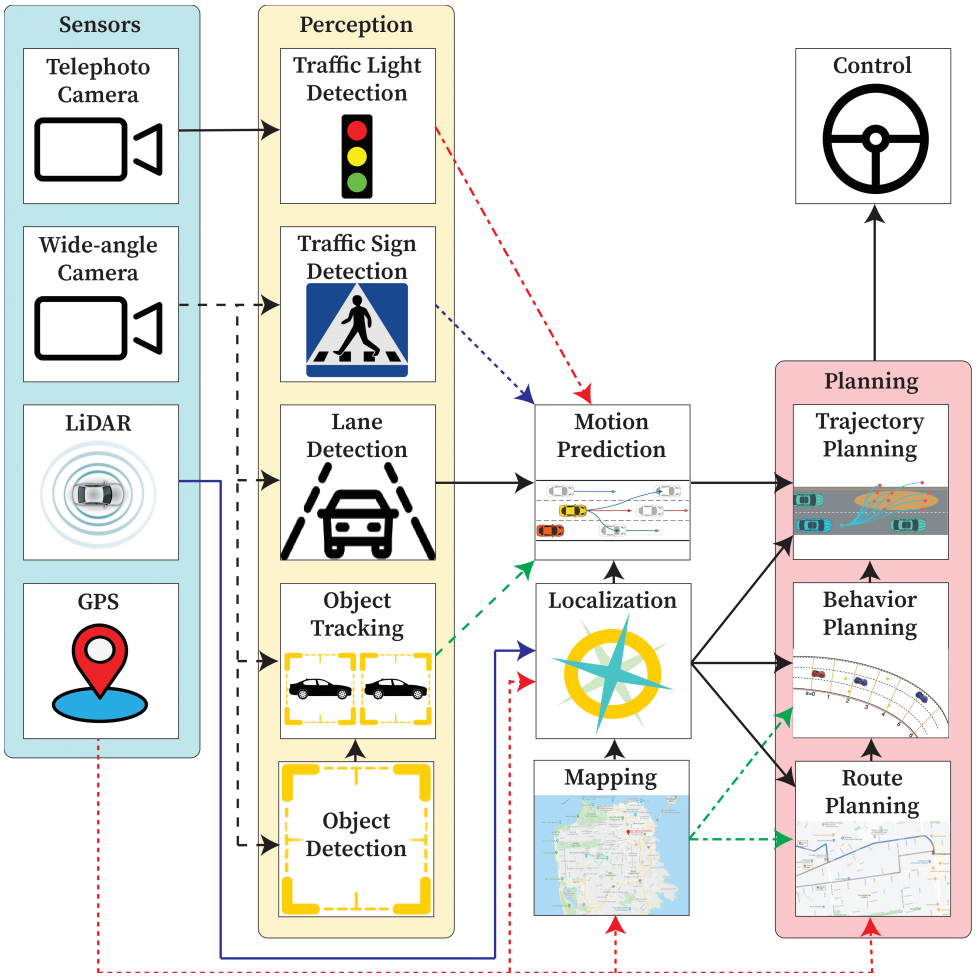


Figure 1.6: Autonomous Driving Stack (ADS) modular pipeline
Source: *Pylot: A modular platform for exploring latency-accuracy tradeoffs in autonomous vehicles* [4]

layer, where the future trajectory of the ego-vehicle is computed and the driving commands are sent to the physical layer (e.g. Drive-by-Wire [2]). Here are some of the most important challenges:

1. Heterogeneity of traffic participants. Traffic partipants (specially those which are dynamic) can be roughly classified as cyclists, pedestrians or other vehicles. The prediction model should be capable of differentiating the motion patterns of heterogeneous traffic participants, in such a way fine-grained classification (detection module) is quite beneficial to include additional metadata along with the past observations.

2. Complexity of road structure. Road structures are highly diverse and complex, specially in highways and urban areas, which noticeably affect the motion behaviours of traffic participants.

3. Variable number of interactive agents. The prediction model must deal with a number of associated traffic participants within a certain area that can vary from time to time, such as intersections or roundabouts. Then, while driving, a comprehensive

representation of the scene must be able to accommodate an arbitrary number of involved traffic participants.

4. Multimodality of driving behaviours. In real-world, despite we know the behaviour our vehicle will carry out, the motion patterns of other traffic participants can be considered inherently multimodal since there is usually more than one reasonable option for a driver to choose, specially in intersections, when the number of lanes increases or even in the same lane with different velocity profiles (constant velocity, sudden break, sudden acceleration). In that sense, a robust and reliable MP model is expected to be human-like and capture different plausible motion modalities where an agent can travel in the prediction horizon.

5. Complex interpendencies among traffic participants and road infrastructure. Agent-Agent, Agent-Road and Road-Road interpendencies are of great importance for MP and interaction modeling, even more taking into account the complexity of road structures and heterogeneity of traffic participants aforementioned. As expected, an agent future trajectory will be affected not only by its own past trajectory and driving objectives (given by the behaviour planner) but also by other surrounding agents past trajectories, traffic rules and physical constraints.

## 1.5. Objectives and Structure of this Thesis

The main scope of this thesis is to study the SOTA and development of novel and efficient interaction-aware Deep Learning based MP models, focusing on long-term (from 3 to 6 s) prediction horizon and AD, where traffic participants can range from trucks to pedestrians, instead of models focused on pedestrian trajectory prediction. The main inputs that will be used throughout this work are the physical (map) information and historical states (that may include agent position, velocity, orientation, object type and category) of traffic participants in Bird's Eye View (BEV), assuming these objects have been previously tracked by our ego-vehicle (also referred as the autonomous car). Though the evaluation of these methods will be done using a single target agent, as proposed by some of the most important prediction datasets, like Argoverse 1 [5] and Argoverse 2 [6], some of the proposed methods will be trained considering multi-agent. In this thesis, the solutions to the aforementioned challenges will be discussed and investigated progressively. In order to achieve the main scope, the following objectives will be met:

1. Research of SOTA MP, focused on Deep Learning (DL) and the AD paradigm.

2. Propose of several MP architectures, studying the progressive incorporation of DL mechanisms and different sources of information and metadata, achieving SOTA accuracy while reducing in millions of parameters previous models as well as inference time.

3. Validate the proposed models in downstream applications, such as decision-making or behaviour planning, taking into account former stages of the perception layer (detection and tracking) instead of static files (benchmarks) in hyper-realistic simulation, as a preliminary stage before implementing it in a real-world vehicle.

The organization of this document has been done as follows:

- Chapter 2 reviews the contextual factors, a MP methods classification according to the context encoding or representation approaches and SOTA databases and simulators to validate the algorithms.
- Chapter 3 presents a technical background, mostly focused on physics-based methods and DL mechanisms to deal with temporal sequences and interactions, to deeply understand the proposed methods.
- Chapter 4 addresses our integration between single-yet-powerful Multi-Object Tracking (MOT) and HD map information as a preliminary stage before computing unimodal predictions.
- Chapter 5 illustrates our Generative Adversarial Network (GAN)-based proposal, the first DL-based vehicle MP method of this thesis, considering both physical context, computing acceptable target points from the driveable area around the target agent, and social context, computing the past trajectory as a temporal sequence via recurrent networks and social interactions with attention mechanism.
- Chapter 6 presents our efficient baselines, where high-level and well-structured physical context is structured in the form of centerlines, Graph Neural Network (GNN)-based approaches are studied to model more complex agent-agent interactions and transformer encoders are employed at the end of the chapter for powerful-yet-efficient context encoding.
- Chapter 7 illustrates the final model of the thesis which takes into account agent-agent, agent-map, map-agent and map-map interactions, using a novel scene representation with heuristic proposals, graph-based encoding, DL-based goal areas proposals and motion refinement.
- Chapter 8 addresses the integration of the final model of the thesis with upstream and downstream modules to contribute the entire pipeline and closed-loop for AD.
- Chapter 9 summarizes the thesis and provides some promising directions for future work in the areas of MP and validation.

# Chapter 2

# Related Works

*Llegaré a ser el mejor, El mejor que habrá jamás*
*Mi causa es ser su entrenador, Tras poderlos capturar.*
*Viajaré a cualquier lugar, Llegaré a cualquier rincón*
*Y al fin podré desentrañar, El poder de su interior.*
*¡Pokémon! Hazte con todos (solos tú y yo),*
*Es mi destino, mi misión*
*¡Pokémon! Tú eres mi amigo fiel,*
*Nos debemos defender.*

Opening 1 de Pokémon: "Gotta catch 'em all!"
Autor original: Jason Paige

## 2.1. Introduction

One of the crucial tasks that ADSs must face during navigation, specially in arbitrarily complex urban scenarios, is to predict the behaviour of dynamic obstacles [5], [7]. In a similar way to humans that pay more attention to nearby obstacles and upcoming turns than considering the obstacles far away, the perception layer of an ADS must focus more on the salient regions of the scene, particularly on the more relevant dynamic agents to predict their future behaviour before conducting a maneuver, such as lane changing or accelerating. In that sense, before proceeding with the study of the different methods of the SOTA of MP in the field of AD, one important thing to note is that this thesis is focused on non-conditional motion prediction, also referred as Passive Motion Prediction (PMP), where the prediction of surrounding agents is not influenced by the future decisions of the ego-vehicle or even other agents, referred as Conditional Motion Prediction (CMP) in the literature. Most existing works [8]–[13] focus on a passive prediction scheme, where the future states of a particular agent are predicted given its past information, other surrounding agents information and interactions as well as the physical context. Then, downstream planning modules, specially the behaviour planning module (also referred as decision-making layer, as stated in Section 1.3), the ego-vehicle (our vehicle) future actions are computed according to the predicted trajectories in a passive manner, that is,

without modifying the output of the prediction model, and the global route previously calculated.

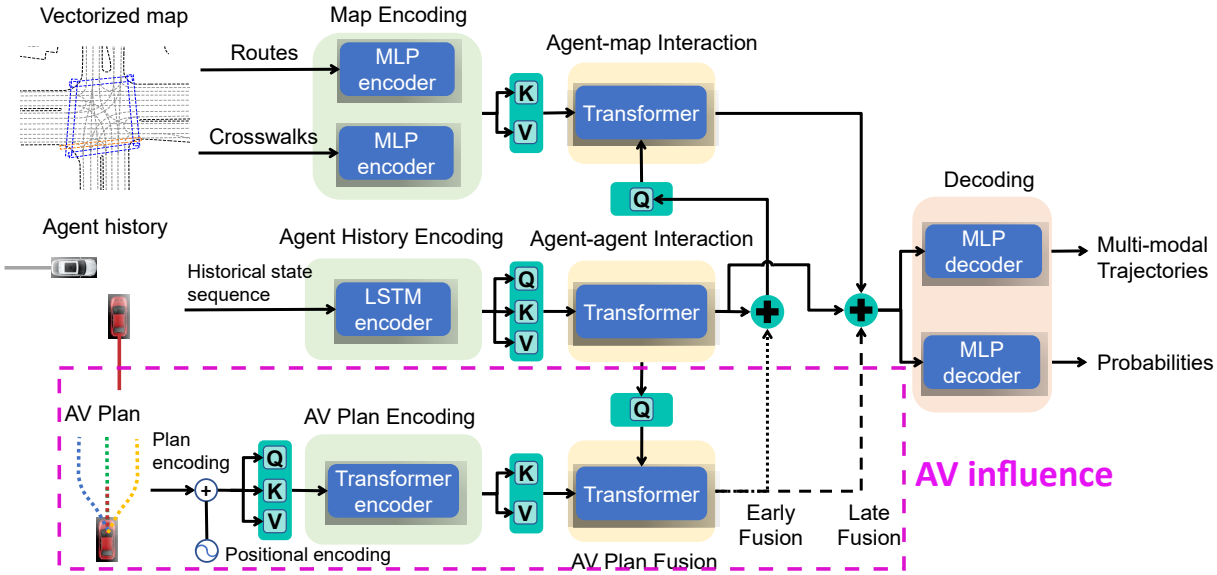


Figure 2.1: Example of a Conditional Motion Prediction (CMP) network.
We highlight the influence of the AD in the prediction of surrounding agents.
Source: *Conditional Predictive Behavior Planning with Inverse Reinforcement Learning for Human-like Autonomous Driving* [14]

Nevertheless, to ensure safety under various predicted trajectories of the surrounding agents, our ADS must overly conservative with inefficient maneuvers, specifically in arbitrarily complex traffic scenarios, because PMP models ignore the fact that the future states of an agent can influence the future actions of other agents, what is the most realistic situation. To this end, researchers recently started to explore a more coherent interactive prediction and planning framework which relies on predicting the surrounding agents future trajectories conditioned on the ego-vehicle future actions [15] [16] [17], as a preliminary state to implement a fully-interaction graph where the future states of all agents (either autonomous prototypes or human-driven) influence in the decision of all agents. Under such frameworks, the ADS can reason over potential actions while considering its influence on surrounding agents, as observed in Figure 2.1, inducing less conservative and more efficient maneuvers in highly interactive scenarios. [14] propose a learning-based behaviour planning framework that learns to predict conditional multi-agent future trajectories, evaluating decisions from real-world human data. Moreover, they propose a two-stage learning process where the prediction model is trained first conditioned on the ADS future actions, and then used as an environment model in the learning of the cost function with maximum entropy Inverse Reinforcement Learning (IRL). [18] argue that CMP-based models essentially learns the posterior distribution of future trajectories conditioned on the future states of the ego-vehicle, where this future trajectory is treated as an observation, whilst safe and realistic prediction models should build the MP to approximate the future trajectory distribution under the intervention of enforcing the ADS future states, referring this new task as Interventional Behaviour Prediction (IBP).

As aforementioned, the algorithms studied and developed throughout this thesis do not focus on the joint study of the prediction and behaviour planning modules, but on building efficient and powerful PMP algorithms without considering the future states of the autonomous agents as an additional condition.

Once the differences between CMP and PMP have been illustrated, we proceed with the problem formulation, main contextual factors and classification of prediction methods.

## 2.2. Problem Formulation of Motion Prediction

Given a sequence of past trajectories $a_P = [a_{-obs'_{len}+1}, a_{-obs'_{len}+2}, ..., a_0]$ for an agent, we aim to predict its future steps $a_F = [a_1, a_2, ..., a_{pred_{len}}]$ up to a fixed time step $pred_{len}$. Running in a specific traffic scenario, each agent will interact with static HD maps $m$ and the other dynamic actors, meeting the corresponding traffic and social rules. Therefore, the probabilistic distribution that we want to capture is $p(a_F|m, a_P, a_P^O)$, where $a_P^O$ denotes the other agents observed states. The output of most existing methods is a set of trajectories $A_F = \{a_F^k\}_{k\in[0,K-1]} = \{(a_1^k, a_2^k, ..., a_{pred_{len}}^k)\}_{k\in[0,K-1]}$ for each agent, where $K$ represents the number of modes or plausible future directions, due to the inherent uncertainty associated to the prediction problem. This set of trajectories for each agent will be used by downstream decision modules. On top of that, TNT (Target-driven trajectory prediction) [19] is one of the first methods that introduces specific preliminary future positions in the problem formulation, also referred as goals, being TNT [19]-like methods distribution approximated as:

$$\sum_{\tau\in T(m,a_P,a_P^O)} p(\tau|m, a_P, a_P^O)p(a_F|\tau, m, a_P, a_P^O) \tag{2.1}$$

where $T(m, a_P, a_P^O)$ is the space of candidate goals depending on the driving context.

However, the map space $m$ is large, and the goal space $T(m, a_P, a_P^O)$ requires careful design. In that sense, some methods expect to accurately predict the actor motion by extracting good features. For example, LaneGCN [13] tries to approximate $p(a_F|m, a_P, a_P^O)$ by modeling $p(a_F|M_{a_0}, a_P, a_P^O)$, where $M_{a_0}$ is a "local" map features that is related to the actor's state $a_0$ at final observed step $t = 0$. To extract $M_{a_0}$, they use $a_0$ as an anchor to retrieve its surrounding map elements and aggregate their features. We found that not only the "local" map information is important, but also the goal area maps information is of great importance for accurate trajectory prediction. So, we reconstructed the probability as:

$$\sum_{\tau} p(\tau|M_{a_0}, a_P, a_P^O)p(M_\tau|m, \tau)p(a_F|M_\tau, M_{a_0}, a_P, a_P^O) \tag{2.2}$$

We directly predict possible goals $\tau$ based on actors' motion histories and driving context. Therefore, GANet is genuinely end-to-end, adaptive, and efficient. Then, we apply the predicted goals as anchors to retrieve the map elements in goal areas explicitly and aggregate their map features as $M_\tau$.

## 2.3. Contextual Factors and Classification of Motion Prediction methods

This section studies the contextual factors (inputs) and classification of MP in the field of AD according to its encoding method of the different inputs and output types. Figure 2.2 [20] summarizes the main inputs and outputs of these methods.

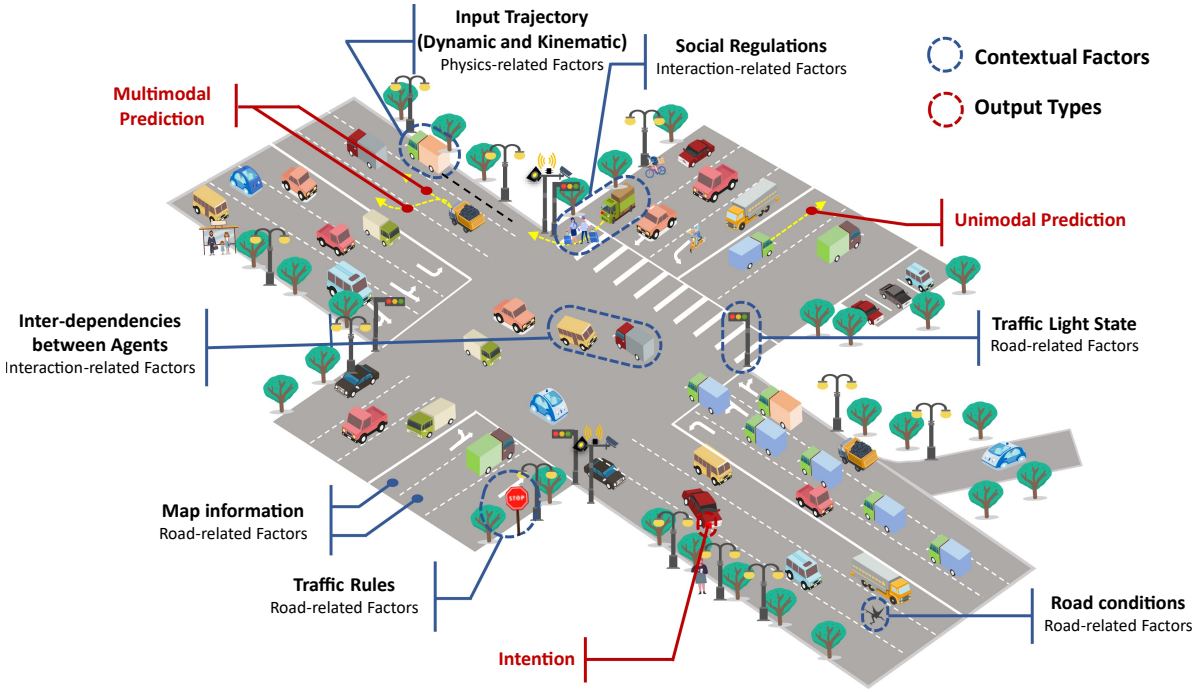


Figure 2.2: Contextual factors and output types in Vehicle Motion Prediction
Source: *A survey on trajectory-prediction methods for autonomous driving* [20]

In order to model the future states of surrounding agents, MP models must pay attention to the current environment, where some contextual factors can be clearly identified:

- Physics-related factors refer to the kinematic and dynamic variables of the agents, specifically to their spatio-temporal variables (such as position, velocity, acceleration, object type or mass) as well as past behaviours.
- Interaction-related factors include the inter-dependencies and social regulations between agents maneuvers. It is important to consider that traffic agents can be either non-relevant pedestrians on the sidewalk as well as an extremely relevant truck in front of the ego-vehicle.

- Road-related factors include the corresponding traffic rules (lane type, traffic signals, stops, etc.) as well as the modeling of the map (usually HD-map), including its topological, semantic and geometrical information.

On the other hand, regarding the output types, MP methods need to provide the future trajectories of traffic participants. Nevertheless, these methods can provide these future trajectories in different ways, even though these outputs can be unified as a single output, depending on the application:

- Unimodal prediction. In the unimodal case, the prediction method only returns a single future trajectory, without taking into account other possible behaviours.
- Multimodal prediction. Models that generate a multimodal prediction compute multiple $K$ future trajectories (also referred as modes in the literature) with the probability of each future trajectory. The higher the mode probability (also referred as score), the more probable this particular behaviour (turn left with a certain velocity and acceleration) should be. This output type is specially useful for fast-changing and highly interactive situations where multiple options are available. One important thing to note is that multimodal methods must be designed in order to not only reason in terms of different maneuvers (keep straight, turn right, lane change, etc.) but also different velocity profiles (constant velocity, acceleration, sudden break, etc.) regarding the same maneuver.
- Maneuver, also referred as intention, can be part of the final output or just be an intermediate step in the method. MP methods usually produce maneuver intention to assist in the subsequent prediction.

As we will study throughout this section, most prediction methods focus on the multimodal output with an associated probability for each mode, since this is the most realistic way to imitate the human brain during navigation. First of all, there are plenty of problems during navigation, since there is a high uncertainty of traffic behavior and a large number of different situations. That means that one cannot use a discrete number of situations and a discrete number of car movements. Second, the main tasks of ADS, like ensuring safe and efficient operations and anticipating a multitude of possible behaviors of traffic actors in its surroundings, provide a large need in knowing the position of all vehicles beforehand. Multimodal means that we have multiple predictions for each timeframe. Figure 2.3 illustrates an interesting traffic scenario in the Argoverse 1 [5] Motion Forecasting dataset, processed by one our algorithms. The **target agent** is getting close to an intersection, where several future maneuvers are plausible. In both cases (unimodal and multimodal, which are the most common ones), the model must reason the future trajectory of the target agent based on its past observations, interactions with other agents and physical context. On the left (2.3a) illustrates the unimodal case, where a single trajectory is predicted. On the right (2.3b), multiple trajectories (or modes) with associated

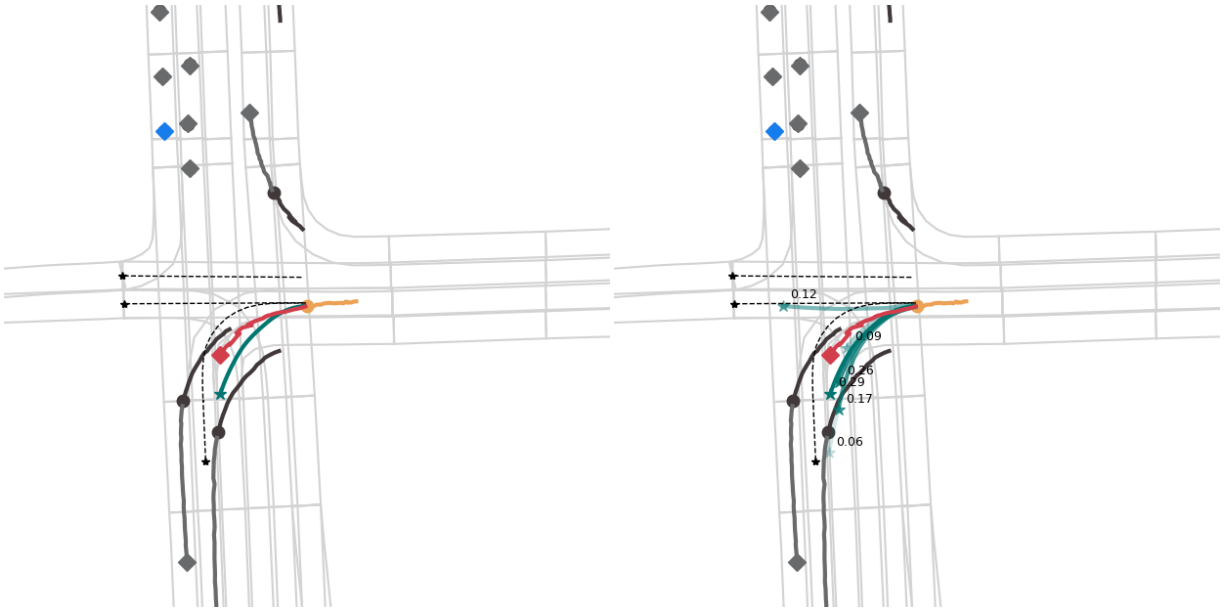


(a) Unimodal prediction (b) Multimodal prediction

Figure 2.3: Modeling multimodality of future 3-second agent trajectories with one of our algorithms; We represent: our vehicle (**ego**), the **target agent**, and **other agents**. We can also see the **ground-truth** trajectory of the target agent, our **multimodal predictions** (with the corresponding confidences) and **plausible centerlines**. Circles represent last observations and diamonds last future positions.

probabilities are predicted, with most modes turning left and one mode keeping straight since in similar situations the agent could also perform this behaviour with a similar context. The main point of having this multimodality is to remove too generalized solutions. A lot of different algorithms study this problem, where quite similar inputs would produce similar predictions, while in reality this does not happens.

After defining the contextual factors and output types, a classification of the prediction methods according to different modeling approaches is illustrates. Over the last two decades, MP can be divided into four parts in chronological order: Physics-based, classic Machine Learning-based, Reinforcement Learning-based and Deep Learning-based, as shown in Figure 2.4. The remaining content of this section, based on the study performed by [20], illustrates the main algorithms used in each part, especially focusing on DL since in this work we focus on predictive techniques for scene understanding based on deep models.

### 2.3.1. Physics-based Motion Prediction

Physics-based methods are the first and simplest methods used by researchers. Although the accuracy of these methods is relatively low, more and more models use the idea of physics-based models to improve the accuracy. Physics-based methods have more accurate results when the movement of vehicles can be accurately described by kinematics or dynamics models, but the physical model of the traffic participants is constantly changing, such that most of these methods are only suitable for short-term prediction (no

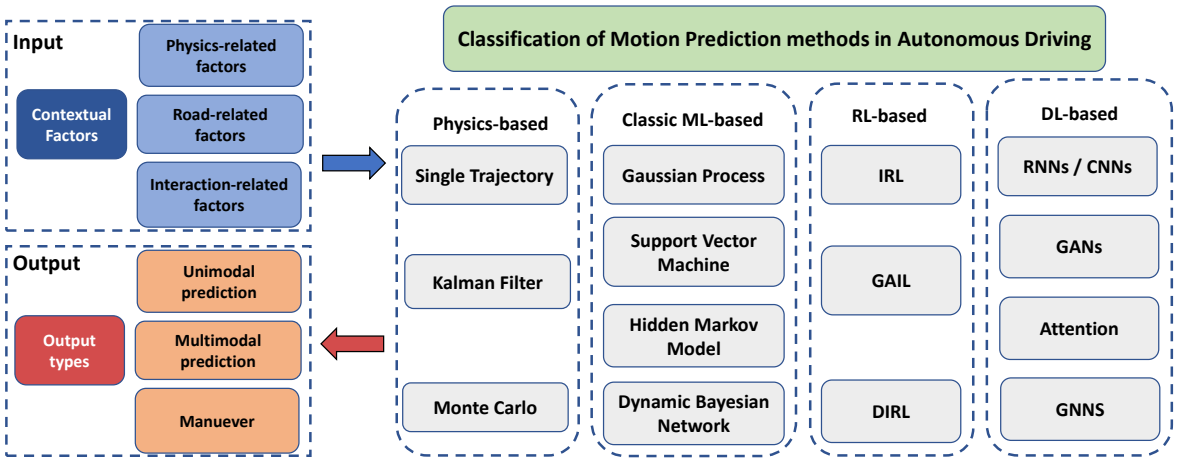


Figure 2.4: Contextual factors and output types in Vehicle Motion Prediction

more than 1-s). Dynamics models can be quite complex, including many inherent parameters and introducing an extra computation burden, in such a way that researchers prefer simple dynamic methods for motion prediction. In terms of vehicle MP, the bicycle model is usually employed to model the vehicle physics, driven by the front wheels [21], [22]. In the literature three main types of physics-based models are distinguished, where the main different is the way in which the uncertainty is handled: Single Trajectory, Kalman Filter-based and Monte Carlo-based.

#### 2.3.1.1. Single-Trajectory

One of the most straightforward methods to predict an agent trajectory is to directly apply the agent current state to the physic model. In order to increase the accuracy and stability of the estimation, the vehicles are mostly assumed to comply with motion models that describe their dynamic behavior. In the past, numerous motion models (with different degrees of complexity) have been proposed for this task [22]–[24]. A first systematization can be achieved by defining different levels of complexity. At the lower end of such a scale, linear motion models are situated. These models assume a Constant Velocity (CV) or a Constant Acceleration (CA). Their major advantage is the linearity of the state transition equation which allows an optimal propagation of the state probability distribution. On the other hand, these models assume straight motions and are thus not able to take rotations (especially the yaw rate) into account.

A second level of complexity can be defined by taking rotations around the $z$-axis into account. The resulting models are sometimes referred to as curvilinear models. They can be further divided by the state variables which are assumed to be constant. The most simple model of this level is the Constant Turn Rate and Velocity (CTRV) model. By

defining the derivative of the velocity as the constant variable, the Constant Turn Rate and Acceleration (CTRA) model can be derived. Both CTRV and CTRA assume that there is no correlation between the velocity $v$ and the yaw rate $\omega$. As a consequence, disturbed yaw rate measurements can change the yaw angle of the vehicle even if it is not moving.

In order to avoid this problem, the correlation between $v$ and $\omega$ can be modeled by using the steering angle $\Phi$ (angle between the axis of motion and the direction of the front wheels) as constant variable and derive the yaw rate from $v$ and $\Phi$. The resulting model is called Constant Steering Angle and Velocity (CSAV). Again, the velocity can be assumed to change linearly, which leads to the Constant Curvature and Acceleration (CCA) model.

From a geometrical point of view, nearly all curvilinear models are assuming that the vehicle is moving on a circular trajectory (either with a constant velocity or acceleration). The only exception is the CTRA model which models a linear variation of the curvature and thus assumes that the vehicle is following a clothoid.

While in theory curvilinear models describe the motion of road vehicles very accurately, errors may result from highly dynamic effects such as drifting or skidding. While models which are able to cope with such effects do exist, they will not be considered here for two reasons: Firstly, most ITS applications are designed for scenarios with non-critical dynamics. Secondly, the required information for estimating the additional parameters (e.g. slip from every tire, lateral acceleration) are not observable by exteroceptive sensors. Furthermore, these methods are not able to consider the road-related factors and the uncertainty of the current state is unreliable for long-term prediction in such a way these single trajectory models should only be used for estimating unimodal trajectories of the surrounding agents in the short-term. We further study the state transition equations of physics-based models in Chapter 3 since they will be used in the algorithms proposed in this thesis as preliminary proposals for the DL models.

#### 2.3.1.2. Kalman Filter

Kalman Filter (KF)-based methods aim to solve one of drawbacks of physics-based models: In real-world, the states of agents are not perfectly known since they present an associated noise. KF-based methods model the uncertainty oir noise of the current agent state and its physic model by means of a Normal (Gaussian) distribution. Compared to the single trajectory methods, the main advantage is that KF methods consider the uncertainty of the predicted trajectory, specially when using its Extended (EKF) or Unscented (UKF) where non-linearities can be modeled. As proposed by the original algorithm [25], the prediction and update steps are combined into a loop where the mean value and covariance matrix of the agent state is computed for each future step, calculated as an average trajectory with related uncertainty.

Nevertheless, these KF-based methods are unimodal Gaussian distributions which are not enough to represent agents interactions. In that sense, [26] propose an Interactive Multiple Model (IMM) to compute a multimodal prediction. Moreover, [27] model a set of Kalman Filters used to describe physical models of the vehicles and switch between them, defined as Switched Kalman Filter (SKF). [28] propose IMM-KF, a novel Interacting Multiple Model Kalman Filter which takes interaction-related factors (social regulation, inter-dependencies) into consideration, as shown in Figure 2.2.

#### 2.3.1.3. Monte Carlo

In the same way KF methods aimed to solve the associated noise to the physics state of the agent, Monte Carlo method aims to simulate the state distribution approximately since an analytical expression for the predicted state distribution is usually unknown without any assumptions of the linearity or the model's Gaussian nature. This method randomly samples the input variables and applies the physics model to compute potential future trajectories. In order to ensure the plausibility of the future behaviour in the context of AD, the generated future states are usually filtered with a lateral acceleration lower than the actual allowable lateral acceleration [29], though other vehicle physical limitation can also be used such that the input of the model will be more realistic. [30] present a model that identifies a preliminary maneuver and then applies the Monte Carlo method to compute future trajectories by the identified maneuver. Furthermore, [31] first use the Monte Carlo algorithm to predict future trajectories and then utilize MPC (Model Predictive Control) algorithm to refine these preliminary future trajectories.

### 2.3.2. Classic Machine Learning based Motion Prediction

Classic ML MP methods make use of data-driven models to predict trajectories instead of only considering the physical model. These methods determine the probability distribution by mining data features. These methods provide new ideas for MP, which promote the development of learning-based approaches. With more factors to be considered, the accuracy of these methods keeps increasing, being most of them maneuver-based (which is provided or identified in advance) in order to subsequently estimate the future states of the agents by first judging the corresponding maneuver. Regarding the field of vehicle MP, we can find in the literature four main types of classic ML methods: Gaussian Process, Support Vector Machine (SVM), Hidden Markov Model (HMM) and Dynamic Bayesian (Network). Figure **??** illustrates some these methods.

#### 2.3.2.1. Gaussian Process

Gaussian Process (GP) applied in ML [34] is identified as an stochastic process (collection of random variables indexed time or space) such that every finite collection of those

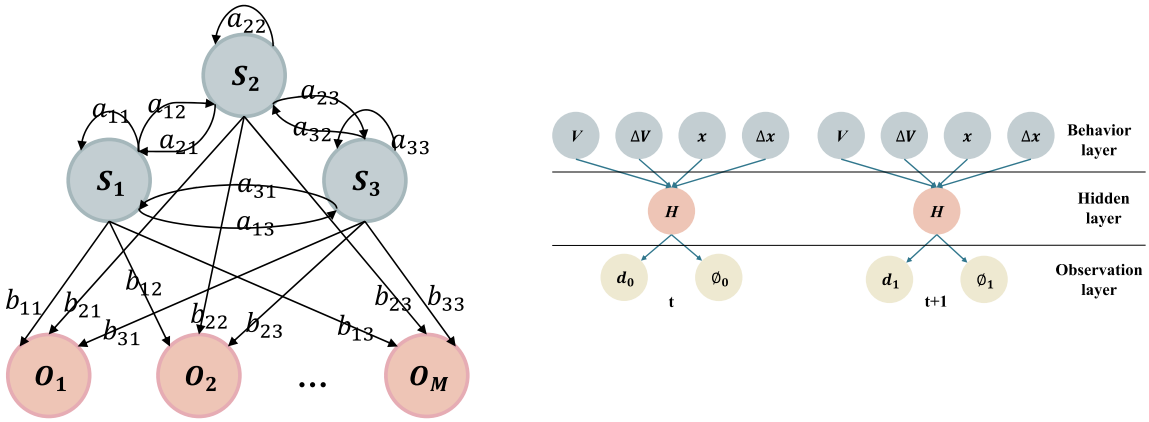


(a) Hidden Markov Model

(b) Dynamic Bayesian Network

Figure 2.5: Some typical Classic Machine Learning algorithms in Motion Prediction, like Hidden Markov Model and Dynamic Bayesian Network.
Source (a): *Improved driving behaviors prediction based on fuzzy logic-hidden markov model (fl-hmm)* [32]
Source (b): *Probabilistic intention prediction and trajectory generation based on dynamic bayesian networks* [33]

random variables has a multivariate normal distribution, i.e. every finite linear combination of them is normally distributed. This stochastic process may be used to solve the prototype trajectory method [35], [36], which a maneuver-based method that divides agents trajectories into a collection of several types of prototype trajectories. First, past trajectories are regarded as the samples of the GP, sampled along the time axis, being these samples represented by $N$ discrete points to map the $N$-dimensional space, which is equivalent to satisfy the $N$-dimensional Gaussian distribution. Therefore, the main task of the GP model regarding the prototype trajectory method is to determine the parameters of GP through the samples. Once these parameters have been obtained by means of the stochastic, the prototype trajectory method measures the similarity between the input historical trajectory and the computed prototype set to predict the most plausible future motion. GP can also be used to model interaction-related factors, as shown in Figure 2.2. [37] solve the frozen robot problem, where the environment surpasses a certain level of complexity and the robot planner decides to freeze in place to avoid collisions, by means of GP for joint collision avoidance. Furthermore, [38] apply GP and Dirichlet Process (DP) to define motion processes and apply a non-parametric Bayesian network to extract potential motion patterns.

#### 2.3.2.2. Support Vector Machine (SVM)

Support Vector Machine (SVM) increases the level of complexity over previous methods, being able to learn and recognize an agent maneuver in a complex environment. The main idea of SVM is to find the support vector that meets the classification requirements and determine the optimal hyperplane which can maximize the interval of the classified data. In particular, when applied to the MP problem in AD, driving maneuvers are usu-

ally classified into several categories: keep straight, turn left, turn right, break, etc. In that sense, it uses the kernel function to convert the input data to high-dimensional and perform linear classification in the space to identify the current driving maneuvers so as to predict the future steps. [39] apply SVM to identify a lane changing maneuver, using the position, velocity, acceleration and steering wheel angle of the corresponding vehicle as input features for identification. [40] propose a layered architecture method combining SVM and Bayesian filtering to identify lane-changing maneuvers so as to obtain more accurate identification results. Furthermore, [41] make use of SVM to identify the maneuvers of traffic participants. Nevertheless, according to the SVM definition which output the characteristics of classification probability, the user must present the categories or possible maneuvers in advance which will will also impact the final prediction results.

#### 2.3.2.3. Hidden Markov Model (HMM)

As aforementioned, SVM can be effective in classification problems, but in the field of MP in AD not as effective as a Hidden Markov Model (HMM). This is one of the most popular maneuver-based classic ML MP methods, which uses Markov Chain. The Markov Chain refers to a stochastic process describing a sequence of possible events in which the probability of each event depends only on the state attained in the previous event, i.e. , the state at time $t+1$ of the system is only related to the previous time $t$, and the state transition probability is not related to time. Figure 2.5a illustrates this model. The mathematical expression is:

$$\begin{aligned} &\mathrm{P}\left(S_{n+1}=s \mid S_1=s_1, S_2=s_2 \cdots, S_n=s_n\right) \\ &\quad=\mathrm{P}\left(S_{n+1}=s \mid S_n=s_n\right). \end{aligned} \tag{2.3}$$

In real life, we can only observe the distinct state that is exposed on the surface, but no intuitive representation of its hidden states exists. Therefore, it is necessary to establish a Markov process with hidden states and get the essential states of events through the observable states set related to the hidden states probability, which is the so-called Hidden Markov Model. HMM is represented by $(S, O, A, B, \pi)$[50], as shown in Figure 2.5a:

- $S=\{S_1, S_2, \cdots S_N\}$ represents the hidden states sequence
- $O=\{O_1, O_2, \cdots O_M\}$ represents the observation sequence
- $A$ represents the transition probability matrix between hidden states
- $B$ is the output matrix, representing the transition probability of hidden states to output states
- $\pi$ is the initial probability matrix, representing the initial probability distribution in hidden states

When HMM is used in the trajectory prediction, the historical states of traffic participants are represented by observation sequence $O$, and HMM solves the most likely future observation sequence. [32] combine HMM with Fuzzy Logic for driver maneuver prediction. In [42], HMM is used for trajectory prediction and risk assessment, and the results of are fed into the decision-making and planning system. Although traditional HMM methods have achieved a great success in predicting driver's maneuvers, they do not consider the impact of interaction-related factors in the prediction process, such that its prediction results are not accurate enough in actual traffic scenes. To solve this issue, [43] propose a vehicle trajectory prediction model based on HMM and Variational Gaussian Mixture Models (GMM) considering interaction-related factors. The vehicle interaction information is obtained by finding the optimal solution of the energy function.

#### 2.3.2.4. Dynamic Bayesian Network (DBN)

Dynamic Bayesian Networks (DBNs) [44] solve the aforementioned issue of HMM when modeling the inter-dependencies among traffic participants, since in order to improve the accuracy of MP, the prediction model should consider at least both vehicle states and the interaction effect between traffic participants. While Bayesian Networks describe static systems, DBNs introduce the concept of time segments to solve timing issues in probabilistic models. Time segment refers to a time template materialized according to DBN, which discretizes continuous time into countable points with preset time granularity.

Generally, the preset time granularity should be consistent with the actual state acquisition frequency, and DBN is trained according to the sensor sampling frequency as the time segment. Besides, the inference and learning methods of DBN need to be converted into Bayesian Networks before they can be directly applied. The architecture of DBN includes a behavior layer, a hidden layer, and an observation layer, as shown in Figure 2.5b. The behavior layer represents the network input information, and the observation layer represents the driver's maneuver. DBN models the effect of interaction between traffic participants when applied to trajectory prediction and perform well in classic machine learning-based methods. Using this architecture, Gindele et al. [59] model the driving maneuvers of multiple vehicles. The input information includes all vehicle states, vehicle interaction relationships, road structures, observation states, etc. [45] apply DBN to judge driving maneuvers and utilize the kinematics model corresponding to each driving maneuver to predict the trajectory. In [46], the vehicle maneuver is predicted by game theory, and then the vehicle motion is judged by DBN which considers the interaction-related factors. In [47], DBN is designed to consider physics-related factors, road-related factors, and interaction-related factors. As maneuver-based methods, DBN models obtain high recognition performance and have been used in several real-world tests [48]. However, DBN still faces the error problem from recognizing maneuvers to generating


Figure 2.6: Description of (a) Reinforcement Learning and (b) Inverse Reinforcement Learning
Source: *A survey on trajectory-prediction methods for autonomous driving* [20]

trajectories. Many methods can only judge two or three maneuvers, such as lane-keeping and lane-changing, and the model's generalization ability is not strong.

### 2.3.3. Reinforcement Learning based Motion Prediction

Reinforcement learning (RL) is one of three basic ML paradigms, alongside supervised learning and unsupervised learning. RL is an area of machine learning concerned with how intelligent agents ought to take actions in an environment in order to maximize the notion of cumulative reward. When RL is used in the field of MP for AD, most methods use the Markov decision process (MDP) to maximize the expected cumulative reward and generate optimal driving policies by learning expert demonstrations, most of which are planning-based methods. A MDP is a tuple $(\boldsymbol{S}, \boldsymbol{A}, \boldsymbol{P}, \boldsymbol{R}, \gamma)$, where $\boldsymbol{S}$ is a finite set of states, $\boldsymbol{A}$ is a finite set of actions, $\boldsymbol{P}$ is a state transition probability matrix, $P^a_{ss'} = \mathbb{P}\left[S_{t+1} = s' \;\; S_t = s, A_t = a\right]$, $\boldsymbol{R}$ is a reward function, $R^{\mathrm{a}}_s = \mathbb{E}\left[R_{t+1} \mid S_t = s, A_t = a\right]$, and $\gamma$ is a discount factor. To find the best decision process over all policies, the optimal state-value function $v_\star(s)$ and the optimal action-value function $q_\star(s, a)$ can be calculated as:

$$\begin{aligned} v_*(s) &= \max_a \left[ R^a_s + \gamma \sum_{s' \in A} P^a_{ss'} v_* \left(s'\right) \right], \\ q_*(s, a) &= R^a_s + \gamma \sum_{s' \in A} P^a_{ss'} \max_{a'} q_* \left(s', a'\right). \end{aligned} \tag{2.4}$$

Using MDP, the RL-based methods can be classified as Inverse Reinforcement Learning (IRL) methods, Generative Adversarial Imitation Learning (GAIL) methods, and Deep IRL (DIRL) methods, which will be discussed below.

#### 2.3.3.1. Inverse Reinforcement Learning (IRL)

Usually, MDP assumes that the reward function is already provided. However, the driver's behavior is always complicated such that manually specifying the weight of the

reward function is inappropriate [49]. IRL learns the reward function according to the expert demonstration (trajectory) to generate the corresponding optimal driving policy as shown in Figure 2.6b, in contrast to the RL approach where we must know the weight of a reward associated to a specific action. These IRL methods may be divided into groups: maximum margin-based and maximum entropy-based methods, where the main difference is the way of learning the weights of the reward function.

Maximum margin-based methods optimize the reward function weights by minimizing the feature expectations between the expert demonstration and the predicted trajectory. For example, [50] use maximum margin planning framework to learn reward functions and learn driving maneuvers for ADSs. However, most margin-based methods are ambiguous in the matching of feature expectations, because some degeneracies can also satisfy the optimal policy of expert demonstration.

On the other hand, Maximum entropy-based methods are more popular because they can use multiple reward functions to explain the ambiguity of experts's behavior [51], most of which are based on linear mapping and can be formulated as:

$$r(\Phi(s)) = \theta^{\top}\Phi(s) \tag{2.5}$$

where $r$ is the approximation of reward function; $\Phi$ is a function to output the features of the state $s$, and the weight $\theta$ will be acquired by training. Several works apply maximum entropy-based IRL (MaxEnt-IRL) to behavior prediction for AVs. In [52], using MaxEnt-IRL acceptability-dependent behavior models are learned from expert's trajectories to generate the stochastic behavior, then the optimum behavior model is chosen by maximizing the social acceptability. [53] leverage IRL with Deep Q-Networks (DQN) to extract the rewards with large state spaces. In [54], interaction-related factors are considered to accomplish probabilistic prediction for ADSs. The distribution for future trajectories is formulated by driving maneuvers. Based on the decision-making mechanism, reward functions are learned using a polynomial trajectory sampler with discrete latent driving intentions in [55].

#### 2.3.3.2. Generative Adversarial Imitation Learning (GAIL)

Instead of learning the reward function from experts' demonstration with IRL, Generative Adversarial Imitation Learning (GAIL) [56] uses the method of GAN to do imitation learning in RL. GAIL directly extracts policies from data where, as proposed by a GAN [57], the core idea of GAIL is that the generator generates a trajectory similar to the expert trajectory as much as possible, and the discriminator tries to judge whether it is an expert trajectory as much as possible. Many articles use GAIL to complete trajectory prediction for AD. [58] extend GAIL to the optimization of RNN to demonstrate human driver behaviors, and policies and actions are evaluated by the discriminator. In [59],

a parameter-sharing extension of GAIL is proposed to model the interaction between multi-agent and can provide agents with domain-specific knowledge. To overcome the shortcomings of GAIL, which only models the next state using the current state, [60] propose a method combining a partially observable Markov decision process (POMDP) within the GAIL framework, and the model is trained using the reward function from the discriminator.

#### 2.3.3.3. Deep Inverse Reinforcement Learning (DIRL)

Since the prediction problem in AD is usually non-linear, i.e. the agent does not traverse in a straight path, it is necessary to use non-linear mapping for generalizable function approximations. In that sense, Deep Inverse Reinforcement Learning (DIRL) is proposed [61] to approximate complex and nonlinear reward functions, which can be expressed as:

$$r(\Phi(s)) = f(\theta, \Phi(s)) \tag{2.6}$$

where $f$ is a nonlinear function. Some DIRL methods take historical trajectories as input. [62] consider the driving style and the road geometry, where the authors first use RL to design MDP, then learn the optimal driving policy from IRL, and use the deep neural network (DNN) to approximate the reward function. In [63], trajectories of traffic participants are encoded by LSTM and the reward network is learned by FCN. Currently, more DIRL-based methods directly use raw perception data. [64] apply FCN for mapping the lidar data to traversability maps. The network is pre-trained to regress to a manual prior cost map and the initialize weights will be fine-tuned by the maximum entropy DIRL network. [65] use RL ConvNet and state visiting frequency (SVF) ConvNet to encode the vehicle's kinematics and obtain the weight of the reward function by back-propagating the loss gradient [66] between expert SVF from expert demonstration and policy SVF from lidar data.

### 2.3.4. Deep Learning based Motion Prediction

The Deep Learning (DL) methods are the last type of MP methods covered in Chapter since its different approaches are, by far, the most used at this moment in the field of MP in AD to predict the future trajectory of traffic participants., being this thesis focused in these particular methods. Most traditional predictions methods [20], which usually only consider physics-related factors (like the velocity and acceleration of the target vehicle that is going to be predicted) and road-related factors (prediction as close as possible to the road centerline), are only suitable for short-time prediction tasks [20] and simple traffic scenarios, such as constant velocity (CV) in a highway or a curve (Constant Turn Rate Velocity, CTRV) where a single path is allowed, i.e. multiple choices computation are not

required. Recently, MP methods based on DL have become increasingly popular since they are able not only to take into account these above-mentioned factors but also consider interaction-related factors (like agent-agent [67], agent-map [68] and map-map [13]) in such a way the algorithm can adapt to more complex traffic scenarios (intersections, sudden breaks and accelerations, etc.). It must be consider that multimodal, specially in the field of vehicle motion prediction, does not refer necessarily to different directions (e.g. turn to the left, turn to the right, continue forward in an intersection), but it may refer to different predictions in the same direction that model a sudden positive or negative acceleration, so as to imitate a realistic human behaviour in complex situations. As expected, neither classical nor machine learning (ML) methods can model these situations [20].

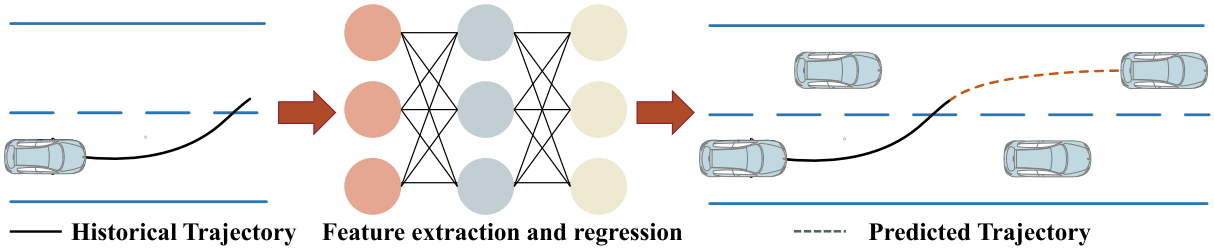


Figure 2.7: Deep Learning methods applied in Motion Prediction
Source: *A survey on trajectory-prediction methods for autonomous driving* [20]

The main DL-based approaches are: Convolutional Neural Networks (CNNs), Recurrent Neural Networks (RNNs), GANs, Attention mechanisms and GNNs. Figure 2.7 illustrates the main idea of using DL to predict the future trajectories of the agents. Since this thesis is focused on developing efficient and accurate DL-based MP models in the field of AD, the theoretical explanation of these different neural networks used in our pipelines will be explained in the Chapter 3 3 along with some physics-based models theory to fully-understand the proposed models. The input is represented by, at least, the physics-factors of the corresponding, though road-factors and interaction-factors are present in most DL algorithms. Then, a neural network extracts the most important features and outputs a future trajectory according to the training process in a supervised way.

In order to classify DL based MP methods, we can identify the different factors (physics, interaction and road) and determine which type of neural network is employed to extract features of the corresponding input. In the literature we mainly distinguish the following inputs and outputs: Motion history (physics-based factors), Social information (interaction-based factors), Map information (road-relared factors), how the model returns the output trajectory and its corresponding distribution. Table 2.1 summarizes several SOTA methods.

Table 2.1: Main state-of-the-art Deep Learning methods for Motion Prediction. Main categories are Encoder (splitted into motion history, social info (agent interactions) and map info (physical information)), Decoder, Output representation and Distribution over future trajectories

| **Method** | **Encoder** | | | **Decoder** | **Output** | **Trajectory Distribution** |
|---|---|---|---|---|---|---|
| | Motion history | Social info | Map info | | | |
| SocialLSTM [69] | LSTM | spatial pooling | – | LSTM | states | samples |
| SocialGan [67] | LSTM | maxpool | – | LSTM | states | samples |
| Jean [70] | LSTM | attention | – | LSTM | states | GMM |
| TNT [19] | polyline | maxpool, attention | polyline | MLP | states | weighted set |
| LaneGCN [13] | 1D-conv | GNN | GNN | MLP | states | weighted set |
| WIMP [17] | LSTM | GNN+attention | polyline | LSTM | states | GMM |
| VectorNet [71] | polyline | maxpool, attention | polyline | MLP | states | unimodal |
| SceneTransformer [72] | attention | attention | polyline | attention | states | weighted set |
| HOME [8] | raster | attention | raster | conv | states | heatmap |
| GOHOME [9] | 1D-conv+GRU | GNN | GNN | MLP | states | heatmap |
| MP3 [73] | raster | conv | raster | conv | cost function | weighted samples |
| CoverNet [74] | raster | conv | raster | lookup | states | GMM w/ dyn. anch. |
| DESIRE [75] | GRU | spatial pooling | raster | GRU | states | samples |
| MFP [15] | GRU | RNNs+attention | raster | GRU | states | samples |
| MANTRA [76] | GRU | – | raster | GRU | states | samples |
| PRANK [77] | raster | conv | raster | lookup | states | weighted set |
| IntentNet [68] | raster | conv | raster | conv | states | unimodal |
| Multimodal [78] | raster | conv | raster | conv | states | weighted set |
| MultiPath [79] | raster | conv | raster | MLP | states | GMM w/ static anchors |
| MultiPath++ [10] | LSTM | RNNs+maxpool | polyline | MLP | control poly | GMM |
| PLOP [80] | LSTM | conv | raster | MLP | state poly | GMM |
| Trajectron++[7] | LSTM | RNNs+attention | raster | GRU | controls | GMM |
| CRAT-PRED[12] | LSTM | GNN+attention | – | MLP | states | weighted set |
| R2P2 [81] | GRU | – | polyline | GRU | motion | samples |
| DKM [82] | raster | conv | raster | conv | controls | weighted set |

- **Motion history**: Most methods encode the sequence of past observed states using 1D-convolution [13] [70], able to model spatial information, or via a recurrent net [69] (LSTM, GRU), which are more useful to handle temporal information. Other methods that use a raster version of the whole scenario represent the agent states rendered as a stack of binary mask images depicting agent oriented bounding boxes [8]. On the other hand, other approaches encode the past history of the agents in a similar way to the road components of the scene given a set of vectors or polylines [19], [71] that can model the high-order interactions among all components, or even employing attention to combine features across road elements and agent interactions [72].

- **Social information**: In complex scenarios, motion history encoding of a particular target agent is not sufficient to represent the latent space of the traffic situation, but the algorithm must deal with a dynamic set of neighbouring agents around the target agent. Common techniques are aggregating neighbour motion history with a permutation-invariant set operator: soft attention [72], a combination of soft attention and RNN [10] / GNN [12] or social pooling [67], [69]. Raster based approaches rely on 2D convolutions [79] [73] over the spatial grid to implicitly capture agent interactions in such a way long-term interactions are dependent on the neural network receptive fields.

- **Map information**: High-fidelity maps [83] have been widely adopted to provide offline information (also known as physical context) to complement the online infor-

mation provided by the sensor suite of the vehicle and its corresponding algorithms. Recent learning-based approaches [68], [84], [85], which present the benefit of having probabilistic interpretations of different behaviour hypotheses, require to build a representation to encode the trajectory and map information. Map information is probably the feature with the clearest dichotomy: raster vs vector treatment. The raster approach encodes the world around the particular target agent as a stack of images (generally from a top-down orthographic view, also known as Bird's Eye View). This world encoding may include from agent state history, agent interactions and usually the road configuration, integrated all this different-sources information as a multi-channel image [8], in such a way the user can use an off-the-shelf Convolutional Neural Network (CNN) based pipeline in order to leverage this powerful information. Nevertheless, this representation has several downsides: constrained field of view, difficulty in modeling long-range interactions and even difficulty in representing continuous physical states due to the inherent world to image (pixel) discretization. On the other hand, the polyline approach may describe curves, such as lanes, boundaries, intersections and crosswalks, as piecewise linear segments, which usually represents a more compact and efficient representation than using CNNs due to the sparse nature of road networks. Some state-of-the-art algorithms not only describe the world around a particular agent as a set-of-polylines [17] [19] in an agent-centric coordinate system, but they also leverage the road network connectivity structure [13] [86] treating road lanes as a set of nodes (waypoints) and edges (connections between waypoints) in a graph neural network so as to include the topological and semantic information of the map.

- **Decoder**: Pioneering works of DL based MP usually adopt the autoencoder architecture, where the decoder is often represented by a recurrent network (GRU, LSTM, etc., specially designed to handle temporal information) to generate future trajectories in an autoregressive way, or by CNNs [8] [9] / MLP [13] [12] using the non-autoregressive strategy. The method may use an autoregressive strategy where the pipeline generates tokens (in this case, positions or relative displacements) in a sequential manner, in such a way the new output is dependent on the previously generated output, whilst MLP [12], CNN [8] or transformer [72] based strategies usually follow a non-autoregressive strategy, where from a latent space the whole future trajectory is predicted.

- **Output**: The most popular model output representation is a sequence of states (absolute positions) or state differences (relative displacements for any dimension considered). The spacetime trajectory may be intrinsically represented as a continous polynomial representation or a sequence of sample points. Other works [8] [9] first predict a heatmap and then decode the corresponding output trajectories after sampling points from the heatmap, whilst [73] [87] learn a cost function evaluator of

trajectories that are enumerated heuristically instead of being generated by a learned model.

- **Trajectory Distribution**: The choice of output trajectory distributions has several approaches on downstream applications. Regardless the agent to be predicted is described as a (non-)holonomic [88] platform, an intrinsic property of the motion prediction problem is that the agent must follow one of a diverse set of possible future trajectories. A popular choice to represent a multimodal prediction are Gaussian Mixture Models (GMMs) due to their compact parameterized form, where mode collapse (associated frequently to GMMs) is addressed through the use of trajectory anchors [79] or training tricks [78]. Other approaches model a discrete distribution via a collection of trajectory samples extracted from a latent space and decoded by the model [81] or over a set of trajectories (fixed or a priori learned) [13].

## 2.4. Motion Prediction Datasets

As stated in previous sections, MP (also referred in the literature and benchmarks as Motion Forecasting) addresses the problem of predicting future states (or occupancy maps) for dynamic actors within a local environment. Some examples of relevant actors for autonomous driving include: vehicles (both parked and moving), pedestrians, cyclists, scooters, and pets. Predicted futures generated by a forecasting system are consumed as the primary inputs in motion planning, which conditions trajectory selection on such forecasts. Generating these forecasts presents a complex, multi-modal problem involving many diverse, partially-observed, and socially interacting agents. Table 2.2 [6] shows an interesting comparison between different SOTA datasets in the field of vehicle MP.

Table 2.2: Comparison between different SOTA vehicle MP datasets. Hyphens "-" indicate that attributes are either not applicable, or not available. "Mined for interestingness" is defined as true if interesting scenarios/actors are mined *after data collection*, instead of taking all/random samples. † Public leaderboard counts as retrieved on Aug. 27, 2021.

Source: *Argoverse 2: Next generation datasets for self-driving perception and forecasting* [6]

| | Argoverse 1 [5] | Interaction [89] | Lyft [90] | Waymo [91] | NuScenes [92] | Yandex [93] | Argoverse 2 [6] |
|---|---|---|---|---|---|---|---|
| # Scenarios | 324k | - | 170k | 104k | 41k | 600k | 250k |
| # Unique Tracks | 11.7M | 40k | 53.4M | 7.6M | - | 17.4M | 13.9M |
| Average Track Length | 2.48 s | 19.8 s | 1.8 s | 7.04 s | - | - | 5.16 s |
| Total Time | 320 h | 16.5 h | 1118 h | 574 h | 5.5 h | 1667 h | 763 h |
| Scenario Duration | 5 s | - | 25 s | 9.1 s | 8 s | 10 s | 11 s |
| Test Forecast Horizon | 3 s | 3 s | 5 s | 8 s | 6 s | 5 s | 6 s |
| Sampling Rate | 10 Hz | 10 Hz | 10 Hz | 10 Hz | 2 Hz | 5 Hz | 10 Hz |
| # Cities | 2 | 6 | 1 | 6 | 2 | 6 | 6 |
| Unique Roadways | 290 km | 2 km | 10 km | 1750 km | - | - | 2220 km |
| Avg. # tracks per scenario | 50 | - | 79 | - | 75 | 29 | 73 |
| # Evaluated object categories | 1 | 1 | 3 | 3 | 1 | 2 | 5 |
| Multi-agent evaluation | × | ✓ | ✓ | ✓ | × | ✓ | ✓ |
| Mined for Interestingness | ✓ | × | - | ✓ | × | × | ✓ |
| Vector Map | ✓ | × | × | ✓ | ✓ | × | ✓ |
| Download Size | 4.8 GB | - | 22 GB | 1.4 TB | 48 GB | 120 GB | 58 GB |
| # Public Leaderboard Entries† | 194 | - | 935 | 23 | 18 | 3 | - |

As observed, multiple vehicle MP exist in the literature. Yandex is the dataset with the highest number of scenarios, total recorded time and amount of data, but there are very few entries and all of them dated from 2021, so, at the moment of writing this thesis, the research community is not focused in this dataset anymore. On the other hand, Lyft has the highest number of entries, but the number of unique roadways is limited to 10 km and it does not provide a vector map. Interaction is limited to some interesting scenarios, with very few unique tracks and roadways compared to the other datasets. Overall, these datasets have common goals of enabling motion prediction and improving the safety and efficiency of autonomous driving systems. However, their coverage, data size, features, and limitations vary, which makes it important to consider the specific requirements and use cases when choosing a dataset for research or development purposes.

Regarding this, we conclude the best vehicle MP datasets in the literature are NuScenes, Waymo, Argoverse 1 and Argoverse 2. In that sense, since the DL part of the thesis was started (around 2021) approximately when Argoverse 1 had a lot of interest from the research community, and, on top of that, they recently released (Argoverse 2) the largest MP dataset to date (including mpre evaluated object categories, not only vehicles, multi-agent evaluation and unique roadways to prevent overfitting), we finally decided to build our algorithms upon the Argoverse 1 and Argoverse 2 datasets.

### 2.4.1. Argoverse 1 Motion Forecasting results

The Argoverse 1 Motion Forecasting dataset is a widely used dataset in the field of autonomous driving for studying and developing algorithms related to motion prediction. It includes HD maps and a detailed map API to get the corresponding rasterized or vector information of the map. This dataset is a curated collection of 324,557 scenarios (particularly, 205942 training samples, 39472 validation samples and 78143 test samples), each 5 seconds long, for training and validation. Data was sampled at 10 Hz, where each sample contains the BEV position (x,y) of all agents in the scene in the past 2s (20 observed points), the local map, and the labels are the 3s (30 predicted points) future positions of one target agent in the scene. For training and validation, full 5-second trajectories are provided, while for testing, only the first 2 seconds trajectories are given.

Table 2.3 shows our estimated distribution of the target agent's maneuver in the dataset, regarding the most common use cases in urban scenarios, such as going straight, turn and lane change. We can observe how most sequences are focused on keeping the same lane, considering that this category not only merges those scenarios where the agent is conducting a trivial constant velocity trajectory.

Table 2.3: Estimated distribution of the Target Agent Maneuver in the Argoverse 1 Motion Prediction Dataset.

| Maneuver | Training | Validation |
|---|---|---|
| Going straight | 191024 (92.75%) | 34958 (90.70%) |
| Left turn | 7860 (3.82%) | 1880 (4.88%) |
| Right turn | 4757 (2.31%) | 1238 (3.21%) |
| Left lane change | 1084 (0.53%) | 284 (0.74%) |
| Right lane change | 1217 (0.59%) | 184 (0.48%) |

### 2.4.2. Argoverse 2 Motion Forecasting results

The last MP algorithm of the thesis has been developed using the Argoverse 2 Motion Forecasting dataset instead of Argoverse 1 since it provides way more utilities and traffic scenarios to design our method. While Argoverse 1 provides a substantial amount of labeled data, it may still have limitations in capturing the full diversity of real-world driving scenarios. Building upon the success of Argoverse 1, the Argoverse 2 Motion Forecasting dataset provides an updated set of prediction scenarios collected from a self-driving fleet. The design decisions enumerated below capture the collective lessons learned from both our internal research/development, as well as feedback from more than 2,700 submissions by nearly 260 unique teams[1] across 3 competitions [94]:

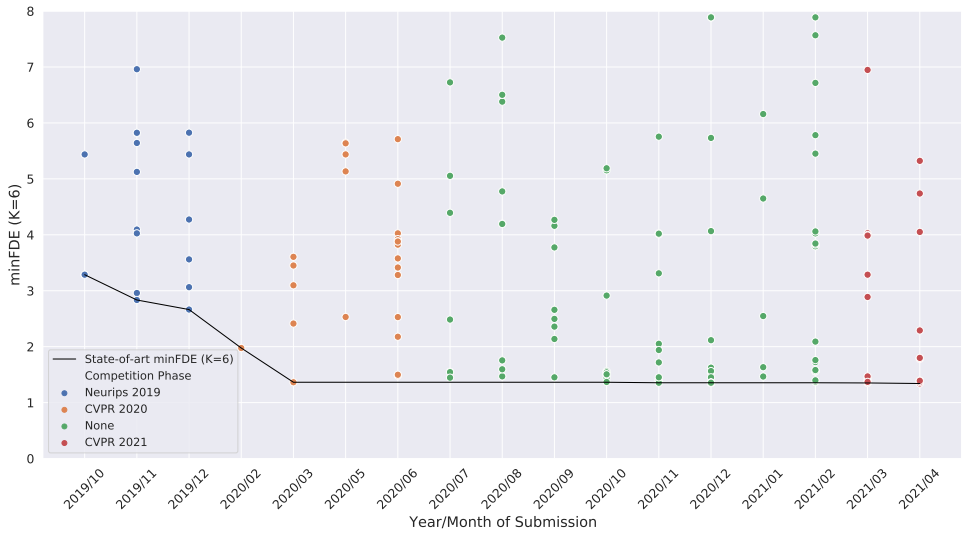


Figure 2.8: MinFDE metric values for submissions on Argoverse 1.1 over time. Individual points indicate submissions to the public leader board. Colors indicate specific competition phases. The solid black line indicates SOTA performance. The research community made massive gains which have plateaued since early 2020. However, we note that the number and diversity of methods performing at or near the SOTA continues to grow. Additionally, later competitions sorted the leaderboard by "Miss Rate" and probability weighted FDE, and those metrics showed progress. Still, minFDE did not improve significantly.

- **Motion forecasting is a safety critical system in a long-tailed domain.** Consequently, our dataset is biased towards diverse and interesting scenarios con-

[1]This count includes private submissions not posted to the public leaderboards.

taining different types of focal agents. Our goal is to encourage the development of methods that ensure safety during tail events, rather than to optimize the expected performance on "easy miles".

- **There is a "Goldilocks zone" of task difficulty.** Performance on the Argoverse 1 test set has begun to plateau, as shown in Figure **??** of the appendix. Argoverse 2 is designed to increase prediction difficulty incrementally, spurring productive focused research for the next few years. These changes are intended to incentivize methods that perform well on extended forecast horizons (3 s $\rightarrow$ 6 s), handle multiple types of dynamic objects (1 $\rightarrow$ 5), and ensure safety in scenarios from the long tail. Future Argoverse releases could continue to increase the problem difficulty by reducing observation windows and increasing forecasting horizons.

- **Usability matters.** Argoverse 1 benefited from a large and active research community—in large part due to the simplicity of setup and usage. Consequently, we took care to ensure that existing Argoverse models can be easily ported to run on Argoverse 2. In particular, we have prioritized intuitive access to map elements, encouraging methods which use the lane graph as a strong prior. To improve training and generalization, all poses have also been interpolated and resampled at exactly 10 Hz (Argoverse 1 was approximate). The new dataset includes fewer, but longer and more complex scenarios; this ensures that total dataset size remains large enough to train complex models but small enough to be readily accessible.

### 2.4.3. Evaluation metrics

Most MP datasets (either in the field of AD or others focused on pedestrian motion prediction) use the same metrics to evaluate the performance of the different proposed algorithms. In this work we focus on the most important ones (minimum Average Displacement Error (minADE) and minimum Final Displacement Error (minFDE)) to evaluate our model with respect to the SOTA both in terms of validation and in the corresponding leaderboard (test):

1. The minimum Average Displacement Error (minADE, also referred as $ADE_{k=N}$) measures the average *L2* between the best predicted trajectory and the ground-truth trajectory over all time steps. The best here refers to the trajectory (or mode) that has the minimum average error. It is defined as:

$$minADE = \min_{i=1}^{N} \left( \frac{1}{T} \sum_{t=1}^{T} \sqrt{\left(x_{i,t}^{pred} - x_{i,t}^{gt}\right)^2 + \left(y_{i,t}^{pred} - y_{i,t}^{gt}\right)^2} \right)$$

where $N$ is the total number of predictions, $T$ is the number of time steps, $(x_{i,t}^{pred}, y_{i,t}^{pred})$ are the predicted coordinates of vehicle $i$ at time step $t$, and $(x_{i,t}^{gt}, y_{i,t}^{gt})$

are the ground truth coordinates of vehicle $i$ at time step $t$. The minADE metric penalizes the algorithm for the worst average displacement error among all the predictions.

2. The minimum Final Displacement Error (minFDE) measures the minimum *L2* distance between the final predicted position and the corresponding ground-truth position. The best here refers to the trajectory (or mode) that has the minimum average error. It is defined as:

$$minFDE = \min_{i=1}^{N} \sqrt{\left(x_{i,T}^{pred} - x_{i,T}^{gt}\right)^2 + \left(y_{i,T}^{pred} - y_{i,T}^{gt}\right)^2}$$

where $(x_{i,T}^{pred}, y_{i,T}^{pred})$ are the predicted coordinates of vehicle $i$ at the last time step $T$, and $(x_{i,T}^{gt}, y_{i,T}^{gt})$ are the ground truth coordinates of vehicle $i$ at the last time step $T$. The minFDE metric penalizes the algorithm for the worst final displacement error among all the predictions.

In this work, except for the GAN-based model (see Section **??**) which is focused on unimodal prediction, we report results for $k = 1$ (unimodal case, only the mode with the best confidence is considered) and $k = 6$ as this is the standard in the Argoverse 1 and 2 Motion Forecasting datasets in order to compare with other models.

## 2.5. Comparison of *state-of-the-art* simulators in Autonomous Driving

The last section of this chapter focuses on justifying the necessity of why a hyper-realistic simulator is required to validate the algorithms instead of only using graphics and metrics of the corresponding dataset, a brief comparison with the SOTA and the simulator we will use in the experimental results to validate the corresponding algorithms.

A fully-autonomous driving architecture (L5 in the J3016 SA [1]) is still years away, mainly due to technical challenges, but also due to social and legal ones [95]. The Society of Automotive Engineers (SAE) stated a taxonomy with five levels [1] of driving automation, in which the level zero stands for no automation and level five for full-automation. Level one (L1) includes primitive ADAS (Advanced Driver Assistance Systems) such as Adaptive Cruise Control, stability control or anti-lock braking systems [96]. Once the system has longitudinal and lateral control in a specific use case (although the driver has to monitor the system at all times), level two (L2) becomes a feasible technology. Then, the real challenge arises above this level. Level three (L3) is conditional automation, that is, the system has longitudinal and lateral control in specific use cases, so the driver does not have to monitor the system at all times. However, the system recognizes the performance limits and the driver is requested to resume control (s/he must be in position) within a sufficient

time margin. In that sense, the takeover maneuver (transition from automatic to manual mode) is an issue yet to be solved. Since recent studies [97] [98] have demonstrated how it increases the likelihood of an accident during the route, in particular if the driver is not aware of the navigation.

Besides this, we find levels four and five, in which human attention is not required anymore in specific use cases (L4) or any weather condition and road conditions (L5), which represent an open and challenging problem. The environment variables, from surrounding behaviour to weather conditions, are highly stochastic and difficult to model. In that sense, no industry organization has shown a ratified testing methodology for L4/L5 autonomous vehicles. The AD community gives a simple reason: despite the fact that some regulations have been defined for these levels and current automotive companies/research groups are very good at testing the individual components of the AD architecture using the corresponding datasets [99] [89], [92], there is a need to test intelligent vehicles full of advanced sensors [100] in an end-to-end way. In this context, artificial intelligence is increasingly being involved in processes such as detecting the most relevant objects around the car (DL based multi-object tracking systems), or evaluating the current situation of the vehicle to conduct the safest decision (e.g. Deep Reinforcement Learning applied to behavioural systems). Moreover, it is important to consider the presence of sensor redundancy in order to establish a safe navigation in such a way the different sensors and associated algorithms are integrated together, to validate the whole system and not just individual components.

Regarding urban environment complexity, in order to validate a whole AD architecture the system must be tested in countless environments and scenarios, which would escalate the cost and development time exponentially with the physical approach. Considering this, the use of photo-realistic simulation (virtual development and validation testing) and an appropriate design of the driving scenarios are the current keys to build safe and robust AV. These simulators have evolved from merely simulating vehicle dynamics to also simulating more complex functionalities. Simulators intended to be used for test self-driving technology must have requirements that extend from simulating physical car models to several sensor models, path planning, control and so forth and so on. Some state-of-the-art simulators [101] for testing self-driving vehicles are as following:

- **MATLAB/Simulink** [102] published its Automated Driving Toolbox, that provides several tools which facilitate the design, simulation and testing of automated driving systems and Advanced Driver Assistance Systems (ADAS). One of its key features is that OpenDRIVE [103] road networks can be imported into MATLAB and may be used for varios testing and design purposes. This Automated Driving toolbox also supports Hardware-in-the-Loop (HIL) testing as well as C/C++ generation, which enables faster prototyping.

- **CarSim** [104] is a vehicle simulator commonly used by academia and industry. Its newest version supports moving objects and sensors that benefit simulations involving self-driving tecnology and ADAS. These moving objects may be linked to 3D objects with their own embedded animations, such as vehicles, byciclists or pedestrians.

- **PreScan** [105] provides a simulator framework to design self-driving cars and ADAS. It presents PreScan's automatic traffic generator which enables manufacturers to validate their autonomous navigation architectures providing a variety of realistic environments and traffic conditions. This simulator also supports HIL simulation, quite common for evaluating Electronic Control Units (ECUs) used in real-world applications.

- **CARLA (CAR Learning to Act)** [106] an open-source autonomous driving simulator implemented as a layer over Unreal Engine 4 (UE4) [107]. This simulation engine provides to CARLA an ecosystem of interoperable plugins, a realistic physics and a state-of-the-art image quality. CARLA is designed as a server-client system so as to support this functionality provided by UE4, where the simulation is rendered and run by the server. The environment is composed of 3D models of static objects, such as buildings, infrastructure or vegetation, as well as dynamic objects like pedestrians, cyclists or vehicles. These objects are designed using low-weight geometric textures and models though maintaining visual realism by making use of variable level of detail and carefully crafting the materials. Moreover, one of the main advantages when using CARLA is the possibility to modify in an easy way the vehicle on-board sensors and their features in order to obtain accurate data, the weather and even the possibility to create realistic traffic scenarios.

- **Gazebo** [108] is an scalable, open-source, flexible and multi-robot 3D simulator. It supports the recreation of both outdoor and indoor environments in which there are two core elements that define the 3D scene, also known as world and model. The world is used to represent the 3D scene, defined in a Simulation Description File (SDF) and a model is basically any 3D object. Gazebo uses Open Dynamic Engine (ODE) as its default physic engine.

- **LGSVL (LG Electronics America R&D Center)** [109] is the most recent simulator for testing autonomous driving technology, focused on multi-robot simulation. It is based on the Unity game engine [110], providing different bridges for message passing between the simulator backbone and the autonomous driving stack. LGSVL provides a PythonAPI to control different environment entitities, such as weather conditions, the position of the adversaries, etc. in a similar way to the CARLA simulator. It also provides Functional Mockup Interface (FMI) so as to integrate vehicle dynamics platform to the external third party dynamics models.

In Table 2.4, we provide a comparison summary where all six simulators described in this paper are further compared.

Table 2.4: Comparison of some *state-of-the-art* simulators for AD

| **Requirements** | **MATLAB (Simulink)** | **CarSim** | **PreScan** | **CARLA** | **Gazebo** | **LGSVL** |
|---|---|---|---|---|---|---|
| **Perception**: Sensor models supported | Y | Y | Y | Y(1) | Y(2) | Y(3) |
| **Perception**: support for different weather conditions | N | N | Y | Y | N | Y |
| **Camera Calibration** | Y | N | Y | Y | N | N |
| **Path Planning** | Y | Y | Y | Y | Y | Y |
| **Vehicle Control**: Support for proper vehicle dynamics | Y | Y | Y | Y | Y | Y(3) |
| **3D Virtual Environment** | U | Y | Y | Y, Outdoor (Urban) | Y, Indoor and Outdoor | Y, Outdoor (Urban) |
| **Traffic Infrastructure** | Y, allows to build lights model | Y | Y | Y, Traffic lights, Intersections, Stop signs, lanes | Y, allows to manually build all kinds of models | Y |
| **Traffic Scenario simulation**: Support of different types of Dynamic objects | Y | Y | Y | Y | N(2) | Y |
| **2D/3D Ground Truth** | Y | N | N | Y | U | Y |
| **Interfaces to other software** | Y, with Carsim, Prescan,ROS | Y, with Matlab(Simulink) | Y, with MATLAB(Simulink) | Y, with ROS, Autoware | Y, with ROS | Y, with Autoware, Apollo, ROS |
| **Scalability** via a server multi-client architecture | U | U | U | Y | Y | Y |
| **Open Source** | N | N | N | Y | Y | Y |
| **Well-maintained/Stable** | Y | Y | Y | Y | Y | Y |
| **Portability** | Y | Y | Y | Y, Windows, | Y, Windows, | Y, Windows, |

In order to choose the right simulator, there is a set of criteria [101] that may serve as a metric to identify which simulators are most suitable for our purposes, such as perception (sensors), multi-view geometry, traffic infrastructure, vehicle control, traffic scenario simulation, 3D virtual environment, 2D/3D groundtruth, scalability via a server multi-client architecture and last but not the least, open-source.

Figure 2.9: CARLA simulator overview

In that sense, we identify that MATLAB/Simulink is designed to simulate simple scenarios, with efficient plot functions and computation. It is usually connected to CarSim, where the user can control the vehicle models from CarSim and build their upper control algorithms in MATLAB/Simulink to do a co-simulation project, but the realism, the quality of the sensors and the complexity is limited. PreScan presents better capabilities to build realistic environments and simulate different weather conditions, unlike MATLAB and CarSim. Gazebo is quite popular as a robotic simulator, but the effort and time needed to create complex and dynamic scenes does not make it the first choice for testing self-driving technology.

Then, we have two simulators as our final options: LGSVL and CARLA. At the moment of writing this thesis, they are the most suited simulators for end-to-end testing of unique functionalities offered by autonomous vehicles, such as perception, mapping, vehicle control or localization. Most of their features, summarized in [101] are identical (open-source, traffic generation simulation, portability, 2D/3D groundtruth, flexible API and so forth and so on), with the only difference that LGSVL does not present camera calibration to perform multi-view geometry or Simultaneous Localization and Mapping (SLAM). Regarding this, we decided to use the CARLA simulator since the performance is very similar to LGSVL and the group had previous experience in the use of this simulator.

## 2.6. Summary

In order to finish this Chapter, we perform a brief comparison between the different methods (Physics-based, Classic ML, Reinforcement Learning and DL) in terms of accuracy, prediction horizon, computation cost and applications in the AD field.

Table 2.5: Summary of Motion Prediction methods features. Short-term and long-term characterize prediction horizons of no more than 1-s and no less than 3-s, respectively.

| Methods | Accuracy | Prediction Horizon | Computation Cost | Applications |
|---|---|---|---|---|
| Physics-based | High in short-term prediction, low in other prediction horizon | Short | Small | Colision risk analysis |
| Classic Machine Learning-based | Good at recognizing maneuvers but generalization ability is poor | Medium | Medium | Maneuver recognition |
| Deep Learning-based | High in considering some factors | Long | Relatively high | More and more applied in real-world |
| Reinforcement Learning-based | Relatively high, prediction methods are relatively few | Long | High | More applied in planning |

- Physics-Based Methods are suitable for the movement of vehicles, which can be accurately described by kinematics or dynamics models. Given a suitable physics model, these methods can be applied to a variety of scenarios at small computational cost and in a short time but without training. However, the prediction results based on such models heavily depends on the inputs and the model selection. The inputs are closely related to human or machine drivers, influenced by the driving environment or the interactions with other participants. Therefore, without the capability to describe such factors, physics-based models are limited to short-term prediction and in static scenes. Because of its simplicity and fast response, these methods can be easily used in real applications for ADSs, such as collision risk analysis.
- Classic Machine Learning-Based Methods, compared with physics-based methods, are able to consider more factors and its accuracy is relatively high with a longer prediction length at a higher computing cost. Most of these methods are maneuver-based methods, which predicts the trajectory with the maneuver known as a prior. However, vehicle maneuvers of human drivers are usually diverse and vary greatly in different scenarios such that the generalization ability of is poor. In real applications for AVs, such methods are used in scenarios such as lane change studies, leveraging their advantages in maneuver recognition.
- Reinforcement Learning-Based Methods imitate the human decision-making process and obtain the reward function through learning the expert demonstration to generate the corresponding optimal driving policy. They can continuously evolve through learning and adapt to complex environments and long prediction horizons. Such methods probably generate higher accuracy trajectories than deep learningmethods in a longer time domain. However, most of these methods are typically computationally expensive in their recovery of an expert cost function and require long training times. In real applications for AVs, reinforcement learning-based trajectory prediction methods are more applied to trajectory planning, taking its advantages in the decision-making process.
- Deep Learning-Based Methods can perform accurate predictions in a longer time horizon with respect to traditional methods that are only suitable for simple scenes and short-term prediction. By means of powerful neural networks, such as RNNs,

CNNs, GANs, Attention mechanisms or GNNs for feature extraction, physics-related, interaction-related and road-related factors are processed as inputs to the model. Furthermore, they can adapt to more complex environments and a longer prediction horizon. DL-based methods require to use a large amount of data for training. Besides, with the increase of consideration factors and the increase of the number of network layers, the computing costs and time increases sharply. Such methods can naturally generate multi-modal trajectories, which is consistent with the diversity of vehicles' maneuvers. In real applications for AVs, it is necessary to reach a balance between calculation time and model complexity to ensure the real-time performance and safety of AVs. At present, more and more real-world trials use thesemethods to predict thefuture trajectory of traffic participants.

As observed in Table 2.5 and discussed in this section summarizing the different MP algorithms, we focus this thesis on DL methods since they are the most suitable methods for long-term prediction with a relatively high computation cost, specially focusing on the ability of extracting and combining the latent spaces of the different inputs by means of SOTA algorithms.

Furthermore, the validation framework (both in terms of datasets and AD simulator) is defined. In this thesis we choose Argoverse 1 and Argoverse 2 as databases to build our DL-based MP algorithms, since both are extensively used by the research community to build this kind of algorithms, and CARLA to validate the prediction methods in a holistic way (that is, integrated with other layers such as decision-making or control) in a hyper-realistic AD simulator as a preliminary stage before implementing it in a real-world platform.

# Chapter 3

# Theoretical Background

*Desde que el mundo cambió,*
*estamos mucho más unidos con los Digimon,*
*luchamos juntos contra el mal.*
*Algo extraño pasaba,*
*Digievolucionaban, en tamaño y color,*
*Ellos son los Digimon.*

Opening 1 de Digimon: "Butterfly"
Autor original: Kōji Wada

## 3.1. Introduction

As commented in previous sections, the MP algorithms covered by this thesis range from tracking multiple objects and subsequent prediction with physics-based methods to the most recent SOTA techniques to compute the deep traffic context and then decode multimodal predictions with associated confidences, assuming the physical information is given and surrounding participants have been multi-tracked beforehand. Throughout this Chapter, an in-depth theoretical study will be made of those algorithms, neural networks or heuristics that form a direct part of the development of this work in order to address the proposed methods in future chapters.

First of all, we will start with the mathematical formulation of the methods to perform physics-based Multi-Object Tracking, from the well-known techniques Kalman Filter [25] for the agents states estimation to the Hungarian algorithm [111] for the association of detections and trackers, which represents the preliminary stage before carrying out the subsequent prediction. On top of that, since several single-trajectory models (Constant Turn Rate and Velocity (CTRV), Constant Turn Rate and Acceleration (CTRA)) are used to compute the most plausible centerlines in the Argoverse 1 [5] and Argoverse 2 [6], we will review the state transition equations to properly understand the constraints for each model. Furthermore, the principal DL techniques (e.g. 1D-CNN, LSTM, GCN, Attention mechanisms) and training losses used in this work to encode and decode the aimed

multimodal will be stated, first a general mathematical formulation and applications and then how the corresponding technique is used in the MP field.

## 3.2. Physics-based algorithms

As stated in Chapter 2 Section 2.1, initially researchers rely on physics-based methods which are basic and straightforward. These methods may not offer high accuracy, but many models use the underlying idea of physics-based models to improve their accuracy. Physics-based approaches yield better results when the movement of vehicles is described by kinematics or dynamics models accurately. Nevertheless, the physical model of traffic participants is constantly evolving, so most physics-based models are only applicable for short-term predictions of no more than one second. In this Section we will study the mathematical formulation of the physics-based prediction algorithms, as well as the data association problem regarding the Multi-Object Tracking stage, that are directly related to our algorithm proposed in Chapter 4.

### 3.2.1. Kalman Filter under the hood

The Kalman Filter [25] is a recursive algorithm used for estimating the state of a dynamic system in the presence of noise. It is widely used in various fields such as engineering, control systems, and robotics. The algorithm works by combining a prediction of the system state based on a mathematical model with measurements (updates) from sensors to improve the accuracy of the state estimation, as shown in Figure 3.1. The Kalman Filter is a powerful algorithm for state estimation, and it has many variations and extensions that can handle various types of systems and measurements. The filter can be applied to non-linear systems using the Extended Kalman Filter or the Unscented Kalman Filter, and it can handle multiple models using the multiple model Kalman Filter. The filter can also be used for smoothing, which involves estimating the state of the system based on past and future measurements.

In its most simple version, the Kalman filter assumes that the system can be described using a set of linear equations, where the state of the system can be represented by a vector $\mathbf{x}_k$, and the measurements can be represented by a vector $\mathbf{z}_k$. The Kalman filter also assumes that the noise in the system follows a Gaussian distribution.

The state estimation process is performed in two steps: the prediction step and the update step. In the prediction step, the current state of the system is predicted based on the previous state and a mathematical model of the system. In the update step, the predicted state is corrected based on a measurement from a sensor.

The prediction step can be represented using the following equations:

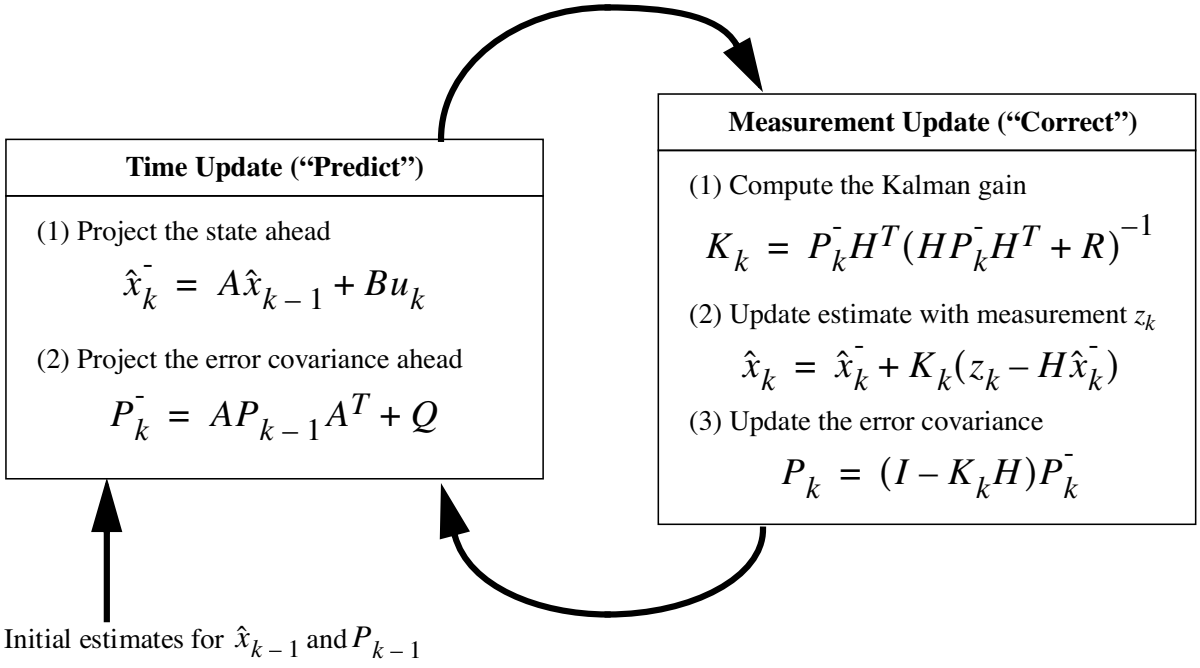


Figure 3.1: Overview of the Kalman Filter Predict-Update cycle. The Kalman filter keeps track of the estimated state of the system and the variance or uncertainty of the estimate. The estimate is updated using a state transition model and measurements
Source: *An introduction to the kalman filter* [112]

$$\begin{aligned} \hat{\mathbf{x}}_k^- &= \mathbf{A}\hat{\mathbf{x}}_{k-1} + \mathbf{B}\mathbf{u}_k \\ \mathbf{P}_k^- &= \mathbf{A}\mathbf{P}_{k-1}\mathbf{A}^T + \mathbf{Q} \end{aligned} \tag{3.1}$$

where $\hat{\mathbf{x}}_k^-$ is the predicted state of the system at time $k$, $\hat{\mathbf{x}}_{k-1}$ is the estimated state of the system at time $k-1$, $\mathbf{A}$ is the state transition matrix, $\mathbf{B}$ is the control-input matrix, $\mathbf{u}_k$ is the control input at time $k$, $\mathbf{P}_k^-$ is the predicted error covariance matrix, and $\mathbf{Q}$ is the process noise covariance matrix. Note that the state transition, control-input and process noise covariance matrix values do not depend on the timestep time $k$.

On the other hand, the update step can be represented using the following equations:

$$\begin{aligned} \mathbf{K}_k &= \mathbf{P}_k^- \mathbf{H}_k^T (\mathbf{H}\mathbf{P}_k^- \mathbf{H}^T + \mathbf{R})^{-1} \\ \hat{\mathbf{x}}_k &= \hat{\mathbf{x}}_k^- + \mathbf{K}_k(\mathbf{z}_k - \mathbf{H}_k\hat{\mathbf{x}}_k^-) \\ \mathbf{P}_k &= (\mathbf{I} - \mathbf{K}_k\mathbf{H})\mathbf{P}_k^- \end{aligned} \tag{3.2}$$

where $\mathbf{K}_k$ is the Kalman gain, $\mathbf{H}$ is the measurement matrix, $\mathbf{R}_k$ is the measurement noise covariance matrix and $\mathbf{I}$ the identity matrix of the corresponding dimension. The Kalman gain determines the relative weight given to the predicted state and the measurement, and is adjusted based on the measurement noise covariance matrix. The measurement matrix relates the measurements to the state variables, and is used to convert the measurements into the same units as the state variables.

### 3.2.2. Hungarian algorithm formulation

The Hungarian algorithm [111], also known as the Munkres algorithm or the Kuhn-Munkres algorithm, is an efficient algorithm for solving the assignment problem in combinatorial optimization. The main concept behind this algorithm is an assignment problem that involves finding the optimal assignment of $n$ workers to $n$ jobs, given the cost of assigning each worker to each job.

The Hungarian algorithm works by iteratively finding a set of independent zero-cost assignments, which correspond to a perfect matching in a bipartite graph. These assignments are then used to reduce the problem size and find a new set of independent zero-cost assignments, until all workers are assigned to jobs.

The Hungarian algorithm has a time complexity of $\mathrm{O}(n^3)$, which makes it one of the most efficient algorithms for solving the assignment problem. In this algorithm, the cost matrix C is assumed to be an $n \times n$ matrix, where each element $C_{i,j}$ represents the cost of assigning worker i to job j. The matrix M represents the matching, where each element $M_{i,j}$ is 1 if worker i is assigned to job j, and 0 otherwise.

As observed in Algorithm 1, the Hungarian algorithm iteratively finds an uncovered zero in the cost matrix C and adds it to the matching M, while also adjusting the cost matrix to ensure that all rows and columns are covered by the matching. This is done by finding the minimum uncovered cost in each row and subtracting it from all uncovered costs in the row, and finding the minimum cost in each uncovered column and adding it to all uncovered costs in the column. Once all rows and columns are covered, the algorithm returns the final matching $M$.

In conclusion, the Hungarian algorithm is a powerful optimization algorithm that solves the assignment problem in polynomial time. The algorithm has a wide range of applications and can be easily adapted to handle various constraints and objectives. The algorithm is also guaranteed to find the optimal solution to the assignment problem, which makes it a valuable tool in many practical settings.

### 3.2.3. State Transition Equations of Single-Trajectory Models

As stated in Chapter 2 Section 2.3.1.1, Single-trajectory prediction methods are used in the field of motion estimation and control, to predict the future state of an object

**Algorithm 1:** The Hungarian algorithm for solving the minimum cost perfect matching problem

**Input :** A cost matrix $C$ of size $n \times n$
**Output:** A minimum cost perfect matching
Initialize the label vectors $u_i = \min_{j \in 1,\dots,n} C_{i,j}$ and $v_j = 0$ for all $i, j$; Initialize the empty matching $M$; **while** $|M| < n$ **do**
  Choose an unmatched row $i$; Initialize the set $T = i$ and the predecessor vector $P = \emptyset$; **while** *true* **do**
    Let $S$ be the set of columns $j$ such that $i \in T$ and $C_{i,j} = u_i + v_j$; If $|S| > 0$, choose any column $j$ in $S$; **else**
      Choose a column $j$ such that $v_j = \min_{k \in 1,\dots,n} v_k$ and let $S$ be the set of rows $i$ such that $j \in M$ or $C_{i,j} = u_i + v_j$; Increment each $u_i$ for $i \in T$ by $\delta = \min_{i \in T, j \in S}(u_i + v_j - C_{i,j})$; Decrement each $v_j$ for $j \in S$ by $\delta$; **for** *each row* $i \in T$ *and each column* $j \in S$ **do**
        **if** $C_{i,j} = u_i + v_j$ **then**
          Add the edge $(i, j)$ to the alternating tree represented by $M$ and $P$; **if** $j$ *is unmatched* **then**
            Augment $M$ along the alternating tree to create a larger matching; **return** the updated matching $M$;
          **end**
          **else**
            Add $j$ to $T$ and continue the while loop;
          **end**
        **end**
      **end**
    **end**
  **end**
**end**

based on its current state and motion. In these methods, the agents are mostly assumed to comply with motion models that describe their dynamic behavior in such a way these are not able to consider the road-related factors and the uncertainty of the current state is unreliable for long-term prediction. Then, these models should only be used for estimating unimodal trajectories of the surrounding agents in the short-term (no more than 1-s).

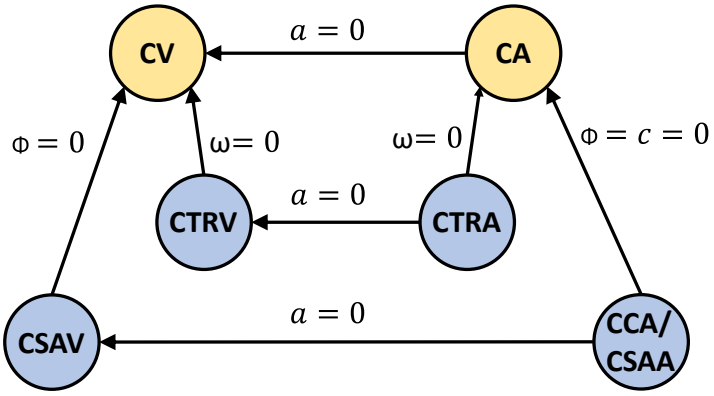


Figure 3.2: Overview of Single Trajectory prediction methods. Every sophisticated model can be transformed into a simpler one by setting one state veriable to zero
Source: *Comparison and evaluation of advanced motion models for vehicle tracking* [113]

Several single-trajectory prediction models have been proposed in the literature, including Constant Velocity (CV), Constant Acceleration (CA), Constant Turn Rate and Velocity (CTRV), Constant Turn Rate and Acceleration (CTRA), Constant Speed and

Angular Velocity (CSAV), and Constant Curvature Acceleration (CCA)/Constant Speed and Angular Acceleration (CSAA), as illustrated in Figure 3.2:

- Constant Velocity (CV) model assumes that the object moves at a constant velocity and its future position can be predicted by simply extrapolating its current velocity vector. This model is simple and computationally efficient, but it may not accurately capture the object's motion if it changes its velocity.
- Constant Acceleration (CA) model is an extension of the CV model, assuming that the object can also change its acceleration in a linear manner. This model can provide more accurate predictions of the object's future position and velocity, but it may not be suitable for objects with more complex motion patterns.
- Constant Turn Rate and Velocity (CTRV) model assumes that the object moves in a circular trajectory with a constant turn rate and velocity magnitude. This model is useful for predicting the motion of objects such as drones or missiles, but it may not accurately represent the motion of objects with more complex trajectories.
- Constant Turn Rate and Acceleration (CTRA) model is an extension of the CTRV model, allowing the object to change its acceleration while maintaining a constant turn rate. This model is often used in applications such as autonomous driving or aircraft navigation, where objects can accelerate or decelerate.
- Constant Speed and Acceleration Vector (CSAV) model assumes that the object moves along a straight line with a constant speed and acceleration vector. This model can be useful for predicting the motion of objects such as trains or boats.
- Constant Acceleration and Angle (CAA) model assumes that the object moves along a constant heading angle and can change its acceleration in a linear manner. This model can be useful for predicting the motion of objects such as bicycles or motorcycles.

It can be observed how a sophisticated model can be transformed into a simpler one by setting one state veriable to zero. For example, CTRA is transformed to CTRV if the agent acceleration $a$ is set to zero. Similarly, CTRA is transformed to CA if the angular speed $\omega$ is set to 0. In this Section we particularly focus on the prediction equations and differences of the most commonly used single-trajectory prediction methods in the field of AD to predict the future motion of a moving object: CTRV and CTRA.

#### 3.2.3.1. Constant Turn Rate Velocity (CTRV)

The Constant Turn Rate and Velocity (CTRV) model is a mathematical model used in the field of autonomous navigation to predict the future motion of a moving object.

The model assumes that the object moves along a smooth, continuous path, and that its velocity and turn rate are constant.

The model describes the motion of the object using a set of differential equations that relate the rate of change of the object's state to its current state and any external inputs. The state of the object is described using five variables: the x and y coordinates of its position, its velocity magnitude, its heading angle (or direction of travel), and its turn rate.

The CTRV model predicts the future position of the object by using the current position, velocity, heading angle, and turn rate, and propagating them forward in time. The model assumes that the velocity and turn rate remain constant throughout the prediction interval.

The prediction equations for the CTRV model are described as follows:

$$\begin{aligned} x_{k+1} &= x_k + \frac{v_k}{\omega_k}\left[\sin(\psi_k + \omega_k \Delta t) - \sin(\psi_k)\right] \\ y_{k+1} &= y_k + \frac{v_k}{\omega_k}\left[\cos(\psi_k) - \cos(\psi_k + \omega_k \Delta t)\right] \\ v_{k+1} &= v_k \\ \psi_{k+1} &= \psi_k + \omega_k \Delta t \\ \omega_{k+1} &= \omega_k \end{aligned} \tag{3.3}$$

where:

$x_k$ and $y_k$ are the coordinates of the object's position at time step $k$ $v_k$ is the velocity magnitude at time step $k$ $\psi_k$ is the heading angle (in radians) at time step $k$ $\omega_k$ is the turn rate (in radians per second) at time step $k$ $\Delta t$ is the time step size.

The first two equations predict the object's position at the next time step, based on its current position, velocity, heading angle, and turn rate. The third and fifth equations predict that the velocity and turn rate will remain constant. The fourth equation predicts the object's heading angle at the next time step, based on its current heading angle and turn rate.

Overall, the CTRV model is a useful tool for predicting the motion of a moving object and can be used in a variety of applications, such as robotics, aviation, and space exploration.

#### 3.2.3.2. Constant Turn Rate Acceleration (CTRA)

The Constant Turn Rate and Acceleration (CTRA) model is an extension of the Constant Turn Rate and Velocity (CTRV) model, allowing the object to change its acceleration

while maintaining a constant turn rate. This makes the CTRA model more accurate for predicting the motion of objects that can accelerate or decelerate, such as cars or aircraft.

The state of the object in the CTRA model is described using variables such as the x and y coordinates of its position, its velocity magnitude, its heading angle, its turn rate, and its acceleration magnitude. The motion of the object is modeled using the following set of equations:

$$\begin{aligned} x_{k+1} &= x_k + \frac{v_k}{\omega_k}\left[\sin(\theta_k + \omega_k \Delta t) - \sin(\theta_k)\right] \\ y_{k+1} &= y_k - \frac{v_k}{\omega_k}\left[\cos(\theta_k + \omega_k \Delta t) - \cos(\theta_k)\right] \\ \theta_{k+1} &= \theta_k + \omega_k \Delta t \\ v_{k+1} &= v_k + a_k \Delta t \\ \omega_{k+1} &= \omega_k \end{aligned} \tag{3.4}$$

where $x_k$ and $y_k$ are the object's position coordinates at time $k$, $\theta_k$ is its heading angle, $v_k$ is its velocity magnitude, $\omega_k$ is its turn rate, and $a_k$ is its acceleration magnitude. $\Delta t$ is the time step between predictions.

The first two equations describe the object's position updates based on its current position, velocity, heading angle, turn rate, and the time step. The third equation describes the object's heading angle update based on its current heading angle and turn rate. The fourth equation describes the object's velocity update based on its current velocity and acceleration. The last equation assumes that the object's turn rate remains constant over time.

In summary, the CTRA model is a useful tool for predicting the motion of objects that can accelerate or decelerate while maintaining a constant turn rate. The model's equations include variables such as the object's position, velocity, heading angle, turn rate, and acceleration magnitude, and they are based on the kinematic equations of motion.

#### 3.2.3.3. CTRV vs CTRA

The CTRV model assumes that the object moves along a smooth, continuous path, and that its velocity and turn rate are constant. This means that the object moves in a circular trajectory with a fixed radius. The state of the object is described using variables such as the x and y coordinates of its position, its velocity magnitude, its heading angle, and its turn rate.

On the other hand, the CTRA model assumes that the object can change its acceleration while maintaining a constant turn rate. This makes the CTRA model more accurate for predicting the motion of objects that can accelerate or decelerate, such as cars or air-

craft. The state of the object in the CTRA model is described using similar variables to the CTRV model, but with an additional variable to represent the object's acceleration.

The prediction equations for the CTRV model are based on the kinematic equations for circular motion, where the object's position, velocity, and heading angle change in a continuous and smooth manner. In contrast, the prediction equations for the CTRA model include an additional term for the object's acceleration, which allows for more accurate predictions of the object's future motion when it can accelerate or decelerate.

In terms of implementation, the CTRA model requires more computational resources due to the additional term for acceleration, which increases the complexity of the equations. This can make the CTRV model more computationally efficient and faster to calculate in real-time applications. However, the CTRA model is more accurate in predicting the motion of objects with varying acceleration and is often used in applications such as autonomous driving or aircraft navigation.

In summary, the main differences between the CTRV and CTRA prediction models are that the CTRA model includes an additional term for acceleration in its prediction equations, allowing for more accurate predictions of the motion of objects with varying acceleration, while the CTRV model assumes a constant velocity and turn rate and is more computationally efficient.

## 3.3. Deep Learning algorithms

In this section the mathematical formulation of the DL layers employed in this thesis is covered. In particular, these are the 1D-CNN, Long Short-Term Memory (LSTM), GAN, Attention mechanism and GNN layers. We briefly introduce each layer, as well as the corresponding mathematical formulation to enhance the comprehension of the learning-based methods proposed in this thesis.

### 3.3.1. Convolutional Neural Networks

Convolutional neural networks (CNNs) are commonly used for image and signal processing tasks. The type of CNN architecture used depends on the nature of the input data. Here are the differences between the three types of CNNs:

- 1D Convolutional Neural Networks (1D CNNs): 1D CNNs are used for processing sequential data such as time series data, speech signals, and text data. The input to a 1D CNN is a one-dimensional sequence of data, such as a time series of sensor readings. 1D CNNs typically have fewer parameters and are computationally efficient compared to 2D and 3D CNNs.

- 2D Convolutional Neural Networks (2D CNNs): 2D CNNs are used for processing 2D images. The input to a 2D CNN is a two-dimensional image represented as a matrix of pixels. The convolutional layers in a 2D CNN apply filters that slide over the image to extract local features. The output of each convolutional layer is a set of 2D feature maps. 2D CNNs are widely used for image classification, object detection, and image segmentation.

- 3D Convolutional Neural Networks (3D CNNs): 3D CNNs are used for processing 3D volumetric data such as CT scans, MRI images, and video data. The input to a 3D CNN is a three-dimensional volume represented as a sequence of 2D images. The convolutional layers in a 3D CNN apply filters that slide over the 3D volume to extract local features. The output of each convolutional layer is a set of 3D feature maps. 3D CNNs are used for tasks such as medical image analysis, video classification, and action recognition.

In summary, 1D CNNs are used for processing sequential data (such as time series data, audio signals, and text), 2D CNNs are used for image processing, and 3D CNNs are used for volumetric data. As we will see in Chapter **??**, in this work we focus on 1D CNNs. The basic building blocks of a 1D CNN are convolutional layers, which learn local patterns in the input data by applying a set of filters to it, as illustrated in Figure 3.3. Each filter slides over the input sequence and performs a dot product operation at each position to generate a feature map. These feature maps capture the presence of certain patterns at different positions in the input sequence.

The architecture of a 1D CNN typically consists of several convolutional layers, followed by one or more fully connected layers for classification or regression. The output of each convolutional layer is fed into the next layer, with optional pooling layers in between to reduce the spatial dimension of the feature maps. The final output of the network is obtained by passing the output of the last fully connected layer through a suitable activation function, such as softmax for classification or linear for regression.

Let $x$ be a 1-dimensional input sequence of length $n$, represented as a vector $x = [x_1, x_2, ..., x_n]$. Let $k$ be a filter of length $m$, represented as a vector $k = [k_1, k_2, ..., k_m]$. We can apply the filter $k$ to the input sequence $x$ by computing a convolution operation:

$$(k * x)_i = \sum_{j=1}^{m} k_j x_{i+j-m} \tag{3.5}$$

where $*$ denotes the convolution operation, and $i$ ranges from $m$ to $n$. This operation produces a new sequence of length $n - m + 1$, representing the local features extracted from the input sequence $x$ by the filter $k$.

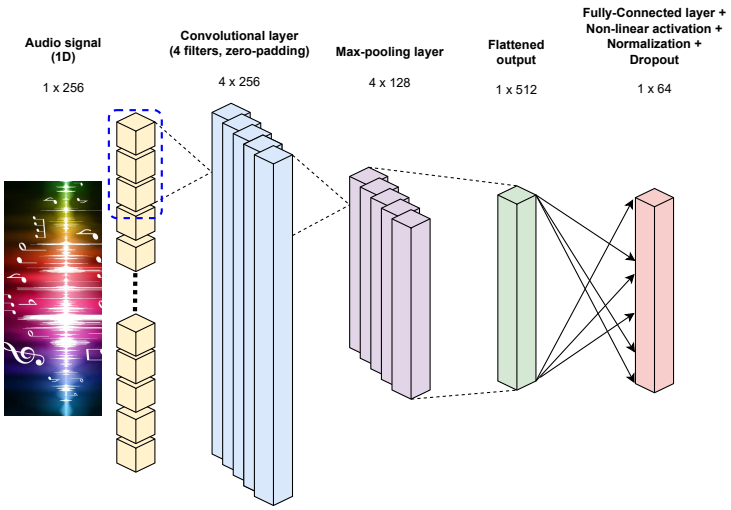


Figure 3.3: Example of CNN architecture to process 1D-input signals

To learn multiple filters and extract different types of features, we use multiple convolutional layers in the network. Each layer applies a set of filters, and produces a set of feature maps. The feature maps can be computed as:

$$h_{i,j} = f(\sum_{k=1}^{m} W_{j,k} x_{i+k-m} + b_j) \tag{3.6}$$

where $h$ is the feature map at position $i$ and filter $j$, $W$ is the weight matrix of the $j$-th filter, $b$ is the bias term for the $j$-th filter, and $f$ is an activation function (such as ReLU or sigmoid).

After each convolutional layer, we typically apply a pooling layer to reduce the dimensionality of the features and increase the translation invariance of the network. The most common pooling operation is max pooling, which selects the maximum value within a window of size $p$:

$$y_{i,j} = \max_{k=0}^{p-1} h_{i+k,j} \tag{3.7}$$

where $y$ is the output of the pooling layer at position $i$ and filter $j$.

Finally, we can use one or more fully connected layers to perform the final classification or regression task. The output of the pooling layer is flattened into a vector, and fed into a set of fully connected layers, with optional dropout regularization and batch normalization:

$$z_j = f(\sum_{i=1}^{n} W_{i,j} y_i + b_j) \tag{3.8}$$

where $z$ is the output of the $j$-th fully connected layer, $W$ is the weight matrix, $y$ is the flattened output of the pooling layer, $b$ is the bias term, and $f$ is an activation function.

### 3.3.2. Recurrent Neural Networks

Recurrent Neural Networks (RNNs) are a type of neural network that are designed to process sequential data, where the order of the input matters. They are widely used in a variety of applications such as natural language processing, speech recognition, image captioning, and time series prediction.

The general theory of RNNs is that they have a feedback loop in their architecture that allows information to be passed from one time step to the next, thereby enabling the network to capture dependencies between the inputs at different time steps. The input at each time step is fed into the network along with the output from the previous time step, and the network uses this information to generate a new output.

There are several types of RNNs, including the basic RNN, the Gated Recurrent Unit (GRU), and the Long Short-Term Memory (LSTM) [114]. The basic RNN is the simplest form of RNN, where the output at each time step is a function of the input at that time step and the output from the previous time step. However, it suffers from the vanishing gradient problem, where the gradients become exponentially small as they propagate through time, making it difficult to learn long-term dependencies.

The GRU is a variation of the basic RNN that uses gating mechanisms to control the flow of information through the network. It has fewer parameters than the LSTM and can be faster to train, but it may not perform as well as the LSTM on tasks that require more complex temporal dependencies.

#### 3.3.2.1. Long Short-Term Memory

LSTM networks were introduced to address the vanishing gradient problem in standard RNNs. They achieve this by using a memory cell to store information over long periods of time, and three gating mechanisms to control the flow of information through the network. Figure 3.4 provides a detailed overview of the LSTM cell structure, illustrating the workflow from the previous cell output and input at time $t-1$ in order to compute the current cell state and hidden state at time $t$.

The three gates are called the input gate, forget gate, and output gate, and they are responsible for deciding which information to store in the memory cell, which information to forget, and which information to output, respectively.

The equations for the input, forget, and output gates are as follows:

- Input gate: $i_t = \sigma(W_i \cdot [h_{t-1}, x_t] + b_i)$
- Forget gate: $f_t = sigmoid(W_f * [h_{t-1}, x_t] + b_f)$
- Input gate: $o_t = sigmoid(W_o * [h_{t-1}, x_t] + b_o)$

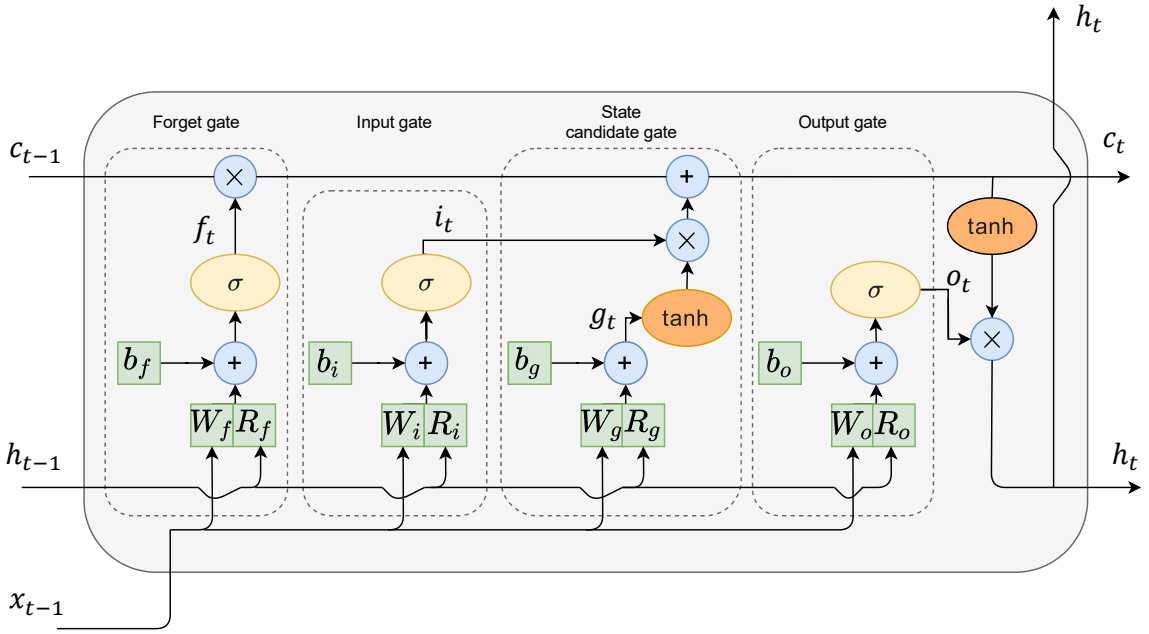


Figure 3.4: Overview of the LSTM cell structure

where $x_t$ is the input at time $t$, $h_{t-1}$ is the hidden state from the previous time step, $i_t$ is the input gate activation, $f_t$ is the forget gate activation, and $o_t$ is the output gate activation. $W_i$, $W_f$, and $W_o$ are weight matrices, and $b_i$, $b_f$, and $b_o$ are bias vectors.

On the other hand, the memory cell is updated based on the input, forget, and output gates, as well as a new candidate value that is computed based on the current input and hidden state. The equations for the memory cell and candidate value are as follows:

$$\begin{aligned} \tilde{C}t &= \tanh(W_c \cdot [ht-1, x_t] + b_c) \\ C_t &= f_t \cdot C_{t-1} + i_t \cdot \tilde{C}_t \end{aligned} \tag{3.9}$$

where $\tilde{C}t$ is the candidate value, $C_t$ is the new memory cell value, and $Ct-1$ is the previous memory cell value. $W_c$ is a weight matrix and $b_c$ is a bias vector.

Finally, the hidden state at time $t$ is computed based on the output gate and the new memory cell value, using the following equation:

$$h_t = o_t \cdot \tanh(C_t) \tag{3.10}$$

This equation scales the memory cell value by the output gate activation, then applies a hyperbolic tangent function to obtain the new hidden state.

In summary, LSTMs use a memory cell and three gating mechanisms to learn long-term dependencies in sequential data. The input, forget, and output gates control the flow of information through the network, while the memory cell stores information over

time. The equations for LSTMs involve computing the input, forget, and output gate activations, the candidate value, the new memory cell value, and the new hidden state.

### 3.3.3. Generative Adversarial Networks

A discriminative model is a type of machine learning model that learns the relationship between the input features and the target output directly. The goal of a discriminative model is to learn a decision boundary that separates different classes in the input data. In other words, discriminative models focus on learning the conditional probability distribution of the target variable given the input features.

Discriminative models are often used in supervised learning tasks, such as classification and regression, where the goal is to predict a target variable based on a set of input features. Common examples of discriminative models include logistic regression, support vector machines, and neural networks.

Unlike generative models, which learn the joint probability distribution of the input and target variables, discriminative models do not model the probability distribution of the input data explicitly. Instead, they focus on learning a mapping function that directly maps the input features to the target output.

In 2014, a breakthrough paper introduced Generative adversarial networks (GANs) [57], a clever new way to leverage the power of discriminative models to get good generative models. At their heart, GANs rely on the idea that a data generator is good if we cannot tell fake data apart from real data. In statistics, this is called a two-sample test - a test to answer the question whether datasets $X = \{x_1, \ldots, x_n\}$ and $X' = \{x'_1, \ldots, x'_n\}$ were drawn from the same distribution. This allows to improve the data generator until it generates something that resembles the real data. At the very least, it needs to fool the classifier even if our classifier is a state of the art deep neural network. GANs are a powerful technique for generating realistic samples that are similar to some training data. A GAN consists of two neural networks, a generator network and a discriminator network. The generator and discriminator networks are trained in a two-player game, where the generator tries to produce samples that fool the discriminator, and the discriminator tries to correctly classify between real and generated data. The objective function for a GAN is a min-max game between the generator and discriminator, and can be optimized using gradient descent or some other optimization algorithm. Some common applications where GANs are widely used are generating realistic images, videos, audio, data augmentation or style transfer.

The generator network takes as input a random noise vector, and generates a sample that is meant to mimic real data. The discriminator network takes as input a sample, and tries to distinguish between real data and generated data. The two networks are trained in a two-player game, where the generator tries to produce samples that fool the

discriminator, and the discriminator tries to correctly classify between real and generated data.

The objective function for a GAN can be formulated as a min-max game between the generator and discriminator. The generator tries to minimize the probability that the discriminator correctly classifies the generated samples as fake, while the discriminator tries to maximize the probability that it correctly classifies the real and generated samples.

The objective function for a GAN can be written as:

$$\begin{aligned} \min_{\theta_G} \max_{\theta_D} V(D,G) &= \mathbb{E}x \sim pdata(x)[\log D(x)] + \mathbb{E}z \sim p_z(z)[\log(1 - D(G(z)))] \\ &= \mathbb{E}x \sim p_{data}(x)[\log D(x)] + \mathbb{E}_{z \sim p_z(z)}[\log(1 - D(G(z;\theta_G)))] \end{aligned} \tag{3.11}$$

where $\theta_G$ and $\theta_D$ are the parameters of the generator and discriminator networks, respectively, $x$ is a real sample from the training data distribution $p_{data}$, $z$ is a noise vector sampled from a prior distribution $p_z$, and $G(z;\theta_G)$ is the generated sample from the generator network.

The first term of the objective function represents the expected log-probability of the discriminator correctly classifying a real sample as real. The second term represents the expected log-probability of the discriminator correctly classifying a generated sample as fake.

During training, the generator network is updated to minimize the objective function with respect to $\theta_G$, while the discriminator network is updated to maximize the objective function with respect to $\theta_D$. This can be done using gradient descent or some other optimization algorithm.

There are some well-known types of GANs, such as:

- Deep Convolutional GANs (DCGANs): These are GANs that use convolutional neural networks (CNNs) in the generator and discriminator networks. DCGANs are commonly used for image generation and have been shown to produce high-quality, realistic images.
- Wasserstein GANs (WGANs): These are GANs that use the Wasserstein distance instead of the traditional Kullback-Leibler (KL) divergence or Jensen-Shannon (JS) divergence for measuring the difference between the real and generated distributions. WGANs have been shown to produce more stable training and generate higher-quality samples.
- CycleGANs: These are GANs that are designed for image-to-image translation tasks, where the goal is to transform an image from one domain to another. CycleGANs use two generators and two discriminators to learn the mapping between the two domains.

Nevertheless, in this work we focus on a particular type of GAN, known as conditional GAN or cGAN, where the generator is conditioned on some additional information, such as class labels or image annotations. The additional information is used to control the generated output, allowing for more specific generation of data.

#### 3.3.3.1. GAN vs cGAN

The main difference between the original GAN and cGAN is that the original GAN generates samples without any control over the generated output, whereas the cGAN generates samples conditioned on some additional information.

In the original GAN, the generator network takes as input a random noise vector, and generates a sample that is meant to mimic real data. The discriminator network takes as input a sample, and tries to distinguish between real data and generated data. The goal of the original GAN is to train the generator network to generate samples that are indistinguishable from real data.

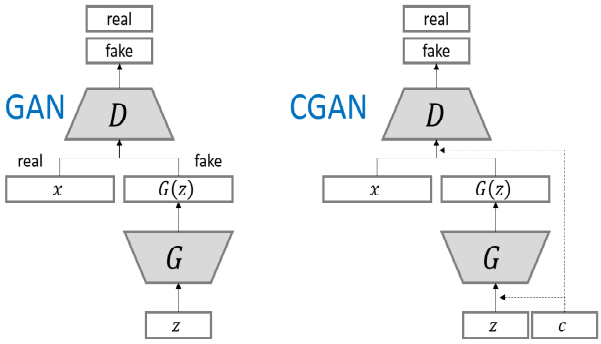


Figure 3.5: Comparison between the original Generative Adversarial Network (GAN) and conditional GAN (cGAN)

In contrast, a cGAN is a GAN that is conditioned on some additional information, such as class labels or image annotations. The generator network in a cGAN takes as input both a random noise vector and a condition vector, and generates a sample that is conditioned on the additional information. The discriminator network also takes as input both the sample and the condition vector, and tries to distinguish between real data and generated data based on the condition. Figure 3.5 illustrates the differences between the original GAN and the corresponding conditioned architecture.

The cGAN can be used for a variety of applications, such as image-to-image translation, where the additional information is an input image that is translated to a different output image. For example, a cGAN can be trained to convert grayscale images to color images, or to transform images of one type of object to another type of object.

The training process for a cGAN is similar to that of the original GAN, but the loss function for the generator and discriminator networks are modified to include the

condition vector. Specifically, the loss function for the generator network includes a term that measures how well the generated samples match the condition vector, in addition to the term that measures how well the generated samples fool the discriminator. Similarly, the loss function for the discriminator network includes a term that measures how well the discriminator can identify the condition vector, in addition to the term that measures how well it can distinguish between real and generated data.

The cGAN can be used for a variety of applications, such as image-to-image translation, where the additional information is an input image that is translated to a different output image. For example, a cGAN can be trained to convert grayscale images to color images, or to transform images of one type of object to another type of object.

### 3.3.4. Attention Mechanism

The attention mechanism is a computational method used in deep learning models to help the model focus on the most important parts of the input data. It is commonly used in natural language processing, speech recognition, and computer vision.

The basic idea of attention is to compute a set of weights that indicate the relative importance of different parts of the input. These weights are then used to compute a weighted sum of the input, which is used as the output of the attention mechanism.

The attention mechanism can be formulated mathematically using the following equations:

First, we compute a set of "keys", "values", and a "query" vector, which are used to compute the attention weights:

$$K = k_1, k_2, ..., k_n V = v_1, v_2, ..., v_n q = [q_1, q_2, ..., q_d] \tag{3.12}$$

where $n$ is the number of elements in the input, and $d$ is the dimension of the query vector. Next, we compute the attention weights using a function that compares the query vector to each of the keys:

$$a_i = \text{softmax}(q^T k_i) \tag{3.13}$$

where $a_i$ is the attention weight for the $i$th element of the input. Finally, we compute the output of the attention mechanism as a weighted sum of the values:

$$o = \sum_{i=1}^{n} a_i v_i \tag{3.14}$$

#### 3.3.4.1. Positional Encoding

In the attention mechanism, positional encoding is used to incorporate the order of the input sequence into the model. Positional encoding involves adding a fixed-length vector to the input embeddings that encodes the position of each element in the sequence.

The mathematical formulation of positional encoding is as follows:

$$\mathrm{PE}_{(pos,2i)} = \sin\left(\frac{pos}{10000^{2i/d}}\right) \tag{3.15}$$

$$\mathrm{PE}_{(pos,2i+1)} = \cos\left(\frac{pos}{10000^{2i/d}}\right) \tag{3.16}$$

where $pos$ is the position of the element in the sequence, $i$ is the index of the dimension, and $d$ is the dimension of the input embeddings. The positional encoding vectors are added to the input embeddings before they are passed through the self-attention mechanism.

The choice of the constants used in the positional encoding formulation, such as the use of the sine and cosine functions and the value of 10000, is arbitrary but has been shown to work well in practice. The positional encoding vectors add a sinusoidal pattern to the input embeddings that allows the model to distinguish between elements at different positions in the sequence.

Positional encoding has been shown to be an effective way of incorporating sequential information into transformer-based models, and it has been used successfully in a variety of natural language processing tasks, including machine translation, language modeling, and sentiment analysis.

#### 3.3.4.2. Multi-Head Attention

Multi-head attention is a type of attention mechanism used in deep learning models, particularly in transformer-based architectures, to allow the model to attend to multiple parts of the input simultaneously. It involves splitting the input into multiple heads and computing separate attention scores for each head, which are then combined to produce the final output.

The multi-head attention mechanism can be formulated mathematically using the following equations:

First, we split the keys, values, and query vectors into multiple "heads", each of which has its own set of learned weight matrices:

$$K_i = k_{i,1}, k_{i,2}, ..., k_{i,n} \tag{3.17}$$

$$V_i = v_{i,1}, v_{i,2}, ..., v_{i,n} \tag{3.18}$$

$$Q_i = q_{i,1}, q_{i,2}, ..., q_{i,n} \tag{3.19}$$

where $n$ is the number of elements in the input, and $i$ is the index of the head.

Next, we compute the attention weights and outputs for each head separately, using the same equations as in the basic attention mechanism:

$$a_{i,j} = \text{softmax}(Q_i^T K_{i,j}) \tag{3.20}$$

$$o_i = \sum_{j=1}^{n} a_{i,j} V_{i,j} \tag{3.21}$$

Finally, we concatenate the outputs from all the heads and multiply by a learned weight matrix to produce the final output:

$$\text{MultiHead}(Q, K, V) = \text{Concat}(\text{head}_1, \ldots, \text{head}_h) W^O \tag{3.22}$$

where $\text{head}_i$ is the output of the $i$th head, and $h$ is the number of attention heads.

The multi-head attention mechanism allows the model to attend to multiple parts of the input at once, which can be useful for capturing complex relationships between different parts of the input. It is often used in transformer-based architectures for natural language processing and other tasks.

#### 3.3.4.3. Self-Attention vs Cross-Attention

Self-attention is a type of attention mechanism used in deep learning models, particularly in transformer-based architectures, that allows the model to attend to different parts of the input sequence to compute a representation of each input element.

In self-attention, the input sequence is transformed into three different vectors: the query vector, the key vector, and the value vector. These vectors are then used to compute the attention score for each element of the input sequence with respect to every other element in the sequence. The attention scores are used to weight the value vectors, which are then combined to produce the final output.

The mathematical formulation of self-attention is as follows:

$$\text{SelfAttention}(X) = \text{softmax}\left(\frac{QK^T}{\sqrt{d_k}}\right) V \tag{3.23}$$

where $X$ is the input sequence, $Q$, $K$, and $V$ are the query, key, and value vectors, respectively, and $d_k$ is the dimension of the key vectors. The softmax function is applied row-wise to the matrix $\frac{QK^T}{\sqrt{d_k}}$, resulting in an attention matrix that has the same dimensions

as $X$. The attention matrix is then used to weight the value vectors $V$, which are combined to produce the final output.

The query, key, and value vectors are obtained through linear transformations of the input embeddings. The exact way in which these transformations are carried out can vary depending on the specific architecture, but in general they involve matrix multiplications with learnable weight matrices.

Self-attention has been shown to be a powerful mechanism for capturing long-range dependencies in sequential data, and it has been used successfully in a variety of natural language processing tasks, including machine translation, language modeling, and sentiment analysis.

On the other hand, in cross-attention, one of the input sequences serves as the query sequence, while the other sequence serves as the key-value sequence. The query sequence is transformed into a query vector, while the key-value sequence is transformed into key and value vectors. The query vector is then used to compute the attention score for each element in the query sequence with respect to every element in the key-value sequence. The attention scores are used to weight the value vectors, which are then combined to produce the final output.

The mathematical formulation of cross-attention is as follows:

$$\text{CrossAttention}(Q, K, V) = \text{softmax}\left(\frac{QK^T}{\sqrt{d_k}}\right)V \tag{3.24}$$

where $Q$, $K$, and $V$ are the query, key, and value vectors, respectively, and $d_k$ is the dimension of the key vectors. The softmax function is applied row-wise to the matrix $\frac{QK^T}{\sqrt{d_k}}$, resulting in an attention matrix that has the same dimensions as the query sequence. The attention matrix is then used to weight the value vectors, which are combined to produce the final output.

Compared to self-attention, which operates on a single sequence, cross-attention operates on two sequences. The key-value sequence provides additional information that can help the model compute more accurate representations of the elements in the query sequence. Cross-attention is commonly used in machine translation models, where one of the input sequences is the source language and the other sequence is the target language.

The main differences between self-attention and cross-attention are:

Self-attention operates on a single sequence, while cross-attention operates on two sequences. In self-attention, the query, key, and value vectors are all derived from the same input sequence, while in cross-attention, the key-value sequence provides the key and value vectors. Self-attention is used to capture relationships between elements within a sequence, while cross-attention is used to capture relationships between elements in different sequences.

#### 3.3.4.4. Transformer

Along this section the attention mechanism has been stated, from the main idea to the differences between self-attention and cross-attention. The Transformer model wraps-up all these concepts into a single and elegant architecture which allows the model to weigh the importance of different parts of the input sequence when computing a representation of each element in the sequence. Introduced in 2017 [115], it has become the absolute standard for Natural language Processing (NLP) tasks such as language modeling, question answering or machine translation. Figure 3.6 depicts the Transformer architecture proposed in the original paper.

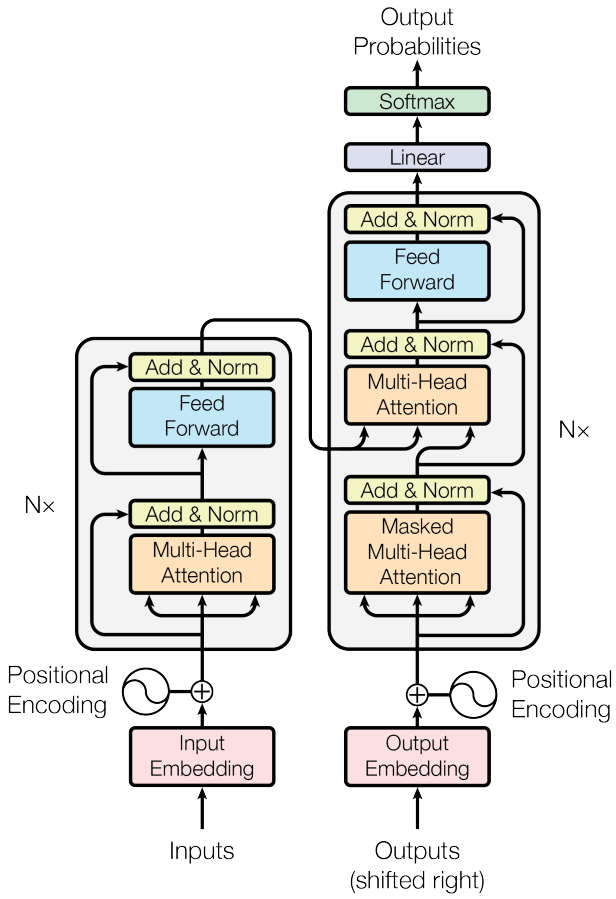


Figure 3.6: Overview of the Transformer architecture
Source: *Attention Is All You Need* [115]

The Transformer architecture consists of an encoder and a decoder. The encoder takes as input a sequence of embeddings, such as word embeddings or character embeddings, and produces a sequence of hidden states that capture the information in the input sequence. The decoder takes as input the encoder hidden states and produces a sequence of output embeddings that represent the output sequence.

The encoder consists of multiple layers, each of which contains two sub-layers: a self-attention sub-layer and a feedforward sub-layer. In the self-attention sub-layer, the model computes a representation of each element in the input sequence by attending to all

the other elements in the sequence. The feedforward sub-layer applies a pointwise fully connected layer to each position in the sequence independently and identically.

The decoder also consists of multiple layers, each of which contains three sub-layers: a self-attention sub-layer, a cross-attention sub-layer, and a feedforward sub-layer. In the self-attention sub-layer, the model attends to the previously generated output embeddings to compute the next output embedding. In the cross-attention sub-layer, the model attends to the encoder hidden states to incorporate information from the input sequence. The feedforward sub-layer applies a pointwise fully connected layer to each position in the sequence independently and identically.

The Transformer architecture uses residual connections and layer normalization to facilitate training of deep neural networks. Residual connections allow information to flow directly from one layer to another, bypassing the intermediate layers, which can help prevent the vanishing gradient problem. Layer normalization normalizes the input to each sub-layer to have zero mean and unit variance, which can help stabilize the training process.

Overall, the Transformer architecture has achieved state-of-the-art results on a wide range of natural language processing tasks, and its success has led to the development of a variety of transformer-based architectures, such as BERT, GPT, and T5.

### 3.3.5. Graphs

A Graph is the type of data structure that contains nodes and edges. A node can be a person, place, or thing, and the edges define the relationship between nodes. The edges can be directed and undirected based on directional dependencies.

Graphs are excellent in dealing with complex problems with relationships and interactions. They are used in pattern recognition, social networks analysis, recommendation systems, and semantic analysis. Creating graph-based solutions is a whole new field that offers rich insights into complex and interlinked datasets.

Nevertheless, Graph-based data structures have drawbacks, and researchers must understand them before developing graph-based solutions.

- A graph exists in non-euclidean space. It does not exist in 2D or 3D space, which makes it harder to interpret the data. To visualize the structure in 2D space, you must use various dimensionality reduction tools.

- Graphs are dynamic; they do not have a fixed form. There can be two visually different graphs, but they might have similar adjacency matrix representations. It makes it difficult for us to analyze data using traditional statistical tools.

- Large size and dimensionality will increase the graph's complexity for human interpretations. The dense structure with multiple nodes and thousands of edges is harder to understand and extract insights.

#### 3.3.5.1. Graph Neural Networks

GNNs are a class of neural networks that operate on graphs, which are collections of nodes and edges. A typical graph is represented by a set of node features, represented by a matrix $X \in \mathbb{R}^{N \times D}$, where $N$ is the number of nodes, and $D$ is the number of features associated with each node. Each node is also connected to other nodes via edges, which are represented by an adjacency matrix $A \in 0, 1^{N \times N}$, where $A_{ij} = 1$ if there is an edge between nodes $i$ and $j$, and 0 otherwise.

- A graph exists in non-euclidean space. It does not exist in 2D or 3D space, which makes it harder to interpret the data. To visualize the structure in 2D space, you must use various dimensionality reduction tools.
- Graphs are dynamic; they do not have a fixed form. There can be two visually different graphs, but they might have similar adjacency matrix representations. It makes it difficult for us to analyze data using traditional statistical tools.
- Large size and dimensionality will increase the graph's complexity for human interpretations. The dense structure with multiple nodes and thousands of edges is harder to understand and extract insights.

The basic idea behind GNNs is to iteratively update the node representations using information from the graph neighborhood. Specifically, at each iteration, each node aggregates information from its neighbors, and the resulting aggregated representation is used to update the node's own representation. This process is typically repeated for multiple iterations until convergence. GNNs were introduced when Convolutional Neural Networks failed to achieve optimal results due to the arbitrary size of the graph and complex structure.

One common way to implement this idea is to use the following update rule:

$$h_i^{(l+1)} = f(h_i^{(l)}, \sum_j A_{ij} h_j^{(l)}) \tag{3.25}$$

where $h_i^{(l)}$ is the representation of node $i$ at iteration $l$, $f$ is a non-linear activation function, and $\sum_j A_{ij} h_j^{(l)}$ is the sum of the representations of the neighbors of node $i$ at iteration $l$.

By stacking multiple layers of such updates, a GNN can learn increasingly complex representations of the graph.

There are several types of neural networks, such as:

- Graph Auto-Encoder Networks, which learn graph representation using an encoder and attempt to reconstruct input graphs using a decoder. They are commonly used in link prediction as Auto-Encoders are good at dealing with class balance.
- Recurrent Graph Neural Networks(RGNNs) are able to learn the best diffusion pattern, and they can handle multi-relational graphs where a single node has multiple relations. They are commonly used in generating text, machine translation, speech recognition or generating image descriptions
- Gated Graph Neural Networks (GGNNs) improve Recurrent Graph Neural Networks by adding a node, edge, and time gates on long-term dependencies, being the common uses similar to RGNNs.

Nevertheless, in this work we focus on a particular type of GNN, that is, Graph Convolutional Networks, which are the most common GNN type used in of MP in the field of AD.

#### 3.3.5.2. Graph Convolutional Networks

The majority of GNNs are Graph Convolutional Networks (GCNs), which are a specific type of GNN that use convolutional operations to aggregate information from the graph neighborhood. GCNs were introduced when Convolutional Neural Networks failed to achieve optimal results due to the arbitrary size of the graph and complex structure. The basic idea behind GCNs is to treat the graph as a signal and use convolutional operations to extract features by inspecting neighboring nodes. GCNs aggregate node vectors, pass the result to the dense layer, and apply non-linearity using the activation function.

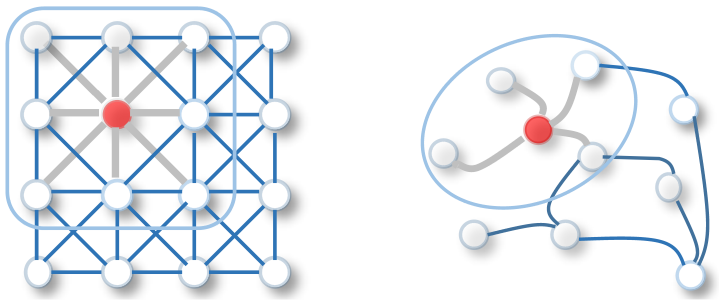

Figure 3.7: Overview of the sliding kernel of a 2D-CNN vs GCN
Source: *A comprehensive survey on graph neural networks* [116]

The major difference between GCN and CNN is that it is developed to work on non-euclidean data structures where the order of nodes and edges can vary, as it can be

appreciated in Figure 3.7. In 2D convolution, each pixel in an image is taken as a node where neighbours are determined by the filter size. The 2D convolution takes the weighted average of pixel values of the red node along with its neighbors. The neighbours of a node are ordered and have a fixed size. On the other hand, to get a hidden representation of a given node red, one simple solution of the graph convolutional operation is to take the average value of the node features of the red node along with its neighbors. Different from image data, the neighbors of a node are unordered and variable in size.

The convolution in GCN is the same as a convolution in convolutional neural networks. It multiplies neurons with weights (filters) to learn from data features. A convolutional operation on a graph is defined as:

$$H^{(l+1)} = \sigma(D^{-\frac{1}{2}}AD^{-\frac{1}{2}}H^{(l)}W^{(l)}) \tag{3.26}$$

where $H^{(l)}$ is the matrix of node representations at iteration $l$, $W^{(l)}$ is the weight matrix of the $l$-th layer, $A$ is the adjacency matrix of the graph, $D$ is the degree matrix of the graph, and $\sigma$ is a non-linear activation function.

The operation $D^{-\frac{1}{2}}AD^{-\frac{1}{2}}$ is a normalization step that scales the adjacency matrix by the inverse square root of the degree matrix. This normalization ensures that nodes with different degrees have similar influence in the convolutional operation. By stacking multiple layers of such convolutions, a GCN can learn increasingly complex features of the graph.

### 3.3.6. Training

Training is the process of iterating through a dataset to make the network learn the optimal mapping (combination of weights) from input to desired output in the data samples. In each iteration, a forward pass through the network is performed, computing the output of each layer until the end. This produces the output response of the network, which is then compared to a desired output with a defined Loss function (L). This function estimates the amount of error, which is back-propagated through the network to update its weights with the aim of minimizing the error.

Regarding the supervised training paradigm, Backpropagation is an algorithm used for training artificial neural networks (ANNs) used to update the weights and biases of the neurons in the network based on the error between the predicted output and the actual output.

The backpropagation algorithm consists of two phases: the forward pass and the backward pass. During the forward pass, the input is fed into the network and propagated through the layers to obtain the predicted output. During the backward pass, the error between the predicted output and the actual output is computed and used to update the weights and biases of the neurons in the network.

The backpropagation algorithm is based on the chain rule of calculus, which allows the gradient of the loss function with respect to each weight and bias to be computed recursively from the output layer to the input layer of the network. The gradient descent algorithm is then used to update the weights and biases in the direction of the negative gradient of the loss function. In that sense, the main losses used in this work are described throughout the remaining content of this Chapter.

#### 3.3.6.1. Optimizer and learning rate

There are several optimizers commonly used for training deep neural networks in the literature, such as Stochastic Gradient Descent (SGD) [117], Adagrad [118], Root Mean Square Propagation (RMSprop) [119] or Adadelta [120]. In this work we use one of the most extended, the ADAM [121] optimizer. It is a popular optimization algorithm used in deep learning, particularly for training neural networks. It is an adaptive learning rate optimization algorithm that is well suited for large datasets and high-dimensional parameter spaces.

The basic idea behind ADAM is to compute adaptive learning rates for each parameter based on estimates of the first and second moments of the gradients. The algorithm computes a moving average of the gradients and their squared values, and uses these estimates to update the parameters with a learning rate that adapts to the local curvature of the loss function. The algorithm also includes bias-correction terms to ensure that the estimates are unbiased, especially in the early stages of training when the estimates are highly uncertain.

The update rule for ADAM can be expressed mathematically as follows:

$$\begin{aligned} m_t &= \beta_1 m_{t-1} + (1-\beta_1) g_t \\ v_t &= \beta_2 v_{t-1} + (1-\beta_2) g_t^2 \\ \hat{m}_t &= \frac{m_t}{1-\beta_1^t} \\ \hat{v}t &= \frac{v_t}{1-\beta_2^t} \\ \theta t + 1 &= \theta_t - \frac{\alpha}{\sqrt{\hat{v}_t} + \epsilon} \hat{m}_t \end{aligned} \tag{3.27}$$

where $\theta_t$ is the parameter vector at time step $t$, $g_t$ is the gradient vector, $m_t$ and $v_t$ are the first and second moment estimates at time step $t$, $\hat{m}_t$ and $\hat{v}_t$ are the bias-corrected moment estimates, $\alpha$ is the learning rate, $\beta_1$ and $\beta_2$ are the decay rates for the moment estimates, and $\epsilon$ is a small constant to prevent division by zero.

The algorithm starts with initializing $m_0$ and $v_0$ as zero vectors, and $\theta_0$ as the initial parameter vector. At each iteration, the gradient vector $g_t$ is computed using a batch of

training data, and the moment estimates $m_t$ and $v_t$ are updated according to the first two lines of the update rule. The bias-corrected moment estimates $\hat{m}_t$ and $\hat{v}_t$ are then computed using the next two lines of the update rule. Finally, the parameter vector $\theta_t$ is updated using the last line of the update rule.

The hyperparameters $\alpha$, $\beta_1$, $\beta_2$, and $\epsilon$ can be tuned to optimize performance on a particular dataset and neural network architecture.

On the other hand, The learning rate is a key hyperparameter in the optimization process of machine learning algorithms, including optimizer updates like the ADAM optimizer. The learning rate controls the step size taken in the direction of the negative gradient during each iteration of the optimization process.

If the learning rate is too small, the optimization process will be slow and may get stuck in local minima. On the other hand, if the learning rate is too large, the optimization process may overshoot the minimum and oscillate back and forth, or even diverge.

In the context of the ADAM optimizer, the learning rate is used to adjust the size of the update step taken in the direction of the estimated gradient. The update step is multiplied by the learning rate, which determines the size of the step. A larger learning rate will result in larger update steps, and a smaller learning rate will result in smaller update steps.

In practice, the learning rate is usually set through a process called hyperparameter tuning, where different values of the learning rate are tried on a validation set to find the optimal value that results in the best performance of the model on the test set.

One common technique to adjust the learning rate during training is called learning rate scheduling. This involves decreasing the learning rate over time, often according to a predetermined schedule or based on the performance of the model on a validation set. This technique can help improve the convergence and stability of the optimization process, particularly in the later stages of training when the model is close to the optimal solution.

Overall, the learning rate plays a crucial role in the optimization process of machine learning algorithms, including optimizer updates like the ADAM optimizer. Selecting an appropriate learning rate is important for achieving fast and stable convergence to the optimal solution.

#### 3.3.6.2. Regression losses

A regression loss is a type of loss function used in regression problems to measure the difference between the predicted and true values of a continuous variable. In other words, it is a way to quantify how well a machine learning model is able to predict numerical values based on input data.

In regression problems, the goal is to learn a function that maps input features to output values. A regression loss is used to train the model by penalizing the difference between the predicted and true output values. The loss function is typically minimized during training, so that the model learns to make more accurate predictions. There are several types of regression loss functions, such as the Quantile loss, Log-Cosh or Mean Absolute Error (MAE). In this work we mainly focus on the Mean Square Error (MSE) and SmoothL1, also known as Huber loss.

**3.3.6.2.1. Mean Square Error loss** The Mean Squared Error (MSE) loss is a commonly used loss function in regression problems. It measures the average squared difference between the predicted and true values of a continuous variable. The MSE loss is given by:

$$MSE(y, \hat{y}) = \frac{1}{n}\sum_{i=1}^{n}(y_i - \hat{y}_i)^2 \tag{3.28}$$

where $y_i$ is the true value of the $i$-th data point, $\hat{y}_i$ is the predicted value, and $n$ is the number of data points.

The MSE loss penalizes large errors more strongly than small errors, since it uses the square of the difference between the predicted and true values. This makes it sensitive to outliers and can lead to overfitting if the data contains extreme values.

The MSE loss is used in many regression problems, such as linear regression, polynomial regression, and neural networks. It is often used as a performance metric to evaluate the quality of the model's predictions.

**3.3.6.2.2. SmoothL1 loss** SmoothL1 loss, also known as Huber loss, is a loss function used in regression problems to measure the difference between the predicted and true values of a continuous variable. It is a variant of the L1 loss that is less sensitive to outliers and has a smooth gradient near zero.

The SmoothL1 loss function can be defined as follows:

$$L(y, \hat{y}) = \begin{cases} \frac{1}{2}(y - \hat{y})^2 & \text{if } |y - \hat{y}| < 1 \\ |y - \hat{y}| - \frac{1}{2} & \text{otherwise} \end{cases} \tag{3.29}$$

where $y$ is the true value, $\hat{y}$ is the predicted value, and $|\cdot|$ represents the absolute value function.

The SmoothL1 loss function behaves like the L1 loss for small errors and like the L2 loss for large errors. Specifically, for errors smaller than 1, it uses the squared difference

between the predicted and true values, which has a smooth gradient. For larger errors, it uses the absolute difference, which is less sensitive to outliers than the squared difference.

The SmoothL1 loss is used in regression problems when the data contains outliers or when the model needs to be less sensitive to large errors. It is commonly used in object detection and localization tasks, where the predicted bounding boxes can be highly sensitive to small changes in the input data.

**3.3.6.2.3. Softmax loss** The softmax loss, also known as the cross-entropy loss, is a commonly used loss function in classification problems. It measures the difference between the predicted probability distribution and the true probability distribution of a categorical variable. The softmax loss is given by:

$$CE(y, \hat{y}) = -\frac{1}{n} \sum_{i=1}^{n} \sum_{j=1}^{k} y_{i,j} \log(\hat{y_{i,j}}) \tag{3.30}$$

where $y_{i,j}$ is the true probability of the $i$-th data point belonging to class $j$, $\hat{y_{i,j}}$ is the predicted probability, $n$ is the number of data points, and $k$ is the number of classes.

The softmax function is applied to the output of the model to obtain a probability distribution over the classes. The predicted probability of class $j$ is given by:

$$\hat{y_{i,j}} = \frac{e^{z_{i,j}}}{\sum_{l=1}^{k} e^{z_{i,l}}} \tag{3.31}$$

where $z_{i,j}$ is the unnormalized score or logit for class $j$ of the $i$-th data point.

The softmax loss penalizes the model more heavily for predictions that are far from the true probabilities. It encourages the model to assign higher probabilities to the correct classes and lower probabilities to the incorrect classes.

The softmax loss is used in many classification problems, such as image classification, natural language processing, and speech recognition. It is often used as a performance metric to evaluate the quality of the model predictions.

**3.3.6.2.4. Negative Log-Likelihood loss** Negative Log Likelihood (NLL) loss is a loss function commonly used in classification problems, particularly in deep learning models that output probabilities for each class. It is a type of maximum likelihood estimation (MLE) loss, which means it attempts to maximize the likelihood of the predicted probabilities given the true labels.

The NLL loss function can be defined as follows:

$$L(y_i, \hat{y_i}) = -\log(\hat{y_{i,y_i}}) \tag{3.32}$$

where $y_i$ is the true label of the $i$-th data point, $\hat{y}_i$ is the predicted probability distribution for that point, and $\hat{y_{i,y_i}}$ is the predicted probability for the true label.

The NLL loss penalizes the model for assigning low probabilities to the true label, while rewarding it for assigning high probabilities. It is a logarithmic loss function, which means that the penalty for low probabilities increases exponentially as the predicted probability approaches zero.

The NLL loss is used in classification problems because it provides a gradient that can be used to update the model parameters during training, in order to improve the accuracy of the predicted probabilities. It is commonly used in conjunction with softmax activation function, which ensures that the predicted probabilities sum to one across all classes.

**3.3.6.2.5. Winner-Takes-All loss** Winner-Takes-All (WTA) loss is a loss function used in clustering problems, particularly in competitive learning models. It is a type of unsupervised learning, which means that it does not require labeled data for training.

The WTA loss function can be defined as follows:

$$L(y_i, f(x_i)) = \begin{cases} 0 & \text{if } y_i = \arg\max_j f_j(x_i) \\ 1 & \text{otherwise} \end{cases} \tag{3.33}$$

where $y_i$ is the true cluster of the $i$-th data point, $f_j(x_i)$ is the activation of the $j$-th neuron in the output layer for that point, and $\arg\max_j f_j(x_i)$ is the index of the neuron with the highest activation.

The WTA loss function penalizes the model for assigning a data point to the wrong cluster. It works by forcing each neuron in the output layer to specialize in a particular cluster, such that the neuron with the highest activation for a given point corresponds to the true cluster of that point.

The WTA loss is used in clustering problems because it encourages the model to learn a set of representative clusters that capture the structure of the data, without requiring any prior knowledge of the true labels. It is commonly used in conjunction with competitive learning algorithms, such as self-organizing maps (SOMs), that use local competition between neurons to learn a topology-preserving mapping from the input space to the output space.

**3.3.6.2.6. Hinge loss** Hinge loss is a loss function used in classification problems, particularly in support vector machines (SVMs). It is a type of max-margin loss, which means it attempts to maximize the margin between the decision boundary and the data points.

The hinge loss function can be defined as follows:

$$L(y_i, f(x_i)) = \max(0, 1 - y_i f(x_i)) \tag{3.34}$$

where $y_i$ is the true label of the $i$-th data point, $f(x_i)$ is the predicted score for that point, and 1 is a margin hyperparameter that determines the width of the margin.

If $y_i f(x_i) \geq 1$, then the point is correctly classified and the loss is zero. If $y_i f(x_i) < 1$, then the point is misclassified and the loss is proportional to the distance between the predicted score and the correct score. The loss function penalizes misclassifications linearly, with a slope of -1 for negative misclassifications and 0 for positive misclassifications.

The hinge loss is used in SVMs because it encourages the model to find a decision boundary that maximizes the margin between the classes, while still correctly classifying the data points. This results in a more robust and generalizable model.

#### 3.3.6.3. Regularization techniques

Regularization techniques in deep learning are used to prevent overfitting and improve the generalization performance of a model. Overfitting occurs when a model fits the training data too closely and captures noise or irrelevant patterns, resulting in poor performance on new, unseen data. Here are some commonly used regularization techniques in deep learning:

L1 and L2 regularization: L1 and L2 regularization are two popular regularization techniques that add a penalty term to the loss function during training. L1 regularization adds the sum of the absolute values of the weights to the loss function, while L2 regularization adds the sum of the squares of the weights. This encourages the model to learn simpler and more generalizable representations by shrinking the weights towards zero.

Dropout: Dropout is a regularization technique that randomly drops out some units (neurons) in a layer during training. This forces the remaining units to learn more robust and diverse representations that generalize better to new data. Dropout has been shown to be effective in reducing overfitting, particularly in deep neural networks with many layers.

Data augmentation: Data augmentation is a technique that artificially increases the size of the training set by generating new examples from existing ones. This can be done by applying transformations such as rotations, translations, flips, or adding noise to the input data. Data augmentation can help reduce overfitting by increasing the diversity of the training data and improving the generalization performance of the model.

Early stopping: Early stopping is a technique that monitors the performance of the model on a validation set during training and stops the training process when the performance starts to degrade. This prevents the model from overfitting to the training data and allows it to generalize better to new data.

Batch normalization: Batch normalization is a technique that normalizes the activations of a layer by subtracting the batch mean and dividing by the batch standard deviation. This helps stabilize the distribution of the activations and reduces the internal covariate shift, which can improve the training process and reduce overfitting.

Weight decay: Weight decay is a technique that adds a penalty term to the loss function during training, similar to L2 regularization. The penalty term is proportional to the square of the weights, and it encourages the model to learn smaller and simpler weights, which can reduce overfitting.

These are some of the commonly used regularization techniques in deep learning. They can be combined and tuned to improve the performance of a model on a specific task and dataset.

Moreover, another interesting technique to help the model improve during training is hard-mining. Hard-mining is a technique in deep learning used to improve the training of a model by focusing on the samples that are most difficult to classify correctly.

During training, the model makes predictions on a batch of training data, and the loss function is computed based on the difference between the predicted values and the true values. In hard-mining, the training samples that contribute the most to the loss function are identified, and these samples are given more importance during training.

The idea behind hard-mining is that by focusing on the difficult samples, the model is forced to learn more discriminative features that can better distinguish between the different classes. This can lead to better generalization performance and improved accuracy on the test data.

There are several ways to implement hard-mining in deep learning, including:

- Hard negative mining involves selecting the training samples that are misclassified with the highest confidence by the model and including them in the next batch of training data. By focusing on the difficult negative samples, the model can learn to better distinguish between the different classes and reduce the number of false negatives.
- Hard positive mining involves selecting the training samples that are misclassified with the lowest confidence by the model and including them in the next batch of training data. By focusing on the difficult positive samples, the model can learn to better distinguish between the different classes and reduce the number of false positives.
- Curriculum learning involves gradually increasing the difficulty of the training data over time. The model is first trained on easy samples and then gradually exposed to more difficult samples. This can help the model learn more robust and generalizable features by gradually increasing the complexity of the training data.

- Overall, hard-mining is a useful technique in deep learning for improving the training of a model by focusing on the difficult samples. By incorporating hard-mining into the training process, the model can learn more discriminative features and improve its generalization performance on new, unseen data.

## 3.4. Summary

In this chapter, the mathematical background of various physics-based and DL-based techniques used for MP models is thoroughly examined. The chapter aims to provide a comprehensive understanding of these methods and their applications in the field of motion prediction.

The chapter begins by introducing the physics-based techniques, starting with the Kalman Filter. The Kalman Filter is a recursive algorithm used to estimate the state of a dynamic system by incorporating noisy measurements. Its mathematical foundation, including the state-space model and the prediction and update steps, is discussed in detail. Next, the Hungarian Algorithm is presented, which is a combinatorial optimization algorithm used for data association in multiple object tracking. The chapter delves into the mathematical formulation of the Hungarian Algorithm and how it can be applied to motion prediction tasks.

Moving on to the physics-based models, the chapter explores the CTRV and CTRA models. These models are widely used for trajectory prediction and capture the motion dynamics of objects by considering their position, velocity, and acceleration. The mathematical equations for these models are examined, highlighting how they can be utilized to predict future motion paths.

The chapter then transitions to deep learning-based techniques, which have gained significant attention in recent years due to their ability to capture complex patterns and dependencies in data. Several models are discussed in detail, starting with the 1D-Convolutional Neural Network (CNN). The mathematical architecture of the 1D-CNN is explained, emphasizing its ability to extract spatial and temporal features from sequential data for motion prediction.

Next, the LSTM model is introduced, which is a type of recurrent neural network (RNN) specifically designed to handle sequence data. The chapter provides an overview of the LSTM architecture, including its memory cell and gate mechanisms, which enable it to capture long-term dependencies and predict future motion accurately.

The chapter then explores GANs and their application in motion prediction. GANs consist of a generator and discriminator network that compete against each other, resulting in the generation of realistic and coherent motion trajectories. The mathematical formulation of GANs and their training process are examined in detail.

Furthermore, the Graph Convolutional Network (GCN) is discussed, which is a deep learning model capable of operating on graph-structured data. The chapter explains how GCNs can be used to represent and predict motion patterns in scenarios where objects interact with each other.

Finally, the Attention mechanism is examined, which is a component commonly integrated into deep learning models to focus on relevant parts of the input data. The chapter explores the mathematical formulation of the Attention mechanism and its application in motion prediction models, highlighting its ability to assign different weights to different input features based on their relevance.

Overall, this chapter provides a comprehensive overview of the mathematical foundations of various physics-based and deep learning-based techniques used in motion prediction models. By understanding the underlying principles and equations of these models, researchers and practitioners can gain a deep understanding of their capabilities and make informed decisions regarding their application in different scenarios.

# Chapter 4

# SmartMOT: Exploiting the fusion of HD maps and Multi-Object Tracking for Real-Time scene understanding

*Avanzad, sin temor a la oscuridad.*
*Luchad jinetes de Theoden.*
*Caerán las lanzas, se quebrarán los escudos.*
*Aún restará la espada.*
*Rojo será el día, hasta el nacer del sol.*
*Cabalgad, cabalgad, cabalgad hacia la desolación*
*y el fin del mundo. Muerte, muerte, muerte.*

Discurso de Theoden, Rey de Rohan
El Señor de los Anillos: El Retorno del Rey

## 4.1. Introduction

In order to achieve a reliable navigation, ADSs must perform safe driving behaviours following conventional traffic rules. In that sense, the perception layer represents one of the most important modules of an Autonomous Driving (AD) stack, responsible of analyzing the online information, also referred as the traffic situation, through the use of a global perception system [122] which involves different on-board sensors as: Light Detection And Ranging (LiDAR), Inertial Measurement Unit (IMU) , RAdio Detection And Ranging (RADAR), Differential-Global Navigation Satellite System (D-GNSS), Wheel odometers or Cameras.

One of the key concepts when developing safe ADSs is the perception of the environment. Furthermore, the reliability of a Collision Avoidance System (CAS) lies on the performance of the environment detector and its ability to predict future situations. In that sense, a real-time MOT system, which goal is to associate detections (usually in the 3D or BEV space) in a sequence, is essential for AD applications, representing in most

cases the preliminary stage before predicting the subsequent future trajectories of these obstacles in the scene, giving the car a valuable reaction time to avoid critical situations or to anticipate its behaviour for the corresponding traffic scenario. The improvements in object detection in the last years have allowed the research community, specially those groups related to AD, to focus on MOT techniques as a preliminary stage before implementing MP, yielding higher accuracy at the cost of computational cost and complexity, making its use prohibitive in real-time systems.

MOT systems aim to estimate the orientation, location and scale of all the objects in the environment over time. While object detection only captures the information of the environment in a single frame, a tracking system must take temporal information into account, filtering outliers (*a.k.a.*false positives) in consecutive detections and being robust to partial or full occlusions. When travelling throughout a route programmed by the path-planner, the vehicle may detect an undetermined number of unforeseen objects over which the MOT module should consider only the most relevant from a safety point of view (such as pedestrians, cyclists or cars) to predict and monitor their trajectories. Then, the vehicle can use the evolution of the scene over time to infer driving behaviour and motion patters for improved MP.

Most MOT approaches [123], [124] model the state of each obstacle with its 3D position, scale, orientation and their corresponding linear and angular velocity. These approaches introduce an unnecessary complexity and computational cost to the system since most traffic scenes can be described in terms of 2D position, angular and linear velocity, apart from the orientation and scale of the resulting bounding box, that is, a BEV perspective, as depicted in Figure 4.1.

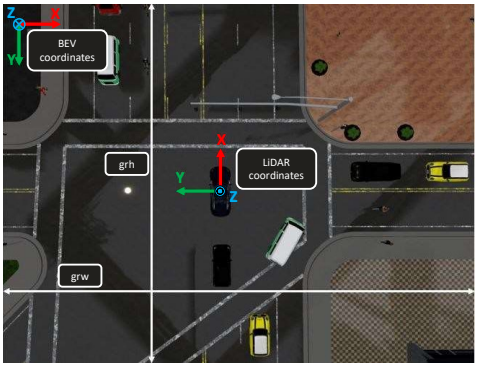


Figure 4.1: LiDAR to BEV coordinates transformation illustrated in the CARLA simulator

## 4.2. SmartMOT

In order to solve the problem of monitoring the relevant objects in an efficient way, we propose SmartMOT [125], a simple-yet-accurate combination of traditional techniques such as the Kalman Filter (KF) [25] and Hungarian algorithm (HA) [111] for state es-

timation and data association respectively to solve the tracking-by-detection paradigm. Moreover, as mentioned in Section 4.1, the core interest of SmartMOT is the incorporation of HD map semantic, geometric and topological information, in addition to the ego-vehicle status, so as to enhance the efficiency and reliability of the tracking system and subsequent predictions, as observed in Figure 4.2.

The remaining content of this chapter summarizes the SmartMOT pipeline, being made up by: (1) 3D object detection module that returns the bounding boxes; (2) Monitored Area computation to filter non-relevant objects, *e.g.*the VRUs that are inside the sidewalk far away the road or the vehicles that are located in a lane in which lane change is not allowed, (3) BEV Kalman filter that predicts the object state from the current frame and updates the object state based on the detected bounding boxes at current frame, (4) Hungarian algorithm which associates the current trackers with new detections, (5) Birth and Death memory that deals with the disappeared trajectories (unmatched trajectories exceeding $age_{max}$ frames) and the newly appeared trajectories (matched trajectories exceeding $f_{min}$ frames) and finally (6) CTRV model which performs short-term physics-based motion prediction of the updated trackers information using both the linear and angular velocity information. As observed, except for the pre-trained object detector module (or ground-truth with the corresponding noise, if used), our MOT system does not need any training and can be directly used for inference.

### 4.2.1. 3D Object Detection

The first step our MOT algorithm must carry out is to detect the obstacles in the environment around the ego-vehicle. As we will see in Chapter **??**, in order to avoid perspective distortion, we make use of some well known 3D and 2D object detection approaches [126], [127] to perform sensor fusion and retrieve the bounding boxes in the 3D space. Nevertheless, since this thesis do not focus on the object detection stage of the perception layer, some experiments are conducted assuming ground-truth detection including Gaussian noise in the $x$,$y$,$z$ to simulate real-world detections. Then, at a given frame $t$, the detections provided by the object detection module are given in the following form:

$$\mathbf{D}_t = [\mathbf{D}_t^1, \mathbf{D}_t^2, ..., \mathbf{D}_t^N] \tag{4.1}$$

Where $N$ is the number of detected 3D bounding boxes at a given frame and threshold. At this point, instead of using all the 3D information of the object [123], [124], we take its projection on the floor plane (BEV information), to reduce the complexity and computational cost of the tracking stage, specially in those urban scenarios full of vehicles, based on the assumption that the height ($z$) dimension is not as important as other coordinates ($x$-axis, $y$-axis) in a context of self-driving navigation. Detected 3D bounding boxes are

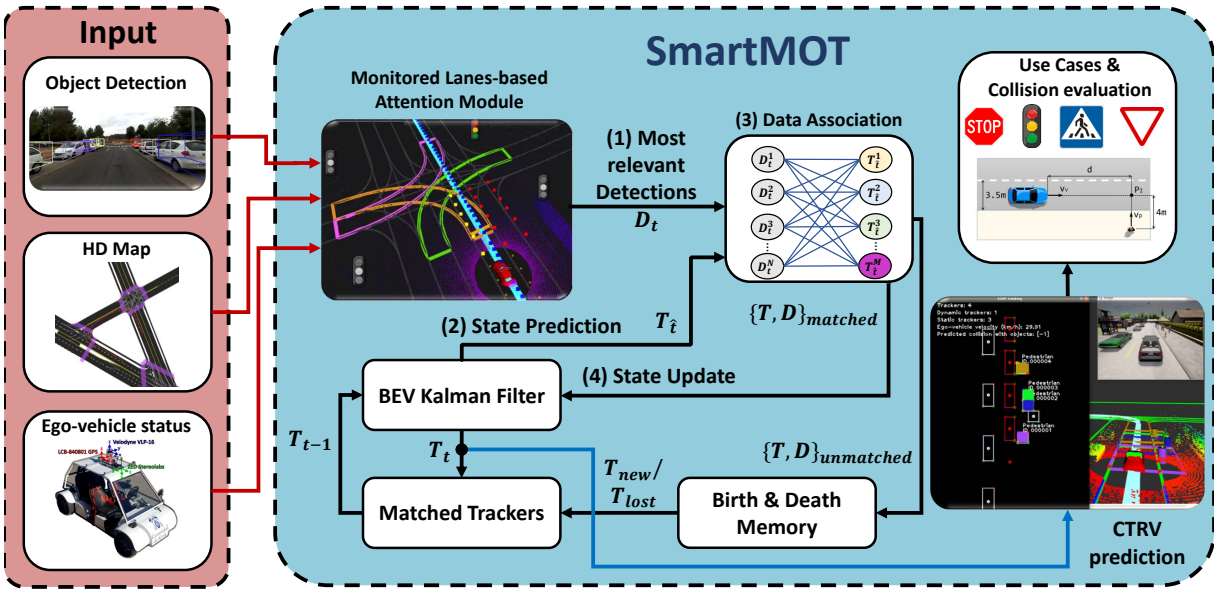


Figure 4.2: **SmartMOT pipeline**: **(1)** The object detection module, mapping layer and localization layer provide the 3D bounding boxes at frame $t$, monitored lanes and ego-vehicle status data respectively; **(2)** A Monitored Lanes-based Attention Module filters the non-relevant traffic participants and transforms the remaining into the BEV image plane; **(3)** A BEV Kalman filter predicts the state of trajectories in frame *t-1* to current frame $\hat{t}$ throughout the prediction step; **(4)** detections at frame $t$ and predicted trajectories at $\hat{t}$ are matched using the Khun-Munkres (*a.k.a.*Hungarian) algorithm; **(5)** matched trajectories are updated based on their corresponding matched detections and every tracker is evaluated again based on its particular monitorized area, to obtain updated trajectories at frame $t$; **(6)** Unmatched trajectories and detections are used to delete disappeared trajectories or create new ones respectively; **(7)** Updated trackers at frame $t$ are predicted using a CTRV model and then evaluated using the monitors module.

referred to the LiDAR coordinate system. A grid is applied to establish a relation between real-world and image dimensions to discretize the possible positions of the detected bounding boxes and decrease the complexity and computational cost of the tracking module. This grid is featured by a rectangle, whose center is located at the LiDAR position on the vehicle, where *grw* and *grh* represent its width and height in LiDAR coordinates $m$ (meters) respectively. Then, each detection in Equation 4.2 is represented as the tuple:

$$\mathbf{D}_t^i = [x_m, y_m, w_m, l_m, \theta, type, score] \tag{4.2}$$

Where $x_m, y_m$ correspond to the object centroid in LiDAR coordinates $(m)$, $w_m$ and $l_m$ correspond to the width and length of the object respectively $(m)$, $\theta$ its orientation angle around the LiDAR Z-axis, object type and detection confidence. Figure 4.1 illustrates the transformation from the source coordinate system (LiDAR), measured in $m$ and placed at the ego-vehicle, to the target coordinate system (BEV), measured in $px$ (pixels) and placed on the top-left corner of the grid, which is the most common way to work with images in computer vision. In other words, we deal with the MOT problem from the BEV image perspective, in order to adapt MOT algorithms originally designed for computer vision purposes.

Equations 4.3 and 4.4 show the transformation matrix between both coordinate systems, including both the rotation and the translation ($\frac{gw}{2}$ and $\frac{gh}{2}$), where a $\mathbf{LiDAR}_{point} = [x_m, y_m, z_m, 1]^T$ is given as the column vector in homogeneous coordinates.

$$\mathbf{T} = \begin{bmatrix} 0 & -1 & 0 & \frac{grw}{2} \\ -1 & 0 & 0 & \frac{grh}{2} \\ 0 & 0 & -1 & 0 \\ 0 & 0 & 0 & 1 \end{bmatrix} \tag{4.3}$$

$$\mathbf{BEV}_{point} = \mathbf{T} \cdot \mathbf{LiDAR}_{point} \tag{4.4}$$

At this point, each detection is represented by the tuple shown in Equation 4.2, but now $x_m, y_m$ represent the obstacle centroid in BEV image perspective. Furthermore, the resolution of the BEV image can be modified, in such a way the image width in pixels is given to the algorithm and the image height is calculated according to the aspect ratio of the real world with respect to the width of the image in pixels. Finally, to convert a point from real-word units $(m)$ to camera units $(px)$, we apply the corresponding scale factor to each coordinate:

$$\begin{bmatrix} x_{px} \\ y_{pc} \end{bmatrix} = \begin{bmatrix} \frac{gpw}{grw} & 0 \\ 0 & \frac{gph}{grh} \end{bmatrix} \begin{bmatrix} x_m \\ y_m \end{bmatrix} \tag{4.5}$$

However, it is very common to have different scales for $x$ and $y$-axis since it is more interesting to have a further view in the $x$ LiDAR axis rather than a large side sweep in terms of $y$ LiDAR axis. Considering this hypothesis, the right way to obtain the width and length of the BEV LiDAR bounding box in *pixels* is to obtain the corners of the rotated bounding box in pixels and then compute the *L2* (*a.k.a.*Euclidean distance) among the corresponding corners to obtain the width and length in *pixels*. Nevertheless, the object detector provides the rotation angle of the obstacle (featured as $\theta$) according to its own coordinate system and not around the ego-vehicle coordinate system. Regarding this constraint, to calculate the dimensions of the bounding box in pixels, three steps must be followed:

$$c1_m = (x_m - \frac{l_m}{2}, y_m - \frac{w_m}{2})$$
$$c2_m = (x_m - \frac{l_m}{2}, y_m + \frac{w_m}{2})$$
$$c3_m = (x_m + \frac{l_m}{2}, y_m - \frac{w_m}{2})$$
$$c4_m = (x_m + \frac{l_m}{2}, y_m + \frac{w_m}{2})$$

First, we assume a horizontal bounding box ($\theta = 0$) at the BEV image coordinate system origin, where *c1* corresponds to the top-left corner (*c2*, *c3* and *c4* are placed clockwise). Then, using the above equations for each corner, the Euclidean distance is applied between *c1* and *c2* to obtain the width in pixels, in the same way that the Euclidean distance is applied between *c1* and *c4* to obtain the length in pixels.

$$w_{px} = \sqrt{(c1_{px,x} - c2_{px,x})^2 + (c1_{px,y} - c2_{px,y})^2} \tag{4.6}$$

$$l_{px} = \sqrt{(c4_{px,x} - c2_{px,x})^2 + (c4_{px,y} - c2_{px,y})^2} \tag{4.7}$$

Finally, the first four variables of the detection tuple shown in Equation 4.2 are converted into pixels, in such a way the tracking algorithm will monitor these bounding boxes in the BEV image by using the following tuple:

$$\mathbf{D}_{t,i} = [x_{px}, y_{px}, w_{px}, l_{px}, \theta, type, score] \tag{4.8}$$

### 4.2.2. Monitored Lanes-based Attention Module

ADSs need to locate itself in the environment to know what is happening around in order to make decisions and execute a correct navigation like a human driver would. When we talk about localization, the first thing we need is a map where to be located

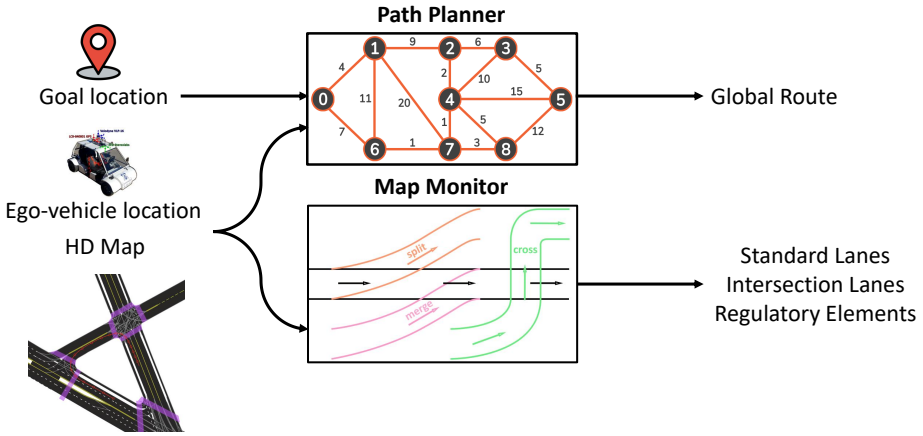


Figure 4.3: Path Planning and Map Monitoring Outline

and, particularly for vehicles, this is road map. Road maps used by current navigators, *e.g.*Google Maps, are not valid for AV because of data type and the fact that they are not accurate enough to be used for autonomous driving. Here is where HD maps appear to solve this problem.

A HD map is usually a text file describing the real-world features related to the road map and its location within a 2D/3D space, and can do things that other sensors cannot [128]: First, they have an *infinite range* and, therefore, can *see* even into occluded areas. Second, HD maps will never fail due to environmental conditions. Lastly, HD maps contain highly refined data. This information can be used by different modules of an AV, (including localization, vehicle control, path planning, perception and system management) drastically reducing the computational load and complexity in comparison to other more complex methods, providing robustness and reliability to the system.

In terms of mapping information, we may distinguish three main categories:

- Topological information provides the connectivity between geometry features. Particularly in the field of AD, this is usually the network of roads. This kind of information can allow vehicles to traverse the most energy-efficient route, based on traffic speed, road grade or distance, as well as ensure that ADSs obey traffic regulation orders, such as one-way streets or the corresponding regulatory elements (pedestrian crossing, traffic light, stop signal, etc.).

- Geometric information provides the geometry or shape of other environmental features which can be static (permanent obstruction, such as buildings, bridges or tunnels), temporary (exist for only a limited amount of time, like traffic cones, parked vehicles or temporary road works) and dynamic features (moving people, objects or vehicles). Most of these features are incorporated by means of perception systems,

specially in terms of dynamic features, in order to include that information in the HD map for successful motion planning and prediction.

- Semantic information returns the *meaning* of aforementioned features, such as road speed limit, road classification, lane information or even the relational information among the different lanes, *i.e.*how lanes work together, different types of lanes, where vehicles must stop and where vehicles can and cannot turn.

As illustrated, providing rich physical contextual information allows ADSs to make informed decisions in different driving scenarios. In our group, we particularly make use of the OpenDrive [103] HD map format, which has been mainly used for two different purposes, as shown in Figure 4.3:

- Global Path Planning, which uses a specific path planner which inputs are the HD map information and the ego-vehicle current location to retrieve an optimal (usually optimized based on the travelled distance) global route towards an specific goal.
- Map monitoring, responsible for monitoring the most relevant static and dynamic map elements around the ego-vehicle at each timestep, such as standard lanes (current, back), intersection lanes (merge, split and cross) and regulatory elements (e.g. give way, stop, pedestrian crossing, traffic light).

In particular, given a pre-defined global route, in this thesis we focus our interest on designing a map monitor module, responsible for retrieving the most relevant lanes around the ego-vehicle to enhance real-time perception and scene understanding requirements.

#### 4.2.2.1. Map Monitor

In a similar way to humans that pay more attention to close obstacles, people walking towards them or upcoming turns rather than considering the presence of building or people far away, the perception layer of a self-driving car must be modelled to focus more on the salient regions of the scene [129] and the more relevant agents to predict the future behaviour of each traffic participant. In that sense, high-fidelity maps have been widely adopted to provide offline (also known as context) information to complement the online information provided by the sensor suite of the vehicle and its corresponding algorithms. Recent learning-based approaches [130] [79] [71] [68], which present the benefit of having probabilistic interpretations of different behaviour hypotheses, require to build a representation to encode the trajectory and map information. [130] assumes that detections around the vehicle are provided and focuses its work on behaviour prediction by encoding entity interactions with ConvNets. Intentnet [68] proposes to jointly detect traffic participants (mostly focused on vehicles) and predict their trajectories using raw LiDAR pointcloud and rendered HD map information. PRECOG [16] aims to capture

the future stochasiticity by flow-based generative models. Furthermore, MultiPath [79] uses ConvNets as encoder and adopts pre-defined trajectory anchors to regress multiple possible future trajectories.

As observed, recent DL-based techniques use relatively complicated filters to predict, in an accurate way, the spatial features of the obstacles in the scene, increasing the complexity and computational cost of the system. On the other hand, traditional methods for behaviour prediction are rule based, where multiple behaviour hypothesis are generated based on constraints from the road maps. As stated above, road maps present some clear advantages over other perception sensors: They have "infinite range", so they can extract information even into occluded areas. Second, they do not fail under challenging environmental conditions, such as intense fog or rain. Third, recent HD maps contain highly refined data (in which many hours or days of human verification and preprocessing to reduce noise and uncertainty), quite useful to perform safe navigation. Then, HD maps can be an additional sensor that cannot fail unless the road infrastructure changes, providing meaningful, accurate and useful information in real-time operation.

Regarding this, we design a Map Monitor in charge of monitoring the surrounding area of the vehicle. The inputs of the Map Monitor are the information provided by the Map Parser module (in charge of getting the information of the map from the HD map file and transform it into custom classes that can be used by other modules like Planning or Perception) and the waypoint route previously obtained by the path planner. The main goal of the Map Monitor is to only monitor the most relevant map elements around the ego-vehicle given the route provided by the global planner (or a new route if the local planer decides to recalculate the route).

First, the path planner returns the route which is divided in segments separated by a given distance and calculates in which segment of the route the ego-vehicle is found, activating a flag in such a way the Map Monitor can start operating. Otherwise, in case the ego-vehicle cannot be located inside the route, the Map Monitor is deactivated. Secondly, a monitor callback is called periodically every time the ego-vehicle status (position, velocity, orientation, etc.) is received, as observed in Figure 4.2. This callback evaluates, if the Map Monitor module is active, calculates the monitored elements frontwards and backwards for a given distance which is proportional to the ego-vehicle velocity given a braking distance linear model that establishes a linear regression between two arrays of velocity and braking distance data. Nevertheless, we make use of a threshold distance to avoid not monitoring if the ego-vehicle is stopped.

The monitored elements are:

- **Standard Lanes**: Current, back and the corresponding left and right lanes. Current lane is monitored from current position to a dynamic distance depending on the velocity of the ego-vehicle. Back lane is monitored from current position to back a proportional distance of the dynamic current lane obtained distance. Left and right

lanes are monitored the same distance that current and back only if the lane marking from the HD map data allows the lane change.

- **Intersection Lanes**: Other lanes that intersect the current monitored lane are checked. Intersection lanes can have different roles: split (1 lane splits into 2 or more), merge (2 or more lanes merge into 1) and cross (a lane crosses a part of the current lane). To calculate the intersection lanes, each lane of every junction (junctions are areas where more than 2 roads meet) in the current lane is evaluated. The polygon of each lane is calculated and evaluated if is inside the polygon of the current lane. It is important to consider that roundabouts are considered as a set of multiple junctions.

- **Regulatory Elements**: The monitored elements are stops, giveaways, traffic lights, speed limits and crosswalks. The regulatory elements are only monitored for the next intersection affecting the route.

An example of our map monitor module in the CARLA simulator [106] using the ROS [131] visualizator (R-VIZ) may be observed in Figure 4.4:

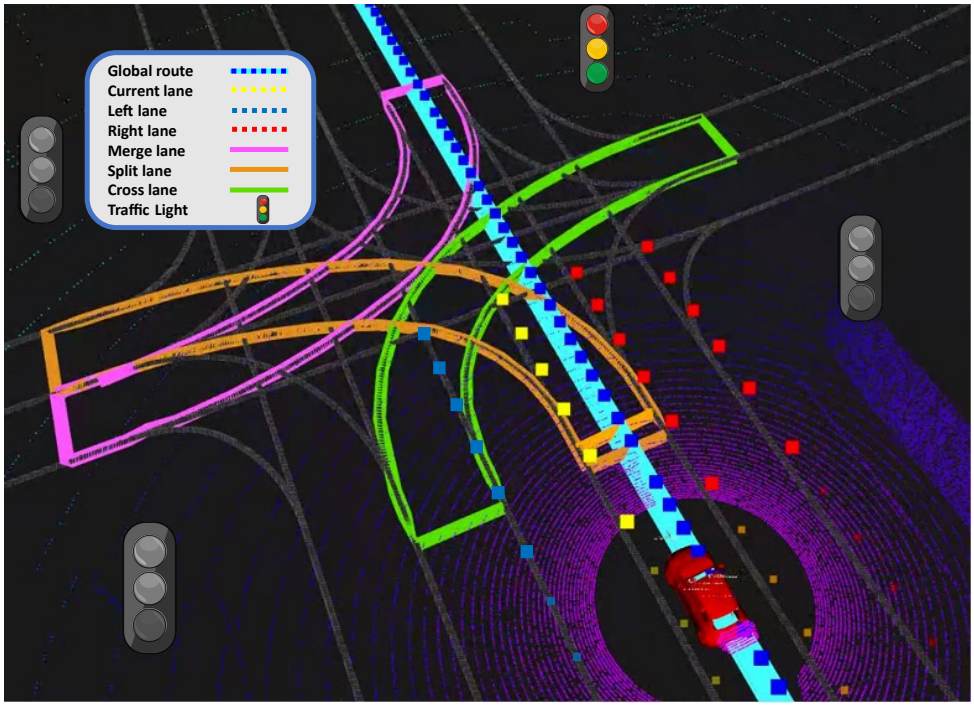


Figure 4.4: Monitored area in the CARLA simulator using ROS visualizator (R-VIZ). It can be appreciated the visualization of the global route, standard lanes, intersection lanes and different traffic lights (regulatory elements). Note that the relevant traffic light is coloured while remaining ones are masked.

As illustrated in Figure 4.2, once the object detections have been provided and the monitored area has been computed, the Monitored Lanes-based Attention Module helps us to increase the efficiency and robustness of the system to avoid tracking and predicting all obstacles in the environment, which would escalate the computational cost especially

in arbitrarily complex urban scenario. This attention module is not focused on DL since the main purpose is to filter non-relevant obstacles in an efficient and interpretable way, such as agents driving way in opposite direction lanes, parked vehicles or pedestrians who are chatting on the sidewalk. The filtering process carried out by our Monitored Lanes-based Attention Module is summarized as follows:

**Algorithm 2:** Jordan's Curve theorem to determine if a point is inside a polygon

```
Data: point, polygon
Result: isInside
crossings ← 0;
for i from 0 to (polygon.length - 1) do
    vertex1 ← polygon[i];
    vertex2 ← polygon[(i + 1) mod polygon.length];
    if (point.y > min(vertex1.y, vertex2.y)) and (point.y ≤ max(vertex1.y,
     vertex2.y)) then
        if point.x ≤ max(vertex1.x, vertex2.x) then
            if vertex1.y ≠ vertex2.y then
                xIntersection ← (point.y - vertex1.y) * (vertex2.x - vertex1.x) /
                 (vertex2.y - vertex1.y) + vertex1.x;
                if vertex1.x == vertex2.x or point.x ≤ xIntersection then
                    crossings ← crossings + 1;
                end
            end
        end
    end
end
isInside ← (crossings % 2 == 1);
return isInside;
```

1. First, we determine the lanes of interested around the vehicle, till a given threshold. The minimum information will be the current front and back lane information (mandatory for the Adaptive Cruise Control and Unexpected Pedestrian use cases), as well as left and right lane information if lane change is available considering the presence of a discontinuous line. Moreover, if an intersection is near the ego-vehicle, other lanes of interest such as merging, splits and intersections are considered, which are specially useful in urban scenarios when the vehicle faces a roundabout or other vehicles incorporation in an intersection.

2. In order to consider an agent as relevant, we study the presence of this agent in our monitored lanes in an elegant and efficient way. The main idea is to find the polygon segment (two nodes on the left, same on the right) closest to the agent. To do that, we iteratively compute the *L2* distance between the agent position (transformed into

global (*a.k.a.*map) coordinates) and the left way nodes (starting from the beginning) of a certain lane. Note that it is irrelevant to take either the left or right lane in terms of observing if the detection is inside a polygon made up by four nodes of the lane, such as there exists the same number of nodes for both ways. For example, in the case of an agent located in front of the vehicle, the distance will decrease since the subsequent left way nodes are closer to the agent.

3. Once the new calculated distance is greater than the previous value, that means the closest segment with nodes $N_0$ and $N_1$ are found. Taking the same lane indexes in the right way, we obtain a 4-side polygon in which the detection is evaluated using the Jordan curve theorem [132], as depicted in Algorithm 2. In this theorem, the input parameters are a point and a polygon, where, by means of a simple-yet-accurate ray casting algorithm, a loop is used to iterate over the polygon vertices and performs the necessary checks to determine the number of crossings. The Jordan's Curve Theorem states that a point is inside a polygon if the number of crossings from an arbitrary direction is odd. Consequently, in our particular case, if the object detection lies outside the closest polygon segment, the traffic participant is considered as non-relevant.

4. Nevertheless, despite this proposal is coherent for non-holonomic obstacles with more constrained behaviours like cars, vans or trucks, the behaviour of Vulnerable Road Users (VRUs), such as pedestrians or cyclists, is usually difficult to predict. Hence, we widen the closest segment area a certain threshold $L$ to the sidewalk so as to track the closest VRUs to the road.

### 4.2.3. BEV Kalman Filter: State Prediction

Once we have obtained the most relevant BEV detections of the environment, a BEV Kalman Filter is used to track the objects. To predict the state of object trajectories from the previous frames to the current frame, we approximate objects inter-frame displacement using a constant velocity model which is independent of other objects in the scene and of the LiDAR motion. Regarding this, the estimation of the measured variables in the following frame are:

$$x_{px}(\hat{t}) = x_{px}(t) + v_x \quad ; \quad y_{px}(\hat{t}) = y_{px}(t) + v_y$$
$$s(\hat{t}) = s(t) + v_s \quad ; \quad \theta(\hat{t}) = \theta(t) + v_\theta$$

Since we formulate the tracking problem over the BEV plane, we remove all variables related to the third dimension of the object, such as its $z$ coordinate of the 3D bounding box centroid, its associated velocity and the height of the obstacle. On the other hand, since our tracking-by-detection algorithm is inspired by the well-established SORT (Single

Online and Real Time) [133] tracking model, originally proposed to track pedestrians using videos as input, some additional variables are included in the object state, such as the aspect ratio and the scale of the bounding box. The aspect ratio can be defined as the relation between the width and the length of the obstacle. Likewise, the scale represents the area of the target bounding box. Then, the state of each object tracker (usually referred as trajectory tracker in the literature) can be expressed as:

$$\mathbf{T}_t^j = [x_{px}, y_{px}, s, r, \theta, x_{px}^{'}, y_{px}^{'}, s^{'}, \theta^{'}] \tag{4.9}$$

Note that the angular velocity $\theta^{'}$ is used in the state space to improve the prediction of the obstacle in later frames. Furthermore, as shown in [133], the aspect ratio of the bounding box is considered to be constant. As observed in Figure 4.2, at every frame $t$, a tuple $\mathbf{T}_t = [\mathbf{T}_t^1, \mathbf{T}_t^2, ..., \mathbf{T}_t^M]$ is returned by the data association module, where each element correspond to an association between a detection and a tracker. Note that $M$ represents the current number of trackers. Then, based on these associations between trackers of the previous frame and current detections, and assuming a Kalman Filter of first order (constant velocity model), the tuple $\mathbf{T}_{\hat{t}}$ is calculated, where each element corresponds to the predicted trajectory ($\mathbf{T}_{\hat{t}}^j$) in the current frame $t$ expressed as:

$$\mathbf{T}_{\hat{t}}^j = [x_{px}(\hat{t}), y_{px}(\hat{t}), s(\hat{t}), r, \theta(\hat{t}), x_{px}^{'}, y_{px}^{'}, s^{'}, \theta^{'}] \tag{4.10}$$

This tuple of predicted trajectories based on the previous frame associations, in addition to the current frame detections, represents the inputs to the data association algorithm at frame $t$.

### 4.2.4. Data association

In order to associate the detections $\mathbf{D}_t$ and the trackers information after the Kalman Filter state prediction $\mathbf{T}_{\hat{t}}$, the Hungarian algorithm is applied. The resulting affinity matrix presents $N$ rows (number of detections at frame $t$) and $M$ columns, which correspond to the number of predicted trajectories based on the information of frame $t-1$. Each element of the matrix corresponds to the Intersection over Union (IoU) in the BEV plane between every pair of predicted trajectory and detection. Then, following the principles stated in Algorithm 1, we solve the bipartite graph matching problem, rejecting the matching if the BEV-IoU metric is lower than a given hyperparameter $IoU_{th}$, giving rise to a set of matched detections ($\mathbf{D}_{matched}$) and predicted trackers ($\mathbf{T}_{matched}$) with the same length $H$ (the number of matches), as well as a set of unmatched detections ($\mathbf{D}_{unmatched}$), where $P = N - H$ is the number of unmatched detections, and a set of unmatched trajectories ($\mathbf{T}_{unmatched}$), where $Q = M - H$ is the number of unmatched detections.

### 4.2.5. BEV Kalman Filter - Object State Update

As observed in Figure 4.2, once we have the corresponding sets of matched detections and trajectories, based on the Kalman Filter prediction-update cycle, we update the state space of each trajectory based on its corresponding matched detection. To do that, we use the weighted average between the matched detection values and the state space of the trajectory tracker, according to [25].

On the other hand, in the same way that [123], we appreciate that this state update step does not work properly for obstacle orientation. The reason is simple: Unless the object detector is based on sensor fusion and vision information is included, the object detector cannot distinguish if the obstacle is rotated 0 or $\pi$, $\frac{\pi}{2}$ and $\frac{3\pi}{2}$, and so on, around its $z$-axis. That is, the orientation may differ by $\pi$ in two consecutive frames. Then, if no orientation correction is applied, the Kalman Filter associated to the tracker can get easily confused, since it tries to adapts itself to the new orientation value rotating the object by $\pi$ in following frames, giving rise to a low BEV-IoU between new detections and predicted trajectories. However, regarding the assumption that obstacles must move smoothly and its orientation cannot be modified by $\pi$ in one frame (0.02 s assuming a frequency of 10 Hz), when this happens the orientation of the corresponding matched detection or matched tracker can be considered wrong. To solve this problem, the detection module only considers angle from 0 to $\pi$ (that is, if an angle exceeds $\pi$, it is substracted to the provided angle). Moreover, if the difference of orientation between a given matched detection and its corresponding matched trajectory is greater than $\frac{\pi}{2}$, as stated before, either the orientation of the detection or the orientation of the tracker is wrong. Finally, we add $\pi$ to the orientation of the tracker with the aim to be consistent with the matched detection.

### 4.2.6. Deletion and Creation of Track Identities

When obstacles leave and enter the aforementioned monitored lanes, unique identities must be destroyed or created accordingly. In most tracking algorithms it is known as the Birth and Death Memory, which is based on the set of unmatched trackers and detections provided by the data association algorithm, where the unmatched trackers represent potential objects leaving the monitored area, in the same way that unmatched detections represent potential objects entering in the area of interest.

In order to avoid tracking of false positives or non-relevant obstacles, a new tracker is not created until the unmatched detection has been continuously detected in the next $f_{min}$ frames. Then, the tracker is initialized with the features of the detected bounding box, and the associated velocities set to zero. Note that, as stated in [133], since the velocity associated to the measured variables is unobserved at this moment (i.e., tracker initialization), the covariance initializes the value of the velocities (in the present work,

velocity of the $x_{px}, y_{px}$ centroid, scale $s$ and rotation angle $\theta$) with large values, reflecting their uncertainty.

To avoid removing true positives trajectories from the scene, they are not terminated unless they are not detected during consecutive $a_{max}$ frames. This assumption prevents an unbounded growth in the number of localisation errors and trackers due to predictions over long duration where the object detector does not provide any correction. Note that since this work does not consider object re-identification for simplicity, an object should leaves the scene and then reappers, according to the SORT algorithm, if it is initialized with a new tracker under a new identity. As shown in Figure 4.2, the inputs to the Matched Trackers module are the updated matched trajectories from the BEV Kalman Filter and a set of created and deleted trackers, which jointly represent the input trajectories for the prediction step in the following frame.

### 4.2.7. CTRV prediction

The last stage of our SmartMOT pipeline is a physics-based MP model to predict the future behaviour of the agents in the short-term. In particular, we make use of the previously studied CTRV model. Once the tracker information (position, velocity and orientation) has been retrieved in real-world coordinates (instead of BEV image coordinates), we are able to differentiate between static and dynamic agents. Then, given the ego-vehicle status and dynamic agents short-term prediction, we are able to analyze the risk of collision or to carry out the state of the current behaviour (Adaptive Cruise Control, Pedestrian Crossing, etc.) in such a way SmartMOT can send a signal to suddenly stop the car. Further experiments will be detailed in Chapter 4.3. Figure 4.5 illustrates an example of the filtering process, tracking-by-detection paradigm and CTRV prediction.

## 4.3. Experimental results

As stated in Section 4.2, SmartMOT is a tracking pipeline that leverages HD map information to subsequently conduct a physics-base unimodal prediction. To validate this algorithm, we first validate the proposed tracking algorithm using the KITTI MOT benchmark. Then, we conduct an interesting study of how integrating the monitored area can reduce the risk of collision and/or the impact velocity on the Vulnerable Road User (VRU).

### 4.3.1. Multi-Object Tracking performance

In order to evaluate our proposed MOT system pipeline, we carry out the evaluation in the KITTI MOT benchmark based on the method proposed by [123]. The KITTI MOT benchmark is composed of 29 testing and 21 training/validation video sequences,

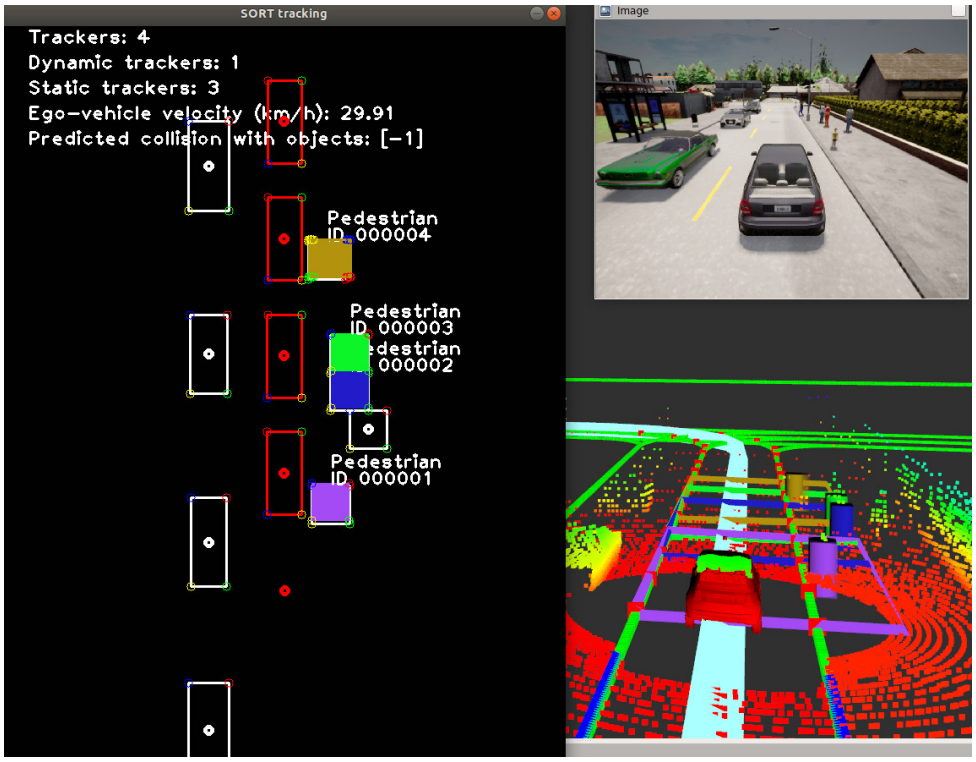


Figure 4.5: Vulnerable Road Users (VRUs) are considered on the sidewalk if the they are close enough to the closest segment of the corresponding centerline.

where each sequence is provided with the corresponding RGB images (left and right camera of the stereo pair), LiDAR point cloud and the corresponding calibration file. Since KITTI does not provide any annotation (*i.e.*, the groundtruth) for the testing split, we decided to evaluate our system in the training/validation split. Moreover, although KITTI distinguish among eight different classes for the object type, our work focus on the car subset, since it is the class that contains the most number of instances over the whole benchmark.

#### 4.3.1.1. Multi-Object Tracking metrics

Mainstream metrics applied to MOT systems are extracted from CLEAR MOT metrics [134], such as MOTA (Multi-Object Tracking Accuracy), MOTP (Multi-Object Tracking Precision), ML/MT (Number of Mostly Lost/Tracked trajectories), IDS (Number of identity swutches), FRAG (Number of fragmentations generated by false negatives) and FN/FP (Number of false negatives/positives). These metrics provide a comprehensive assessment of tracking performance by considering aspects such as accuracy, precision, and overall performance:

**4.3.1.1.1. MOTA (Multi-Object Tracking Accuracy)** The MOTA metric is commonly used to evaluate the performance of multi-object tracking algorithms. It measures the overall tracking accuracy by considering the false positives (FP), false negatives (FN),

and identity switches (IDS) in the tracking results. The formula for calculating MOTA is given as:

$$MOTA = 1 - \frac{\text{FN} + \text{FP} + \text{IDS}}{\text{GT}} \tag{4.11}$$

where:

- FN (False Negatives) represents the number of ground truth objects that were not correctly detected by the tracking algorithm.
- FP (False Positives) represents the number of false detections made by the tracking algorithm.
- IDS (Identity Switches) represents the number of times the algorithm incorrectly switches the identity of a tracked object.
- GT (Ground Truth) represents the total number of ground truth objects in the video sequence.

A higher MOTA value indicates better tracking accuracy, with a perfect tracking result yielding MOTA = 1.

**4.3.1.1.2. MOTP (Multi-Object Tracking Precision)** The MOTP metric is used to assess the localization accuracy of a multi-object tracking algorithm. It measures the average precision of the tracked object positions by considering the distance between the predicted locations and their corresponding ground truth locations. The formula for calculating MOTP is given as:

$$MOTP = \frac{\sum_{i=1}^{N} d_i}{N} \tag{4.12}$$

where:

- $N$ represents the total number of matched object pairs between the predicted and ground truth locations.
- $d_i$ represents the Euclidean distance between the predicted location and the ground truth location for the $i$-th matched object pair.

The MOTP metric ranges between 0 and 1, with a higher value indicating better localization accuracy. A perfect tracking result with exact object positions would yield MOTP = 1.

**4.3.1.1.3. Integral metrics: AMOTA and AMOTP** Nevertheless, these metrics analyze the DAMOT system performance at a given threshold, not taking into account the confidence provided by the object detector and possibly misunderstanding the capability of the method. That means they do not take into account the full spectrum of precision and accuracy over different thresholds. Moreover, these traditional metrics evaluate the performance of the MOT system on the image plane (by projecting the detected 3D bounding box onto the image plane), which does not demonstrate the full strength of 3D DATMO. In that sense, AB3DMOT [123] recently presented a 3D extension of the KITTI 2D MOT evaluation, known as KITTI-3DMOT, which focuses on the dimensions, orientation and centroid position of the 3D bounding box instead of the projection onto the image plane to evaluate the performance of the MOT system. Moreover, two new integral MOT metrics are introduced in order to solve the problem of evaluating the MOTA and MOTP of the system across all thresholds, known as AMOTA and AMOTP (Average MOTA and MOTP), as shown in Equation 4.13:

$$AMOTA = \frac{1}{L} \sum_{\{\frac{1}{L}, \frac{2}{L}, \ldots, 1\}} (1 - \frac{FP + FN + IDS}{num_{gt}}) \tag{4.13}$$

Where $L$ is the number of different recall values. Note that IDS, FP and FN are modified according to the results of each threshold value. Likewise, AMOTP can be estimated by integrating MOTP across all recall values.

#### 4.3.1.2. MOT leaderboard

Table 4.1: Comparative of Multi-Object Tracking pipelines using the KITTI-3DMOT evaluation tool in the validation set (car class). We bold in **black the best results for each category**

| Method | AMOTA (%) | AMOTP (%) | MOTA (%) | MOTP (%) | IDs |
|---|---|---|---|---|---|
| SmartMOT [125] (tracking only) using PointPillars [126] (Ours) | 39.90 | **79.31** | **94.20** | 82.06 | 150 |
| mmMOT [135] | 33.08 | 72.45 | 74.07 | 78.16 | 10 |
| FANTrack [136] | **40.03** | 75.01 | 74.30 | 75.24 | 35 |
| Monocular 3D [137] | 31.37 | 64.29 | 62.38 | 68.26 | **1** |

We compare our proposed MOT pipeline (PointPillars as 3D object detector [126], BEV Kalman Filter, with the state space specified in Section 4.2 as data estimator and Hungarian algorithm as data association algorithm) against modern open-sourced 3D MOT systems such as mmMOT [135], FANTrack [136] and Monocular3D [137] using the proposed KITTI-3DMOT. Results are observed in Table **??**, where we achieve results that are on-pair with other SOTA tracking methods. Note that these results were obtained with default values of the hyperparameters in the tracking stage ($age_{max} = 1$, $min_{hits} = 1$, $IoU_{thr} = 0.1$). For a deeper information of these hyperparameters, we refer the reader

to the next subsection, where we conduct an ablation study to analyze the influence of maximum age or minimum threshold in the data association cost matrix to achieve the best tracking results.

#### 4.3.1.3. MOT ablation

Once we decide to implement a specific tracking-by-detection configuration, we carry out an ablation study that allows us to observe the performance in function of the tracking hyperparameters. These are:

- $age_{max}$**:** Maximum number of frames for a tracker (Kalman Filter) to be associated again to a certain detection
- $min_{hits}$**:** Minimum number of consecutive frames in which a tentative tracker must be associated to a detection to be considered as an actual tracker
- $IoU_{thr}$**:** Threshold to match a predicted trajectory and a detection in the data association module

Table **??** shows an ablation study by modifying these parameters. With a threshold $IoU_{thr}$ of 0.01 we get quite similar results in terms of MOTA and MOTP, decreasing by 36 % the number of identity switches (150 to 54). On the other hand, increasing the minimum number of hits allows us to reduce the identity switching noticeably, overcoming one of the main drawbacks associated to the motion metric proposed by SORT. Moreover, modifying the maximum age to consider a tracker has left the scene barely modifies the studied metrics. Finally, we bold in black the best values for each metric and in blue our final configuration ($age_{max} = 1$, $min_{hits} = 3$, $IoU_{thr} = 0.1$) that achieves an impressive number of 2 identity switches and quite acceptable CLEAR and integral metrics, which are key as a preliminary stage to predict the short-term for each trajectory in the motion prediction stage.

Table 4.2: Ablation study of the final tracking stage configuration of SmartMOT using the KITTI-3DMOT evaluation tool in the validation set (car class). We bold the best results in **black** and the second best in **blue** for each metric

| $age_{max}$ | $min_{hits}$ | $IoU_{thr}$ | AMOTA (%) | AMOTP (%) | MOTA (%) | MOTP (%) | IDs |
|---|---|---|---|---|---|---|---|
| 1 | 1 | 0.1 | **39.90** | 79.31 | 94.20 | 82.06 | 150 |
| 1 | 1 | 0.01 | 39.84 | 70.96 | 95.13 | 81.84 | 54 |
| 1 | 1 | 0.25 | 39.37 | **79.35** | 89.10 | 82.42 | 682 |
| **1** | **3** | **0.1** | **39.54** | **71.24** | **91.38** | **83.23** | **2** |
| 1 | 5 | 0.1 | 39.26 | 71.36 | 88.84 | **83.68** | 3 |
| 2 | 1 | 0.1 | 39.49 | 79.24 | 94.91 | 81.48 | 154 |
| 3 | 1 | 0.1 | 39.50 | 79.15 | **95.16** | 81.15 | 152 |

Finally, our final system configuration is as following: We use PointPillars trained over 1,187,840 training steps using the KITTI MOT benchmark database, the BEV Kalman Filter formulated in the previous section, an $IoU_{th} = 0.1$ as the threshold to associate a detection with a tracker the data association module, and $min_{hits} = 3$, $age_{max} = 1$ values for the birth and death module respectively.

#### 4.3.1.4. Qualitative results in CARLA and our campus

In this subsection we may appreciate some qualitative results both in simulation and in our real-world prototype using SmartMOT. One of the best advantages of CARLA is the possibility to create ad-hoc urban layouts by means of an OpenSCENARIO [138] script definition where town, vehicles, climate conditions and also driving behaviours are defined, helpful to validate AD algorithms (specially those focused on the perception layer) under different traffic and weather conditions.

In terms of simulation, we reproduce a very common situation (as observed in the KITTI dataset) which is the *ego_vehicle* driving in narrow streets full of parked obstacles aside, evaluating its performance in night conditions. Despite this is probably the major disadvantage when using camera information (very poor performance in night conditions), we get impressive results in this situation, as illustrated in Figure 4.6. This is pretty much coherent since LiDAR sensors are not passive sensors like cameras but they supply their own illumination source, which hits objects the reflected energy is detected and measured by the sensor in order to compute the distance to the object.

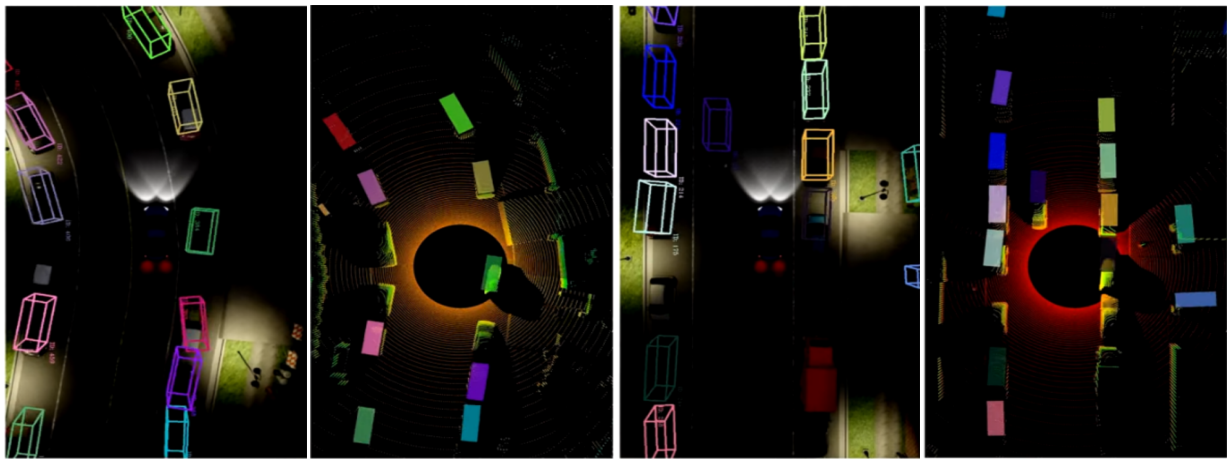

(a) (b) (c) (d)

Figure 4.6: Detection and Tracking of Multiple Objects in the parked aside vehicles at night traffic scenario considering a curved trajectory (a,b) and straight trajectory (c,d)

On the other hand, in terms of our real-world prototype, we focus on implementing a 360º real-time and power-efficient MOT pipeline in an efficient way. Perception systems in autonomous driving must process a huge amount of information coming from at least one sensor in order to understand the environment. However, the physical space

occupied by the processing units in the vehicle or their power consumption are metrics to be deeply analyzed, even more if these processing units will be integrated in an electric vehicle, where the state of the batteries is crucial. In that sense, the current approach is to use powerful but power-efficient AI embedded systems as computation devices for autonomous machines, since they present a remarkable ratio between performance and power consumption in a reduced-size hardware. Regarding the advantage of using neural networks in GPU, these embedded systems present a powerful GPU unit as well as fast storages based on solid state disks and a large RAM memory size. At the time of writing this paper, the best ratio of performance vs power consumption and size is represented by the NVIDIA Jetson embedded computing boards. NVIDIA Jetson is the world's leading AI computing platform for GPU-accelerated parallel processing in mobile embedded systems. These kits allow to implement state-of-the-art frameworks and libraries to conduct accelerated computing, such as CUDA, cuDNN or TensorRT (Tensor RealTime).

Table 4.3: Comparative of inference frequency between the NVIDIA Jetson AGX Xavier and our PC desktop (Intel Core i7-9700, 16GB RAM) with CUDA-based NVIDIA GeForce RTX 1080 Ti 11GB VRAM

| Stage | Frequency AGX Xavier (Hz) | Frequency PC desktop (Hz) | Ratio |
|---|---|---|---|
| Detection | 7.3 | **41.7** | 5.7x |
| Tracking | 15 | **101.9** | 6.7x |

In this particular work we make use of the NVIDIA Jetson AGX Xavier, which is as far as we know one of the most powerful AI embedded system specially designed for autonomous machines. Table 4.3 shows a comparative between the embedded system and our PC frequency in the inference stage, where the detection (PointPillars) is reduced by almost 6 times and the tracking by almost 7 times. Nervertheless, although the detection and tracking frequencies are on the border to be considered real-time according to the requirements of the perception systems for autonomous machines, the embedded system consumes 30 W whilst only the 1080 Ti GPU consumes 250 W at full power respectively. Considering that the embedded system computation power is reduced by 6.2 times (average between the detection and tracking frequency ratios) but only the GPU (not considering the whole PC desktop) presents a power consumption 8.3 higher, makes the current NVIDIA Jetson AGX Xavier a better suitable option for large scale-deployment in the autonomous driving field rather than using desktop graphic cards. Distributing several sensor processing across multiple embedded systems for parallelization will result in lower power consumption than using conventional GPUs in future autonomous driving prototypes. Qualitative results of running our DAMOT pipeline in our own vehicle, equipped with a VLP-16 LiDAR instead of the HDL-64 shown in CARLA and KITTI, are illustrated in Figure 4.7. It can be appreciated that although the obtained results are slightly worse than with the KITTI dataset (equipped with a HDL-64 sensor), we

obtain quite promising results, validating the pipeline studied in this work both in terms of accuracy and real-time operation.

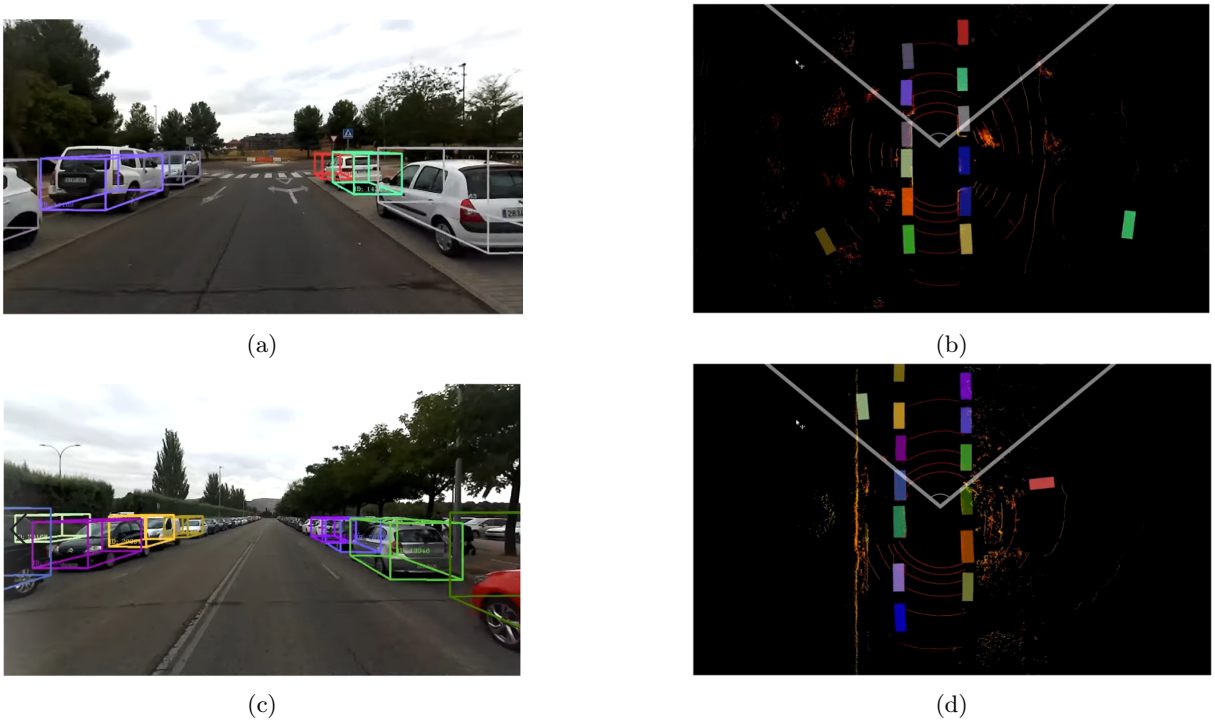

(a) (b) (c) (d)

Figure 4.7: Detection and Tracking of Multiple Objects in our campus with our real-world vehicle

### 4.3.2. EuroNCAP-based validation

A considerable amount of research works and studies, related to pedestrian detection and collision avoidance behavior are present in the literature, where the main objective is to validate the perception and control modules. Nevertheless, as stated before, we aim to demonstrate how incorporating HD map information helps the whole AD stack to anticipate faster the behaviour of the traffic participants in the corresponding traffic scenarios. Then, common metrics for all frameworks must be used to evaluate the whole architecture, where all modules are integrated. Regarding this, New Car Assessment Programs (NCAPs) protocols are introduced, evaluating the safety of vehicles for different traffic situations and Advanced Driver Assistance Systems, such as Child Occupant Protection (COP), Speed Assist Systems (SAS) or Autonomous Emergency Braking (AEB). Euro-NCAP [139] is introduced in 1997, representing the widely most adopted performance assessment within the scope of the collaboration of European Union countries. China New Car Assessment Program (C-NCAP) [140] is presented (2006) as a research and development benchmark for vehicle manufacturers in Asia, being most of its protocols based on Euro-NCAP. National Highway Transportation Safety Administration (NHTSA), funded in 1970 as an agency of the Department of Transportation of United States, published [141] its guidance documents and regulations on vehicles equipped with ADAS. As observed, these programmes do not present specific protocols in order to eval-

uate AD stacks, presenting noticeable differences, such as different scenarios, parameters and evaluation metrics.

Regarding this, in order to evaluate SmartMOT, we adopt the validation method proposed by [142], which proposes to generalize the VRU v.10.0.3 protocol [143], representing a baseline to compare the performance of different pipelines for the particular situation (both in simulation and real-world) of an Unexpected Vulnerable Road User (VRU) jumping into the road during the navigation, where an Autonomous Emergency Braking (AEB) behaviour must be executed.

#### 4.3.2.1. Implementation details of the EuroNCAP scenario

Figure 4.8 illustrates this traffic situation, in which the VRU (a pedestrian in this particular case) starts in the closest sidewalk to the vehicle in a perpendicular position to the vehicle orientation. Once the vehicle starts the navigation and the L2 distance between the ego-vehicle centroid and the VRU centroid is lower than a certain threshold $d$, the VRU starts its path to unexpectedly cross the road in such a way the ego-vehicle must detect, track and forecast its future trajectory in order to avoid the collision or at least reduce the impact velocity as much as possible. Then, the protocol consists on reproducing the CPNA crash avoidance scenario, with a fixed VRU velocity ($v_p$) of 5 km/h and a variable ego-vehicle velocity that ranges from 10 km/h to 60 km/h. It is important to note that the threshold $d$ is not fixed, but it is ego-vehicle velocity dependent, that is, the pedestrian must start walking in such a way the impact point ($P_I$) (Figure **??**) is in the center of the lane for each particular velocity.

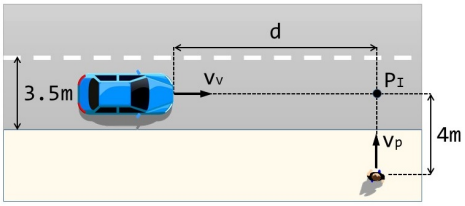


Figure 4.8: Car to Pedestrian Nearside Adult (CPNA) scenario

Regarding the evaluation metrics, a score for each test is calculated based on the velocity reduction of the vehicle, as following:

- For a vehicle velocity $v_v$ less than or equal to 40km/h:
  - If the vehicle stops without collision, the highest score is achieved:

$$score_{test} = score_{max} \tag{4.14}$$

  - Otherwise, if the vehicle collides, its score is defined as follows:

$$score_{test} = \frac{v_{test} - v_{impact}}{v_{test}} \cdot score_{max} \tag{4.15}$$

- For $v_v$ higher than 40km/h:
  - If the vehicle is able to reduce its speed in at least 20 km/h, the highest score is achieve:

$$v_{impact} \leq v_{test} - 20 \rightarrow score_{test} = score_{max} \tag{4.16}$$

  - Otherwise, if the vehicle collides at a velocity greater than the velocity under test less a threshold of 20 km/h, no score is achieve:

$$v_{impact} > v_{test} - 20 \rightarrow score_{test} = 0 \tag{4.17}$$

Finally, the final score of a particular pipeline is given by the arithmetic mean of the results obtained in each CPNA crash avoidance test for different weather conditions. For further details about the validation protocol, we refer the reader to [142].

#### 4.3.2.2. Experimental results in the EuroNCAP-based scenario

In this section we obtain some interesting both qualitative and quantitative results, evaluating our AD stack [144] in the CPNA crash avoidance scenario using two different perception layer strategies. On the one hand, we implement the perception module stated by [145] which tracks all objects in the environment regardless their topological information and considers a naive velocity dependent rectangular monitored area in front of the vehicle to determine the distance to the nearest object in the route as well as to predict the collision. On the other hand, we use SmartMOT to track and predict the future trajectories of only the most relevant obstacles around the vehicle, that is, those in which the human in manual driver should pay attention throughout the route, such as VRUs close to the road, vehicles in intersections and lanes where the lane change maneuver is allowed, etc. Qualitative results may be found in the following play list SmartMOT [1], where the SmartMOT performance is illustrated.

Regarding urban environment complexity, in order to validate a whole AD architecture the system must be tested in countless environments and scenarios, which would escalate the cost and development time exponentially with a physical approach. Considering this, the use of photo-realistic simulation (virtual development and validation testing) and an appropriate design of the driving scenarios are the current keys to build safe and robust AV.

In our work we propose the use of CARLA (CAR Learning to Act) [106] as the best open-source simulator to reach our goals, taking even more importance when analyzing the behaviours the vehicle can face in these complex traffic scenarios. One of the best advantages of CARLA is the possibility to create ad-hoc urban layouts, useful to validate the navigation architecture in challenging driving scenarios. This code can be downloaded from the ScenarioRunner repository, associated to the CARLA GitHub. The

[1] SmartMOT: https://cutt.ly/uk9ziaq

ScenarioRunner is a module that allows the user to define and execute traffic scenarios for the CARLA simulator. In the present case, we define several scenarios according to the CPNA crash avoidance traffic situation, modifying the velocity of the ego-vehicle and the presence of other traffic participants. All test were carried out in a PC desktop (Intel Core i7-9700k, 32GB RAM with CUDA-based NVIDIA GeForce RTX 2080 Ti 11GB VRAM), using the version 0.9.10.1 version of CARLA as well as the corresponding ROS Bridge, responsible of communicating the CARLA environment with our ROS-based architecture, and ScenarioRunner modules. In particular, we make use of the OpenScenario standard, supported by ScenarioRunner, where both the VRU and ego-vehicle features can be modified to accomplish the Euro-NCAP requirements.

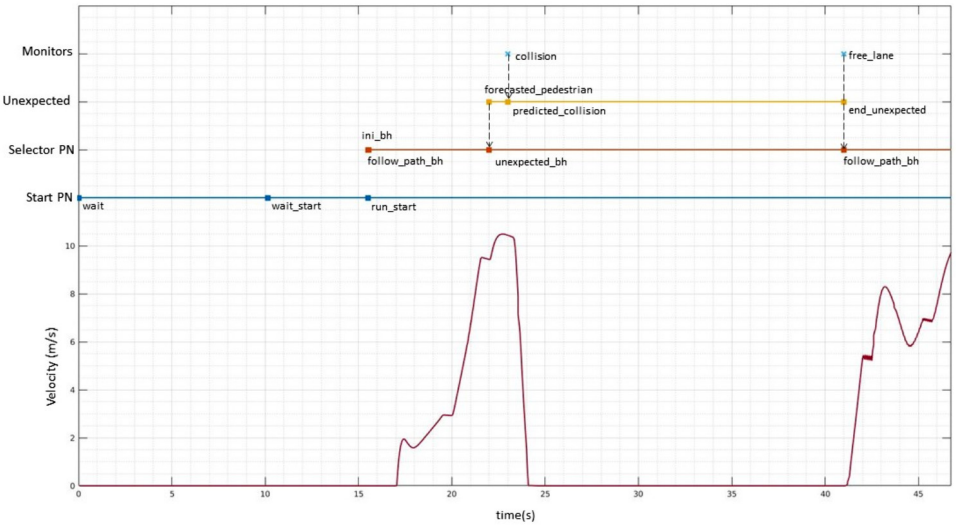


Figure 4.9: Unexpected Vulnerable Road User (VRU) temporal diagram. At the top, the events produced by our monitors and map manager modules. In the middle, the selector, and start (background) PNs of our decision-making layer. At the bottom, the velocity of the car throughout the navigation

In order to appreciate the behaviour of the vehicle during navigation, we incorporate a very illustrative temporal diagram (Figure **??**), representing a powerful manner to qualitatively validate how the architecture behaves in an end-to-end manner, since we can observe how the car behaves considering the different actions and events [144] provided by the executive layer, which is actually the output of the whole architecture before sending commands to the motor. As observed, the ego-vehicle starts far away from the adversary and starts its navigation. At second 22 a pedestrian that is in the sidewalk is detected, so tracking-by-detection and subsequent motion prediction must be carried as fast as possible to avoid collision, since the scenario is designed in such a way that the pedestrian must start walking in such a way the impact point ($P_I$) (Figure 4.8) is in the center of the lane for each particular velocity. After that, our prediction module intersects the ego-vehicle forecasted trajectory and the pedestrian forecasted trajectory. If the Intersection over Union (IoU) is greater than a threshold (in this case, 0.01), a *predictedcollision* flag is activated and the low-level (reactive) control, which always runs in the background of the

decision-making layer, performs an emergency break until the car is stopped in front of the obstacle. Navigation is resumed once the obstacle leaves the driving lane. Table 4.4 compares the performance of the architecture by implementing [145] and a rectangular monitorized lane to retrieve the nearest object in route and predict collision against our proposal, where it can be appreciated that for velocities greater than 40 km/h, using HD map semantic and geometric information gives the car a valuable reaction time to anticipate the VRU behaviour and avoid the collision, achieving the highest score.

Table 4.4: Comparison of our two different perception strategies in the Car to Pedestrian Nearside Adult (CPNA) scenario. We bold the best score in **black**.

| **CPNA** | | | | | |
|---|---|---|---|---|---|
| $v_{test}$ | $score_{max}$ | **Rectangular area + [145]** | | **SmartMOT** | |
| | | $v_{impact}$ | *score* | $v_{impact}$ | *score* |
| 10 km/h | 1.00 | 0.0 km/h | 1.00 | 0.0 km/h | 1.00 |
| 20 km/h | 1.00 | 0.0 km/h | 1.00 | 0.0 km/h | 1.00 |
| 30 km/h | 2.00 | 0.0 km/h | 2.00 | 0.0 km/h | 2.00 |
| 40 km/h | 3.00 | 0.0 km/h | 3.00 | 0.0 km/h | 3.00 |
| 50 km/h | 2.00 | 23.82 km/h | 2.00 | 0.0 km/h | 2.00 |
| 60 km/h | 1.00 | 44.23 km/h | 0.00 | 0.0 km/h | 1.00 |
| **Total** | 10.00 | | 9.00 | | **10.0** |

Figure 4.10 shows different analysis of the CPNA crash avoidance scenario with variable ego-vehicle and the incorporation of other traffic participants in the scenario (4.10c **??**). $T_0$ corresponds with the moment the vehicle either stops or collides, and crosses **x** represent the moment in which the system sends a predicted collision signal to the executive layer, so it is coherent that crosses in tests where the ego-vehicle collides with the VRU are shifted to the right (prediction collision signal was given in time). Left column tracks all objects around the vehicle and adopts a geometric monitorized area to estimate the nearest distance and predicted collision, whilst right column uses HD map information to help in the Multi-Object Tracking and motion prediction tasks, monitoring only the most relevant traffic participants around the vehicle that is, the main purpose of SmartMOT.

As observed, using HD map information is able to avoid collision until a ego-vehicle velocity of 80 km/h, where SmartMOT is not able to send a signal of predicted collision (output of the system, as shown in Figure 4.2) in time, colliding at a velocity of 39.78 km/h. Nevertheless, this velocity at the moment of collision is even lower that the impact velocity (44.23 km/h) when testing the system under 60 km/h condition not using HD map in the MOT stage, illustrating how incorporating additional semantic and geometric map information helps the vehicle to react faster or at least mitigate the effect of collision. Moreover, we simulate both perception strategies using the most common velocities in urban scenarios, which range from 30 to 50 km/h, including 4.10c **??** static adversaries (in particular, vehicles and pedestrians) which do not actually in the traffic scenario to fulfill the particular requirements stated by [142] protocol. As expected, tracking all objects around the ego-vehicle and using the rectangular monitorized area suffers when the number of traffic participants is increased around the ego-vehicle, whilst SmartMOT

holds this exponential increase by analyzing the objects and their corresponding role as relevant obstacles considering the information provided by the HD map, avoiding the collision in all situations.

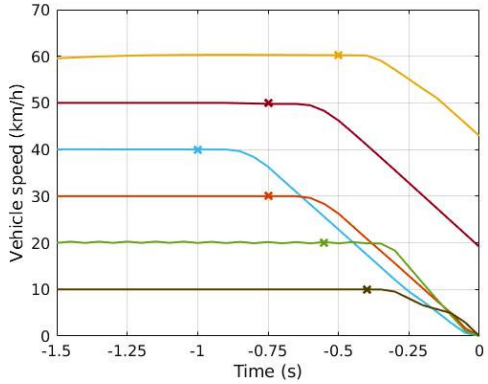


(a) Rectangular monitored area without adversaries

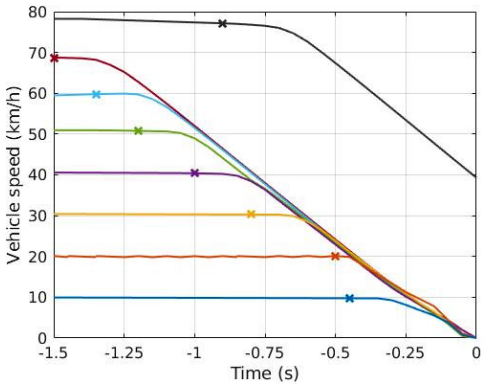


(b) SmartMOT area without adversaries

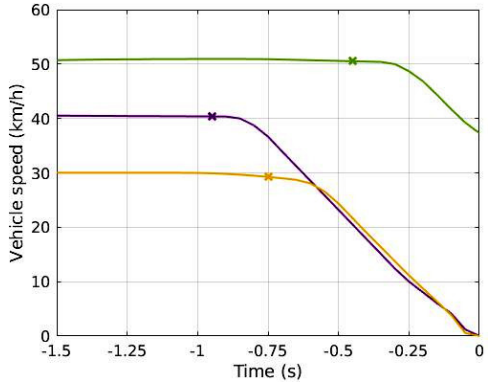


(c) Rectangular monitored area with adversaries

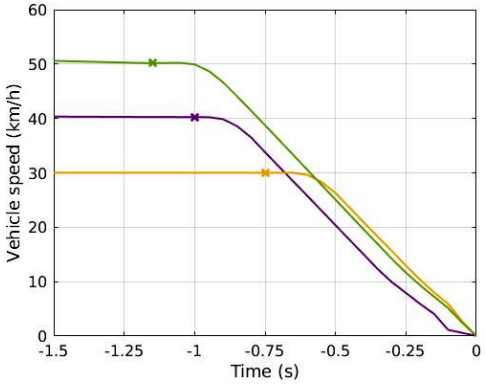


(d) SmartMOT area with adversaries

Figure 4.10: Analysis of the Car to Pedestrian Nearside Adult (CPNA) crash avoidance scenario with variable ego-vehicle velocity. Left column (Figures **??** and **??**) adopts a rectangular monitorized area to estimate the nearest distance and predicted collision, Right column (Figures 4.10b and 4.10d) uses HD map information for this purpose. On the other hand, first row shows the scenario without additional traffic participants, second row analyzes the crash avoidance scenario including additional traffic participants to the road, monitorized sidewalk area and non-relevant sidewalk area. Crosses in the lines represent the moment in which the system sends a predicted collision signal to the executive layer

## 4.4. Summary

In this chapter we propose SmartMOT, a simple-yet-powerful pipeline that fuses the concepts of tracking-by-detection and HD map information to design a real-time and power-efficient Multi-Object Tracking (MOT) and Motion Prediction pipeline used to track and predict the future trajectories of only the most relevant obstacles around the ego-vehicle, incorporating a Monitored Lanes-based Attention Module to the pipeline, improving the way in which the vehicles are considered as relevant, and an additional module to evaluate different behavioural use cases and background behaviours.

Then, experimental results focus on validating the tracking stage in the KITTI dataset. Once the best hyperparameters are obtain by means of an ablation study, an end-to-end validation of our pipeline in the Unexpected VRU scenario is carried out, following an Euro-NCAP-based validation protocol, illustrating how integrating map information in the pipeline can minimize or at least reduce the impact velocity with the VRU by reducing the computational complexity of the problem. Moreover, a temporal graph is depicted, representing a very intuitive and powerful manner to appreciate how the integration of this extended version of SmartMOT gives the vehicle a valuable time to anticipate the corresponding behaviours. We hope that our distributed pipeline can serve as a solid baseline on which others can build on to advance the state-of-the-art in fusing perception data and map information to perform real-time motion prediction and decision-making evaluation in arbitrarily complex urban scenarios.

# Chapter 5

# Exploring GAN for Vehicle Motion Prediction

*Avanzad, sin temor a la oscuridad.*
*Luchad jinetes de Theoden.*
*Caerán las lanzas, se quebrarán los escudos.*
*Aún restará la espada.*
*Rojo será el día, hasta el nacer del sol.*
*Cabalgad, cabalgad, cabalgad hacia la desolación*
*y el fin del mundo. Muerte, muerte, muerte.*

Discurso de Theoden, Rey de Rohan
El Señor de los Anillos: El Retorno del Rey

## 5.1. Introduction

Despite the fact that SmartMOT illustrates a simple-yet-powerful tracking and prediction pipeline, traditional methods for MP in the field of AD are based on physical kinematic constraints and road map information with handcrafted rules. Though these approaches are sufficient in many simple situations (*i.e.*vehicles moving in constant velocity or straightforward intersections), they fail to capture the rich behavior strategies and interaction in complex scenarios, in such a way they are only suitable for simple prediction scenes and short-time prediction tasks [20]. In that sense, as commented in Chapter 2.3.4, recently DL based methods have dominated this task and they usually follow an encoder-decoder paradigm.

The main challenge in the MP is the human driver behaviour can neither be modeled and consequently predicted properly, specially in negotiating situations [144] [70] with many participants where considering agent-environment/agent-agent interactions [129] plays a determinant role. Then, resulting trajectories may not be necessarily feasible, not covering the full spectrum of possible trajectories that a vehicle can take. In that sense, a more natural way of capturing the feasible directions [146] is to first compute a set of

intermediate target points from a distribution of acceptable positions. In this chapter we explore the influence of attention mechanisms in generative models, in particular based on Generative Adversarial Network (GAN) [57], to carry out the task of motion prediction.

Our model considers both physical context, computing acceptable target points from the driveable area around the target agent, and social context, LSTM (Long Short-Term Memory) [114] based encoder as input to a Multi-head self-attention module, as input of our generator, which combines the scene understanding around the agent vehicle (target agent to predict its trajectory) and the corresponding noise vector associated to generative models to compute the trajectories using a LSTM decoder, as illustrated in Figure 5.1. In this context, the discriminator is applied in order to force the generator model to produce more realistic samples (*i.e.*trajectories), hence, to improve the performance.

Prior knowledge on MP in pedestrian datasets like ETH [147] or UCY [148] usually focuses on deep methods such as LSTMs [114] and GANs [57]. SocialLSTM [69] proposes an LSTM-based model that can jointly predict the paths of all agents in the scene taking into account the common sense rules and social conventions using a social-pooling module. SocialGAN [67] enhances SocialLSTM with a generative adversarial framework, introducing a variety loss that encourage the network to cover the space of plausible paths and proposing a novel pooling global social pooling vector that encodes the subtle cues for all agents involved in the scene. SoPhie [129] considers not only the path history of all agents but also the physical context information (captured by a top-view static image, computing salient regions of the scene), combining physical and social attention mechanisms in order to help the model knows what to extract and where to focus. Goal-GAN [146] predicts the most likely goal points of the agent of interesting, estimating a set of trajectories towards these potential future candidates using both physical and social context, as proposed by [129]. On the other hand, in the context of vehicle prediction [5], [92], prior information takes more importance regarding the risk at certain velocities in urban / highway environments in order to perform safe navigation.

As stated in Chapter 2.3.4, HD maps have been widely adopted to provide a preliminary raw physical context and then apply data-driven approaches. Recent learning-based approaches [68], [130], which present the benefit of having probabilistic interpretations of different behaviour hypotheses, require to build a representation to encode the trajectory and map information. [130] assumes that detections around the vehicle are provided and focuses its work on behaviour prediction by encoding entity interactions with ConvNets. Intentnet [68] proposes to jointly detect traffic participants (mostly focused on vehicles) and predict their trajectories using raw LiDAR pointcloud and rendered HD map information. PRECOG [16] aims to capture the future stochasiticity by flow-based generative models. Furthermore, MultiPath [79] uses ConvNets as encoder and adopts pre-defined trajectory anchors to regress multiple possible future trajectories.

Furthermore, as commented in previous sections, in a similar way to humans that pay more attention to close obstacles, people walking towards them or upcoming turns rather than considering the presence of people or building far away, the perception layer of a self-driving car must be modelled to focus more on the more relevant features of the scene. Social Attention is a mechanism that allows selective interactions within relevant agents. SoPhie [129] computes a different context vector for each agent, in such a way other agents features are sorted in terms of their relative distance to the agent of interest. Then, a soft attention mechanism is used to compute a context feature vector, which represents the social context. Nevertheless, a fixed size ($N_{\max}$ agents) list that considers the context of all agents is sensitive to small variations [70] of other agents positions. In that sense, SocialWays [149] presents a hand-crafted relative geometric feature to produce a set of normalized weights, in such a way the context vector represents a convex sum of other feature vectors (context of each agent) that is invariant to the ordering.

However, these attention mechanisms were not designed to model complex interactions, no more than angles and distances due to the inherent problem of pedestrian prediction, in such a way we must find this challenging interactions in the vehicle motion prediction task to account for specific behaviours like overtaking, Adaptive Cruise Control (ACC), emergency braking or yielding. GRIP [150] proposes a graph representation of vehicle neighbours, taking into account local interactions among vehicles withing a $d$ distance threshold around the target agent.

[151] use a dot product attention module (inspired from the attention mechanism proposed by [115] for sentence translation), allowing joint forecast of every agent in the scene without spatial limitations, considering long range interactions regardless the ordering of the input vehicles tracks and the number of vehicles. Moreover, [151] combines this dot product with a spatio-temporal graph representation to take into account temporal and spatial dependencies of the agents, such as their absolute/relative positions and time step movements. [70] present a multi-head extension of this dot attention mechanism, where each agent is embedded by means LSTMs before computing the dot product attention in order to produce social interactions.

## 5.2. Attention-based GAN approach

In this work, we aim to develop a model [152] that can successfully predict plausible future trajectories in the context of vehicle prediction, taking into account not only the past trajectory of the corresponding agent but also the past state of the most relevant obstacles around it and HD map information to compute a set of acceptable target points representing the physical constraints for our problem.

When vehicles drive through a traffic scenario, they usually aim to reach partial goals, depending on their predefined navigation route and scene context (both physical and

social), until they finally arrive at their final destination. Formally, given a certain goal, vehicles must face different traffic rules and other agents along their way to reach their final destination. Regarding this, our model takes computes both the social context and acceptable target points for the corresponding agent given its past trajectory and then generates plausible trajectories towards the estimated goals. As illustrated in Figure 5.1, our model consists of three main blocks:

- *Target Points Extractor*: Combines HDMap information and dynamic features of the target agent (speed and orientation) to generate acceptable target points in the driveable area.
- *Attention module*: Computes the agent's dynamic features recursively by means a LSTM unit and uses a Multi-Head Self Attention module to capture complex social interactions among agents.
- *GAN module*: Given the target points and highlighted social features, this module generates plausible and realistic trajectories using a LSTM based decoder, which represents the generator. Discriminator is applied to enhance the performance of the generator by forcing it to compute more realistic predictions.

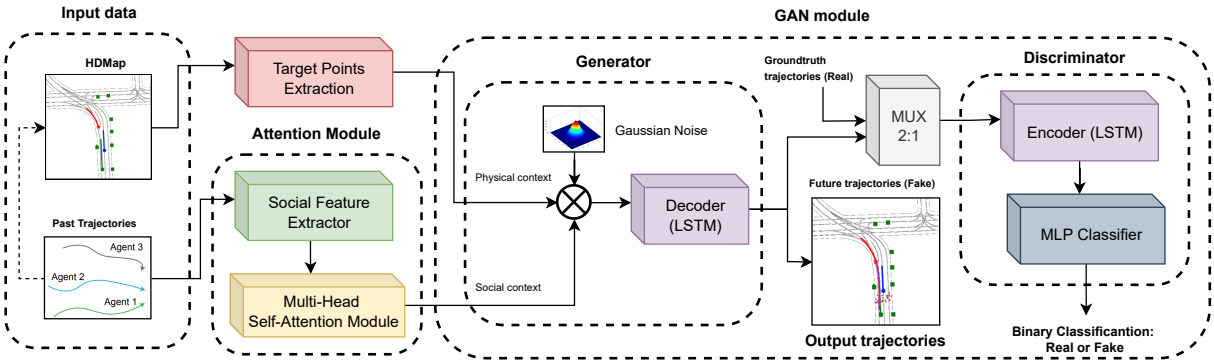


Figure 5.1: Overview of our **Attention-based Generative Model**. We distinguish three main blocks: 1) **Target points extractor**, which uses HDMap information and agent past trajectory to compute acceptable target points, 2) **Attention module**, responsible for encoding the trajectories of the surrounding vehicles and applying Multi-Head Self-Attention, 3) **LSTM based GAN module**, which consists of a LSTM based decoder as the "generator", in charge of taking into account the estimated target locations and the dynamic feature to generate the future trajectories, and a discriminator to force the generator to produce more realistic predictions.

Figure 5.1 illustrates an overview of our model. Next, we describe the different blocks of our model.

### 5.2.1. Target points extraction

Multiple approaches have tried to predict realistic trajectories by means of learning physically feasible areas as heatmaps or probability distributions of the agent future location [8], [129], [146]. These approaches require either a top-view RGB BEV image of

the scene, or a HD Map with exhaustive topological, geometric and semantic information (commonly codified as channels). This information is usually encoded using a CNN and fed into the model together with the social agent information [71], [129], [146].

In our model, we propose we estimate the range of motion (360º) using a minimal HD Map representation that includes only the feasible area, where we can discretize the feasible area $\mathcal{F}$ (represented by a discrete grid of the *width* x *height* BEV map image where the pixels are driveable) as a subset of $r$ randomly sampled points $\{p_0, p_1 ... p_r\}$ from such area in the map (easy to extract from a 1-channel binarized HD image) considering the orientation and velocity in the last observation frame for the agent. This step can be considered as pre-processing of the HD Map, therefore the model never sees the HD map image nor the whole graph of nodes.

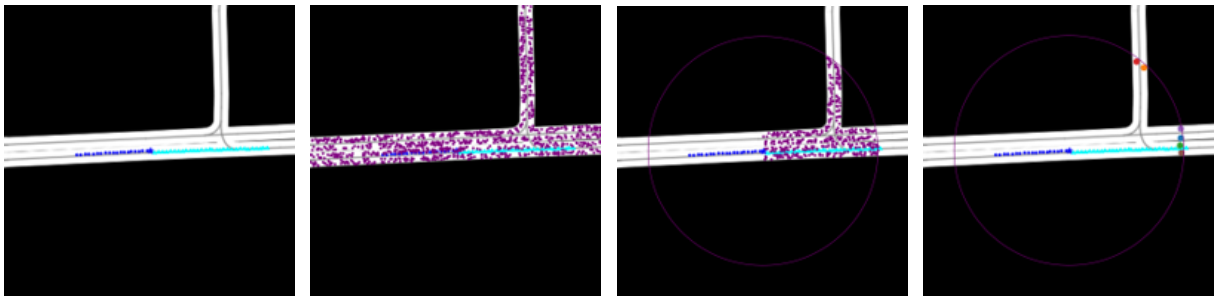

(a) (b) (c) (d)

Figure 5.2: Target Points Estimation from the Feasible area process: (a): Agent Past Trajectory (past observations and ground-truth), (b) Feasible area discretization (random points in the driveable area), (c) Non-holonomic-based dynamic filter (both angle and velocity), (d) Multimodal clustering to get the final proposals

Figure 5.2 summarizes step-by-step the whole process. First, we calculate the driveable area (white area in Figure 5.2) around the vehicle considering a hand-defined $d$ threshold.

Then, we consider the dynamic features of the agent of interest in the last observation frame $t_{obs}$ to compute acceptable target points in local coordinates. As we will detail in future sections, the Argoverse 1 Motion Forecasting dataset focuses on estimating the future prediction of a particular target agent. On top of that, the aforementioned dynamic features (orientation and velocity) are not provided, in such a way they must be calculated. Since the trajectory data are noisy with tracking errors, as expected from a real-world dataset, simply interpolating the coordinates between consecutive time steps, assuming constant frequency, results in noisy estimation. Then, in order to estimate the orientation and velocity of the target agent in the last observation frame $t_{obs}$, we compute a vector for each feature given:

$$\begin{aligned} \theta_i &= \arctan\left(\frac{y_i - y_{i-1}}{x_i - x_{i-1}}\right) \\ v_i &= \frac{X_i - X_{i-1}}{t_i - t_{i-1}} \end{aligned} \tag{5.1}$$

where $X_i$ represents the 2D position of the agent at each observed frame $i$ as state above. Once both vectors are computed, we obtain a smooth estimation as proposed by [153] of the heading angle (orientation) and velocity by assigning less importance (higher forgetting factor) to the first observations, in such a way immediate observations are the key states to determine the current spatio-temporal variables of the agent, as depicted in Equation 5.2, which applies to both the orientation and velocity vector:

$$\hat{\psi}_{T_h} = \sum_{t=0}^{T_h} \lambda^{T_h - t} \psi_t \tag{5.2}$$

where $T_h$ is the number of observed frames, $\psi_t$ is the estimated orientation/velocity at the $t_i$ frame, $\lambda \in (0, 1)$ is the forgetting factor, and $\hat{\psi}_{t_obs}$ is the smoothed orientation/velocity estimation at the last observed frame. After estimating these variables, we calculate the range of motion around the target agent as a circle with radius: $H * \psi_v$ where $\psi_v$ is the estimated velocity using Equation 5.2 and $H = 3$ is the time-horizon of 3s. After that, we randomly sample $r$ points $p \in \mathcal{F}$ in this range considering a constant velocity model during the prediction horizon and the estimated orientation, assuming non-holonomic constraints [88] which are inherent of standard road vehicles, that is, the car has three degrees of freedom, its position in two axes and its orientation, and must follow a smooth trajectory in a short-mid term prediction. Finally, we estimate $k$ target points (one per mode required in the future prediction) by means of the k-means [154] clustering algorithm. This clustering method, originally from signal processing, that aims to partition n observations into k clusters in which each observation belongs to the cluster with the nearest mean (cluster centers or cluster centroid), serving as a prototype of the cluster. In this particular model, we focus on unimodal prediction, that is, the model must reason the most plausible future trajectory based on the agents past observations, attention-based social interaction and target points as physical context.

This representation not only reunites information about the feasible area around the agent, but also represents potential **Target points** [146] (*i.e.*potential destinations or end-of-trajectory points for the agents). Moreover, this information is *"cheap"* and *interpretable*, therefore, we do not need further exhaustive annotations from the HD Map in comparison with other methods like HOME, which gets as input a 45-channel encoded map [8]. We concatenate this information, as 2D vector $\mathcal{V}$, together with the model social context features to generate more realistic trajectories (see Figure 5.1).

### 5.2.2. Attention module

Our model takes as social input the past $n$ observations in map (global) coordinates for each agent in the scene, encoding these trajectories as a preliminary stage before feeding a Multi-Head Self-Attention (MHSA) [115] module that computes the social context of the scene, as observed in Fig. 5.1. The past trajectory of an agent is transformed to relative

(local coordinates) displacement vectors $(\Delta x_i^t, \Delta y_i^t)$ and embedded into a higher dimensional vector with a Multi-Layer Perceptron (MLP), which serves as input of the LSTM unit, dynamic feature extractor to capture the speed and direction of the corresponding agent. Then, the hidden state of the LSTM ($h_{ME}$) is used by the MHSA module that learns complex social interactions while being invariant to their number and ordering, avoiding a fixed size ($N_{\max}$ agents) list which would be sensitive to small variants in the agent's positions. In this context, each agent of the scene should pay attention to specific features from the most relevant agents around it. The Multi-Head Self-Attention module consists of several heads that given the encoded trajectories produces feature vectors that encode all pairwise relations among agent's information.

### 5.2.3. GAN module

To capture the stochastic nature of motion prediction, state-of-the-art methods leverage the power of generative models, such as Variational Autoencoders (VAEs) and Generative Adversarial Networks (GANs). In our work we use an adversarial framework in order to train our trajectory generator, responsible for generating physically and realistic feasible trajectories. In a GAN, the Generator (which after being trained will be the inference network) and Discriminator networks compete in a two-player min-max game [57], as observed in Equation 5.3. While the generator aims at producing feasible trajectories, the discriminator learns to differentiate between fake and real samples, in other words, ground-truth (which are feasible by definition) and inferred trajectories, in such a way the tasks of the discriminator is to enhance the performance of the generator by forcing it to compute more realistic predictions, more and more similar to the ground-truth trajectory. As a result, the generator should be able to produce outputs which the discriminator cannot discriminate clearly, indicating that the output is realistic.

$$\begin{aligned}\min_{Gen}\max_{Dis} V(Dis, Gen) = E_{X\sim p_{data}(X)}[\log Dis(X,Y)] \\ + E_{z\sim p_z(z)}[\log(1 - Dis(X, Gen(X,z)))],\end{aligned} \tag{5.3}$$

In the present case, the generator, also identified as the routing module, is represented by a decoder LSTM ($LSTM_{gen}$) and the discriminator by a classifier LSTM ($LSTM_{dis}$) so as to estimate the temporally dependent future states. Similar to the conditional GAN proposed by [129], the input to our generator is a concatenation of a white noise vector $z$ sampled from a multivariate normal distribution, being the physical context (goal points in relative coordinates in the last observation frame, $C_{Ph(i)}^{t_{obs}}$) and social context (interactions among agents, $C_{So(i)}^{1:t_{obs}}$) its conditions. Then, the generated future trajectory for a particular agent is modelled as Equation 5.4:

$$\hat{Y}_i^{t_{obs}:t_{pred}} = LSTM_{gen}\Big(C_{Ph(i)}^{t_{obs}}; C_{So(i)}^{1:t_{obs}}; z\Big) \tag{5.4}$$

On the other hand, the input of the discriminator is a randomly chosen trajectory sample from the either predicted future trajectory or ground-truth for the corresponding agent up to $t = t_{obs} + t_{pred}$ frame, i.e. $T_i^{t_{obs}:t_{pred}} \sim p(\hat{Y}_i^{t_{obs}:t_{pred}}, Y_i^{t_{obs}:t_{pred}})$.

$$\hat{L}_i^{t_{obs}:t_{pred}} = LSTM_{dis}(T_i^{t_{obs}:t_{pred}}) \tag{5.5}$$

Then, the discriminator returns a label $\hat{L}_i^{t_{obs}:t_{pred}}$ for the chosen trajectory indicating whether the trajectory is ground-truth (real) $Y_i^{t_{obs}:t_{pred}}$ or predicted (fake) $\hat{Y}_i^{t_{obs}:t_{pred}}$, being the labels 0 and 1 for fake and real trajectories respectively. Equation 5.5 summarizes the discriminator working principles.

### 5.2.4. Losses

To train our GAN-based model, we use the following losses:

$$\begin{aligned} W^* = \underset{W}{\operatorname{argmin}} \quad \mathbb{E}_{i,\tau}[&\lambda_{gan}\mathcal{L}_{GAN}\Big(\hat{L}_i^{t_{obs}:t_{pred}}, L_i^{t_{obs}:t_{pred}}\Big) + \\ &\lambda_{ade}\mathcal{L}_{L2}(\hat{Y}_i^{t_{obs}:t_{pred}}, Y_i^{t_{obs}:t_{pred}}) + \\ &\lambda_{fde}\mathcal{L}_{L2}(\hat{Y}_i^{t_{obs}+t_{pred}}, Y_i^{t_{obs}+t_{pred}})], \end{aligned} \tag{5.6}$$

where $W$ is the collection of the weights of all networks used in our model and the different $\lambda$ represent the corresponding regularizers between these losses. As stated in Equation 5.3, $\mathcal{L}_{GAN}$ represents the min-max game where the generator tries to minimize the function while the discriminator tries to maximize it. ADE loss function is commonly used to compute the average error between the predicted trajectories and the corresponding ground-truth. Moreover, we add FDE loss function to explicitly optimize the distribution towards the final real point.

## 5.3. Experimental Results

### 5.3.1. Dataset

We evaluate our work on the well-established and public available Argoverse Motion Forecasting dataset [5], including the training, validation and testing subsets from its official website [155].

It consists of 205942 training samples, 39472 validation samples and 78143 samples. Each sample in the Argoverse Dataset has a length of 5 seconds, with an observation window of 2 seconds and a prediction window of 3 seconds, including the corresponding labels of the agents (AGENT, as the target agent, AV, the vehicle that captures the scene and OTHER, representing the remaining relevant obstacles) and a global map from the cities of Pittsburgh and Miami. The sampling frequency is 10Hz. The main goal here is to predict the 3s future position of the target agent in the scene, which is supposed to be the vehicle that faces the most challenging traffic scenarios.

### 5.3.2. Metrics

Previous works **mercat2020multiattentmotion**, [79], [129] report the minimum Average Displacement Error (minADE$_K$), which averages the $L2$ distances between the ground truth and predicted output across all timesteps and minimum Final Displacement error (FDE$_K$), which computes the $L2$ distance between the final points of the ground-truth and the predicted final position, taking the best $K$ trajectory sample of each agent compared to the ground truth. In the present work, we use $K = 1$ (unimodal case).

### 5.3.3. Implementation details

All local test were conducted in a PC desktop (AMD Ryzen 9 5900X, 32GB RAM with CUDA-based NVIDIA GeForce RTX 3090 24GB VRAM, Ubuntu 18.04).

We design our dataloader to sample in each batch a 30/70 proportion of straight and curved trajectories (regarding the target agent's whole trajectory). We classify a trajectory as straight or curve estimating a first degree trajectory by means the RANSAC algorithm with the highest number of inliers (tolerance $t$ set to 2m, max trials=30, min samples=60% total observations). Then, if the actual trajectory presents 20% or more consecutive points further than $t$ with respect to the closest point of the fitted trajectory, the whole sequence is labelled as curve. We do this to focus in the training process in non-linear prediction, which represents one the key challenges in vehicle motion prediction.

Regarding the ablation study, we train the different models for 150 epochs using Adam optimizer with learning rate 0.001 and default parameters, linear LR Scheduler with factor 0.5 decay on plateaus (5k iterations) and batch size 64. The loss function is weighted by setting $\lambda_{gan}$=1.4, $\lambda_{ade}$=1 and $\lambda_{fde}$=1.5, giving more importance to the adversarial loss and the final displacement error. Similar to [129], the LSTM encoder (attention block) encodes trajectories using a single layer MLP with an embedding dimension of 16. We set all LSTM units to have 32 hidden dimensions. The number of target points is set also to 32 in order to compute the physical context. Moreover, in order to calculate these target points we consider the same prediction horizon $t_{pred} = 3s$ to estimate the distance

travelled assuming a constant velocity model. To make our model more robust to scene orientation, we augment the training data adding some white noise ($\mu = 0, \sigma = 0.25$, [m]) to the observation data, rotating the scene and also dropping and replacing (with their last frame) some observations of the past trajectory in order to make the trained model general enough so as to perform well on the unseen traffic scenarios in the split test which different scene geometries such as left/right turning or emergency braking.

### 5.3.4. Model results

In this section, we perform an ablation study and compare our method's performance against state-of-the-art results on the Argoverse Motion Forecasting benchmark (split test). Additionally, we conduct a statistical analysis on the Argoverse validation set for the ADE and FDE metrics, distinguishing the performance between straight and curved trajectories.

Table **??** illustrates the comparison with some Argoverse baseline methods. Our baseline (*) is represented by the system pipeline illustrated in Fig. **??**, that is, LSTM based GAN with Multi-Head Self-Attention, without target points extractor. We conduct an ablation study to observe the influence of incorporating target points and class balance to our baseline. As expected, by explicitly defining the locations an agent is likely to be at a fixed prediction horizon for a given input trajectory and scene geometry, we are able to improve our baseline. Additionally, since nonlinear trajectories are more challenging than standard straight trajectories, we also observe how enforcing the class balance (straight, curve) during training is able to improve performance.

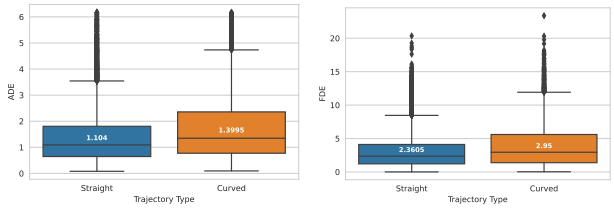


Figure 5.3: Statistical results on the Argoverse Validation Dataset. We show the boxplots for ADE and FDE metrics. We distinguish between straight and curved trajectories. We highlight the median (Q2) in each boxplot.

On the other hand, we analyze our performance on the Argoverse Validation Dataset, we use 31000 samples: 23012 straight and 7988 curved trajectories. We show in Figure 5.3 the boxplots for the ADE and FDE metrics. As stated before, our method, as most methods, struggles with curved trajectories, the overall ADE and FDE is "always" better for the straight trajectory cases. The median provides a robust estimator of our trajectories error. Note that we detected multiple outliers in our analysis, these are due to the unimodal nature of the predicted trajectories that makes difficult for the model to consider multiple possible hypotheses (multimodal).

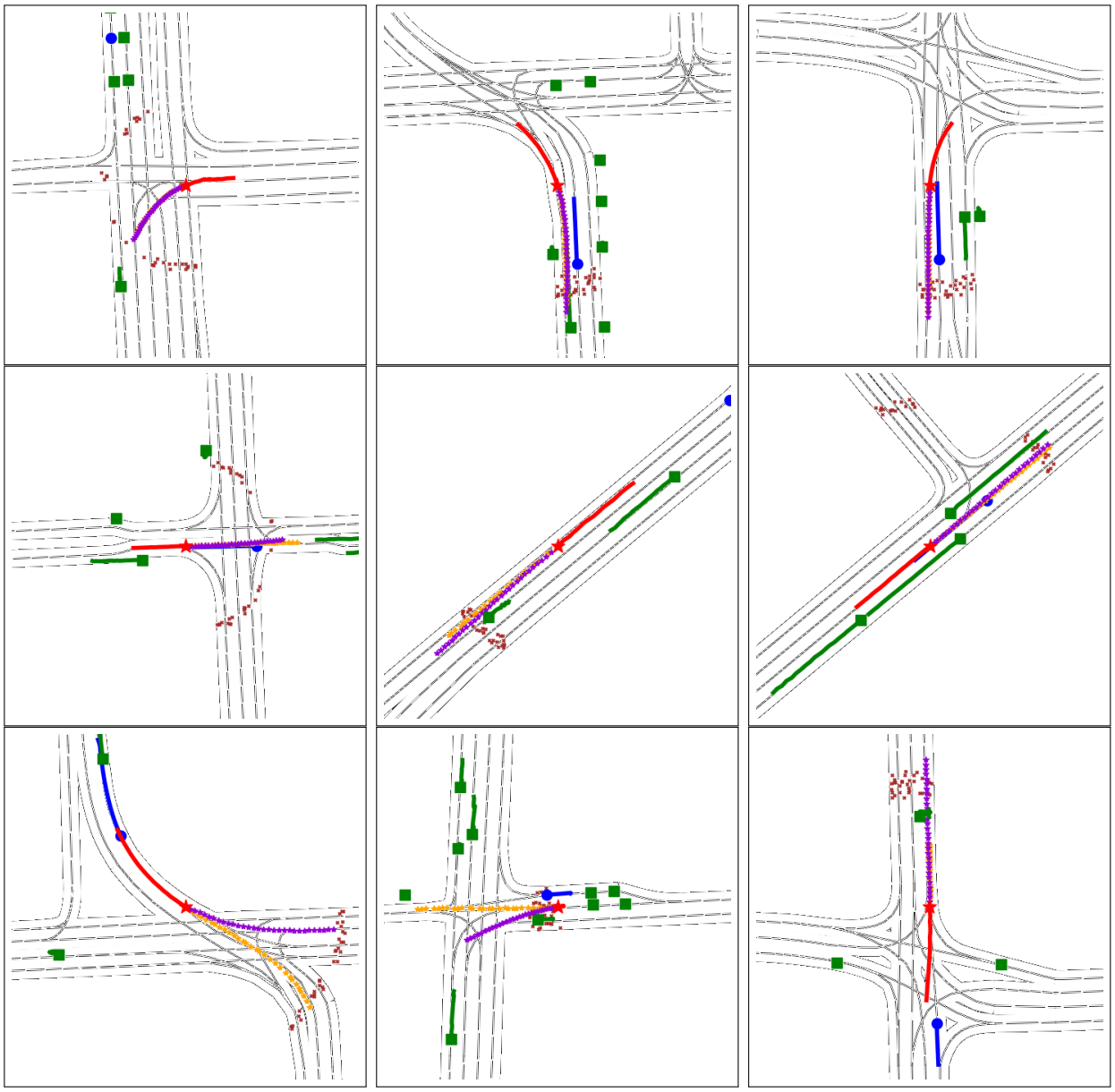

Figure 5.4: Qualitative Results using our best model (including target points extraction and class balance). The legend is as follows: our vehicle (ego), the target agent, and other agents. We can also see the real trajectory, the prediction and potential goal-points. Markers are current positions. First and second rows shows feasible predicted trajectories, whilst the third one shows interesting challenging scenarios in which our current approach is not able to properly reason.

Fig. 5.4 illustrates some qualitative results, all of them considering unimodal prediction towards the precomputed target points, meeting the physical and social constraints in the scenes. It can be clearly appreciated that a naive CTRV (Constant Turn Rate Velocity) could not generalize in these situations, where the vehicle can describe a curved future trajectory given a predominant straight input trajectory and viceversa. On top of that, second row illustrates quite interesting scenarios where the lack of reasoning and multimodality (producing a set of k-trajectories towards the set of target points) is revealed, being situations in which predicting accurately the end-point is difficult, and this the FDE is extremely high. Left image shows how we compute an unimodal prediction

in the wrong direction of a split, even though target points are extracted very close to the groundtruth end point. Center image shows an extreme difficult situation, where the input trajectory is almost in the same place (probably the target agent was stopped in front a traffic light) whilst the groundtruth future trajectory is clearly an acceleration since the last observation frame. Finally, right image shows a deceleration because of the ahead obstacle whilst our model is not able to properly reason the presence of this obstacle in order to meet common sense safety constraints.

## 5.4. Summary

# Chapter 6

# Efficient Baselines for Motion Prediction in Autonomous Driving

*La fuerza de tus convicciones*
*determina tu éxito,*
*no el número de tus seguidores.*

Reamus Lupin
Harry Potter y Las Reliquias de la Muerte, Parte 2

## 6.1. Introduction

As observed in the previous section, our GAN-based model (more specifically the generator) was able to compute the deep context regarding the agents past observations, attention-based social interaction and target points as physical context, but the prediction was limited to the unimodal case. In other words, the GAN-based model is able to reason more complex interactions and future behaviours than SmartMOT (physics-based prediction), but it lacks one of the main features of a deep learning-based model as a preliminary stage before the local planning or decision-making layers: Multimodality. On top of that, at this point of the thesis the literature was re-visited and despite GANs-based approaches [67], [129], [146], [152] provide certain control since they are focused on more simple methods framed in an adversarial training, most competitive approaches on MP benchmarks in the field of AD, such as Argoverse [5], NuScenes [92] or Waymo [91], **do not** use adversarial training, where the training complexity is one the main reasons.

## 6.2. Efficient Baselines

Considering the trade-off between curated input data and complexity, we aim to achieve competitive performance in the MP using powerful DL techniques in terms of prediction

metrics (minADE, minFDE), including attention mechanisms and GNNs, while reducing the number of parameters of operations with respect to other SOTA methods. In particular, we propose two baselines, social and map baseline.

The only inputs for the social baseline are the agent past trajectories and their corresponding interactions. On the other hand, for the map baseline, we propose an extension with respect to our previous target points proposals where, based on a simple-yet-powerful map pre-processing algorithm where the corresponding agent trajectory is initially filtered, the feasible area with which the agent can interact is computed. In spite the fact that topological, semantic and geometric information are involved while computing this area due to road connectivity, we only retrieve the geometric information of the feasible area proposals in an efficient and elegant way. Therefore, our models do not require full-annotated (including, topological, geometric and semantic) HD Map information as input or even rasterized BEV representations of the scene to compute the physical context. Figure 6.1 illustrates an overview of our final approach.

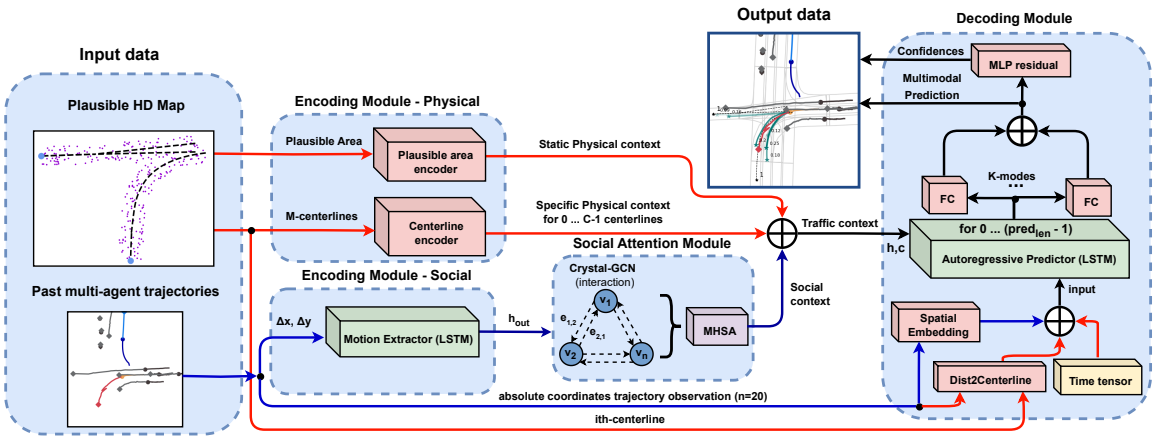


Figure 6.1: Overview of our final efficient baseline model (**Blue links** and **Red links** represent **Social** and **Map** information respectively). We distinguish three main blocks: 1) **Encoding module**, which uses plausible HD Map information (specific centerlines and driveable area around) and agents past trajectories to compute the motion and physical latent features, 2) **Social Attention module**, which calculates the interaction among the different agents and returns the most relevant social features, 3) **Decoding module**, responsible for calculating the multimodal prediction by means of an auto-regressive strategy concatenating low-level map features and social features as a baseline, as well as iterating over the different latent centerlines for specific physical information per mode.

### 6.2.1. Social Baseline

Our social baseline is inspired in the architecture proposed by [12]. It uses as input the past trajectories of the most relevant obstacles as relative displacements to feed the Encoding Module (Figure 6.1). Then, the social information is computed using a GNN, in particular Crystal-Graph Convolutional Network (**Crystal-GCN**) layers [12], [156], and Multi-Head Self Attention (MHSA) [115] to obtain the most relevant agent-agent interactions. Finally, we decode this latent information using an **autoregressive** strategy

where the output at the *i-th* step depends on the previous one for each mode respectively in the Decoding Module. The following sections provide in-depth description of the aforementioned modules.

#### 6.2.1.1. Preprocessing of past trajectories

Multiple methods [12], [13] consider only the vehicles that are observable at *t=0*, handling those agents that are not observed over the full sequence spectrum (observation length = $obs_{len}$ + prediction length = $pred_{len}$) by concatenating a binary flag $b_i^t$ that indicates if the agent is padded or not. In our case, we consider the agents that have information over the full history horizon $T_h = obs_{len} + pred_{len}$ (*e.g.* 5s timeframe for Argoverse), reducing the number of agents to be considered in complex traffic scenarios. Furthermore, to make the model translation and rotation invariant, the coordinate system in our model is BEV centered of a given target agent at $t = 0$, and we use the orientation from the target location given in the same timestamp as the positive $x$-axis. Note that this representation will benefit the model to have a common representation to enhance the generalization of the model and prevent overfitting. Once the scene has been translated and rotated, instead of using absolute 2D-BEV ($xy$ plane), the input for the agent $i$ is a series of relative displacements:

$$\Delta\boldsymbol{\nu}_i^t = \boldsymbol{\nu}_i^t - \boldsymbol{\nu}_i^{t-1} \tag{6.1}$$

Where $\boldsymbol{\nu}_i^t$ represents the state vector (in this case, $xy$ position of the agent $i$ at timestamp $t$.

#### 6.2.1.2. Encoding of past trajectories

Unlike other methods, we do not limit nor fix the number of agents per sequence. Given the relative displacements of all different agents, a single LSTM is used to compute the temporal information of each agent in the sequence:

$$out, \mathbf{h_{out}}, \mathbf{c_{out}} = \text{LSTM}(\Delta\boldsymbol{\nu}^{obs_{len}}, \mathbf{h_{in}}, \mathbf{c_{in}}) \tag{6.2}$$

This LSTM encoder shares the weights for all vehicles in the batch. The input hidden and cell vectors ($\mathbf{h_{in}}, \mathbf{c_{in}}$) are initialized with a tensor of zeros. $\Delta\boldsymbol{\nu}^{obs_{len}}$ represents the relative displacements over the whole past horizon $obs_{len}$. In order to feed the agent-agent interaction module (Social Attention Module in Figure **??**), we take the output hidden vector ($\mathbf{h_{out}}$).

#### 6.2.1.3. Social Attention module

After encoding the past history of each vehicle in the sequence, we compute the agent-agent interactions to obtain the most relevant social information of the scene. For this purpose, we construct an interaction graph using Crystal-GCN [156] [12]. , originally developed for the prediction of material properties, allowing to efficiently leverage edge features. Then, Multi-Head Self-Attention (MHSA) [115] is applied to enhance the learning of agent-agent interactions.

Before creating the **interaction mechanism**, we split the temporal information in the corresponding scenes, taking into account that each traffic scenario may have a different number of agents. The interaction mechanism is defined in [12] as a bidirectional fully-connected graph, where the initial node features $\mathbf{v}_i^{(0)}$ are represented by the latent temporal information for each vehicle $\mathbf{h}_{i,out}$ computed by the motion history encoder. On the other hand, the edges from node $k$ to node $l$ is represented as the vector distance ($\mathbf{e}_{k,l}$) between the corresponding agents at t = $obs_{len}$ in absolute coordinates, where the origin of the sequence ($x = 0, y = 0$) is represented by the position of the target at t = $obs_{len}$:

$$\mathbf{e}_{k,l} = \boldsymbol{\nu}_k^{obs_{len}} - \boldsymbol{\nu}_l^{obs_{len}}, \tag{6.3}$$

Given the interaction graph (nodes and edges), the Crystal-GCN, proposed by [156], is defined as:

$$\mathbf{v}_i^{(g+1)} = \mathbf{v}_i^{(g)} + \sum_{j=0:j\neq i}^{N} \sigma\left(\mathbf{z}_{i,j}^{(g)}\mathbf{W}_{\mathrm{f}}^{(g)} + \mathbf{b}_{\mathrm{f}}^{(g)}\right) \odot \mu\left(\mathbf{z}_{i,j}^{(g)}\mathbf{W}_{\mathrm{s}}^{(g)} + \mathbf{b}_{\mathrm{s}}^{(g)}\right). \tag{6.4}$$

This operator, in contrast to many other graph convolution operators [86] [13], allows the incorporation of edge features in order to update the node features based on the distance among vehicles (the closer a vehicle is, the more is going to affect to a particular node). As stated by [12], we use $L_g = 2$ layers of the GNN ($g \in 0, \ldots, L_g$ denotes the corresponding Crystal-GCN layer) with ReLU and batch normalization as non-linearities between the layers. $\sigma$ and $\mu$ are the sigmoid and softplus activation functions respectively.

Moreover, $\mathbf{z}_{i,j}^{(g)} = (\mathbf{v}_i^{(g)}||\mathbf{v}_j^{(g)}||\mathbf{e}_{i,j})$ corresponds to the concatenation of two node features in the $g_{th}$ GNN layer and the corresponding edge feature (distance between agents), N represents the total number of agents in the scene and $\mathbf{W}$ and $\mathbf{b}$ the weights and bias of the corresponding layers respectively.

After the interaction graph, each updated node feature $\mathbf{v}_i^{(L_g)}$ contains information about the temporal and social context of the agent $i$. Nevertheless, depending on their current position and past trajectory, an agent may require to pay attention to specific social information. To model this, we make use of a scaled dot-product Multi-Head Self-

Attention mechanism [115] which is applied to the updated node feature matrix $\mathbf{V}^{(L_g)}$ that contains the node features $\mathbf{v}_i^{(L_g)}$ as rows.

Each head $h \in 1, \ldots, L_h$ in the MHSA mechanism is defined as:

$$\text{head}_h = \text{softmax}\left(\frac{\mathbf{V}_{Q_h}^{(L_g)}\mathbf{V}_{K_h}^{(L_g)T}}{\sqrt{d}}\right)\mathbf{V}_{V_h}^{(L_g)}. \tag{6.5}$$

where $\mathbf{V}_{Q_h}^{(L_g)}$ (Query), $\mathbf{V}_{K_h}^{(L_g)}$ (Key) and $\mathbf{V}_{V_h}^{(L_g)}$ (Value) represent the $h_{th}$ head linear projections of the node feature matrix $\mathbf{V}^{(L_g)}$ and $d$ is the normalization factor corresponding to the embedding size of each head. For our purpose, we use $L_h = 4$ as the total number of heads.

The result of the softmax weights multiplied by the node feature matrix $\mathbf{V}_{V_h}^{(L_g)}$ (Value) is often referred as the attention weight matrix, representing in this particular case pairwise dependencies among vehicles.

Finally, the updated node feature matrix **SATT** is computed as the combination of the different attention heads in a single matrix:

$$\mathbf{SATT} = (\text{head}_1||\ldots||\text{head}_{L_h})\mathbf{W}_\text{o} + \begin{pmatrix}\mathbf{b}_\text{o}\\ \vdots \\ \mathbf{b}_\text{o}\end{pmatrix}. \tag{6.6}$$

Where each row of the final social attention matrix **SATT** (output of the social attention module, after the GNN and MHSA mechanisms) represents the interaction-aware feature of the agent $i$ with surroundings agents, considering the temporal information under the hood, being $\mathbf{W}_\text{o}$ / $\mathbf{b}_\text{o}$ the corresponding weight and bias of the layer that merges the different attention heads. As this model has been developed upon the Argoverse 1 Motion Forecasting benchmark, we **only consider** the row of the final matrix that takes into account the interactions of the target agent with surrounding obstacles.

### 6.2.2. Map Baseline

As mentioned before, in this work we extend our social baseline using minimal HD map information, from which we discretize the feasible area $\mathcal{P}$ of the target agent as a subset of $r$ randomly sampled points $\{p_0, p_1 ... p_r\}$ (low-level features) around the plausible centerlines (high-level and well-structured features) considering the velocity and acceleration of the corresponding agent in the last observation frame, as observed in Figure 6.2. As stated in Section 5.2, this is a map preprocessing step, therefore the model never sees the HD map (either vectorized or rasterized) image nor the whole graph of nodes.

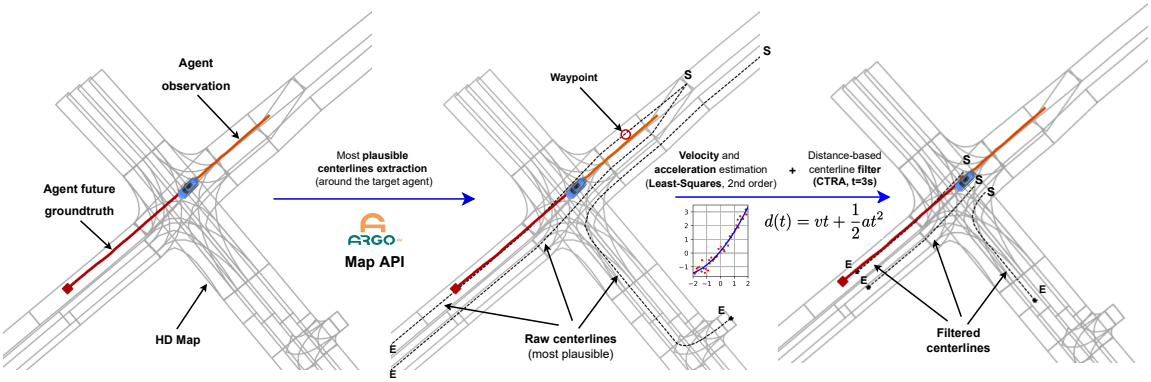


Figure 6.2: Plausible centerlines estimation. Left: General view of the scene, only considering the target agent (**observation (2 s)** and **future ground-truth (3 s)**) and HD Map around its last observation (position of the **blue** vehicle). Center: **Centerlines** proposed by the Argoverse Map API (maximum number of centerlines $M$ set to 3). Right: We filter the input observation by means of Least-Squares (2nd order) algorithm to estimate the velocity and acceleration of the agent. Then, the distance considering a CTRA (Constant Turn Rate Acceleration) model and a prediction horizon of 3 s are used computed to obtain the end-points **E** of the **final proposals**. Start-points **S** are the closest centerlines waypoints to the agent in the last observation frame.

#### 6.2.2.1. Centerlines proposals and Feasible area points

In a similar way to the target points computed in our GAN-based model, we want to compute the heuristic proposals for each agent. Nevertheless, instead of limiting the map baseline to some discrete target points, now we aim to compute the most plausible future centerlines (that is, the center of the lane) as a connection of nodes (waypoints). Considering lane connectivity, multiple approaches have tried to predict realistic trajectories by means of learning physically feasible areas as heatmaps or probability distributions of the agent's future location [8], [129], [146]. [13] represents the map as a set of lanes and their connectivity (predecessor, successor, right neighbour, left neighbour), taking into account all lanes whose distance from the target agent is smaller than 100 m as the input, regardless the orientation or the velocity of the vehicle. On the other hand, [157] encodes static elements such as crosswalks, lane, road boundaries and intersections that are included in a local map 150m x 100m centered in the corresponding vehicle as a multi-channel image. These approaches require either a top-view RGB BEV image of the scene, or a HD map with exhaustive topological, geometric and semantic information (commonly codified as channels). This information is usually encoded using a CNN and fed into the model together with the social agent's information [71], [129], [146].

As observed, when trying to utilize HD map information, specially in terms of lane proposals, most SOTA methods utilize this physical to enhance the latent information to decode the future trajectories, but heavy computation or raw data features are required.

**Effectively** and **efficiently** exploiting HD maps is a must for MP models to produce accurate and plausible trajectories in real-time applications, specially in the field of AD, providing specific map information to each agent based on its kinematic state and geo-

metric HD map information. In that sense, we propose to obtain the most plausible $M$ lane candidates, we make use of the pertinent heuristic functions proposed by the Argoverse 1 Motion Forecasting dataset Map API [5] as illustrated by [17] to choose the closest centerlines to the last observation data of the target agent, which are going to represent its most representative future trajectories. On the other hand, as depicted in the MP dataset used to train this model (Argoverse 1), vehicles are the only evaluated object category as the target agent. Then, considering a vehicle as a rigid structure with non-holonomic [88] features (no abrupt motion changes between consecutive timestamps) and the road driving task is usually described as anisotropic [158] (most relevant features are found in a specific direction, in this case the lanes ahead). In other words, the agent should follow a smooth trajectory in a short-mid term prediction. The heuristic to obtain these centerlines is summarized as follows:

1. Trajectory data presents noise associated to the real-world data capturing the exact position of the previously tracked vehices in real-world scenarios. Regarding this, we filter the agent trajectory as a polynomial curve fitting problem by means of the Least Squares ($2^{nd}$ order) per axis and Savitzky-Golais [159] algorithms to obtain a smooth representation of the position vector.

2. By doing so, and assuming the agent is moving with a constant acceleration, we are able to calculate the subsequent derivatives (velocity and acceleration) of the target agent in $t_{obs_{len}}$. Then, a vector of $obs_{len}$ - 1 and $obs_{len}$ - 2 length is computed to estimate the velocity and acceleration respectively as $V_i = \frac{X_i - X_{i-1}}{t_i - t_{i-1}}$ and $A_i = \frac{V_i - V_{i-1}}{t_i - t_{i-1}}$, where $X_i = [x_i, y_i]$ represents the 2D position of the agent at each observed frame $i$.

3. In order to compute the velocity, acceleration and yaw angle in the last observation frame, we compute a weighted mean by assigning less importance (weight) to the first positions of the corresponding vector and higher importance to the latter states, in such a way immediate past observations are the key states to determine the current spatio-temporal variables of the agent, as depicted in Equation 5.2.

4. We compute the future travelled distance by means of the well-known Constant Acceleration (CA) model:

$$d(t) = x_0 + vt + \frac{1}{2}at^2 \tag{6.7}$$

where $t$ corresponds to the prediction horizon $t_pred$, $x_0$ is equal to 0 since we want to determine the travelled distance from the current position and $v$ and $a$ are the velocity and acceleration in the last observation frame previously calculated. Note that we assume that this is a CTRA model, instead of only Constant Acceleration (CA) in a specific direction, since the orientation is implicit in the lane boundaries. That's why it does not make sense to involve the orientation at frame $t = 0$ in the travelled distance calculation.

5. Get all lane candidates within a bubble, given the agent last observation and Manhattan distance.

6. Expand the bubble until at least 1 lane is found.

7. Once some preliminary proposals are found, we employ the Depth First Search (DFS) algorithm to get all successor and predecessor candidates, merging the past and future candidates and removing the overlapping ones.

8. Then, we process these raw candidates so as to use them as plausible physical information. Given these raw lanes, we aim to limit the number of centerlines to a fixed number $M$. First, given the previously computed smoothed trajectory, we compute the closest centerlines to our current position since they will represent the most realistic future lanes in the traffic scenario. Second, we evaluate the above-mentioned travelled distance along the raw centerlines. We determine the end-point index $p$ of the centerline $m$ as the waypoint (each discrete node of the centerline) where the accumulated distance (considering the $\mathcal{L}_2$ distance between each waypoint) is greater or equal than the above-computed $d(obs_{len})$:

$$p \quad : \quad d(obs_{len}) \leq \sum_{p=start_{point}}^{centerline_{length}} \mathcal{L}_2(w(p+1), w(p)) \tag{6.8}$$

9. Finally, in order to have the same points (particularly, the number of points matches the prediction horizon $t_pred$, also referred as $pred_len$) per centerline, we interpolate them using a $1^{st}$ spline order, considering as start point the last agent observation and as end or goal point the aforementioned travelled distance along the corresponding centerline.

10. Note that if the number of proposed centerlines is lower than a pre-defined number $M$, a virtual centerline is created and padded with zeros.

Figure 6.2 summarizes this HDMap filtering process, where we are able to estimate the preliminary centerlines proposals as a **simplified version of the HD map**. Moreover, Fig. **??** illustrates how after our filtering process the end-points of the plausible centerlines are noticeable closer to the ground-truth prediction at the final timestep.

In addition to these **high-level** and well-structured centerlines, we apply point location perturbations to all plausible centerlines under a $\mathcal{N}(\mu, \sigma)$ [m] distribution [160] in order to discretize the plausible area $\mathcal{P}$ as a subset of $r$ randomly sampled points $\{p_0, p_1 ... p_r\}$ (**low-level** features) around the plausible centerlines. By doing this, we may have a common representation of the plausible area, defined as low-level map features. We make use of a normal distribution $\mathcal{N}$ to calculate these random points as an additional regularization term in a similar way that data augmentation is applied to the past trajectories.

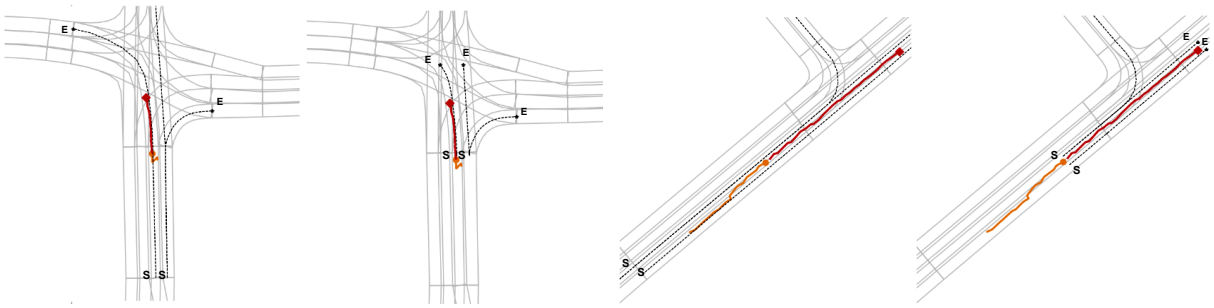


Figure 6.3: Some challenging examples of our preprocessing step to obtain relevant map features. In both scenarios the target agent (**observation (2 s)** and **future ground-truth (3 s)**) presents a noticeable noisy past trajectory and the provided raw **centerlines** do not consider the current kinematic state of the vehicle. (a) The agent is stopped (maybe due to an stop, pedestrian crossing or red traffic light use case). We estimate a minimum travelled distance of 25 m in these situations to determine the centerline end-points **E**. (b) In this scenario, we can observe how the raw centerlines consider way more distance (both ahead and behind) than required. Our kinematic-based filter is able to minimize these proposals in an interpretable way to serve as prior information to the MP model

#### 6.2.2.2. Encoding module of map information

In order to calculate the latent map information, we employ a plausible area and centerline encoder (Figure 6.1) to process the low-level and high-level map features respectively. Each of these encoders are represented by a Multi-Layer Perceptron (MLP). First, we flat the information along the points dimension, alternating the x-axis and y-axis information. Then, the corresponding MLP (three layers, with batch normalization, interspered ReLUs and dropout in the first layer) transforms the interpretable absolute coordinates around the origin ($x = 0, y = 0$) into representative latent physical information. The static physical context (output from the plausible area encoder) will serve as a common latent representation for the different modes, whilst the specific physical context will illustrate specific map information for each mode.

### 6.2.3. Augmented Efficient baseline with Transformer Encoders

Once the social and map baseline encoders are stated, we focus on a more powerful mechanism to encode the spatial and temporal information of inputs by encoding them into feature vectors. In that sense, we focus of designing an effective encoder transformer while keeping its structure as simple and efficient as possible. In a similar way to [161], we adopt the combination of CNN/MLP, attention block and normalization, as observed in Figure 6.4.

In order to encode the centerlines, we first use an MLP-based encoder to transform the input vector at each time stamp ($d_i^t$, which actually represents a plausible position of the target agent) into deep features:

$$f_i^t = MLP_{\text{map}}\left(d_i^t; W_{\text{map}}\right) \tag{6.9}$$

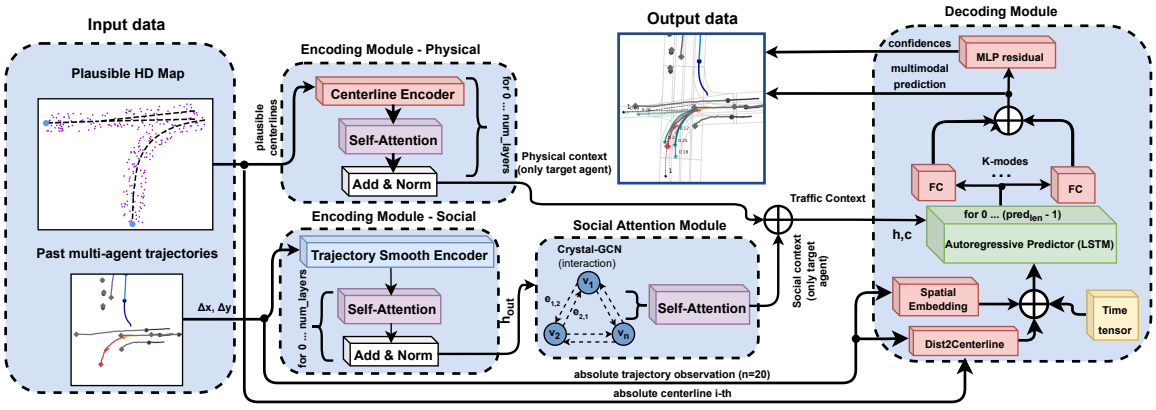


Figure 6.4: Efficient baseline with transformer encoders to process the physical and social input

where $MLP_{\text{map}}$ is a Multi-Layer (3) Perceptron with a ReLU asnon-linear layer and $W_{\text{map}}$ as the weight matrix that is learnable. However, to predict the future trajectory, the separate feature of each vector is insufficient. For example, even if two road segments in the first half have the same structure, the difference in the last half can result in a total difference in geometric meaning. Therefore, we make use of the well-established Multi-Head Self-Attention (MHSA) [115] mechanism to encode the overall set of physical features per agent as a single vector.

To be more specific, we first calculate the query, key and value matrix:

$$q_i^t = W^q f_i^t, k_i^t = W^k f_i^t, v_i^t = W^q f_i^t, \tag{6.10}$$

where $W^q, W^k, W^v$ are the learnable weight matrices. Then, we take these three matrices as the inputs of the weighting block based on softmax:

$$h_i^t = \text{softmax}\left(\frac{q_i^t \cdot k_i^{tT}}{\sqrt{d_k}}\right) v_i^t, \tag{6.11}$$

where $d_k$ is the length of matrix $k$. Finally, we adopt a 2-layer MLP to aggregate the features of vectors within a road segment:

$$h_i = MLP_{agg}\left(h_i^t; W_{agg}\right) \tag{6.12}$$

where $MLP_{agg}$ is a 2-layer MLP with a ReLU non-linear layer and $W_{agg}$ is the weight matrix that is learnable. Now, we have the feature vector for each target agent, stored as a 2D matrix $(M, H)$, where $M$ is the number of road segments and H is the length of hidden features.

For agents, we use similar techniques to encode and aggregate the information. In particular, we use a trajectory encoder block to encode each vector into the form of a feature vector. Then, similar to roads, even two vehicles have the same movement in the

first half of their trajectory, and the differences in the last half of trajectories can lead to a totally different future trajectory. Therefore, we use a MHSA block to encode the overall feature of one trajectory in the observed time period and form a single feature vector for each agent. Finally, a 2-layer MLP-based aggregator is used to construct a single feature vector for each trajectory.

One aspect worth mentioning is the agent encoder. While trajectory data are, unlike roads (well structured) usually non-smooth, as expected from real-world datasets. Then, while we make use of MLP to compute the deep physical features, we use a 1D-CNN based motion encoder in the first stage due to its wider receptive field compared with MLP in such a way the convolutional encoder can smooth the trajectories and reduce the influence of noisy input trajectories.

### 6.2.4. Decoding module

The decoding module is the third component of our baselines, as observed in Figure 6.1. The decoding module consists of an **LSTM** network, which recursively estimate the relative displacements for the future timesteps, in the same way we studied the past relative displacements in the Motion History encoder. Regarding the social baseline, the model uses the social context computed by the Social Interaction Module, only paying attention to the target agent row. Then, only the social context corresponds to the whole *traffic context* of the scenario, representing the input hidden vector of the autoregressive LSTM predictor. On the other hand, in terms of the map baseline, for a mode $m$, we identify the latent *traffic context* as the concatenation of the social context, static physical context and specific physical context as stated in Section 6.2.2.2, which will serve as input hidden vector $\mathbf{h}$ of the LSTM decoder. In both cases (social and map baselines), the cell vector $\mathbf{c}$ is initialized with a vector of zeros of the same dimension.

Regarding the LSTM input, in the social case it is represented by the encoded past $n$ relative displacements of the target agent after a spatial embedding, whilst the map baseline adds the encoded vector distance between the current absolute target position and the current centerline, as well as the current scalar timestamp $t$, as illustrated in Figure 6.1. In both cases (social and map baselines), we process the output of the LSTM using a standard Fully-Connected (FC) layer (one per mode). Once we have the relative prediction in the timestep $t$, we shift the initial past observation data in such a way we introduce our last-computed relative displacement at the end of the vector, removing the first data. We identify this technique as a *temporal decoder*, where a window of size $n$ is analized by the autoregressive decoder in contrast to other techniques [67], [129], [146] where only the last data is considered. Finally, after performing relative displacements to absolute coordinates operation, we obtain our multimodal predictions $\hat{Y} \in \mathbb{R}^{k \times pred_{len} \times data_{dim}}$, where $k$ represents the number of modes, $pred_{len}$ represents the prediction horizon and $data_{dim}$ represents the data dimensionality, in this case $xy$, predictions from the BEV perspective).

Once the multimodal predictions are computed, they are concatenated and processed by a residual MLP to obtain the confidences (the higher the confidence, the most probable the mode must be, and closer to the ground-truth).

### 6.2.5. Losses

We use the standard **Negative Log-Likelihood** (NLL) loss to train our social and map baselines in order to compare the ground-truth points $Y \in \mathbb{R}^{pred_{len} \times data_{dim}} = \{(x_0, y_0)...(x_{pred_{len}}, y_{pred_{len}})\}$ with our multimodal predictions ($\hat{Y} \in \mathbb{R}^{k \times pred_{len} \times data_{dim}}$), given $k$ modalities (hypotheses) $\mathbf{p} = \{(\hat{x}_0^1, \hat{y}_0^1)...(\hat{x}_{pred_{len}}^k, \hat{y}_{pred_{len}}^k)\}$, with their corresponding confidences $\mathbf{c} = \{c_1...c_k\}$ using the following equation:

$$\text{NLL} = -\log \sum_k e^{\log c^k - \frac{1}{2}\sum_{t=0}^{pred_{len}} (\hat{x}_t^k - x_t)^2 + (\hat{y}_t^k - y_t)^2} \tag{6.13}$$

Similar to [70], we assume the ground-truth points to be modeled by a mixture of multi-dimensional independent Normal distributions over time (predictions with unit covariance). Minimizing the NLL loss maximizes the likelihood of the data for the forecast. Nevertheless, the NLL loss tends to overfit most predictions in a similar direction. As stated above, in the motion prediction task, specially in the Autonomous Vehicles field, we must build a model that not only reasons multimodal predictions in terms of different maneuvers (keep straight, turn right, lane change, etc.) but also different velocity profiles (constant velocity, acceleration, etc.) regarding the same maneuver. For this reason, after the baselines models have been trained, as stated by [162], we add as regularization the Hinge (*a.k.a.*max-margin) and **Winner-Takes-All** (WTA) [13], [162] losses to improve the confidences and regressions respectively.

Algorithm 3 illustrates how we compute the max-margin and WTA losses. First, we determine the closest mode $m^*$ to the ground-truth using the $\mathcal{L}_2$ distance, only considering the end-points. Then, WTA loss is computed using Smooth $\mathcal{L}_1$ distance taking into account in this case the whole prediction horizon between the best mode and ground-truth prediction. Finally, we apply the max-margin loss regarding the confidence of the best mode and a margin ($\epsilon$).

**Algorithm 3:** Additional regularization: Hinge and WTA loss

**input:** ground-truth trajectory ($Y \in \mathbb{R}^{pred_{len} \times data_{dim}}$) and output trajectories ($\hat{Y} \in \mathbb{R}^{k \times pred_{len} \times data_{dim}}$), where $k$, $pred_{len}$, and $data_{dim}$ denote the number of modes, prediction horizon, and data dimensionality for the target agent.

**output:** classification loss $\mathcal{L}_{Hinge}$ and regression loss $\mathcal{L}_{WTA}$

**for** $m$ *in* $\{1, 2, \ldots, k\}$ **do**

  $d^m_{wta} \leftarrow$ Euclidean distance between $\hat{Y}^m_{pred_{len}}$ and $Y_{pred_{len}}$;

**end**

$m^* = \arg\min_m d^m_{wta}$;

$\mathcal{L}_{reg,WTA} \leftarrow$ Smooth $\mathcal{L}_1$ loss between $\hat{Y}^{m^*}$ and $Y$;

$\mathcal{L}_{class,Hinge} = \frac{1}{(K-1)} \sum_{m=1 \backslash m \neq m^*}^{K} \max(0, c_k + \epsilon - c_{m^*})$;

**return** $\mathcal{L}_{WTA}$, $\mathcal{L}_{Hinge}$;

Therefore, our loss function is:

$$\mathcal{L} = \alpha \mathcal{L}_{NLL} + \beta \mathcal{L}_{Hinge} + \gamma \mathcal{L}_{WTA} \tag{6.14}$$

## 6.3. Experimental Results

**6.3.0.0.1. Efficiency discussion** In terms of **efficiency discussion**, to the best of our knowledge, very few methods reports efficiency-related information **gilles2021gohome**, [8], [71], [163]. Furthermore, comparing runtimes is difficult, as only a few competitive methods provide code and models. The Argoverse Benchmark [5] provides insightful metrics about the model's performance, mainly related with the predictions error. However, there are no metrics about efficiency (i.e. model complexity in terms of parameters or FLOPs). In the AD context, we consider these metrics as important as the error evaluation because, in order to design a reliable AD stack, we must produce reliable predictions on time, meaning the inference time (related to model's complexity and inputs) is crucial. SOTA methods already provide predictions with an error lesser than 1 meter in the multi-modal case. In our opinion, an accident will rarely happen because some obstacle predictions are offset by one or half a meter, this uncertainty in prediction can be acceptable in the design of AV, but rather because lack of coverage or delayed response time. Despite its high accuracy and fast inference time, LaneGCN [13] makes use of multiple GNN layers that can lead to issues with over-smoothing for map-encoders **li2018deeper**. Moreover, as mentioned in [71], CNN-based models for processing the HD map information are able to capture social and map interactions, but most of them are computationally too expensive. LaneRCNN [86] adds huge number of hyperparameters to the model, making it quite complex since it proposes to capture agent and map interactions with a local interaction graph per agent, not just a single vector.

Table 6.1: Efficiency comparison among SOTA methods. We show the number of parameters for each model, FLOPs, minADE (k=6) in the Argoverse test set, and runtime. Works from [71] focus on unimodal predictions (k=1). *N/A* stands for *Not Available*. Time measured on a RTX 2080 Ti (using batch 32). Some numbers are borrowed from **zhou2022hivt**, **bhattacharyya2022ssllanes**.

| Model | # Par. (M) | FLOPs (G) ↓ | minADE (m) ↓ | Run (ms) ↓ |
|---|---|---|---|---|
| CtsConv [164] | 1.08 | 0.34 | 1.85 | 684 |
| R18-k3-c1-r100 [71] | 0.25 | 0.66 | 2.21 | *N/A* |
| R18-k3-c1-r400 [71] | 0.25 | 10.56 | 2.16 | *N/A* |
| VectorNet [71] | **0.072** | 0.41 | 1.66 | 1103 |
| DenseTNT (w/ 100ms opt.) **gu2021densetntwaymo** | 1.1 | 0.763 | 0.88 | 2644 |
| DenseTNT (w/ goal set pred.) **gu2021densetntwaymo** | 1.1 | 0.763 | 0.85 | 531 |
| LaneGCN [13] | 3.7 | 1.071 | 0.87 | 173 |
| mmTransformer [163] | 2.607 | 0.177 | 0.84 | *N/A* |
| MF-Transformer **he2022multi** | 2.469 | 0.408 | **0.82** | *N/A* |
| HOME+GOHOME **gilles2021gohome** | 0.40 | 0.09 | 0.94 | 32 |
| GAN-based MAPFE4MP (Social baseline) **gomez2022exploringmapbased** | 0.105 | **0.007** | 1.26 | 7 |
| MAPFE4MP (Map baseline) **gomez2022exploringmapbased** | 0.621 | 0.047 | 0.96 | 31 |
| Ours | 1.235 | **0.038** | 0.91 | **16** |

Similar to image classification, where model efficiency depends on its accuracy and parameters/FLOPs, we use the same criteria to compare models. We show the **efficiency comparison** with other relevant methods in Table 6.1. We calculate FLOPs and parameters using a third-party library [1]. Some minor operations were not supported, yet, their contributions to the number of FLOPs were residual and ignored. The results for the other methods are consulted from [8] **gilles2021gohome** [71] **he2022multi**. We calculate FLOPs using the relation: GMACs $\approx 0.5 * $ GFLOPs using https://github.com/facebookresearch/fvcore.

In order to calculate the FLOPs, we follow the common practice [71] [165] [9] of fixing the number of lanes *i.e.,* the number of centerlines is limited to 3. [71] compares its GNN backbone with CNNs of different kernel sizes and map resolution to compute deep map features (decoder operations and parameters are excluded, min), demonstrating how CNN based methods noticeably increase the amount of parameters and operations per second. We do not require CNNs to extract features from the HD map since we use our map-based feature extractor to obtain the feasible area (see Section **??**), assuming anisotropic driving (the most important features are ahead) and non-holonomic constraints, in such a way these features are interpretable in comparison with CNNs high-dimensional outputs. Note that, in both variants (social and map baselines), the self-attention module is used with a dynamic number of input agents, this typically implies a quadratic growth in complexity with the number of agents in the scene [115], yet, this only applies to the MHSA layers.

Even though our method do not obtain the best regression metrics, we achieve comparable results (Table **??**) against other SOTA approaches whilst our number of FLOPs is several orders of magnitude smaller than other approaches **gu2021densetntwaymo** [13], obtaining a good trade-off between model complexity and error (minADE, k=6).

Moreover, as it is well known in machine learning, the number of parameters is not always proportional to the inference speed. In that sense, our transformer approach also

[1] https://github.com/facebookresearch/fvcore

has certain benefits in comparison to LSTM/RNN temporal encoding, since these are non-parallelizable, therefore, despite having more parameters, transformers are faster [115].

We illustrate the qualitative results of our best model.

## 6.4. Summary

Even though our methods do not obtain the best regression metrics, we achieve up-to-pair results (Table **??**) against other SOTA approaches whilst our number of FLOPs is several orders of magnitude smaller than other approaches **gu2021densetntwaymo** [13], obtaining a good trade-off (specially the map baseline) between model complexity and accuracy (minADE, k=6), making it suitable for real-time operation in the field of AD. In our case, considering the top-25 regression metrics we achieve near SOTA results (just 15 cm, which represents 18.5 %, worse in terms of minADE k=6 regarding our final approach) while achieving an impressive reduction of parameters and FLOPs. As observed in Table **??**, if we compare our final model, which includes social information, agents interaction and preliminary road information, and the methods with the closest minADE k=6 [m] (LaneGCN [13], HOME [8] and GOHOME **gilles2021gohome**), we obtain a reduction of 96 %, 99 % and 48 % respectively in terms of FLOPs. It can be observed how including preliminary road information assuming non-holonomic [88] and anisotropic [158] constraints respectively (that is, we mostly focus on the front driveable area) instead of processing the whole map, as well as computing social interactions via graph convolutional networks, boost our model for further integration edge-computing devices with a minimum accuracy loss acceptable for real-world Autonomous Driving applications.

Even though our method do not obtain the best regression metrics, we achieve comparable results (Table **??**) against other SOTA approaches whilst our number of FLOPs is several orders of magnitude smaller than other approaches **gu2021densetntwaymo** [13], obtaining a good trade-off between model complexity and error (minADE, k=6).

Moreover, as it is well known in machine learning, the number of parameters is not always proportional to the inference speed. In that sense, our transformer approach also has certain benefits in comparison to LSTM/RNN temporal encoding, since these are non-parallelizable, therefore, despite having more parameters, transformers are faster [115].

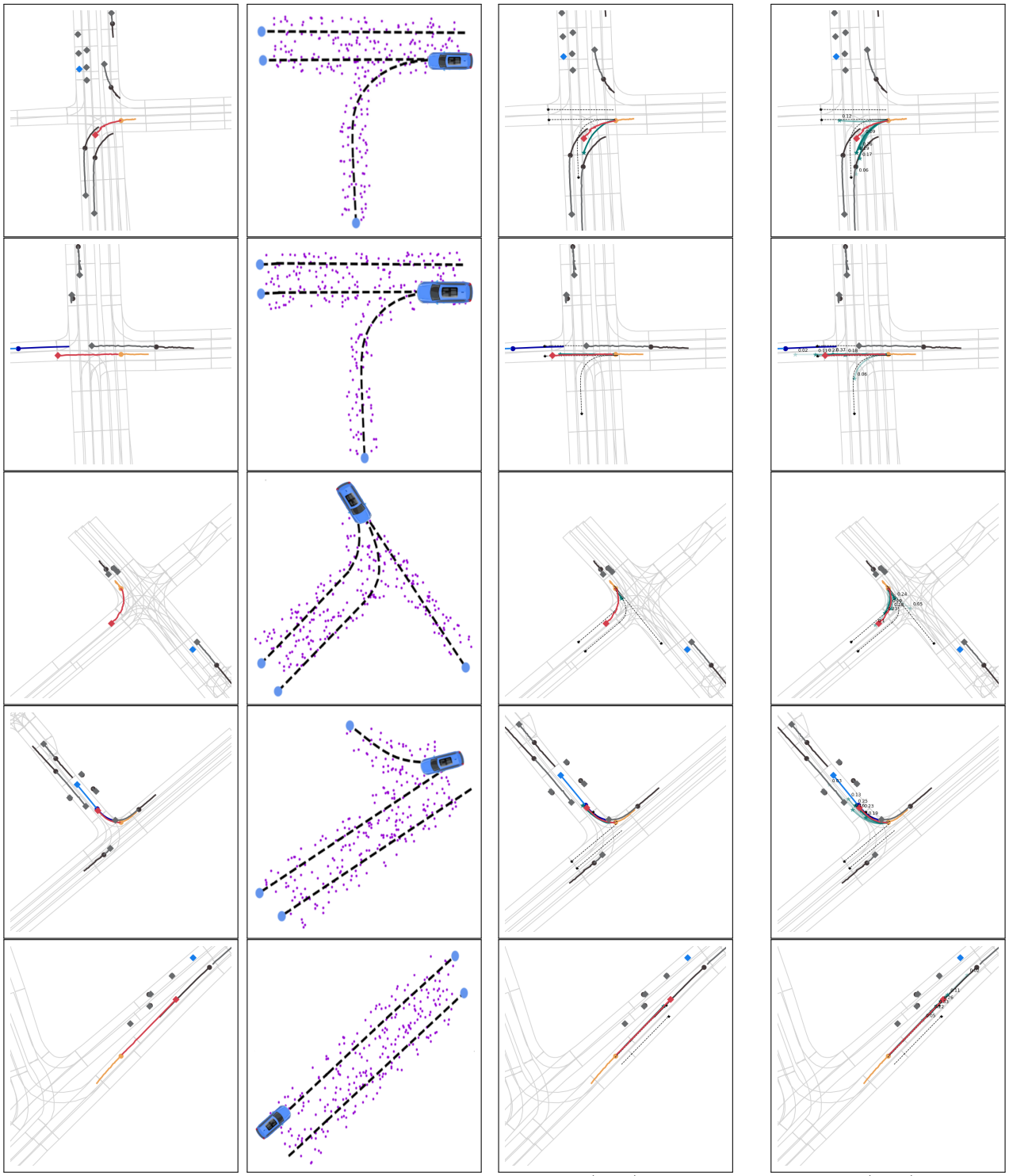

General view | Plausible HDMap | Unimodal (k=1) prediction | Multimodal (k=6) predictions

Figure 6.5: Qualitative Results on challenging scenarios in the Argoverse 1 validation set using our best model. We represent: our vehicle (**ego**), the **target agent**, and other agents. We can also see the **ground-truth** trajectory of the target agent, our **multimodal predictions** (with the corresponding confidences) and **plausible centerlines**. Circles represent last observations and diamonds last future positions. As we can see the plausible HDMap serves as a good guidance to our model, which can predict reasonable trajectories in presence of multiple agents and challenging scenarios. We show, from left to right, a general view of the traffic scenario (including social and map information), our calculated plausible HDMap, unimodal prediction (best mode in terms of confidence) and multimodal prediction ($k = 6$), including confidences (the higher, the most probable)

# Chapter 7

# Improving Multi-Agent Motion Prediction with Heuristic Proposals and Motion Refinement

*La fuerza de tus convicciones*
*determina tu éxito,*
*no el número de tus seguidores.*

Reamus Lupin
Harry Potter y Las Reliquias de la Muerte, Parte 2

## 7.1. Introduction

This is the last and most advanced MP algorithm proposed in this thesis. Based on our previously stated map baseline, we aim to get an efficient model that consider more information about the agents, HD map topological and semantic information (in addition to the previously stated geometric features) and contextual interactions. Note that obtaining and fusing this information (*e.g.*actor-to-actor, map-to-actor) is a research topic by itself [10], [13], [86] and a core part in the ADS pipeline. Here we identify a bottleneck for efficient real-time applications [125], [166], as usually, more (complex) data-inputs implies higher model complexity and inference time [71].

Predicting the future trajectories of the agents without considering their nature might not be optimal (*e.g.*predicting on a pedestrian, a cyclist or a vehicle using the same logic). For this reason, we integrate additional features related to the type and properties of agents (also referred as metadata in the literature). Moreover, we also compute heuristic scene understanding to constrain the model predictions towards the real scene geometry (*e.g.*plausible centerlines and lanes), including lane and boundary topological information or presence of an intersection. As stated by [167], only using lane centerline as input to get the embedding feature of vector map nodes is not enough. The lane centerline can

only provide the topology of the lanes, and other elements of the vector map also contain rich information. For example, the lane boundary can provide traffic rule constraint information such as whether it is possible to conduct the lane change behaviour or not (dashed vs solid line, yellow vs white, etc.). When considering such amount of information, specifically in terms of physical context and interactions, most SOTA methods require an overwhelming model complexity which can be inefficient in terms of computation [71], [83], [164].

## 7.2. Our proposal

To address the aforementioned SOTA limitations, we propose a model [168] to achieve accurate motion prediction, yet, using light-weight transformer-based models for social encoding, GNNs for context interaction, enhanced heuristic proposals and motion refinement, reducing notably the complexity of our model with respect to previous methods such as GANet [11] to avoid these possible constraints. Figure 7.1 illustrates the overall pipeline. We make the following contributions:

1. We present a SOTA method on the Argoverse 2 Motion Forecasting Benchmark, one of the most recent and challenging vehicle MP datasets.
2. Our model uses various attention mechanisms with GNNs, and a motion refinement module to further improve temporal consistency.
3. In comparison to previous methods that rely only on past trajectories and HD map, we additionally use information about the agents (*e.g.*type of agent) and the scene geometry (*e.g.*lane distribution and possible goal points).
4. Our method reduces in millions of parameters previous methods such as GANet [11], and improves over LaneGCN [13].
5. Finally, we provide an open-source framework for MP.

### 7.2.1. Preprocessing of past trajectories and heuristic proposals

The social preprocessing step proposed in this model is slightly different to our previous methods where we only considered those agents that have information over the full history horizon. Now, given the complexity of Argoverse 2, an agent that recently appeared in the scene, even if it was not observed over the whole full sequence spectrum, or even it was occluded for a few timestamps, it can be really relevant to determine the future behaviour of another agent. To this end, as proposed by multiple methods [12], [13], we consider all agents that are observable at $t{=}0$, handling those agents that are not observed over the full sequence spectrum (observation length = $obs_{len}$ + prediction length

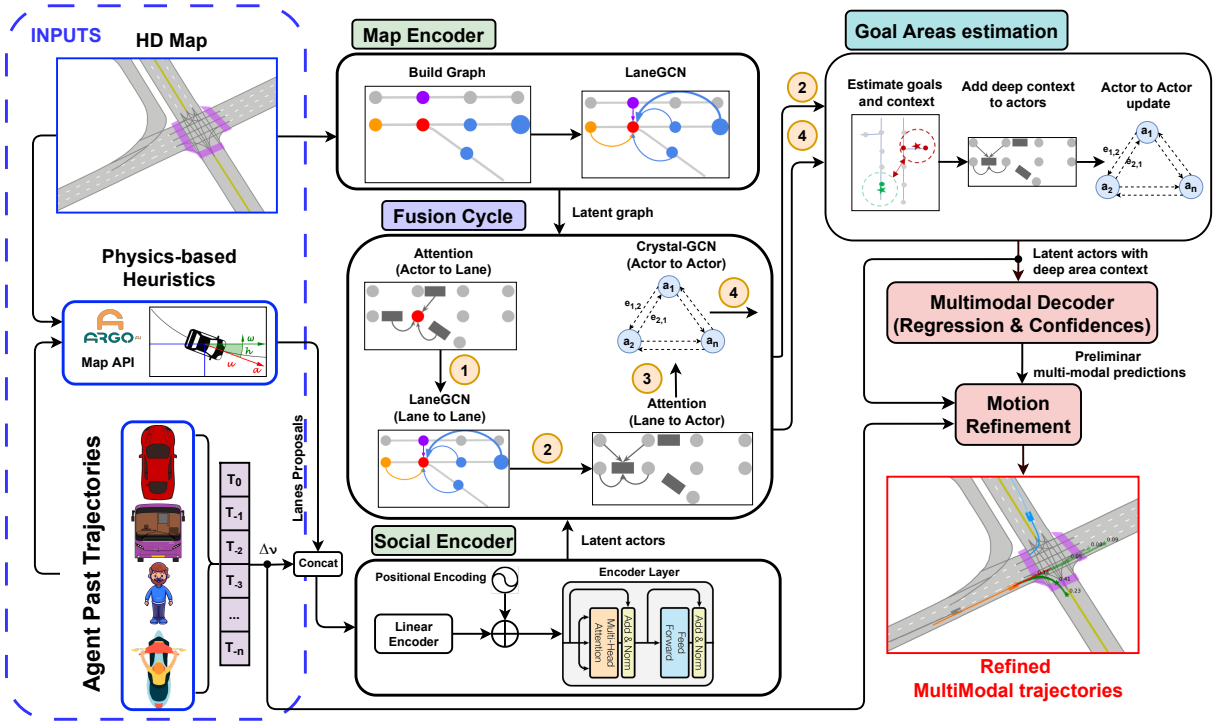


Figure 7.1: Overview of our Motion Prediction pipeline. We distinguish: 1) **Social Encoder**, which uses the agent past trajectories (relative displacements and additional metadata such as the type (*e.g.*car, cyclist, pedestrian) and category, from less to more important) and the corresponding heuristic lane proposals to compute the social features, 2) **Map Encoder**, that constructs a lane graph from the HD Map and uses a LaneConv operator [13] to extract lane node features, 3) **Fusion Cycle**, responsible for fusing agents and map latent features, 4) **Goal Areas estimation**, to predict some goals and their surrounding (area) features are aggregated to the agents, 5) **Multimodal Decoder**, which uses the latent actors with deep area context to generate reliable multi-modal predictions and 6) **Motion Refinement**, in charge of enhancing the quality of the future trajectories taking into account the past trajectories, actors latent features and preliminary predicted trajectories.

$= pred_{len}$) by concatenating a binary flag $b_i^t$ that indicates if the agent is padded or not. On top of that, we only consider the dynamic agents of the scene (vehicles, pedestrians, motorcyclists, cyclists and buses) and discard unknown or static objects (background, construction or riderless bicycle), since dynamic (which can be stopped or not) are the most relevant for the MP task. Given these final agents, we follow the same principles of translation and rotation invariant, as well as relative displacements, to compute the input past trajectories. On top of that, we additionally compute and codify the object type (bus, pedestrian, vehicle, cyclist) and agent importance (unscored, scored and focal track) as additional metadata. As described by Argoverse 2, each track is assigned one of the following labels, which dictate scoring behavior in the Argoverse 2 challenges:

1. Track fragment: Lower quality track that may only contain a few timestamps of observations.

2. Unscored track: Unscored track used for contextual input.

3. Scored track: High-quality tracks relevant to the agent.

4. Focal track: The primary track of interest in a given scenario - scored in the single-agent prediction challenge.

We can appreciate how, in addition to the attention mechanisms of the model which are responsible of computing the most relevant features, the aforementioned track category serves as a good guidance as preliminary information to refer the importance of a specific agent with respect to another one.

In terms of physical information, we aim to increase the number of features of the HD Map as well as its corresponding interactions with the social features. Then, we focus on **Graph-based** methods [86] which construct graph-structured representations from the HD maps, which preserve the connectivity of lanes, and therefore the geometry of the scene. VectorNet [71] is one of the first works in this direction, where the authors propose to encode map elements and actor trajectories as polylines and then use a global interactive graph to fuse map and actor features. We find especially related LaneGCN [13], a method that constructs a map node graph and proposes a novel graph convolution. In that sense, we follow the same principles than these well-established baselines by adopting simple form of vectorized map data as our representation of HD maps. In this case, the map data is represented as a set of polylines (lanes) and their connectivity, where each lane contains a centerline (sequence of 2D BEV points), arranged following the lane direction. For any two lanes which are directly reachable, 4 types of connections are given: predecessor, successor, left neighbour and right neighbour.

Moreover, we propose the use of preliminary plausible area information in a similar way to the heuristic proposals illustrated in Section 6.2.2.1. We follow the same heuristic (filter the agent, calculate the future travelled distance by means a CA model, get all candidates within a bubble, given the agent last observation and Manhattan distance, etc) to compute the most plausible future centerlines for the corresponding agent. It must be considered that in Argoverse 2 the number of categories is modified to 5 (vehicles, pedestrians, motorcyclists, cyclists and buses) insteaf of only 1 (vehicle) in the case of most vehicle MP datasets, including Argoverse 1. So, no centerlines proposals are considered (then, they are created virtually and padded as stated in previous sections) since we assume that pedestrians are not walking on the road, but on the pedestrian crossings or sidewalks. In future works we will work on integrating specific physical information depending on the object type as preliminary map features. Nevertheless, in this particular case, thanks to a more realistic representation of the HD map, we include additional metadata such as lane type (bus, bike, vehicle), presence of intersection (binary flag) or boundaries mark type (dash, solid, yellow), along with the aforementioned centerline relative displacements.

### 7.2.2. Social Encoder

As terms of social encoding, in order to capture more complex features for subsequent features fusion and interaction, we initially adopted GANet [11], based on LaneGCN [13], to encode motion history and scene context for its outstanding performance. In this backbone (given the aforementioned social input: translation and rotation invariant with respect to a target agent, and relative displacements), LaneGCN makes use of use a network with 3 groups/scales of 1D convolutions 1D CNN to process the trajectory input for its effectiveness in extracting multi-scale features and efficiency in parallel computing. The output is a well-structured feature map, whose element at $t = 0$ is used as the actor feature. The network has 3 groups/scales of 1D convolutions. Then, a Feature Pyramid Network (FPN) [169] to fuse the multi-scale features, and apply another residual block to obtain the output tensor. Moreover, GANet applies an LSTM network on FPN output features and use two identical parallel networks to enhance the motion history encoding.

Regarding this, we aimed to improve social encoding taking into account that in spite the fact that LSTMs became popular because they could solve the problem of vanishing gradients, they suffer from *short-term memory* due to the vanishing gradient problem, as well as require a lot of resources to get trained and become ready for real-world applications. In particular, they need high memory-bandwidth because of linear layers present in each cell which the system usually fails to provide for. To solve that, we replace the motion encoder proposed by [11] for a transformer encoder, which is faster than Recurrent Neural Network (RNN)-based models as all the input is ingested once, decreasing the computational complexity. On the other hand, even though the preliminary lane proposals represent physical information, they are quite related to the future intentions of the social information. Then, as depicted in Figure 7.1, we concatenate the agents past trajectories, additional social metadata and heuristic map proposals (including semantic and topological metadata), which is processed by a linear embedding. Then, positional encoding is added to the output embedding explicitly to retain the information regarding the order of past trajectories and future preliminar steps. Finally, these latent features feed the transformer encoder, leveraging the self-attention mechanism and positional encoding to learn complex and dynamic patterns from long-term time series data.

### 7.2.3. Map preprocessing and encoding

In terms of physical context, we adopt MapNet [13] backbone to encode the scene context for its outstanding performance. While other approaches encode the map as a raster image and apply 2D convolutions to extract features, MapNet consists of two steps:

- Build a lane graph from vectorized map data
- Apply a LaneConv operator to the lane graph to output the map features

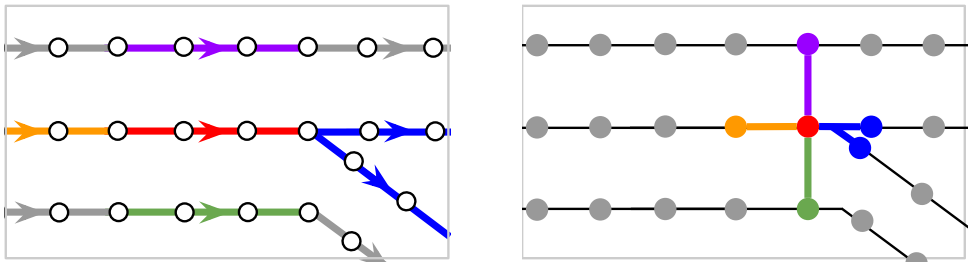

Figure 7.2: Lane graph construction from vectorized map data
Source: *Learning lane graph representations for motion forecasting* [13]

As observed in Figure 7.2, the map data is represented as a set of lanes and their connectivity. Each lane contains a centerline, *i.e.*, a sequence of 2D BEV points, which are arranged following the lane direction. For any two lanes which are directly reachable, 4 types of connections are given: *predecessor*, *successor*, *left neighbour* and *right neighbour*. Given a lane $A$, its predecessor and successor are the lanes which can directly travel to $A$ and from $A$ respectively. Left and right neighbours refer to the lanes which can be directly reached without violating traffic rules. This simple map format provides essential geometric and semantic information for MP, as vehicles generally plan their routes by reference to lane centerlines and their connectivity.

In order to conduct the Lane Graph construction, we first define a lane node as the straight line segment formed by any two consecutive points (grey circles in Figure 7.2) of the centerline. The location of a lane node is the averaged coordinates of its two end points. Following the connections between lane centerlines, we also derive 4 connectivity types for the lane nodes, *i.e.*, *predecessor*, *successor*, *left neighbour* and *right neighbour*. For any lane node $A$, its predecessor and successor are defined as the neighbouring lane nodes that can travel to $A$ or from $A$ respectively. Note that one can reach the first lane node of a lane $l_A$ from the last lane node of lane $l_B$ if $l_B$ is the predecessor of $l_A$. Left and right neighbours are defined as the spatially closest lane node measured by $\ell_2$ distance on the left and on the right neighbouring lane respectively. We denote the lane nodes with $V \in \mathbb{R}^{N\times 2}$, where $N$ is the number of lane nodes and the $i$-th row of $V$ is the BEV coordinates of the $i$-th node. We represent the connectivity with 4 adjacency matrices $\{A_i\}_{i\in\{\text{pre,suc,left,right}\}}$, with $A_i \in \mathbb{R}^{N\times N}$. We denote $A_{i,jk}$, as the element in the $j$-th row and $k$-th column of $A_i$. Then $A_{i,jk} = 1$ if node $k$ is an $i$-type neighbor of node $j$.

#### 7.2.3.1. LaneConv Operator

A natural operator to handle lane graphs is the graph convolution [170]. The most widely used graph convolution operator [171] is defined as $Y = LXW$, where $X \in \mathbb{R}^{N\times F}$ is the node feature, $W \in \mathbb{R}^{F\times O}$ is the weight matrix, and $Y \in \mathbb{R}^{N\times O}$ is the output. The graph Laplacian matrix $L \in \mathbb{R}^{N\times N}$ takes the form $L = D^{-1/2}(I + A)D^{-1/2}$, where $I$, $A$ and $D$ are the identity, adjacency and degree matrices respectively. $I$ and $A$ account for self connection and connections between different nodes. All connections share the same

weight $W$, and the degree matrix $D$ is used to normalize the output. However, this vanilla graph convolution is inefficient in our case due to the following reasons. First, it is not clear what kind of node feature will preserve the information in the lane graphs. Second, a single graph Laplacian can not capture the connection type, *i.e.*, losing the directional information carried by the connection type. Third, it is not straightforward to handle long range dependencies, *e.g.*, akin dilated convolution, within this form of graph convolution. Motivated by these challenges, we introduce our novel specially designed operator for lane graphs, called *LaneConv*.

**7.2.3.1.1. Node Feature** We first define the input feature of the lane nodes. Each lane node corresponds to a straight line segment of a centerline. To encode all the lane node information, we need to take into account both the shape (size and orientation) and the location (the coordinates of the center) of the corresponding line segment. We parameterize the node feature as follows:

$$\mathbf{x}_i = \mathrm{MLP}_{\mathrm{shape}}\left(\mathbf{v}_i^{\mathrm{end}} - \mathbf{v}_i^{\mathrm{start}}\right) + \mathrm{MLP}_{\mathrm{loc}}\left(\mathbf{v}_i\right) \tag{7.1}$$

where MLP indicates a multi-layer perceptron and the two subscripts refer to shape and location, respectively. $\mathbf{v}_i$ is the location of the $i$-th lane node, *i.e.*, the center between two end points, $\mathbf{v}_i^{\mathrm{start}}$ and $\mathbf{v}_i^{\mathrm{end}}$ are the BEV coordinates of the node $i$'s starting and ending points, and $\mathbf{x}_i$ is the $i$-th row of the node feature matrix $X$, denoting the input feature of the $i$-th lane node.

**7.2.3.1.2. LaneConv** The node feature above only captures the local information of a line segment. To aggregate the topology information of the lane graph at a larger scale, we design the following LaneConv operator:

$$Y = XW_0 + \sum_{i \in \{\mathrm{pre,suc,left,right}\}} A_i X W_i \tag{7.2}$$

where $A_i$ and $W_i$ are the adjacency and the weight matrices corresponding to the $i$-th connection type respectively. Since we order the lane nodes from the start to the end of the lane, $A_{\mathrm{suc}}$ and $A_{\mathrm{pre}}$ are matrices obtained by shifting the identity matrix one step towards upper right (non-zero superdiagonal) and lower left (non-zero subdiagonal). $A_{\mathrm{suc}}$ and $A_{\mathrm{pre}}$ can propagate information from the forward and backward neighbours whereas $A_{\mathrm{left}}$ and $A_{\mathrm{right}}$ allow information to flow from the cross-lane neighbours. It is not hard to see that our LaneConv builds on top of the general graph convolution and encodes more geometric (*e.g.*, connection type/direction) information.

**7.2.3.1.3. Dilated LaneConv** Since motion forecasting models usually predict the future trajectories of actors with a time horizon of several seconds, actors with high speed could

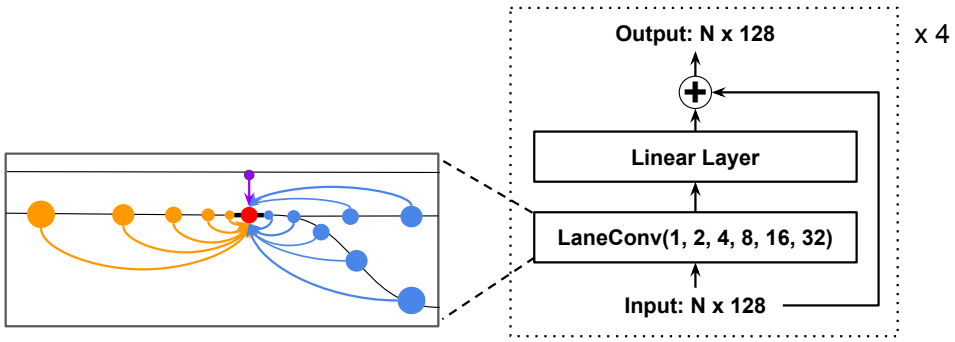


Figure 7.3: LaneGCN architecture. LaneGCN is a stack of 4 multi-scale LaneConv residual blocks, each of which consists of a LaneConv(1,2,4,8,16,32) and a linear layer with a residual connection.
Source: *Learning lane graph representations for motion forecasting* [13]

have moved a long distance. Therefore, the model needs to capture the long range dependency along the lane direction for accurate prediction. In regular grid graphs, a dilated convolution operator [172] can effectively capture the long range dependency by enlarging the receptive field. Inspired by this operator, we propose the *dilated LaneConv* operator to achieve a similar goal for irregular graphs.

In particular, the $k$-dilation LaneConv operator is defined as follows:

$$Y = XW_0 + A^k_{\text{pre}} XW_{\text{pre},k} + A^k_{\text{suc}} XW_{\text{suc},k} \tag{7.3}$$

where $A^k_{\text{pre}}$ is the $k$-th matrix power of $A_{\text{pre}}$. This allows us to directly propagate information along the lane for $k$ steps, with $k$ a hyperparameter. Since $A^k_{\text{pre}}$ is highly sparse, one can efficiently compute it using sparse matrix multiplication. Note that the dilated LaneConv is only used for predecessor and successor, as the long range dependency is mostly along the lane direction.

#### 7.2.3.2. LaneGCN

Based on the dilated LaneConv, we further propose a multi-scale LaneConv operator and use it to build our LaneGCN. Combining Eq. (7.2) and (7.3) with multiple dilations, we get a multi-scale LaneConv operator with $C$ dilation sizes as follows:

$$Y = XW_0 + \sum_{i \in \{\text{left},\text{right}\}} A_i XW_i + \sum_{c=1}^{C} \left( A^{k_c}_{\text{pre}} XW_{\text{pre},k_c} + A^{k_c}_{\text{suc}} XW_{\text{suc},k_c} \right), \tag{7.4}$$

where $k_c$ is the $c$-th dilation size. We denote LaneConv$(k_1, \cdots, k_C)$ this multi-scale layer.

### 7.2.4. Enhanced Actor-Map Fusion Cycle

Once both the map and social latent features are computed, we obtain a 2D feature matrix $X$ where each row $X_i$ indicates the feature of the $i$-th actor, and a 2D matrix $Y$

where each row $Y_i$ indicates the feature of the $i$-th lane node. Then, we make use of the well-established actor-map fusion cycle [13] (also referred as FusionNet in the literature) that transfers and aggregates feature among actors and lane nodes. The behaviour of an actor strongly depends on its context, *i.e.*, other actors and the map. Although the interactions between actors has been explored by previous work, the interactions between the actors and the map, and map conditioned interactions between actors have received much less attention. FusionNet makes use of spatial attention and LaneGCN to capture a complete set of actor-map interactions, as observed in Figure **??**.

FusionNet makes use of a stack of four fusion modules to capture all information flows between actors and lane nodes, *i.e.*, (1) Actors to Lanes (A2L), (2) Lanes to Lanes (L2L), (3) Lanes to Actors (L2A) and (4) Actors to Actors (A2A). This order is not coincidence. Assuming several agents are on the road and all of them have a web service that provides detailed information about geographical regions and sites worldwide (*e.g.*, Google Maps):

- First, agents introduce their real-time traffic information to lane nodes, such as blockage, presence of an accident, etc. In other words, the HD map information is updated with the traffic information of the agents.
- The HD map information of a particular node is propagated to the immediate neighbours, in such a way ...
- ... Further agents are updated with the information of surrounding map nodes, which were previously updated by neighboring nodes.
- Finally, A2A concludes the actor-map fusion cycle handling the interactions between actors and produces the output actor features.

We implement L2L using another LaneGCN, which has the same architecture as the one used in our MapNet. Regarding the A2L, L2A and A2A modules, [13] applies a spatial attention layer as defined in Section 3.3.4. Taking the first module (A2L) as en example, given an actor node $i$, we aggregate the features from its context lane nodes $j$ as follows:

$$\mathbf{y}_i = \mathbf{x}_i W_0 + \sum_j \phi(\text{concat}(\mathbf{x}_i, \Delta_{i,j}, \mathbf{x}_j)W_1)W_2 \tag{7.5}$$

where $\mathbf{x}_i$ represents the feature of the $i$-th node, $W$ a weight matrix, $\phi$ the composition of layer normalization and ReLU, and $\Delta_{ij} = \text{MLP}(\mathbf{v}_j - \mathbf{v}_i)$, where $\mathbf{v}$ denotes the node location.

The context nodes are defined to be the lane nodes whose $\ell_2$ distance from the actor node $i$ is smaller than a threshold. Each of A2L, L2A and A2A has two residual blocks, which consist of a stack of the proposed attention layer and a linear layer, as well as a residual connection.

Nevertheless, as observed in our model (Figure **??**), once implemented FusionNet to compute actor-map interactions, we substitute the final module that models Actor to Actor interactions with a Graph Convolution Operator (GCN), inspired in our previous proposed efficient baselines (Figure 6.1).

### 7.2.5. Goal prediction

In stage two, we predict possible goals for the $i$-th actor based on $X_i$. We apply intermediate supervision and calculate the smooth L1 loss between the best-predicted goal and the ground-truth trajectory's endpoint to backpropagate, making the predicted goal close to the actual goal as much as possible. The goal prediction stage serves as a predictive test to locate goal areas, which is different from goal-based methods using the predicted goals as the final predicted trajectories' endpoint. In practice, a driver's driving intent is highly multi-modal. For example, he or she may stop, go ahead, turn left, or turn right when approaching an intersection. Therefore, we try to make a multiple-goals prediction. We construct a goal prediction header with two branches to predict $E$ possible goals $G_{n,end} = \{g^e_{n,end}\}_{e\in[0,E-1]}$ and their confidence scores $C_{n,end} = \{c^e_{n,end}\}_{e\in[0,E-1]}$, where $g^e_{n,end}$ is the $e$-th predicted goal coordinates and $c^e_{n,end}$ is the $e$-th predicted goal confidence of the $n$-th actor.

We train this stage using the sum of classification loss and regression loss. Given $E$ predicted goals, we find a positive goal $\hat{e}$ that has the minimum Euclidean distance with the ground truth trajectory's endpoint.

For classification, we use the max-margin loss:

$$L_{cls\_end} = \frac{1}{N(E-1)} \sum_{n=1}^{N} \sum_{e\neq\hat{e}} max(0, c^e_{n,end} + \epsilon - c^{\hat{e}}_{n,end}) \tag{7.6}$$

where $N$ is the total number of actors and $\epsilon = 0.2$ is the margin. The margin loss expects each goal to capture a specific pattern and pushes the goal closest to the ground truth to have the highest score. For regression, we only apply the smooth L1 loss to the positive goals:

$$L_{reg\_end} = \frac{1}{N} \sum_{n=1}^{N} reg(g^{\hat{e}}_{n,end} - a^*_{n,end}) \tag{7.7}$$

where $a^*_{n,end}$ is the ground truth BEV coordinates of the $n$-th actor trajectory's endpoint, $reg(z) = \sum_i d(z_i)$, $z_i$ is the $i$-th element of $z$, and $d(z_i)$ is a smooth L1 loss.

Additionally, we also try to add a "one goal prediction" module at each trajectory's middle position aggregating map features to assist the endpoint goal prediction and the whole trajectory prediction. Similarly, we apply a residual MLP to regress a middle goal $g_{n,mid}$ for the $n$-th actor. The loss term for this module is given by:

$$L_{reg\_mid} = \frac{1}{N}\sum_{n=1}^{N} reg(g_{n,mid} - a^*_{n,mid}) \tag{7.8}$$

where $a^*_{n,mid}$ is the ground truth BEV coordinates of the $n$-th actor trajectory's middle position.

The total loss at the goal prediction stage is:

$$L_1 = \alpha_1 L_{cls\_end} + \beta_1 L_{reg\_end} + \rho_1 L_{reg\_mid} \tag{7.9}$$

where $\alpha_1 = 1$, $\beta_1 = 0.2$ and $\rho_1 = 0.1$.

### 7.2.6. GoICrop

We choose the predicted goal with the highest confidence among $E$ goals as an anchor. This anchor is the approximate destination with the highest possibility that the actor may reach based on its motion history and driving context. Because the actors' motion is highly uncertain, we crop maps within 6 meters of the anchor as the goal area of interest, which relaxes the strict goal prediction requirement. The actual endpoint is more likely to appear in candidate areas compared with being hit by scattered endpoint predictions. Moreover, the actor's behavior highly depends on its destination area's context, i.e., the maps and other actors. Although previous works have explored the interactions between actors, the interactions between actors and maps in goal areas and the interactions among actors in the future have received less attention.

Thus, we retrieve the lane nodes in goal areas and apply a GoICrop module to aggregate these map node features as follows:

$$x'_i = \phi_1(x_i W_0 + \sum_j \phi_2(concat(x_i W_1, \Delta_{i,j}, y_j)W_2))W_3 \tag{7.10}$$

where $x_i$ is the feature of $i$-th actor and and $y_j$ is the feature of $j$-th lane node, $W_i$ is a weight matrix, $\phi_i$ is a layer normalization with ReLU function, and $\Delta_{i,j} = \phi(MLP(v_i - v_j))$, where $v_i$ denotes the anchor's coordinates of $i$-th actor and $v_j$ denotes the $j$-th lane node's coordinates.

GoICrop serves as spatial distance-based attention and updates the goal area lane nodes' features back to the actors. We transpose $x_i$ with $W_1$ as a query embedding. The relative distance feature between the anchor of $i$-th actor and $j$-th lane node are extracted by $\Delta_{i,j}$. Then, we concatenate the query embedding, relative distance feature, and lane node feature. An $MLP$ is employed to transpose and encode these features. Finally, the goal area features are aggregated for $i$-th actor.

Previous motion forecasting methods usually focus on the interactions in the observation history. However, actors will interact with each other in the future to follow driving etiquette, such as avoiding collisions.

Since we have performed predictive goal predictions and gotten possible goals for each actor, our framework can model the actors' future interactions.

Hence, we utilize the predicted anchor positions and apply a GoICrop module as equation 7.10 to implicitly model actors' interactions in the future. We consider the other actors whose future anchor's distance from the anchor of $i$-th actor is smaller than 100 meters. In this case, $y_j$ in equation 7.10 denotes the features of $j$-th actor, $v_i$ denotes the anchor's coordinates of $i$-th actor, and $v_j$ denotes the anchor's coordinates of $j$-th actor in $\Delta_{i,j} = \phi(MLP(v_i - v_j))$.

### 7.2.7. Decoding module

In order to get the future trajectories with corresponding scores, as observed in Figure **??**, we take the updated actor features $X$ as input to predict $K$ final future trajectories and their confidence scores in stage three. Specifically, we construct a two-branch multi-modal prediction header similar to the goal prediction stage, with one regression branch estimating the trajectories and one classification branch scoring the trajectories.

For each actor, we regress $K$ sequences of BEV coordinates $A_{n,F} = \{(a^k_{n,1}, a^k_{n,2}, ..., a^k_{n,T})\}_{k\in[0,K-1]}$, where $a^k_{n,t}$ denotes the $n$-th actor's future coordinates of the $k$-th mode at $t$-th step.

For the classification branch, we output $K$ confidence scores $C_{n,cls} = \{c^k_n\}_{k\in[0,K-1]}$ corresponding to $K$ modes.

We find a positive trajectory of mode $\hat{k}$, whose endpoint has the minimum Euclidean distance with the ground truth endpoint.

For classification, we use the margin loss $L_{cls}$ similar to the goal prediction stage. For regression, we apply the smooth L1 loss on all predicted steps of the positive trajectories:

$$L_{reg} = \frac{1}{NT}\sum_{n=1}^{N}\sum_{t=1}^{T} reg(a^{\hat{k}}_{n,t} - a^*_{n,t}) \tag{7.11}$$

where $a^*_{n,t}$ is the $n$-th actor's ground truth coordinates.

To emphasize the importance of the goal, we add a loss term stressing the penalty at the endpoint:

$$L_{end} = \frac{1}{N}\sum_{n=1}^{N} reg(a^{\hat{k}}_{n,end} - a^*_{n,end}) \tag{7.12}$$

where $a^*_{n,end}$ is the $n$-th actor's ground truth endpoint coordinates and $a^{\hat{k}}_{n,end}$ is the $n$-th actor's predicted positive trajectory's endpoint.

The loss function for training at this stage is given by:

$$L_2 = \alpha_2 L_{cls} + \beta_2 L_{reg} + \rho_2 L_{end} \tag{7.13}$$

where $\alpha_2 = 2$, $\beta_2 = 1$ and $\rho_2 = 1$.

### 7.2.8. Motion refinement

A second-stage motion refinement, as proposed by [173], is introduced to further explore the temporal consistency for predicting more accurate future trajectories. The goal is to reduce the offset between ground truth trajectory $Y$ and predicted trajectory $\hat{Y}$. We define this offset as $\Delta Y = Y - \hat{Y}$. In this stage, we leverage three sources of information: 1. Preliminary predictions computed in the decoding module, 2. Prior latent information to the decoding module and 3. Past observations. Using this approach, an MLP model is trained to minimize the offset by predicting a residual $R$ that is added to the original trajectory *i.e.*we use $L_2$ loss to optimize the offset as follows:

$$\mathcal{L}_{\text{off}} = ||Y - \hat{Y} - \hat{R}||_2 = ||\Delta Y - \hat{R}||_2. \tag{7.14}$$

$$\mathcal{L}_{\text{angle}} = \frac{1}{t_f} \sum_{t=1}^{t_f} -cos(\hat{\theta}_t - \theta_t) \tag{7.15}$$

Note that this method can be applied to the pre-trained model from previous stages, which is completely functional, as the main function is to improve the output trajectories.

## 7.3. Experimental Results

We use the Argoverse 2 [6] dataset described in Section 2.4. For each real driving scenario we have the corresponding local HD map, past trajectories of the agents, metadata about the agents (*e.g.*the ype of agent: cyclist, pedestrian, car), and topological information about the scene. Each scenario is 11 seconds long. We consider five seconds of the past trajectory (also known as motion history), and we predict the next six seconds.

**Implementation.** We train our model on 2 A100 GPUs using a batch size of 128 with the Adam optimizer for 42 epochs. The initial learning rate is 1 x 10-3, decaying to 1 x 10-4 at 32 epochs. The latent dimension (regarding map and social features) in most of our experiments is 128. The number of attention heads in the social encoder and motion refinement is 8. The training setup including loss functions follows GANet [11] official implementation as our baseline.

**Augmentations** (i) Dropout and swapping random points from the past trajectory, (ii) point location perturbations under a $\mathcal{N}(0, 0.2)$ [m] noise distribution [160].

Tables 7.1 and 7.2 present the results obtained on the Argoverse 2 Motion Forecasting validation and test sets, respectively. We achieve near state-of-the-art performance in both sets, which is on-pair with the most promising pipelines, while using notably less parameters. As stated throughout this work, we focus on applying efficient methods to help understand future interactions among the different agents, reducing the number of parameters and inference time.

We can appreciate in Table 7.1 the huge influence of the physical context both in terms of accuracy and runtime. GANet [11] shows the best multimodal prediction metrics, with an approximate amount of 6.2M of parameters of 1612 ms given a batch size of 128 traffic scenarios and an average number of 30 agents per scene. As expected, progressively removing the map influence (remove map from decoder, remove goal areas estimation) in the model we decrease the MP performance with a noticeable parameter decrease.

In our case, we study the influence of substituting the modified ActorNet [11], [13] social encoder proposed by GANet, which uses RNNs. Our proposal replaces these by a Linear embedding, a Positional Encoding and Encoder Transformer. Moreover, we add the aforementioned agent metadata (object type and track category), and we substitute the Actor to Actor attention of the fusion cycle for a GCN [12] operator to enhance agents global interaction. It can be appreciated how we obtained a similar performance (both with 128 latent dimension in *Ours-m*, and 64 latent in *Ours-s*), reducing the parameters and inference time.

Finally, our best model, which includes heuristic proposals that serve as a preliminar multi-modal guidance for the model and motion refinement to improve the quality of the final predictions, obtains a performance on pair with [11], reducing the number of parameters and inference time about 21% and 41% respectively. We can appreciate in Table 7.2 how our model generalizes well in the test set, with results (both in uni-modal and multi-modal prediction) up-to-pair with other state-of-the-art algorithms.

Table 7.1: Comparison of methods in the **Argoverse 2 Validation** Set. We show the number of parameters for each model, prediction metrics (minADE, minFDE and brier-minFDE) for the multimodal scenario (k=6) and runtime. Runtime was measured on a single GPU A100-SXM4 (using batch 128). Our experiments are indicated using †. We use as baseline method GANet [11].

| Method | Map | # Par. (M) | minADE (m) ↓ | minFDE (m) ↓ | brier-minFDE (m) ↓ | Runtime (ms) ↓ |
|---|---|---|---|---|---|---|
| GANet [11] | Yes | 6.2 | 0.806 | 1.402 | 2.02 | 1612 |
| GANet w/o Map Decoder [11] | Yes | 5.7 | 0.84 | 1.55 | 2.18 | 1353 |
| GANet w/o Goal Areas [11] | Yes | 4.5 | 0.87 | 1.66 | 2.29 | 1134 |
| GANet w/o map [11] | No | 1.79 | 1.034 | 2.212 | 2.825 | 838 |
| † CRAT-Pred [12] | No | 0.53 | 1.31 | 2.78 | 3.65 | 223 |
| † Ours-base: GANet [11] ActorNet → Attention Transformer | Yes | 5.0 | 0.83 | 1.45 | 2.07 | 923 |
| † Ours-m: Ours-base + A2A → C-GCN + Metadata | Yes | 4.74 | 0.82 | 1.43 | 2.05 | 892 |
| † Ours-s: Ours-base + A2A → C-GCN + Metadata (64 latent size) | Yes | 1.2 | 0.88 | 1.53 | 2.15 | 893 |
| † **Ours:** Ours-m + Proposals + Motion Refinement | Yes | 4.92 | 0.81 | 1.42 | 2.04 | 946 |

We provide advanced qualitative samples in Figure **??**, where we show the HD Map of real traffic scenes, heuristic trajectory proposals in the form of centerlines, and the

multimodal predictions from our model including their respective confidences (the higher, the most probable).

As we discussed in **??**, we designed our model to ensure realistic predictions. We can appreciate that all the predictions are plausible and constrained to the scene geometry *e.g.*lane distribution and centerlines. We believe our heuristic proposals help to regularize the model and produce realistic predictions that would ensure traffic safety. For simplicity, we only illustrate the heuristic proposals for the focal agent and ego-vehicle. We believe our software for qualitative analysis of MP models on the well-known Argoverse 2.0 [6] is fundamental and a core contribution.

Table 7.2: Results on **Argoverse 2 Test** dataset. The "-" denotes that this result was not reported in their paper. Some numbers are borrowed from [11]. For all the metrics, the lower, the better.

| Method | b-minFDE (K=6) | MR (K=6) | minFDE (K=6) | minADE (K=6) | minFDE (K=1) | minADE (K=1) | MR (K=1) |
|---|---|---|---|---|---|---|---|
| DirEC | 3.29 | 0.52 | 2.83 | 1.26 | 6.82 | 2.67 | 0.73 |
| drivingfree | 3.03 | 0.49 | 2.58 | 1.17 | 6.26 | 2.47 | 0.72 |
| LGU | 2.77 | 0.37 | 2.15 | 1.05 | 6.91 | 2.77 | 0.73 |
| Autowise.AI(GNA) | 2.45 | 0.29 | 1.82 | 0.91 | 6.27 | 2.47 | 0.71 |
| Timeformer [174] | 2.16 | 0.20 | 1.51 | 0.88 | 4.71 | 1.95 | 0.64 |
| QCNet | 2.14 | 0.24 | 1.58 | 0.76 | 4.79 | 1.89 | 0.63 |
| *OPPred w/o Ensemble* [167] | 2.03 | 0.180 | 1.389 | 0.733 | 4.70 | 1.84 | 0.615 |
| *TENET w/o Ensemble* [175] | 2.01 | - | - | - | - | - | - |
| Polkach(VILaneIter) | 2.00 | 0.19 | 1.39 | **0.71** | 4.74 | 1.82 | 0.61 |
| GANet | **1.969** | **0.171** | **1.352** | 0.728 | **4.475** | **1.775** | **0.597** |
| Ours | 1.98 | 0.185 | 1.37 | 0.73 | 4.53 | 1.79 | 0.608 |

## 7.4. Summary

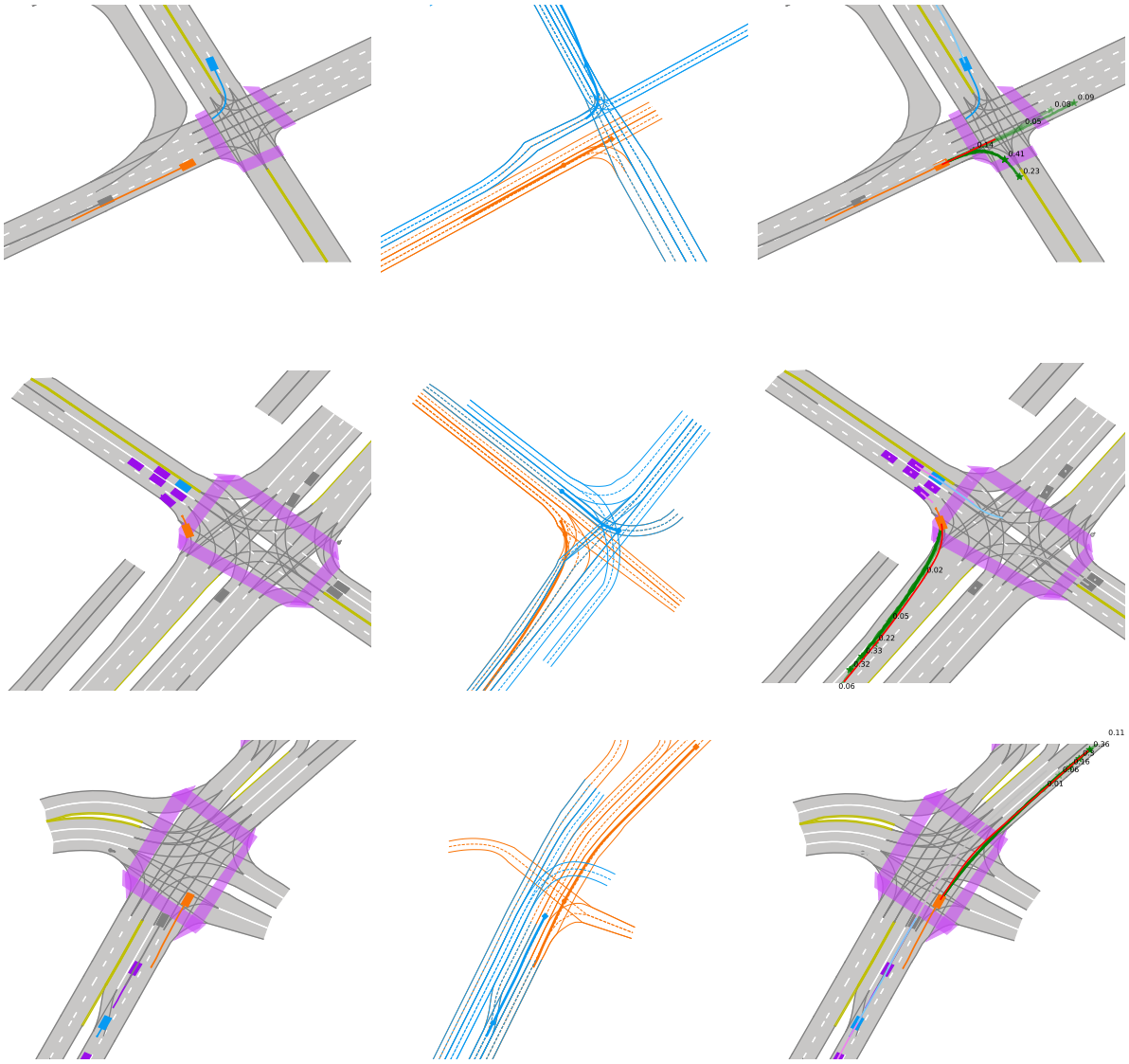

HD Map input | Heuristic proposals | Multimodal (k=6) predictions

Figure 7.4: Qualitative Results on challenging scenarios in Argoverse 2 using our best model. We represent: our vehicle (**ego**), the **focal agent**, the **relevant agents** in the scene, and **other agents**. We can also see the **ground-truth** trajectory of the target agent, our **multimodal predictions** (with the corresponding **confidences**). We also highlight the most important topology of the road, such as pedestrian crossing and boundaries mark type. We show, from left to right, a general view of the traffic scenario (including and map information), the heuristic proposals for each agent (we only include the **ego** and **focal agent** for simplicity) and the multimodal prediction ($k = 6$) for the **focal agent**, including the corresponding confidences (the higher, the most probable)

# Chapter 8

# Applications in Autonomous Driving

*La fuerza de tus convicciones*
*determina tu éxito,*
*no el número de tus seguidores.*

Reamus Lupin
Harry Potter y Las Reliquias de la Muerte, Parte 2

## 8.1. Introduction

In this chapter we will detail the experiments carried out to assess the performance of our prediction algorithms, both in terms of accuracy and computational resources (time, FLoating-point Operations per seconds (FLOPs), parameters) for real-time applications in the field of AD. Regarding the proposed methods, we first make use of some well-established tracking metrics to evaluate the behaviour of our physics-based tracking method; then, we follow the validation method proposed by [142] to check how integrating HD map information in the prediction pipeline can be determinant to decrease the risk of collision or at least to minimize the impact velocity in an EURO-NCAP based scenario. After that, we study the prediction metrics obtained in the Argoverse 1 [5] and Argoverse 2 [6] Motion Forecasting datasets.

Once we have evaluated our different proposals, the best model (including its social and map version) is selected to carry out some challenging applications. First, regarding the decision-making layer using the SMARTS [176] framework based on the SUMO (Simulation of Urban MObility) [177] simulator, we study the influence of the prediction pipeline when computing the most optimal action for the ego-vehicle in contrast to reactive proposals where only the past observations or current adversaries positions are required. Second, the prediction pipeline is integrated in the ADS of our research group using the CARLA [106] (CAR Learning to Act) to study how the ego-vehicle can leverage the scene understanding and the future behaviour prediction of the agents to improve the overall score by means of a holistic validation using the CARLA Leaderboard, inspired in the well-established NHTSA typology.

## 8.2. Decision-Making

The increasing popularity of autonomous vehicles (AVs) has brought with it significant challenges in ensuring safe and effective decision-making, particularly in complex urban driving scenarios [178]. Reinforcement learning (RL) techniques have emerged as a promising solution to address these challenges [179]. They enable AVs to learn from their interactions with the driving environment, without relying on pre-defined rules. However, RL-based approaches still face a number of limitations that can hinder their development, including issues related to state representation.

A key challenge in RL-based AVs is the development of effective state representations that can account for the complexity of urban driving scenarios. Unlike in simpler environments, state representations for urban driving must be able to incorporate a wide range of information, including dynamic features of traffic flows and interactions among different agents. Finding ways to effectively encode this information and develop accurate state representations is essential to enabling RL-based AVs to generalize to various scenarios and make effective driving decisions. Distilling predictive information from scene representations can aid in the development of effective decision-making policies for AVs. By better understanding the potential consequences of different driving actions, RL-based AVs can make more informed decisions that lead to safer and more efficient driving behaviour.

In this section we propose an approach to enhance the efficiency and generalization of RL-based AVs in urban driving scenarios. Specifically, we introduce the use of a Motion Prediction (MP) module to obtain the future positions of the ego-vehicle and the surrounding vehicles (adversaries) in the scenario. These predictions are the input to an RL-based decision-making module that executes high-level actions. Our approach is developed using the Proximal Policy Optimization (PPO) algorithm [180]. We carry out an evaluation in the unsignalized T-intersection scenario shown in Fig. **??** with and without the proposed state representation and provide a comparison with some baseline methods.

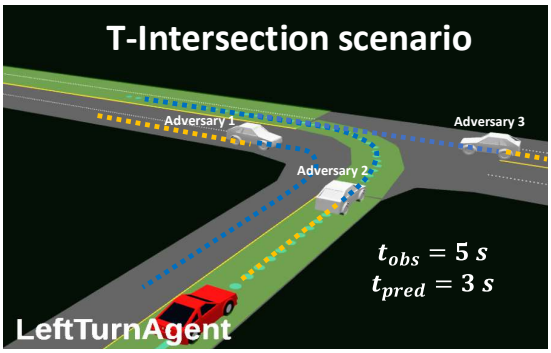


Figure 8.1: Simulation environment. A visualization of the ego-vehicle driving in the T-intersection scenario. The past positions of the adversaries (yellow) and the predicted trajectories (blue) are represented in the scenario.

In recent years, RL has emerged as a promising approach for developing decision-making policies for AVs [181], outperforming ruled-based approaches that usually cannot solve complex situations [182]. However, a large number of interactions with the environment are required to obtain the desired policy. This is why other approaches such as imitation learning [183] and inverse RL [184], based on human experts' behaviours are also used in the literature.

This work is focused on a critical issue for RL-based AVs, which is the state representation problem. Traditional state representations often focus on low-dimensional features such as distance to obstacles, lane positions, and vehicle velocities [185]. However, these representations may not be sufficient to capture the complex interactions among different agents and road structures in urban driving scenarios. To address the state representation problem, some methods have been proposed that use higher-dimensional or learned representations, such as convolutional neural networks [186] and recurrent neural networks [187]; other methods have been proposed to use more detailed representations, such as Bird-Eye-View images [188], image augmentation [189] or occupancy grids [190]. These methods have shown promising results in improving the generalization and robustness of the decision-making approaches. Recently, transformer-based approaches have gained increasing attention for their ability to capture long-term dependencies and interactions among different entities in sequential data. In the context of AVs, transformers have been used to reduce the computational load in end-to-end approaches [191] and anticipate future states with prediction-aware planning [192].

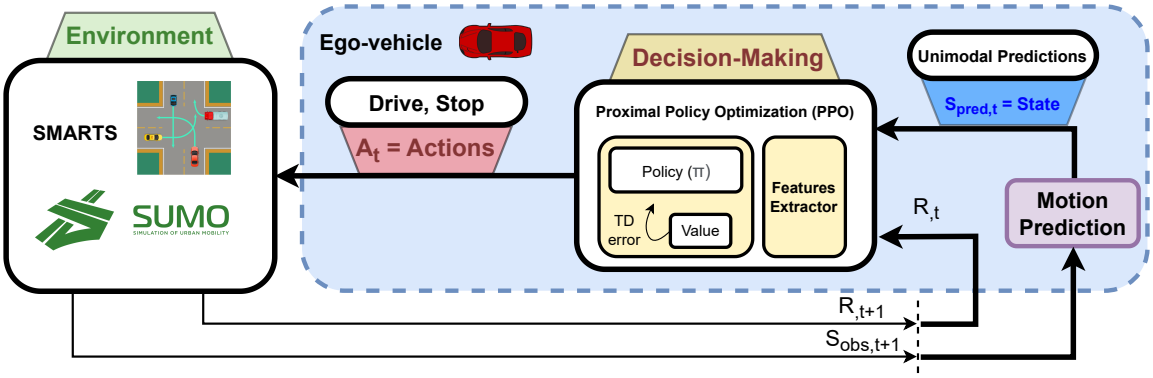


Figure 8.2: An overview of the Augmented Reinforcement Learning with Efficient Social-based Motion Prediction for Autonomous Decision-Making. The observations (both position and ID, so, trackers) of the vehicles in the scenario are obtained from the simulator. The MP module estimates the future positions of these vehicles, taking into account the most plausible score of a multimodal prediction. The decision-making module selects high-level actions based on this information. These actions are executed by the simulator, which provides a new state to the framework.

The objective of this study is to illustrate the efficacy of employing a low-dimensional state representation in conjunction with an MP method. We aim to prove that the proposed framework can lead to good performance in urban scenarios. More specifically, we present the following contributions:

- The augmentation of RL techniques with MP to improve state representation. By predicting vehicle trajectories, we can better capture the complex interactions between different agents and road structures in urban driving scenarios.

- Higher explainability than end-to-end methods. Intermediate states are accessible in our approach. This can help to understand the decisions made.

- We provide a comparison with baseline methods in a standard scenario. We demonstrate that our approach leads to some improvements in performance, particularly in scenarios with high velocities.

The RL framework proposed in this work, which executes high-level decisions to solve urban driving scenarios, is represented in Fig. 8.2. The past observations of the position of adversaries are obtained from the environment. This information is provided to the MP module, which estimates future positions. The PPO algorithm takes these predictions and generates the decision-making output.

We propose two different learning processes: supervised learning for the motion prediction module and a reinforcement learning approach for the decision-making module. These two modules are trained separately, which allows access to the information of the predictions that feed the decision-making module.

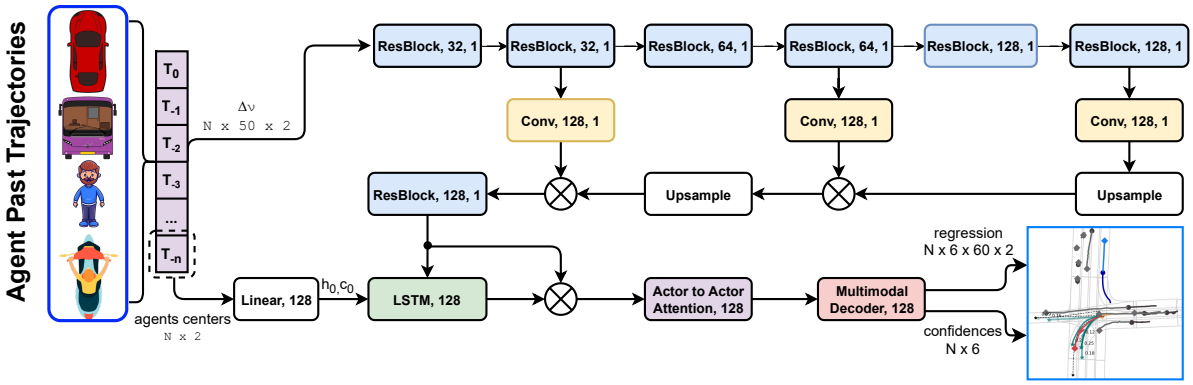


Figure 8.3: Overview of our Efficient Social-based Motion Prediction. The main inputs are the relative displacements and centers (last observations) of the agents in the ego-vehicle frame. The relative displacements and centers are encoded through a sequence of Residual, Convolutional Blocks, LSTM and Attention module. Finally, a multimodal decoder based on residual blocks is used to predict $K$ final future trajectories (modes) and their confidence scores.

Predicting the future behaviour of traffic agents [6] around the ego-vehicle is one of the key unsolved challenges in reaching full self-driving autonomy. In that sense, an Autonomous Driving Stack (ADS) can be hierarchically broken down into the following tasks: (i) perception, responsible for identifying what is around the vehicle, then track and predict what will happen next, (ii) planning and decision-making, deciding what the AD stack is going to do in the near future and (iii) control, that sends the corresponding low-level commands (brake, throttle and steering angle) to the vehicle.

This prediction is required to be multi-modal, which means given the past motion of a particular vehicle and its surrounding scene, there may exist more than one possible future behaviour (also known as modes). Therefore, MP models need to cover the different choices a driver could make (i.e. going straight or turning, accelerations or slowing down) as a possible trajectory in the immediate future or as a probability distribution of the agent's future location. In other words, when an ADS attempts to make a specific action (e.g. left turn), it must consider the future motion of the other vehicles, since the own future actions (also known as decision-making or behaviour planning) depends on the all possible maneuvers of the other agents of the scene for safe driving.

Since our proposed pipeline (Fig. 8.2) is multi-stage to provide a more interpretable framework, we follow the principles of the Argoverse 2 Motion Forecasting dataset [6] to train our prediction model. In our case, we build an efficient model solely based on past trajectories (motion history, $obs_{len} = 50$) and agents interactions, taking into account the corresponding traffic rules, not requiring fully-annotated HD map information, to predict $obs_{len} = 60$ future steps.

The SMARTS [176] framework provides only the positions of the agents in the timestamp $t$. Nevertheless, in order to predict the future $pred_{len}$ trajectories of the agents, we require their corresponding $obs_{len}$ trackers over a certain set of observations. Most vehicle prediction datasets [6] aim to predict the future behaviour of a target agent assuming the surrounding agents have been detected and tracked (so, monitored over time) and the map information is also provided. In that sense, since SMARTS provide the agents in the same order for consecutive timestamps (that is, the agent 5, unless it disappears from the scene, will be the agent 5 again in the next frame), we are able to compute a FIFO (*First Input First Output*) for each agent, not requiring data association [111] to perform this task.

On top of that, as proposed by multiple methods [13], [168], we consider only the vehicles that are observable at *t=0*, handling those agents that are not observed over the full sequence spectrum (observation length = $obs_{len}$ + prediction length = $pred_{len}$) by concatenating a binary flag $b_i^t$ that indicates if the agent is padded or not. In particular, we filter the static elements and track fragments scored by Argoverse 2 to get only the most relevant traffic agents, reducing the number of agents to be considered in complex traffic scenarios. Furthermore, to make the model translation and rotation invariant, the coordinate system in our model is BEV-centered of a given target agent at $t = 0$, and we use the orientation from the target location given in the same timestamp as the positive $x$-axis. Note that this representation will benefit the model to have a common representation to enhance the generalization of the model and prevent overfitting. Once the scene has been translated and rotated, instead of using absolute 2D-BEV ($xy$ plane), the input for the agent $i$ is a series of relative displacements:

$$\Delta \boldsymbol{\nu}_i^t = \boldsymbol{\nu}_i^t - \boldsymbol{\nu}_i^{t-1} \tag{8.1}$$

Where $\boldsymbol{\nu}_i^t$ represents the state vector (in this case, $xy$ position of the agent $i$ at timestamp $t$).

Since our model focus on an efficient encoding of the social information, we base our model on the ActorNet backbone proposed by [13], as observed in Fig. 8.3. While both CNNs and RNNs can be used for temporal data, ActorNet uses an 1D CNN to process the trajectory input for its effectiveness in extracting multi-scale features and efficiency in parallel computing. The output is a temporal feature map, whose element at $t = 0$ is used as the actor feature. The network has 3 groups/scales of 1D convolutions. Each group consists of 2 residual blocks, with the stride of the first block as 2. Then, a Feature Pyramid Network (FPN) [169] is used to fuse the multi-scale features, and apply another residual block to obtain the output tensor. For all layers, the convolution kernel size is 3 and the number of output channels is 128. Layer normalization and the Rectified Linear Unit (ReLU) are used after each convolution.

On top of that, in a similar way to [11], the agents centers (observations at $t = 0$) are encoded through a linear layer to initialize the hidden and cell vector of the LSTM layer, which processes the previously latent motion history. After that, a social attention block is used to compute the most representative agents interaction.

Taking the final actor features after motion history and agents interaction, a multi-modal prediction header outputs the final motion forecasting. For each agent, it predicts $K$ possible future trajectories and their confidence scores. The header has two branches, a regression branch to predict the trajectory of each mode and a classification branch to predict the confidence score of each mode.

For the $m$-th actor, a residual block and a linear layer in the regression branch to regress the $K$ sequences of BEV coordinates is obtained:

$$O_{m,\text{reg}} = \{(\mathbf{p}_{m,1}^k, \mathbf{p}_{m,2}^k, ..., \mathbf{p}_{m,T}^k)\}_{k\in[0,K-1]} \tag{8.2}$$

where $O_{m,\text{reg}}$ is the whole set of regressions and $\mathbf{p}_{m,i}^k$ is the predicted $m$-th actor's BEV coordinates of the $k$-th mode at the $i$-th time step.

On the other hand, for the classification branch, a MLP to $\mathbf{p}_{m,T}^k - \mathbf{p}_{m,0}$ to get $K$ distance embeddings is applied. Finally, each distance embedding is concatenated with the actor feature, applying a residual block and a linear layer to output $K$ confidence scores, $O_{m,\text{cls}} = (c_{m,0}, c_{m,1}, ..., c_{m,K-1})$.

In this particular work, we take the most plausible future trajectory for each agent (both the adversaries and the ego-vehicle) in the following timestamps: *t=0*, *t=10*, *t=20* and *t=30*, which correspond to the current position and the predicted position of the

corresponding agent 1, 2 and 3 seconds in the future respectively. Even though we train our prediction model following the principles of Argoverse 2 (5s and 6s of observation and prediction respectively), given the velocities and traffic density of the experiments run in the SMARTS simulator , we believe that predicting 3s in the future is enough for this purpose to evaluate the high-level actions of decision-making layer preventing overfitting. In future works, we will design more difficult scenearios, up-to-pair with the Argoverse 2 dataset (specially in terms of intersections or lane change behaviours at high speed) where multimodal predictions with higher prediction horizons will be required.

A Markov Decision Process (MDP) is a discrete-time stochastic control process that provides a mathematical framework for modelling decision-making environments. An MDP is a tuple $(S, A, P, R)$ in which $S$ is a set of states named state space, $A$ is a set of actions named action space, $P$ is the probability function and $R$ is a reward function. An algorithm with a given state $s \in S$ takes an action $a \in A$ transitioning to $s'$ with a probability $P(s, a, s')$, and getting a reward $R(s, a, s')$ as shown in Fig. 8.2. This algorithm iterates through this loop to learn a desired behaviour.

The goal in an MDP is to find a good policy for the decision-making system. The objective is to find the optimal policy $\pi*(s)$, that maximizes the cumulative function of the future reward.

We represent the driving scenario as an MDP to develop our decision-making module. We consider the output of the MP module as an input to this module. The state space, action space, and reward functions are defined in this section.

The state is defined by the predicted trajectories of the ego-vehicle and the five closest vehicles in the scenario.

$$s_t = (K_t^{ego}, K_t^1, ..., K_t^5) \tag{8.3}$$

where $K_t^i = (x_{t_0}^i, y_{t_0}^i, x_{t_1}^i, y_{t_1}^i, x_{t_2}^i, y_{t_2}^i, x_{t_3}^i, y_{t_3}^i)$ contains the future estimations of the positions of the vehicles across a future horizon of three seconds. A representation of a state vector is shown in Fig 8.4, where the vehicles' predicted positions are represented.

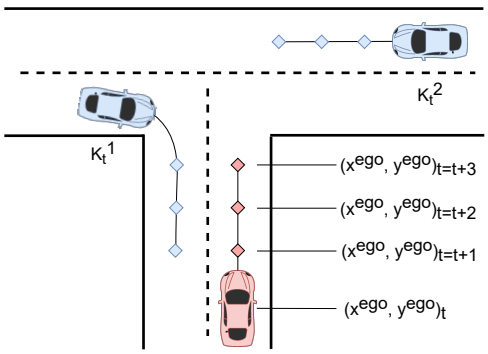


Figure 8.4: The ego-vehicle (red) and the adversaries (blue) predicted positions in the next three seconds are represented.

We propose a discrete action space formed by two actions. A low-level controller implemented by the simulator is in charge of performing smooth driving based on these actions. These actions are focused on the ego-vehicle velocity. The first action aims to reach a desired predefined velocity and the second action reduces the velocity until the vehicle stops. The action space is defined as:

$$a = (Drive, Stop) \tag{8.4}$$

#### 8.2.0.1. Reward Function

The reward function is defined in terms of success or failure. A negative reward is given when there is a collision and a positive reward is given when the vehicle reaches the success point, situated at the end of the scenario.

$$r = k_v * v_{ego} + \begin{cases} 1 & if \quad sucess \\ -1 & if \quad collision \end{cases} \tag{8.5}$$

As shown in Equation 8.5, we add one more factor to the reward function to encourage the ego-vehicle to move. We propose a cumulative reward based on its longitudinal velocity. We use a constant small enough to ensure that the reward per episode is bounded between -1 and 1.

Our approach for the RL implementation (Fig. 8.5) builds upon our previous research [193], where we demonstrated that incorporating a feature extractor module to a PPO algorithm yields improved metrics and faster convergence.

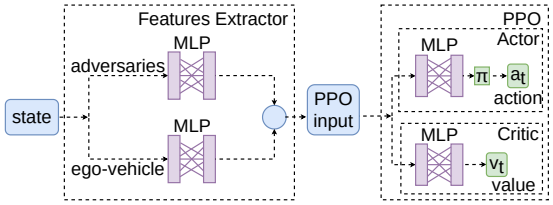


Figure 8.5: The neural network architecture consists of two fully connected layers followed by the concatenation of both adversaries and ego vehicle features. The resulting concatenated features are then passed through an actor-critic structure, which comprises two layers, each containing 128 neurons.

In this implementation, we introduce separate feature extractors for adversaries and the ego-vehicle, which are then concatenated into the input for the PPO algorithm. This algorithm consists of two models: the Actor, responsible for selecting an action based on the policy, and the Critic, which estimates the value function.

To validate the performance of our approach, an intersection scenario is implemented in SMARTS, which is a SUMO [177] based simulation platform for research on autonomous driving.

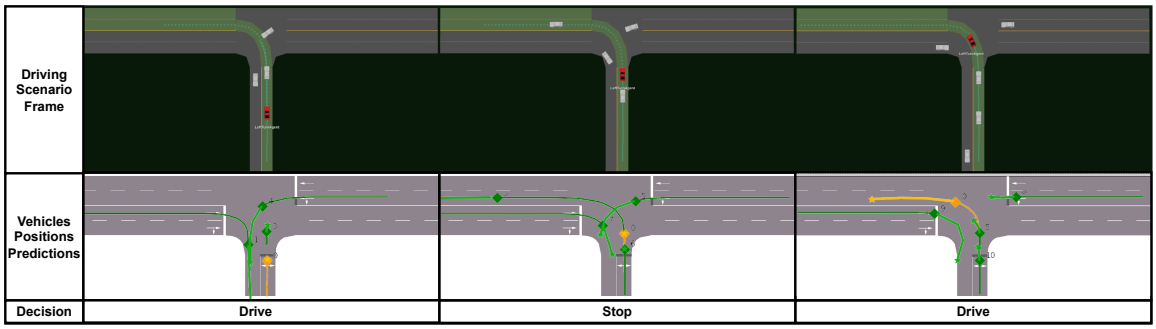


Figure 8.6: Simulation overview of our system behaviour. The red car follows the green path, and each image represents a different frame of the simulation. We also show the predicted positions below each image and the actions taken by the decision-making module.

The scenario is an urban unsignalized T-intersection. The objective is to execute a left turn maneuver in the absence of traffic signal protection, allowing the continuous flow of traffic. Fig. 8.1 illustrates the drivable area (highlighted in green) where the ego-vehicle can navigate to reach the target location. Simulations are reset under three conditions: 1) the ego-vehicle successfully reaches the target, 2) the episodic step surpasses the maximum time steps limit, and 3) the ego-vehicle collides or deviates from the drivable route.

We define different scenario configurations to test the performance of the proposed framework. First, the regular T-intersection scenario which is defined in SMARTS, where a random number of vehicles between [5-10] are spawned every minute, and the maximum velocity of these vehicles is 14 km/h. Then, we propose different configurations increasing the maximum velocity of the adversaries to 30, 60, and 90 km/h.

In decision-making, the success rate serves as a direct measure of the effectiveness of the RL agent in accomplishing the designated task. Besides, the average time of the episode is a common metric used in the literature. These metrics are defined as:

- $success\ [\%] = n_{success}/n_{success}$
- $t_e[s] = \sum t_n/n_{episodes}$

where the number of episodes $n_e$ is 100 and simulation time is measured in seconds.

To evaluate the performance of our approach we first present a comparison with the existing methods for decision-making in the literature and then an ablation study is conducted.

This first study compares the proposed approach with other existing methods for decision-making. The baseline methods used for comparison are Data-regularized Q-learning (DrQ) [189], Soft Actor-Critic (SAC) [194], and PPO. These methods have different features and serve as reference points for evaluating the proposed approach. The results presented in Table 8.1 demonstrate a higher success rate of our proposal.

Two ablative studies are carried out to see how the use of motion prediction in the state representation can improve the performance of the framework. The first approach is to use

Table 8.1: A comparison of the proposed framework against the existing baselines in the T-intersection scenario. The success rate S[%] and the average episode time $t_e$ are presented.

| Metric | Ours | PPO | SAC | DrQ |
|---|---|---|---|---|
| S[%] | **80** | 70 | 68 | 78 |
| $t_e$(s) | 22.3 | 36.4 | 19.2 | 18.2 |

just the position of the vehicles as the input to the decision-making module and the second approach is to use the locations over the past five seconds. We test the three approaches under the previously introduced configurations with different adversaries' velocities, from 15km/h to 90km/h. To correctly evaluate the performance of the decision-making system we propose different metrics that aim to provide a better comprehension of the behaviour. We believe that the success rate is still a good indicator, but we slightly modify the average time, only considering the successful episodes to calculate this metric. In addition, we include a new relevant metric: the average ego-vehicle velocity when a collision takes place $v_c$.

The results presented in Table **??** show that the use of the predicted positions in the state vector avoids more collisions as the velocities increase. Besides, the average collision velocity and the average time to complete the scenario are lower for the proposed approach.

Table 8.2: An ablation study comparing three state representations with the different scenario configurations: Current positions, Past positions, and Future positions. The success rate S[%], the episode time $t_e$ in these successful episodes, and the average velocity of collision $v_c$ are presented.

| | Metric | 15 km/h | 30 km/h | 60 km/h | 90 km/h |
|---|---|---|---|---|---|
| Future | S [%] | 80 | 78 | 78 | 77 |
| | $t_e$ (s) | 22.3 | 23.3 | 23.4 | 23.3 |
| | $v_c$ (km/h) | 4.9 | 5.1 | 5.6 | 5.6 |
| Current | S [%] | 77 | 73 | 70 | 70 |
| | $t_e$ (s) | 25.1 | 23.4 | 23.4 | 23.3 |
| | $v_c$ (km/h) | 5.1 | 5.5 | 6.1 | 6.2 |
| Past | S [%] | 78 | 75 | 72 | 71 |
| | $t_e$ (s) | 24.2 | 23.3 | 23.2 | 23.1 |
| | $v_c$ (km/h) | 4.9 | 5.2 | 5.9 | 6.0 |

Finally, an overview of the behaviour of our system is shown in Fig. 8.6. The ego-vehicle in red follows the trajectory defined in green. Each image represents a different frame of the simulation and the respective predictions of the positions are displayed below. Besides, the action executed by the decision-making module for each frame is shown.

The proposed method incorporates an Efficient Social-based Motion Prediction module, which predicts the future positions of vehicles within the scenario. These predictions improve a Reinforcement Learning-based Decision Making module. The results of the study demonstrate that our approach achieves significant performance improvements, particularly in scenarios involving high velocities.

This research opens up several potential directions for future work. The proposed approach can be evaluated in a broader range of urban driving scenarios to assess its robustness and scalability, up-to-pair with the difficulty of the Argoverse 2 dataset scenarios (specially in terms of intersections or lane change behaviours at high speed) where multimodal predictions with higher prediction horizons will be required. Furthermore, the Reinforcement Learning-based Decision Making module can be enhanced by exploring advanced algorithms.

## 8.3. Holistic Simulation in CARLA

The main contribution of our AD PerDevKit is the creation of a ground-truth generation tool for the surrounding obstacles of the ego-vehicle using CARLA and ROS. For its implementation, as explained in section **??**, the CARLA-ROS brige is used so that the simultaneous execution of CARLA and this tool is not necessary, since the execution of both programs can be very demanding due to the simulator requirements. This way it is possible to record a rosbag (a file with all the ROS messages) with the GT information, so that only an area around the ego-vehicle is analyzed and not the whole obstacles in the CARLA runtime.

The messages created by CARLA contain the information of the different objects of the environment in relation to the map on which it is being used. However, to be used independently, the obstacles must be referenced to the ego-vehicle. Therefore, it is necessary to perform the different transformations to go from a coordinate system based on the map to a coordinate system based on the ego-vehicle.

### 8.3.1. Method for obtaining 2D bounding boxes

While the CARLA-ROS bridge gives access to the 3D bounding boxes of the objects in the environment, it does not provide the projected 2D bounding boxes of these 3D objects in the camera. We perform a series of transformations to go from the coordinates of the world to the pixels containing that object within each image generated by the camera.

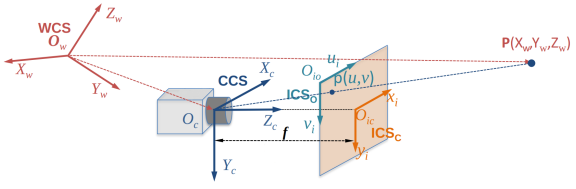


Figure 8.7: Geometry transformation from world to camera

A conversion from the world coordinates to the image ones is necessary to transform the eight vertices of a 3D bounding box into the vertices of a 2D bounding box. For this purpose, it is necessary to apply some geometry transformations as shown in Fig. 8.7.

Using homogeneous coordinates, the correspondence between a 3D point in the World Coordinate System (WCS) and its projected pixel in the Image Coordinate System at origin ($ICS_O$) is calculated applying the following equation:

$$\begin{bmatrix} wu \\ wv \\ w \end{bmatrix} = M_{3x4} \begin{bmatrix} X_w \\ Y_w \\ Z_w \\ 1 \end{bmatrix}$$

where $M_{(3x4)} = M_{int}M_{ext}$ is the camera projection matrix, formed by the product of intrinsic matrix and extrinsic matrix, defined as follow:

$$M_{int} = \begin{bmatrix} f/dx & 0 & u_0 \\ 0 & f/dy & v_0 \\ 0 & 0 & 1 \end{bmatrix}$$

$$M_{ext} = \begin{bmatrix} R_{3x3} & T_{3x1} \\ 0 & 1 \end{bmatrix}$$

being $f$ focal distance, $(dx, dy)$ physical size of the pixel, $(u_0, v_0)$ centre of the image in pixels, $T_{3x1}$ translation matrix and $R_{3x3}$ rotation matrix from the world (WCS) to the camera (CCS).

The steps to perform this conversion are the following:

1. Transformation from World Coordinate System to Camera Coordinate System (WCS/CCS):

   During the geometric transformation of the world coordinates to the image, homogeneous coordinates are used, such a coordinate system adds a fourth component to the three-dimensional coordinates. This coordinate system has a direct equivalence to the Cartesian coordinate system as shown below.

   $$(x, y, z) \rightarrow (x', y', z', w)$$
   $$(x, y, z) = (x'/w, y'/w, z'/w)$$

   Firstly the translation matrix from the world to the camera is obtained.

   $$T_{3x1} = \begin{bmatrix} T_x \\ T_y \\ T_z \end{bmatrix}$$

   Afterwards, the rotation matrix is built over the 3 rotation matrices of the different dimensions.

$$R = R_x(\alpha)R_y(\beta)T_z(\gamma)$$

Based on the translation matrix and the rotation matrix, a matrix of 4x4 dimensions is built, which together with the matrix of the points to be transformed, gives a matrix with the points in the camera coordinate system.

$$P_c = \begin{bmatrix} R_{3x3} & T_{3x1} \\ 0 & 1 \end{bmatrix} \begin{bmatrix} X_w \\ Y_w \\ Z_w \\ 1 \end{bmatrix} = \begin{bmatrix} X_c \\ Y_c \\ Z_c \\ 1 \end{bmatrix}$$

2. Transformation from Camera Coordinate System to Image Coordinate System in the center of the image (CCS/ICS$_C$):

   During the transformation to the image coordinate system, it is necessary to work with the distance between the optical center and the image plane, also called focal length. Thereby a matrix is constructed, which together with the points in the camera coordinate system is obtained in the image coordinate system in the center of the image.

$$\begin{bmatrix} wx \\ wy \\ w \end{bmatrix} = \begin{bmatrix} f & 0 & 0 & 0 \\ 0 & f & 0 & 0 \\ 0 & 0 & 1 & 0 \end{bmatrix} \begin{bmatrix} X_c \\ Y_c \\ Z_c \\ 1 \end{bmatrix}$$

3. Transformation from Image Coordinate System in the center of the image to Image Coordinate System at origin (ICS$_C$/ICS$_O$) in pixels:

   As a last step, the points are transformed to image pixels using the size of the camera sensor as well as the pixel resolution of the image.

$$\begin{bmatrix} wu \\ wv \\ w \end{bmatrix} = \begin{bmatrix} 1/dx & 0 & u_0 \\ 0 & 1/dy & v_0 \\ 0 & 0 & 1 \end{bmatrix} \begin{bmatrix} wx \\ wy \\ w \end{bmatrix}$$

After all this, the vertices from the different 3D bounding boxes of the objects in the environment are brought to the pixels of the images taken, and after this, they are transformed to 2D bounding boxes with the vertices furthest from each object.

### 8.3.2. Calculation of object visibility

One main issue for the GT calculation is that CARLA always render all the objects, even when they are not visible by the camera, LiDAR or Radar, which is a problem for any training process. There are many studies about ray tracing that solve this issue.

These techniques [195] [196] are computationally very expensive so it is very difficult to implement them in real-time.

We propose a method for the calculation of visibility in CARLA and ROS using directly the point cloud calculated by CARLA. A vehicle will be considered as visible, as long as a point of the LiDAR point cloud is found inside an object, in the same way as it is done in the nuScenes dataset [92]. The steps to be performed are the following:

1. Remove objects furthest than the maximum LiDAR distance.
2. Deletion of the points of the point cloud with the height higher or lower than the objects in the surroundings.
3. Elimination of points outside the area in which the objects are located, taking into account all possible rotations.
4. Selection of the visible objects having at least one point in the point cloud taking into account the rotation of the different objects.

In order to obtain a much simplified and reduced GT to work with, the tool has been designed with sensor synchronization as the basis. In this way, GT does not have to be calculated every time data is obtained from a sensor, or in certain timestamps in which data is available. Because of this, it is necessary to activate the CARLA synchronization option for the correct functioning of the tool.

## 8.4. Summary

# Chapter 9

# Conclusions and Future Works

*El mundo no es todo alegría y color,*
*es un lugar terrible y por muy duro que seas*
*es capaz de arrodillarte a golpes*
*y tenerte sometido a golpes permanentemente*
*si no se lo impides.*
*Ni tú ni yo ni nadie golpea mas fuerte que la vida.*
*Pero no importa lo fuerte que golpeas,*
*sino lo fuerte que pueden golpearte*
*hay que soportar sin dejar de avanzar.*
*¡Así es como se gana!*

Discurso de Rocky a su hijo
Rocky Balboa

## 9.1. Conclusions

AD has gained significant attention in recent years, with the development of intelligent vehicles and the increasing need for safe and efficient transportation systems. However, one of the main challenges in the field of AD is scene understanding, which involves the ability of a vehicle to recognize and interpret the objects and events in its environment. Accurate scene understanding, particularly focusing on the future behaviour of the scene, is critical for safe and efficient driving, as it enables the vehicle to make informed decisions and take appropriate actions.

DL has emerged as a powerful tool for scene understanding in autonomous driving, as it can automatically learn representations of complex and high-dimensional data. In particular, deep neural networks have shown remarkable performance in various tasks related to scene understanding, such as object detection, segmentation, classification or prediction. In that sense, the design and implementation of effective DL models for scene understanding is a really active research area, and there is a need for more advanced predictive techniques to improve the performance of autonomous vehicles.

The main scope of this thesis has been the development of novel and efficient interaction-aware DL based MP models, focusing on long-term (from 3 to 6 s) prediction horizon, including social and physical information. Even though the main agent to be predicted will be usually the ego-vehicle, the algorithms proposed in this chapter will be able to properly model the past trajectory and agents interactions based on the specific type of agent, instead of the first DL models proposed in the literature which only focused on pedestrian trajectory prediction [67], [69], [129].

First of all, this chapter will study the incorporation of HD map information to enhance the robustness and reliability of a simple-yet-powerful tracking-by-detection pipeline, based on Kalman Filter and Hungarian algorithm, which subsequently feeds the updated tracker information to perform CTRV prediction. Then, DL will be progressively integrated to encode the past trajectories, social interactions and physical information respectively, including physics-based heuristics to include map information, specially the potential future goals or centerlines candidates. The goal is to develop advanced models that can accurately recognize and interpret the agents states, interactions and context to provide reliable predictions for safe and efficient driving.

## 9.2. Future Works

# List of Publications

The following publications correspond to first author or main co-author. For a complete view of all publications derived from the thesis: All publications [1]:

## Journal Papers

- **Gomez-Huelamo, C.**, Conde, M. V., Barea, R., Ocala, M, & Bergasa, L. M. (2023). Efficient Baselines for Motion Prediction in Autonomous Driving. Transactions on Intelligent Transportation Systems. In submission.
- **Gomez-Huelamo, C.**, Del Egido, J., Bergasa, L. M., Barea, R., Lopez-Guillen, E., Araluce, J., & Antunes, M. (2022). 360º real-time and power-efficient 3D DAMOT for autonomous driving applications. Multimedia Tools and Applications, 81(19), 26915-26940
- **Gómez-Huélamo, C.**, Del Egido, J., Bergasa, L. M., Barea, R., López-Guillén, E., Arango, F., ... & López, J. (2021). Train here, drive there: Ros based end-to-end autonomous-driving pipeline validation in carla simulator using the nhtsa typology. Multimedia Tools and Applications, 1-28

## Conference Contributions

- **Gómez-Huélamo, C.**, Conde, M. V., Gutiérrez-Moreno R, Barea, R., Llamazares A., Antunes M., & Bergasa, L. M. (2022, October). Efficient Context-Aware Graph Transformer for Vehicle Motion Predictio. In 2023 IEEE 26th International Conference on Intelligent Transportation Systems (ITSC). IEEE. In submission.
- Gutiérrez-Moreno R., **Gómez-Huélamo, C.**, Barea. R, López-Guillén E., Arango F., Ortiz, M., & Bergasa, L. M. (2023, October). Augmented Reinforcement Learning with Efficient Social-based Motion Prediction for Autonomous Decision-Making. In 2023 IEEE 26th International Conference on Intelligent Transportation Systems (ITSC). IEEE. In submission.

[1] https://scholar.google.es/citations?user=OWwoG6EAAAAJ&hl=es

- **Gómez-Huélamo, C.**, Conde, M, Barea, R. & Bergasa, L. M. (2023, June). Improving Multi-Agent Motion Prediction with Heuristic Goals and Motion Refinement. In Proceedings of the IEEE/CVF Conference on Computer Vision and Pattern Recognition (CVPR) (pp. 5322-5331). IEEE

- **Gómez-Huélamo, C.**, Conde, M. V., Ortiz, M., Montiel, S., Barea, R., & Bergasa, L. M. (2022, October). Exploring Attention GAN for Vehicle Motion Prediction. In 2022 IEEE 25th International Conference on Intelligent Transportation Systems (ITSC) (pp. 4011-4016). IEEE

- Diaz-Diaz, A., Ocaña, M., Llamazares, Á., **Gómez-Huélamo, C.**, Revenga, P., & Bergasa, L. M. (2022, June). HD maps: Exploiting OpenDRIVE potential for Path Planning and Map Monitoring. In 2022 IEEE Intelligent Vehicles Symposium (IV) (pp. 1211-1217). IEEE.

- **Gómez-Huélamo, C.**, Diaz-Diaz, A., Araluce, J., Ortiz, M. E., Gutiérrez, R., Arango, F., ... & Bergasa, L. M. (2022, June). How to build and validate a safe and reliable Autonomous Driving stack? A ROS based software modular architecture baseline. In 2022 IEEE Intelligent Vehicles Symposium (IV) (pp. 1282-1289). IEEE

- Del Egido, J., **Gómez-Huélamo, C.**, Bergasa, L. M., Barea, R., López-Guillén, E., Araluce, J., ... & Antunes, M. (2020, November). 360 real-time 3d multi-object detection and tracking for autonomous vehicle navigation. In Advances in Physical Agents II: Proceedings of the 21st International Workshop of Physical Agents (WAF 2020), November 19-20, 2020, Alcalá de Henares, Madrid, Spain (pp. 241-255). Cham: Springer International Publishing.

- **Gómez–Huélamo, C.**, Bergasa, L. M., Gutiérrez, R., Arango, J. F., & Díaz, A. (2021, July). Smartmot: exploiting the fusion of hdmaps and multi-object tracking for real-time scene understanding in intelligent vehicles applications. In 2021 IEEE Intelligent Vehicles Symposium (IV) (pp. 710-715). IEEE.

- Gutiérrez, R., Arango, J. F., **Gomez-Huélamo, C.**, Bergasa, L. M., Barea, R., & Araluce, J. (2021, July). Validation Method of a Self-Driving Architecture for Unexpected Pedestrian Scenario in CARLA Simulator. In 2021 IEEE Intelligent Vehicles Symposium (IV) (pp. 1144-1149). IEEE.

- **Gómez-Huélamo, C.**, Del Egido, J., Bergasa, L. M., Barea, R., López-Guillén, E., Arango, F., ... & López, J. (2021). Train here, drive there: Simulating real-world use cases with fully-autonomous driving architecture in carla simulator. In Advances in Physical Agents II: Proceedings of the 21st International Workshop of Physical Agents (WAF 2020), November 19-20, 2020, Alcalá de Henares, Madrid, Spain (pp. 44-59). Springer International Publishing

- **Gómez-Huélamo, C.**, Del Egido, J., Bergasa, L. M., Barea, R., Ocana, M., Arango, F., & Gutiérrez-Moreno, R. (2020, September). Real-time bird's eye view multi-object tracking system based on fast encoders for object detection. In 2020 IEEE 23rd International Conference on Intelligent Transportation Systems (ITSC) (pp. 1-6). IEEE.
- **Gómez-Huelamo, C.**, Bergasa, L. M., Barea, R., López-Guillén, E., Arango, F., & Sánchez, P. (2019, October). Simulating use cases for the UAH Autonomous Electric Car. In 2019 IEEE Intelligent Transportation Systems Conference (ITSC) (pp. 2305-2311). IEEE.

# Bibliography


[1] S. Taxonomy, "Definitions for terms related to driving automation systems for on-road motor vehicles (j3016)", Technical report, Society for Automotive Engineering, Tech. Rep., 2016.

[2] J. F. Arango, L. M. Bergasa, P. A. Revenga, *et al.*, "Drive-by-wire development process based on ros for an autonomous electric vehicle", *Sensors*, vol. 20, no. 21, p. 6121, 2020.

[3] A. Ranga, F. Giruzzi, J. Bhanushali, *et al.*, "Vrunet: Multi-task learning model for intent prediction of vulnerable road users", *arXiv preprint arXiv:2007.05397*, 2020.

[4] I. Gog, S. Kalra, P. Schafhalter, M. A. Wright, J. E. Gonzalez, and I. Stoica, "Pylot: A modular platform for exploring latency-accuracy tradeoffs in autonomous vehicles", in *2021 IEEE International Conference on Robotics and Automation (ICRA)*, IEEE, 2021, pp. 8806–8813.

[5] M.-F. Chang, J. Lambert, P. Sangkloy, *et al.*, "Argoverse: 3d tracking and forecasting with rich maps", in *Proceedings of the IEEE/CVF conference on computer vision and pattern recognition*, 2019, pp. 8748–8757.

[6] B. Wilson, W. Qi, T. Agarwal, *et al.*, "Argoverse 2: Next generation datasets for self-driving perception and forecasting", *arXiv preprint arXiv:2301.00493*, 2023.

[7] T. Salzmann, B. Ivanovic, P. Chakravarty, and M. Pavone, "Trajectron++: Dynamically-feasible trajectory forecasting with heterogeneous data", in *Computer Vision–ECCV 2020: 16th European Conference, Glasgow, UK, August 23–28, 2020, Proceedings, Part XVIII 16*, Springer, 2020, pp. 683–700.

[8] T. Gilles, S. Sabatini, D. Tsishkou, B. Stanciulescu, and F. Moutarde, "Home: Heatmap output for future motion estimation", in *2021 IEEE International Intelligent Transportation Systems Conference (ITSC)*, IEEE, 2021, pp. 500–507.

[9] T. Gilles, S. Sabatini, D. Tsishkou, B. Stanciulescu, and F. Moutarde, "Gohome: Graph-oriented heatmap output for future motion estimation", in *2022 International Conference on Robotics and Automation (ICRA)*, IEEE, 2022, pp. 9107–9114.

[10] B. Varadarajan, A. Hefny, A. Srivastava, *et al.*, "Multipath++: Efficient information fusion and trajectory aggregation for behavior prediction", in *2022 International Conference on Robotics and Automation (ICRA)*, IEEE, 2022, pp. 7814–7821.

[11] M. Wang, X. Zhu, C. Yu, *et al.*, "Ganet: Goal area network for motion forecasting", *arXiv preprint arXiv:2209.09723*, 2022.

[12] J. Schmidt, J. Jordan, F. Gritschneder, and K. Dietmayer, "Crat-pred: Vehicle trajectory prediction with crystal graph convolutional neural networks and multi-head self-attention", in *2022 International Conference on Robotics and Automation (ICRA)*, IEEE, 2022, pp. 7799–7805.

[13] M. Liang, B. Yang, R. Hu, *et al.*, "Learning lane graph representations for motion forecasting", in *Computer Vision–ECCV 2020: 16th European Conference, Glasgow, UK, August 23–28, 2020, Proceedings, Part II 16*, Springer, 2020, pp. 541–556.

[14] Z. Huang, H. Liu, J. Wu, and C. Lv, "Conditional predictive behavior planning with inverse reinforcement learning for human-like autonomous driving", *IEEE Transactions on Intelligent Transportation Systems*, 2023.

[15] C. Tang and R. R. Salakhutdinov, "Multiple futures prediction", *Advances in neural information processing systems*, vol. 32, 2019.

[16] N. Rhinehart, R. McAllister, K. Kitani, and S. Levine, "Precog: Prediction conditioned on goals in visual multi-agent settings", in *Proceedings of the IEEE/CVF International Conference on Computer Vision*, 2019, pp. 2821–2830.

[17] S. Khandelwal, W. Qi, J. Singh, A. Hartnett, and D. Ramanan, "What-if motion prediction for autonomous driving", *arXiv preprint arXiv:2008.10587*, 2020.

[18] C. Tang, W. Zhan, and M. Tomizuka, "Interventional behavior prediction: Avoiding overly confident anticipation in interactive prediction", in *2022 IEEE/RSJ International Conference on Intelligent Robots and Systems (IROS)*, IEEE, 2022, pp. 11 409–11 415.

[19] H. Zhao, J. Gao, T. Lan, *et al.*, "Tnt: Target-driven trajectory prediction", in *Conference on Robot Learning*, PMLR, 2021, pp. 895–904.

[20] Y. Huang, J. Du, Z. Yang, Z. Zhou, L. Zhang, and H. Chen, "A survey on trajectory-prediction methods for autonomous driving", *IEEE Transactions on Intelligent Vehicles*, vol. 7, no. 3, pp. 652–674, 2022.

[21] N. Kaempchen, B. Schiele, and K. Dietmayer, "Situation assessment of an autonomous emergency brake for arbitrary vehicle-to-vehicle collision scenarios", *IEEE Transactions on Intelligent Transportation Systems*, vol. 10, no. 4, pp. 678–687, 2009.

[22] R. Pepy, A. Lambert, and H. Mounier, "Reducing navigation errors by planning with realistic vehicle model", in *2006 IEEE Intelligent Vehicles Symposium*, IEEE, 2006, pp. 300–307.

[23] R. Miller and Q. Huang, "An adaptive peer-to-peer collision warning system", in *Vehicular Technology Conference. IEEE 55th Vehicular Technology Conference. VTC Spring 2002 (Cat. No. 02CH37367)*, IEEE, vol. 1, 2002, pp. 317–321.

[24] J. Hillenbrand, A. M. Spieker, and K. Kroschel, "A multilevel collision mitigation approach—its situation assessment, decision making, and performance tradeoffs", *IEEE Transactions on intelligent transportation systems*, vol. 7, no. 4, pp. 528–540, 2006.

[25] R. E. Kalman, "A new approach to linear filtering and prediction problems", 1960.

[26] N. Kaempchen, K. Weiss, M. Schaefer, and K. C. Dietmayer, "Imm object tracking for high dynamic driving maneuvers", in *IEEE Intelligent Vehicles Symposium, 2004.*, IEEE, 2004, pp. 825–830.

[27] B. Jin, B. Jiu, T. Su, H. Liu, and G. Liu, "Switched kalman filter-interacting multiple model algorithm based on optimal autoregressive model for manoeuvring target tracking", *IET Radar, Sonar & Navigation*, vol. 9, no. 2, pp. 199–209, 2015.

[28] V. Lefkopoulos, M. Menner, A. Domahidi, and M. N. Zeilinger, "Interaction-aware motion prediction for autonomous driving: A multiple model kalman filtering scheme", *IEEE Robotics and Automation Letters*, vol. 6, no. 1, pp. 80–87, 2020.

[29] A. Broadhurst, S. Baker, and T. Kanade, "Monte carlo road safety reasoning", in *IEEE Proceedings. Intelligent Vehicles Symposium, 2005.*, IEEE, 2005, pp. 319–324.

[30] K. Okamoto, K. Berntorp, and S. Di Cairano, "Driver intention-based vehicle threat assessment using random forests and particle filtering", *IFAC-PapersOnLine*, vol. 50, no. 1, pp. 13 860–13 865, 2017.

[31] Y. Wang, Z. Liu, Z. Zuo, Z. Li, L. Wang, and X. Luo, "Trajectory planning and safety assessment of autonomous vehicles based on motion prediction and model predictive control", *IEEE Transactions on Vehicular Technology*, vol. 68, no. 9, pp. 8546–8556, 2019.

[32] Q. Deng and D. Söffker, "Improved driving behaviors prediction based on fuzzy logic-hidden markov model (fl-hmm)", in *2018 IEEE Intelligent Vehicles Symposium (IV)*, IEEE, 2018, pp. 2003–2008.

[33] G. He, X. Li, Y. Lv, B. Gao, and H. Chen, "Probabilistic intention prediction and trajectory generation based on dynamic bayesian networks", in *2019 Chinese Automation Congress (CAC)*, IEEE, 2019, pp. 2646–2651.

[34] C. E. Rasmussen, "Gaussian processes in machine learning", in *Advanced Lectures on Machine Learning: ML Summer Schools 2003, Canberra, Australia, February 2-14, 2003, Tübingen, Germany, August 4-16, 2003, Revised Lectures*, Springer, 2004, pp. 63–71.

[35] J. Joseph, F. Doshi-Velez, A. S. Huang, and N. Roy, "A bayesian nonparametric approach to modeling motion patterns", *Autonomous Robots*, vol. 31, pp. 383–400, 2011.

[36] Q. Tran and J. Firl, "Online maneuver recognition and multimodal trajectory prediction for intersection assistance using non-parametric regression", in *2014 ieee intelligent vehicles symposium proceedings*, IEEE, 2014, pp. 918–923.

[37] P. Trautman and A. Krause, "Unfreezing the robot: Navigation in dense, interacting crowds", in *2010 IEEE/RSJ International Conference on Intelligent Robots and Systems*, IEEE, 2010, pp. 797–803.

[38] Y. Guo, V. V. Kalidindi, M. Arief, *et al.*, "Modeling multi-vehicle interaction scenarios using gaussian random field", in *2019 IEEE Intelligent Transportation Systems Conference (ITSC)*, IEEE, 2019, pp. 3974–3980.

[39] H. M. Mandalia and M. D. D. Salvucci, "Using support vector machines for lane-change detection", in *Proceedings of the human factors and ergonomics society annual meeting*, SAGE Publications Sage CA: Los Angeles, CA, vol. 49, 2005, pp. 1965–1969.

[40] P. Kumar, M. Perrollaz, S. Lefevre, and C. Laugier, "Learning-based approach for online lane change intention prediction", in *2013 IEEE Intelligent Vehicles Symposium (IV)*, IEEE, 2013, pp. 797–802.

[41] G. S. Aoude and J. P. How, "Using support vector machines and bayesian filtering for classifying agent intentions at road intersections", Tech. Rep., 2009.

[42] Y. Wang, C. Wang, W. Zhao, and C. Xu, "Decision-making and planning method for autonomous vehicles based on motivation and risk assessment", *IEEE Transactions on Vehicular Technology*, vol. 70, no. 1, pp. 107–120, 2021.

[43] N. Deo, A. Rangesh, and M. M. Trivedi, "How would surround vehicles move? a unified framework for maneuver classification and motion prediction", *IEEE Transactions on Intelligent Vehicles*, vol. 3, no. 2, pp. 129–140, 2018.

[44] D. Koller and N. Friedman, *Probabilistic graphical models: principles and techniques*. MIT press, 2009.

[45] M. Schreier, V. Willert, and J. Adamy, "An integrated approach to maneuver-based trajectory prediction and criticality assessment in arbitrary road environments", *IEEE Transactions on Intelligent Transportation Systems*, vol. 17, no. 10, pp. 2751–2766, 2016.

[46] M. Bahram, A. Lawitzky, J. Friedrichs, M. Aeberhard, and D. Wollherr, "A game-theoretic approach to replanning-aware interactive scene prediction and planning", *IEEE Transactions on Vehicular Technology*, vol. 65, no. 6, pp. 3981–3992, 2015.

[47] J. Li, B. Dai, X. Li, X. Xu, and D. Liu, "A dynamic bayesian network for vehicle maneuver prediction in highway driving scenarios: Framework and verification", *Electronics*, vol. 8, no. 1, p. 40, 2019.

[48] G. Weidl, A. L. Madsen, D. Kasper, and G. Breuel, "Optimizing bayesian networks for recognition of driving maneuvers to meet the automotive requirements", in *2014 IEEE International Symposium on Intelligent Control (ISIC)*, IEEE, 2014, pp. 1626–1631.

[49] Y. Guan, S. E. Li, J. Duan, W. Wang, and B. Cheng, "Markov probabilistic decision making of self-driving cars in highway with random traffic flow: A simulation study", *Journal of Intelligent and Connected Vehicles*, vol. 1, no. 2, pp. 77–84, 2018.

[50] D. Silver, J. A. Bagnell, and A. Stentz, "Learning autonomous driving styles and maneuvers from expert demonstration", in *Experimental Robotics: The 13th International Symposium on Experimental Robotics*, Springer, 2013, pp. 371–386.

[51] N. Aghasadeghi and T. Bretl, "Maximum entropy inverse reinforcement learning in continuous state spaces with path integrals", in *2011 IEEE/RSJ International Conference on Intelligent Robots and Systems*, IEEE, 2011, pp. 1561–1566.

[52] M. Herman, V. Fischer, T. Gindele, and W. Burgard, "Inverse reinforcement learning of behavioral models for online-adapting navigation strategies", in *2015 IEEE international conference on robotics and automation (ICRA)*, IEEE, 2015, pp. 3215–3222.

[53] S. Sharifzadeh, I. Chiotellis, R. Triebel, and D. Cremers, "Learning to drive using inverse reinforcement learning and deep q-networks", *arXiv preprint arXiv:1612.03653*, 2016.

[54] L. Sun, W. Zhan, and M. Tomizuka, "Probabilistic prediction of interactive driving behavior via hierarchical inverse reinforcement learning", in *2018 21st International Conference on Intelligent Transportation Systems (ITSC)*, IEEE, 2018, pp. 2111–2117.

[55] Z. Huang, J. Wu, and C. Lv, "Driving behavior modeling using naturalistic human driving data with inverse reinforcement learning", *IEEE Transactions on Intelligent Transportation Systems*, vol. 23, no. 8, pp. 10 239–10 251, 2021.

[56] F. Torabi, G. Warnell, and P. Stone, "Generative adversarial imitation from observation", *arXiv preprint arXiv:1807.06158*, 2018.

[57] I. Goodfellow, J. Pouget-Abadie, M. Mirza, *et al.*, "Generative adversarial networks", *Communications of the ACM*, vol. 63, no. 11, pp. 139–144, 2020.

[58] A. Kuefler, J. Morton, T. Wheeler, and M. Kochenderfer, "Imitating driver behavior with generative adversarial networks", in *2017 IEEE Intelligent Vehicles Symposium (IV)*, IEEE, 2017, pp. 204–211.

[59] R. Bhattacharyya, B. Wulfe, D. J. Phillips, *et al.*, "Modeling human driving behavior through generative adversarial imitation learning", *IEEE Transactions on Intelligent Transportation Systems*, 2022.

[60] S. Choi, J. Kim, and H. Yeo, "Trajgail: Generating urban vehicle trajectories using generative adversarial imitation learning", *Transportation Research Part C: Emerging Technologies*, vol. 128, p. 103 091, 2021.

[61] M. Wulfmeier, P. Ondruska, and I. Posner, "Maximum entropy deep inverse reinforcement learning", *arXiv preprint arXiv:1507.04888*, 2015.

[62] C. You, J. Lu, D. Filev, and P. Tsiotras, "Advanced planning for autonomous vehicles using reinforcement learning and deep inverse reinforcement learning", *Robotics and Autonomous Systems*, vol. 114, pp. 1–18, 2019.

[63] T. Fernando, S. Denman, S. Sridharan, and C. Fookes, "Deep inverse reinforcement learning for behavior prediction in autonomous driving: Accurate forecasts of vehicle motion", *IEEE Signal Processing Magazine*, vol. 38, no. 1, pp. 87–96, 2020.

[64] M. Wulfmeier, D. Rao, D. Z. Wang, P. Ondruska, and I. Posner, "Large-scale cost function learning for path planning using deep inverse reinforcement learning", *The International Journal of Robotics Research*, vol. 36, no. 10, pp. 1073–1087, 2017.

[65] Z. Zhu, N. Li, R. Sun, D. Xu, and H. Zhao, "Off-road autonomous vehicles traversability analysis and trajectory planning based on deep inverse reinforcement learning", in *2020 IEEE Intelligent Vehicles Symposium (IV)*, IEEE, 2020, pp. 971–977.

[66] M. Wulfmeier, D. Z. Wang, and I. Posner, "Watch this: Scalable cost-function learning for path planning in urban environments", in *2016 IEEE/RSJ International Conference on Intelligent Robots and Systems (IROS)*, IEEE, 2016, pp. 2089–2095.

[67] A. Gupta, J. Johnson, L. Fei-Fei, S. Savarese, and A. Alahi, "Social gan: Socially acceptable trajectories with generative adversarial networks", in *Proceedings of the IEEE conference on computer vision and pattern recognition*, 2018, pp. 2255–2264.

[68] S. Casas, W. Luo, and R. Urtasun, "Intentnet: Learning to predict intention from raw sensor data", in *Conference on Robot Learning*, PMLR, 2018, pp. 947–956.

[69] A. Alahi, K. Goel, V. Ramanathan, A. Robicquet, L. Fei-Fei, and S. Savarese, "Social lstm: Human trajectory prediction in crowded spaces", in *Proceedings of the IEEE conference on computer vision and pattern recognition*, 2016, pp. 961–971.

[70] J. Mercat, T. Gilles, N. El Zoghby, G. Sandou, D. Beauvois, and G. P. Gil, "Multi-head attention for multi-modal joint vehicle motion forecasting", in *2020 IEEE International Conference on Robotics and Automation (ICRA)*, IEEE, 2020, pp. 9638–9644.

[71] J. Gao, C. Sun, H. Zhao, *et al.*, "Vectornet: Encoding hd maps and agent dynamics from vectorized representation", in *Proceedings of the IEEE/CVF Conference on Computer Vision and Pattern Recognition*, 2020, pp. 11 525–11 533.

[72] J. Ngiam, V. Vasudevan, B. Caine, *et al.*, "Scene transformer: A unified architecture for predicting future trajectories of multiple agents", in *International Conference on Learning Representations*, 2022.

[73] S. Casas, A. Sadat, and R. Urtasun, "Mp3: A unified model to map, perceive, predict and plan", in *Proceedings of the IEEE/CVF Conference on Computer Vision and Pattern Recognition*, 2021, pp. 14 403–14 412.

[74] T. Phan-Minh, E. C. Grigore, F. A. Boulton, O. Beijbom, and E. M. Wolff, "Covernet: Multimodal behavior prediction using trajectory sets", in *Proceedings of the IEEE/CVF Conference on Computer Vision and Pattern Recognition*, 2020, pp. 14 074–14 083.

[75] N. Lee, W. Choi, P. Vernaza, C. B. Choy, P. H. Torr, and M. Chandraker, "Desire: Distant future prediction in dynamic scenes with interacting agents", in *Proceedings of the IEEE conference on computer vision and pattern recognition*, 2017, pp. 336–345.

[76] F. Marchetti, F. Becattini, L. Seidenari, and A. D. Bimbo, "Mantra: Memory augmented networks for multiple trajectory prediction", in *Proceedings of the IEEE/CVF conference on computer vision and pattern recognition*, 2020, pp. 7143–7152.

[77] Y. Biktairov, M. Stebelev, I. Rudenko, O. Shliazhko, and B. Yangel, "Prank: Motion prediction based on ranking", *Advances in neural information processing systems*, vol. 33, pp. 2553–2563, 2020.

[78] H. Cui, V. Radosavljevic, F.-C. Chou, *et al.*, "Multimodal trajectory predictions for autonomous driving using deep convolutional networks", in *2019 International Conference on Robotics and Automation (ICRA)*, IEEE, 2019, pp. 2090–2096.

[79] Y. Chai, B. Sapp, M. Bansal, and D. Anguelov, "Multipath: Multiple probabilistic anchor trajectory hypotheses for behavior prediction", *arXiv preprint arXiv:1910.05449*, 2019.

[80] T. Buhet, E. Wirbel, A. Bursuc, and X. Perrotton, "Plop: Probabilistic polynomial objects trajectory prediction for autonomous driving", in *Conference on Robot Learning*, PMLR, 2021, pp. 329–338.

[81] N. Rhinehart, K. M. Kitani, and P. Vernaza, "R2p2: A reparameterized pushforward policy for diverse, precise generative path forecasting", in *Proceedings of the European Conference on Computer Vision (ECCV)*, 2018, pp. 772–788.

[82] H. Cui, T. Nguyen, F.-C. Chou, *et al.*, "Deep kinematic models for kinematically feasible vehicle trajectory predictions", in *2020 IEEE International Conference on Robotics and Automation (ICRA)*, IEEE, 2020, pp. 10 563–10 569.

[83] Y. B. Can, A. Liniger, O. Unal, D. Paudel, and L. Van Gool, "Understanding bird's-eye view of road semantics using an onboard camera", *IEEE Robotics and Automation Letters*, vol. 7, no. 2, pp. 3302–3309, 2022. DOI: 10.1109/LRA.2022.3146898.

[84] R. Mahjourian, J. Kim, Y. Chai, M. Tan, B. Sapp, and D. Anguelov, "Occupancy flow fields for motion forecasting in autonomous driving", *IEEE Robotics and Automation Letters*, 2022.

[85] B. Ivanovic, K.-H. Lee, P. Tokmakov, *et al.*, "Heterogeneous-agent trajectory forecasting incorporating class uncertainty", *arXiv preprint arXiv:2104.12446*, 2021.

[86] W. Zeng, M. Liang, R. Liao, and R. Urtasun, "Lanercnn: Distributed representations for graph-centric motion forecasting", in *2021 IEEE/RSJ International Conference on Intelligent Robots and Systems (IROS)*, IEEE, 2021, pp. 532–539.

[87] W. Zeng, W. Luo, S. Suo, *et al.*, "End-to-end interpretable neural motion planner", in *Proceedings of the IEEE/CVF Conference on Computer Vision and Pattern Recognition*, 2019, pp. 8660–8669.

[88] B. Triggs, "Motion planning for nonholonomic vehicles: An introduction", 1993.

[89] W. Zhan, L. Sun, D. Wang, *et al.*, "Interaction dataset: An international, adversarial and cooperative motion dataset in interactive driving scenarios with semantic maps", *arXiv preprint arXiv:1910.03088*, 2019.

[90] H. John, Z. Guido, B. Luca, *et al.*, "One thousand and one hours: Self-driving motion prediction dataset", *arXiv preprint arXiv: 2006.14480*, 2020.

[91] S. Ettinger, S. Cheng, B. Caine, *et al.*, "Large scale interactive motion forecasting for autonomous driving: The waymo open motion dataset", in *Proceedings of the IEEE/CVF International Conference on Computer Vision*, 2021, pp. 9710–9719.

[92] H. Caesar, V. Bankiti, A. H. Lang, *et al.*, "Nuscenes: A multimodal dataset for autonomous driving", in *Proceedings of the IEEE/CVF conference on computer vision and pattern recognition*, 2020, pp. 11 621–11 631.

[93] A. Malinin, N. Band, G. Chesnokov, *et al.*, "Shifts: A dataset of real distributional shift across multiple large-scale tasks", *arXiv preprint arXiv:2107.07455*, 2021.

[94] J. Singh, W. Qi, T. Agarwal, and A. Hartnett, *Argoverse motion forecasting competition*, https://eval.ai/web/challenges/challenge-page/454/overview, Accessed: 08-27-2021.

[95] R. Matthaeia, A. Reschkaa, J. Riekena, *et al.*, *Autonomous driving: Technical, legal and social aspects*, 2015.

[96] R. Rajamani, *Vehicle dynamics and control*. Springer Science & Business Media, 2011.

[97] C. Gold, M. Körber, D. Lechner, and K. Bengler, "Taking over control from highly automated vehicles in complex traffic situations: The role of traffic density", *Human factors*, vol. 58, no. 4, pp. 642–652, 2016.

[98] N. Merat, A. H. Jamson, F. C. Lai, M. Daly, and O. M. Carsten, "Transition to manual: Driver behaviour when resuming control from a highly automated vehicle", *Transportation research part F: traffic psychology and behaviour*, vol. 27, pp. 274–282, 2014.

[99] A. Geiger, P. Lenz, and R. Urtasun, "Are we ready for autonomous driving? the kitti vision benchmark suite", in *2012 IEEE Conference on Computer Vision and Pattern Recognition*, IEEE, 2012, pp. 3354–3361.

[100] H. Schöner, "The role of simulation in development and testing of autonomous vehicles", in *Driving Simulation Conference, Stuttgart*, 2017.

[101] P. Kaur, S. Taghavi, Z. Tian, and W. Shi, "A survey on simulators for testing self-driving cars", *arXiv preprint arXiv:2101.05337*, 2021.

[102] R. Lattarulo, J. Pérez, and M. Dendaluce, "A complete framework for developing and testing automated driving controllers", *IFAC-PapersOnLine*, vol. 50, no. 1, pp. 258–263, 2017.

[103] M. Dupuis, M. Strobl, and H. Grezlikowski, "Opendrive 2010 and beyond–status and future of the de facto standard for the description of road networks", in *Proc. of the Driving Simulation Conference Europe*, 2010, pp. 231–242.

[104] R. F. Benekohal and J. Treiterer, "Carsim: Car-following model for simulation of traffic in normal and stop-and-go conditions", *Transportation research record*, vol. 1194, pp. 99–111, 1988.

[105] M. Tideman and M. Van Noort, "A simulation tool suite for developing connected vehicle systems", in *2013 IEEE Intelligent Vehicles Symposium (IV)*, IEEE, 2013, pp. 713–718.

[106] A. Dosovitskiy, G. Ros, F. Codevilla, A. Lopez, and V. Koltun, "Carla: An open urban driving simulator", in *Conference on robot learning*, PMLR, 2017, pp. 1–16.

[107] A. Sanders, *An introduction to unreal engine 4*. AK Peters/CRC Press, 2016.

[108] N. Koenig and A. Howard, "Design and use paradigms for gazebo, an open-source multi-robot simulator", in *Intelligent Robots and Systems, 2004.(IROS 2004). Proceedings. 2004 IEEE/RSJ International Conference on*, IEEE, vol. 3, 2004, pp. 2149–2154.

[109] G. Rong, B. H. Shin, H. Tabatabaee, *et al.*, "Lgsvl simulator: A high fidelity simulator for autonomous driving", in *2020 IEEE 23rd International Conference on Intelligent Transportation Systems (ITSC)*, IEEE, 2020, pp. 1–6.

[110] J. Haas, "A history of the unity game engine", *Diss. WORCESTER POLYTECHNIC INSTITUTE*, 2014.

[111] H. W. Kuhn, "The hungarian method for the assignment problem", *Naval research logistics quarterly*, vol. 2, no. 1-2, pp. 83–97, 1955.

[112] G. Bishop, G. Welch, *et al.*, "An introduction to the kalman filter", *Proc of SIGGRAPH, Course*, vol. 8, no. 27599-23175, p. 41, 2001.

[113] R. Schubert, E. Richter, and G. Wanielik, "Comparison and evaluation of advanced motion models for vehicle tracking", in *2008 11th international conference on information fusion*, IEEE, 2008, pp. 1–6.

[114] S. Hochreiter and J. Schmidhuber, "Long short-term memory", *Neural computation*, vol. 9, no. 8, pp. 1735–1780, 1997.

[115] A. Vaswani, N. Shazeer, N. Parmar, *et al.*, "Attention is all you need", *Advances in neural information processing systems*, vol. 30, 2017.

[116] Z. Wu, S. Pan, F. Chen, G. Long, C. Zhang, and S. Y. Philip, "A comprehensive survey on graph neural networks", *IEEE transactions on neural networks and learning systems*, vol. 32, no. 1, pp. 4–24, 2020.

[117] H. Robbins and S. Monro, "A stochastic approximation method", *The annals of mathematical statistics*, pp. 400–407, 1951.

[118] J. Duchi, E. Hazan, and Y. Singer, "Adaptive subgradient methods for online learning and stochastic optimization.", *Journal of machine learning research*, vol. 12, no. 7, 2011.

[119] F. Zou, L. Shen, Z. Jie, W. Zhang, and W. Liu, "A sufficient condition for convergences of adam and rmsprop", in *Proceedings of the IEEE/CVF conference on computer vision and pattern recognition*, 2019, pp. 11 127–11 135.

[120] M. D. Zeiler, "Adadelta: An adaptive learning rate method", *arXiv preprint arXiv:1212.5701*, 2012.

[121] D. P. Kingma and J. Ba, "Adam: A method for stochastic optimization", *arXiv preprint arXiv:1412.6980*, 2014.

[122] C. Gómez-Huelamo, L. M. Bergasa, R. Barea, E. López-Guillén, F. Arango, and P. Sánchez, "Simulating use cases for the uah autonomous electric car", in *2019 IEEE Intelligent Transportation Systems Conference (ITSC)*, IEEE, 2019, pp. 2305–2311.

[123] X. Weng, J. Wang, D. Held, and K. Kitani, "3d multi-object tracking: A baseline and new evaluation metrics", in *2020 IEEE/RSJ International Conference on Intelligent Robots and Systems (IROS)*, IEEE, 2020, pp. 10 359–10 366.

[124] H.-k. Chiu, J. Li, R. Ambruş, and J. Bohg, "Probabilistic 3d multi-modal, multi-object tracking for autonomous driving", in *2021 IEEE International Conference on Robotics and Automation (ICRA)*, IEEE, 2021, pp. 14 227–14 233.

[125] C. Gómez–Huélamo, L. M. Bergasa, R. Gutiérrez, J. F. Arango, and A. Díaz, "Smartmot: Exploiting the fusion of hdmaps and multi-object tracking for real-time scene understanding in intelligent vehicles applications", in *2021 IEEE Intelligent Vehicles Symposium (IV)*, IEEE, 2021, pp. 710–715.

[126] A. H. Lang, S. Vora, H. Caesar, L. Zhou, J. Yang, and O. Beijbom, "Pointpillars: Fast encoders for object detection from point clouds", in *Proceedings of the IEEE/CVF conference on computer vision and pattern recognition*, 2019, pp. 12 697–12 705.

[127] J. Redmon, S. Divvala, R. Girshick, and A. Farhadi, "You only look once: Unified, real-time object detection", in *Proceedings of the IEEE conference on computer vision and pattern recognition*, 2016, pp. 779–788.

[128] K. Wong, Y. Gu, and S. Kamijo, "Mapping for autonomous driving: Opportunities and challenges", *IEEE Intelligent Transportation Systems Magazine*, vol. 13, no. 1, pp. 91–106, 2020.

[129] A. Sadeghian, V. Kosaraju, A. Sadeghian, N. Hirose, H. Rezatofighi, and S. Savarese, "Sophie: An attentive gan for predicting paths compliant to social and physical constraints", in *Proceedings of the IEEE/CVF conference on computer vision and pattern recognition*, 2019, pp. 1349–1358.

[130] J. Hong, B. Sapp, and J. Philbin, "Rules of the road: Predicting driving behavior with a convolutional model of semantic interactions", in *Proceedings of the IEEE/CVF Conference on Computer Vision and Pattern Recognition*, 2019, pp. 8454–8462.

[131] M. Quigley, K. Conley, B. Gerkey, *et al.*, "Ros: An open-source robot operating system", in *ICRA workshop on open source software*, Kobe, Japan, vol. 3, 2009, p. 5.

[132] H. Tverberg, "A proof of the jordan curve theorem", *Bulletin of the London Mathematical Society*, vol. 12, no. 1, pp. 34–38, 1980.

[133] A. Bewley, Z. Ge, L. Ott, F. Ramos, and B. Upcroft, "Simple online and realtime tracking", in *2016 IEEE international conference on image processing (ICIP)*, IEEE, 2016, pp. 3464–3468.

[134] K. Bernardin and R. Stiefelhagen, "Evaluating multiple object tracking performance: The clear mot metrics", *EURASIP Journal on Image and Video Processing*, vol. 2008, pp. 1–10, 2008.

[135] W. Zhang, H. Zhou, S. Sun, Z. Wang, J. Shi, and C. C. Loy, "Robust multi-modality multi-object tracking", in *Proceedings of the IEEE/CVF International Conference on Computer Vision*, 2019, pp. 2365–2374.

[136] E. Baser, V. Balasubramanian, P. Bhattacharyya, and K. Czarnecki, "Fantrack: 3d multi-object tracking with feature association network", in *2019 IEEE Intelligent Vehicles Symposium (IV)*, IEEE, 2019, pp. 1426–1433.

[137] X. Weng and K. Kitani, "Monocular 3d object detection with pseudo-lidar point cloud", in *Proceedings of the IEEE/CVF International Conference on Computer Vision Workshops*, 2019.

[138] J.-M. Jullien, C. Martel, L. Vignollet, and M. Wentland, "Openscenario: A flexible integrated environment to develop educational activities based on pedagogical scenarios", in *2009 Ninth IEEE International Conference on Advanced Learning Technologies*, IEEE, 2009, pp. 509–513.

[139] M. R. van Ratingen, "The euro ncap safety rating", in *Karosseriebautage Hamburg 2017*, A. Piskun, Ed., Wiesbaden: Springer Fachmedien Wiesbaden, 2017, pp. 11–20, ISBN: 978-3-658-18107-9.

[140] K. Guo, Y. Yan, J. Shi, R. Guo, and Y. Liu, "An investigation into c-ncap aeb system assessment protocol", in *SAE Technical Paper*, SAE International, Sep. 2017. DOI: 10.4271/2017-01-2009. [Online]. Available: https://doi.org/10.4271/2017-01-2009.

[141] Á. Takács, D. A. Drexler, P. Galambos, I. J. Rudas, and T. Haidegger, "Assessment and standardization of autonomous vehicles", in *2018 IEEE 22nd International Conference on Intelligent Engineering Systems (INES)*, 2018, pp. 000 185–000 192. DOI: 10.1109/INES.2018.8523899.

[142] R. Gutiérrez, J. F. Arango, C. Gomez-Huélamo, L. M. Bergasa, R. Barea, and J. Araluce, "Validation method of a self-driving architecture for unexpected pedestrian scenario in carla simulator", in *2021 IEEE Intelligent Vehicles Symposium (IV)*, IEEE, 2021, pp. 1144–1149.

[143] *Euro ncap assessment protocol - vru - v10.0.3*, https://cdn.euroncap.com/media/58230/euro-ncap-assessment-protocol-vru-v1003.pdf, Accessed: 2021-02-10.

[144] C. Gómez-Huélamo, J. Del Egido, L. M. Bergasa, *et al.*, "Train here, drive there: Ros based end-to-end autonomous-driving pipeline validation in carla simulator using the nhtsa typology", *Multimedia Tools and Applications*, pp. 1–28, 2021.

[145] C. Gómez-Huélamo, J. Del Egido, L. M. Bergasa, *et al.*, "Real-time bird's eye view multi-object tracking system based on fast encoders for object detection", in *2020 IEEE 23rd International Conference on Intelligent Transportation Systems (ITSC)*, IEEE, 2020, pp. 1–6.

[146] P. Dendorfer, A. Osep, and L. Leal-Taixé, "Goal-gan: Multimodal trajectory prediction based on goal position estimation", in *Proceedings of the Asian Conference on Computer Vision*, 2020.

[147] S. Pellegrini, A. Ess, K. Schindler, and L. Van Gool, "You'll never walk alone: Modeling social behavior for multi-target tracking", in *2009 IEEE 12th international conference on computer vision*, IEEE, 2009, pp. 261–268.

[148] A. Lerner, Y. Chrysanthou, and D. Lischinski, "Crowds by example", *Comput. Graph. Forum*, vol. 26, pp. 655–664, Sep. 2007. DOI: 10.1111/j.1467-8659.2007.01089.x.

[149] J. Amirian, J.-B. Hayet, and J. Pettré, "Social ways: Learning multi-modal distributions of pedestrian trajectories with gans", in *Proceedings of the IEEE/CVF Conference on Computer Vision and Pattern Recognition Workshops*, 2019.

[150] X. Li, X. Ying, and M. C. Chuah, "Grip: Graph-based interaction-aware trajectory prediction", in *2019 IEEE Intelligent Transportation Systems Conference (ITSC)*, IEEE, 2019, pp. 3960–3966.

[151] A. Vemula, K. Muelling, and J. Oh, "Social attention: Modeling attention in human crowds", in *2018 IEEE international Conference on Robotics and Automation (ICRA)*, IEEE, 2018, pp. 4601–4607.

[152] C. Gómez-Huélamo, M. V. Conde, M. Ortiz, S. Montiel, R. Barea, and L. M. Bergasa, "Exploring attention gan for vehicle motion prediction", in *2022 IEEE 25th International Conference on Intelligent Transportation Systems (ITSC)*, IEEE, 2022, pp. 4011–4016.

[153] C. Tang, W. Zhan, and M. Tomizuka, "Exploring social posterior collapse in variational autoencoder for interaction modeling", *Advances in Neural Information Processing Systems*, vol. 34, pp. 8481–8494, 2021.

[154] M. Ahmed, R. Seraj, and S. M. S. Islam, "The k-means algorithm: A comprehensive survey and performance evaluation", *Electronics*, vol. 9, no. 8, p. 1295, 2020.

[155] *Argoverse benchmark*, https://eval.ai/web/challenges/challenge-page/454/evaluation, Accessed: 2022-03-19.

[156] T. Xie and J. C. Grossman, "Crystal graph convolutional neural networks for an accurate and interpretable prediction of material properties", *Physical review letters*, vol. 120, no. 14, p. 145 301, 2018.

[157] N. Djuric, H. Cui, Z. Su, *et al.*, "Multixnet: Multiclass multistage multimodal motion prediction", in *2021 IEEE Intelligent Vehicles Symposium (IV)*, IEEE, 2021, pp. 435–442.

[158] R. S. Ross, "Planning minimum-energy paths in an off-road environment with anisotropic traversal costs and motion constraints", NAVAL POSTGRADUATE SCHOOL MONTEREY CA, Tech. Rep., 1989.

[159] A. Savitzky and M. J. Golay, "Smoothing and differentiation of data by simplified least squares procedures.", *Analytical chemistry*, vol. 36, no. 8, pp. 1627–1639, 1964.

[160] M. Ye, T. Cao, and Q. Chen, "Tpcn: Temporal point cloud networks for motion forecasting", in *Proceedings of the IEEE/CVF Conference on Computer Vision and Pattern Recognition*, 2021, pp. 11 318–11 327.

[161] Z. Wang, J. Guo, Z. Hu, H. Zhang, J. Zhang, and J. Pu, "Lane transformer: A high efficiency trajectory prediction model", *IEEE Open Journal of Intelligent Transportation Systems*, 2023.

[162] S. Kim, H. Jeon, J. Choi, and D. Kum, "Improving diversity of multiple trajectory prediction based on map-adaptive lane loss", *arXiv preprint arXiv:2206.08641*, 2022.

[163] Y. Liu, J. Zhang, L. Fang, Q. Jiang, and B. Zhou, "Multimodal motion prediction with stacked transformers", in *Proceedings of the IEEE/CVF Conference on Computer Vision and Pattern Recognition*, 2021, pp. 7577–7586.

[164] R. Walters, J. Li, and R. Yu, "Trajectory prediction using equivariant continuous convolution", *arXiv preprint arXiv:2010.11344*, 2020.

[165] J. Gu, Q. Sun, and H. Zhao, "Densetnt: Waymo open dataset motion prediction challenge 1st place solution", *arXiv preprint arXiv:2106.14160*, 2021.

[166] C. Katrakazas, M. Quddus, W.-H. Chen, and L. Deka, "Real-time motion planning methods for autonomous on-road driving: State-of-the-art and future research directions", *Transportation Research Part C: Emerging Technologies*, vol. 60, pp. 416–442, 2015, ISSN: 0968-090X. DOI: https://doi.org/10.1016/j.trc.2015.09.011. [Online]. Available: https://www.sciencedirect.com/science/article/pii/S0968090X15003447.

[167] C. Zhang, H. Sun, C. Chen, and Y. Guo, "Banet: Motion forecasting with boundary aware network", *arXiv preprint arXiv:2206.07934*, vol. 2, 2022.

[168] C. Gómez-Huélamo, M. V. Conde, R. Barea, and L. M. Bergasa, "Improving multi-agent motion prediction with heuristic goals and motion refinement", in *Proceedings of the IEEE/CVF Conference on Computer Vision and Pattern Recognition*, 2023, pp. 5322–5331.

[169] T.-Y. Lin, P. Dollár, R. Girshick, K. He, B. Hariharan, and S. Belongie, "Feature pyramid networks for object detection", in *Proceedings of the IEEE conference on computer vision and pattern recognition*, 2017, pp. 2117–2125.

[170] D. I. Shuman, S. K. Narang, P. Frossard, A. Ortega, and P. Vandergheynst, "The emerging field of signal processing on graphs: Extending high-dimensional data analysis to networks and other irregular domains", *IEEE signal processing magazine*, vol. 30, no. 3, pp. 83–98, 2013.

[171] T. N. Kipf and M. Welling, "Semi-supervised classification with graph convolutional networks", *arXiv preprint arXiv:1609.02907*, 2016.

[172] F. Yu and V. Koltun, "Multi-scale context aggregation by dilated convolutions", *arXiv preprint arXiv:1511.07122*, 2015.

[173] M. Liu, H. Cheng, L. Chen, *et al.*, "Laformer: Trajectory prediction for autonomous driving with lane-aware scene constraints", *arXiv preprint arXiv:2302.13933*, 2023.

[174] T. Gilles, S. Sabatini, D. Tsishkou, B. Stanciulescu, and F. Moutarde, "Thomas: Trajectory heatmap output with learned multi-agent sampling", *arXiv preprint arXiv:2110.06607*, 2021.

[175] Y. Wang, H. Zhou, Z. Zhang, *et al.*, "Tenet: Transformer encoding network for effective temporal flow on motion prediction", *arXiv preprint arXiv:2207.00170*, 2022.

[176] M. Zhou, J. Luo, J. Villella, *et al.*, *Smarts: Scalable multi-agent reinforcement learning training school for autonomous driving*, Nov. 2020. [Online]. Available: https://arxiv.org/abs/2010.09776.

[177] M. Behrisch, L. Bieker, J. Erdmann, and D. Krajzewicz, "Sumo - simulation of urban mobility: An overview", in *in SIMUL 2011, The Third International Conference on Advances in System Simulation*, 2011, pp. 63–68.

[178] E. Yurtsever, J. Lambert, A. Carballo, and K. Takeda, "A survey of autonomous driving: Common practices and emerging technologies", *CoRR*, vol. abs/1906.05113, 2019. arXiv: 1906.05113. [Online]. Available: http://arxiv.org/abs/1906.05113.

[179] B. R. Kiran, I. Sobh, V. Talpaert, *et al.*, "Deep reinforcement learning for autonomous driving: A survey", *CoRR*, vol. abs/2002.00444, 2020. arXiv: 2002.00444. [Online]. Available: https://arxiv.org/abs/2002.00444.

[180] J. Schulman, F. Wolski, P. Dhariwal, A. Radford, and O. Klimov, "Proximal policy optimization algorithms", *CoRR*, vol. abs/1707.06347, 2017. arXiv: 1707.06347. [Online]. Available: http://arxiv.org/abs/1707.06347.

[181] V. Mnih, K. Kavukcuoglu, D. Silver, *et al.*, "Human-level control through deep reinforcement learning", *Nature*, vol. 518, no. 7540, pp. 529–533, Feb. 2015, ISSN: 00280836. [Online]. Available: http://dx.doi.org/10.1038/nature14236.

[182] L. Zhu, F. R. Yu, Y. Wang, B. Ning, and T. Tang, "Big data analytics in intelligent transportation systems: A survey", *IEEE Transactions on Intelligent Transportation Systems*, vol. 20, no. 1, pp. 383–398, 2019. DOI: 10.1109/TITS.2018.2815678.

[183] D. Silver, A. Huang, C. J. Maddison, *et al.*, "Mastering the game of Go with deep neural networks and tree search", *Nature*, vol. 529, no. 7587, pp. 484–489, 2016, ISSN: 0028-0836. DOI: 10.1038/nature16961.

[184] S. Ross, G. J. Gordon, and J. A. Bagnell, "No-regret reductions for imitation learning and structured prediction", *CoRR*, vol. abs/1011.0686, 2010. arXiv: 1011.0686. [Online]. Available: http://arxiv.org/abs/1011.0686.

[185] R. Gutiérrez-Moreno, R. Barea, E. López-Guillén, F. Arango, N. Abdeselam, and L. M. Bergasa, "Hybrid decision making for autonomous driving in complex urban scenarios", in *2023 IEEE Intelligent Vehicles Symposium (IV)*, 2023.

[186] C. Hoel, K. Wolff, and L. Laine, "Automated speed and lane change decision making using deep reinforcement learning", *CoRR*, vol. abs/1803.10056, 2018. arXiv: 1803.10056. [Online]. Available: http://arxiv.org/abs/1803.10056.

[187] T. Tram, A. Jansson, R. Grönberg, M. Ali, and J. Sjöberg, "Learning negotiating behavior between cars in intersections using deep q-learning", *CoRR*, vol. abs/1810.10469, 2018. arXiv: 1810.10469. [Online]. Available: http://arxiv.org/abs/1810.10469.

[188] Z. Zhang, A. Liniger, D. Dai, F. Yu, and L. V. Gool, *End-to-end urban driving by imitating a reinforcement learning coach*, 2021. arXiv: 2108.08265 [cs.CV].

[189] I. Kostrikov, D. Yarats, and R. Fergus, *Image augmentation is all you need: Regularizing deep reinforcement learning from pixels*, 2021. arXiv: 2004.13649 [cs.LG].

[190] M. Moghadam and G. H. Elkaim, *A hierarchical architecture for sequential decision-making in autonomous driving using deep reinforcement learning*, 2019. arXiv: 1906.08464 [cs.RO].

[191] G. Li, Y. Qiu, Y. Yang, *et al.*, "Lane change strategies for autonomous vehicles: A deep reinforcement learning approach based on transformer", *IEEE Transactions on Intelligent Vehicles*, vol. 8, no. 3, pp. 2197–2211, 2023. DOI: 10.1109/TIV.2022.3227921.

[192] R. Valiente, M. Razzaghpour, B. Toghi, G. Shah, and Y. P. Fallah, *Prediction-aware and reinforcement learning based altruistic cooperative driving*, 2022. arXiv: 2211.10585 [cs.RO].

[193] R. Gutiérrez-Moreno, R. Barea, E. López-Guillén, J. Araluce, and L. M. Bergasa, "Reinforcement learning-based autonomous driving at intersections in carla simulator", *Sensors*, vol. 22, no. 21, 2022, ISSN: 1424-8220. DOI: 10.3390/s22218373. [Online]. Available: https://www.mdpi.com/1424-8220/22/21/8373.

[194] T. Haarnoja, A. Zhou, K. Hartikainen, *et al.*, *Soft actor-critic algorithms and applications*, 2019. arXiv: 1812.05905 [cs.LG].

[195] J. Knodt, J. Bartusek, S.-H. Baek, and F. Heide, *Neural ray-tracing: Learning surfaces and reflectance for relighting and view synthesis*, 2021. arXiv: 2104.13562 [cs.CV].

[196] S. M. Koksbang and S. Hannestad, "Studying the precision of ray tracing techniques with szekeres models", *Physical Review D*, vol. 92, no. 2, 2015, ISSN: 1550-2368. DOI: 10.1103/physrevd.92.023532. [Online]. Available: http://dx.doi.org/10.1103/PhysRevD.92.023532.